

# **AUTOMATED DESIGN OPTIMISATION AND SIMULATION OF STITCHED ANTENNAS FOR TEXTILE DEVICES**

By

Abraham Torleele Wiri

A Doctoral Thesis Submitted in Partial Fulfilment of the  
Requirements for the Award of Doctor of Philosophy of  
Loughborough University

July 2019

© by Abraham Torleele Wiri

# Abstract

This thesis describes a novel approach for designing 7-segment and 5-angle pocket and collar planar antennas (for operation at 900 MHz). The motivation for this work originates from the problem of security of children in rural Nigeria where there is risk of abduction. There is a strong potential benefit to be gained from hidden wireless tracking devices (and hence antennas) that can protect their security. An evolutionary method based on a genetic algorithm was used in conjunction with electromagnetic simulation. This method determines the segment length and angle between segments through several generations. The simulation of the antenna was implemented using heuristic crossover with non-uniform mutation. Antennas obtained from the algorithm were fabricated and measured to validate the proposed method.

This first part of this research has been limited to linear wire antennas because of the wide range and flexibility of this class of antennas. Linear wire antennas are used for the design of high or low gain, broad or narrow band antennas. Wire antennas are easy and inexpensive to build. All the optimised linear wire antenna samples exhibit similar performances, most of the power is radiated within the GSM900 frequency band. The reflection coefficient ( $S_{11}$ ) is generally better than -10dB. The method of moment (MoM-NEC2) and FIT (CST Studio Suite 2015) solvers were used for this design. MATLAB is used to as an interface to control computational electromagnetic solvers for antenna designs and analysis. The genetic algorithm procedures were written in MATLAB.

The second part of the work focuses on meshed ground planes for applications at 900 MHz global system for mobile communications (GSM), 2.45 Hz industrial, scientific, and medical (ISM) band and 5 Hz wearable wireless local area networks (WLAN) frequencies. Square ground planes were developed and designed using linear equations in MATLAB. The ground plane was stitched using embroidery machines. To examine the effect of meshing on the antenna performance and to normalise the meshed antenna to a reference, solid patch antenna was designed, fabricated on an FR4 substrate.

A finite grid of resistors was created for numerical simulation in MATLAB. The resistance from the centre to any node of a finite grid of resistors are evaluated using nodal analysis. The probability that a node connects to each node in the grid was computed. The circuit model has been validated against the experimental model by measurement of the meshed ground plane. A set of measurement were collected from a meshed and compared with the numerical values, they show good agreement.

***Keywords- Linear wire antennas; Genetic algorithm; Reproduction operation; Stitched; Embroidery; Meshed ground plane***

# Acknowledgements

I would like to express my heartfelt appreciation and gratitude to my supervisors: Dr. Robert D. Seager and Dr. James A. Flint, for their irreplaceable advice, guidance and shared knowledge throughout my PhD. I would also like to thank Dr. Will Whittow, Dr. Alford Chauraya and Dr. Shiyu Zhang for their shared experience and knowledge towards completing my thesis.

To Prof M.J Ayotamuno, Dean Faculty of Engineering, Rivers State University, Port Harcourt, Nigeria for giving me this opportunity to do a PhD, I sincerely thank you.

My deepest gratitude belongs to Precious my wife and my children; Zina, Barilunanee and Lenu for supporting me, your patient and understanding throughout the research years.

Lastly to my mother; Mrs Baakoasae Stella Wiri for being my first teacher, who died in the middle of this study 2017. Thank you for your inspiration and care.

# Dedication

To my wife Precious, for her unconditional support, love, encouragement and prayers of day and night make me able to get victory and honour.

And, to my children, Zina, Barilunanee and Lenu who inspired me to be strong in spite of many challenges in life. Thank you, Jesus, for all.



# List of Abbreviations

|      |  |
|------|--|
| BW   | Bandwidth                                  |
| CST  | Computer Simulation Technology             |
| dB   | Decibels                                   |
| dBi  | Decibels compared to an isotropic radiator |
| EBG  | Electromagnetic Band Gap                   |
| EM   | Electromagnetic                            |
| FBR  | Front to Back Ratio                        |
| FR4  | Flame Resistant 4, substrate               |
| LC   | Inductor Capacitor                         |
| IBM  | International Business Machines            |
| MIDI | Musical Instrument Digital Interface       |
| PCB  | Printed Circuit Board                      |
| PET  | Polyester                                  |
| RF   | Radio Frequency                            |
| RL   | Resistor Inductor                          |
| RLC  | Resistor Inductor capacitor                |
| SMA  | Sub Miniature version A, connector         |
| TM   | Transverse Magnetic                        |
| VNA  | Vector Network Analyser                    |
| WLAN | Wireless Local Area Network                |

# List of Symbols

| Symbol     | Meaning                                    | Unit       |
|------------|--|------------|
| $Z_0$      | Characteristic impedance                   | $\Omega$   |
| $R_0$      | Real part of Characteristic impedance      | $\Omega$   |
| $X_0$      | Imaginary part of Characteristic impedance | $\Omega$   |
| $\Delta z$ | Length                                     | $mm$       |
| $\rho$     | Resistivity                                | $\Omega.m$ |
| $\sigma$   | Conductivity                               | $S/m$      |

|                 |                            |                           |
|-----------------|----------------------------|---------------------------|
| $\delta$        | Skin depth                 | —                         |
| $\mu_0$         | Permeability of free space | $H/m$                     |
| $\mu_r$         | Relative permeability      | —                         |
| $\varepsilon_0$ | Permittivity of free space | $F/m$                     |
| $\varepsilon_r$ | Relative permittivity      | —                         |
| $\tan \delta$   | Loss tangent               |                           |
| $\lambda$       | Wavelength                 | $m$                       |
| $\alpha$        | Attenuation constant       | $Nm^{-1}$ or $dB^2m^{-1}$ |
| $\beta$         | Phase constant             | —                         |
| $k$             | Wave number                | —                         |
| $\Gamma$        | Reflection Coefficient     | —                         |

## List of Figures

|   |      |
|---|------|
| Figure 1.1 Multifunctional shirt integrated with wearable antennas.....   | 1.3  |
| Figure 1.2 Candidate space for hiding an antenna on garments.....   | 1.5  |
| Figure 2.1 Antenna system.....  | 2.2  |
| Figure 2.2 Standard spherical coordinate system used in antenna measurements.....   | 2.5  |
| Figure 2.3. Positional axis for chamber measurements.....   | 2.5  |
| Figure 2.4 Examples of early wearable applications.....   | 2.6  |
| Figure 2.5 Functional chording keyboard embroidered into a jacket.....  | 2.7  |
| Figure 2.6 Commercial floating lifejacket.....  | 2.12 |
| Figure 2.7 Fabricated textile patch antenna placed conformal on the human arm.....  | 2.13 |
| Figure 2.8 Six e-textile complementary-8 antennas.....  | 2.13 |
| Figure 2.9 Brother Pr1000e embroidery machine.....  | 2.16 |
| Figure 2.10 (a) Sketch of the lock stitches and (b) Bobbin with top thread and looper thread.....   | 2.17 |
| Figure 2.11 Schematic of a woven textile with warp yarns in white and weft yarns in dark grey.....  | 2.18 |
| Figure 2.12 (a) Weft knitted (on left) and warp knitted (on right). The blue yarns represent a particular row inside the fabric. (b) A fabric with knitted tubes..... | 2.19 |

|  |      |
|--|------|
| Figure 2.13 (a) Metal coated wire combined in iron tube; (b) Several diameter reductions of tube; (c) Bundling of tubes; (d) Leaching, realizing fibres..... | 2.21 |
| Figure 2.14 Various conductive threads.....  | 2.22 |
| Figure 2.15 Standard design of copper yarn twisted with polyester fibres.....  | 2.23 |
| Figure 2.16 Photographs of prototype evolved antennas.....   | 2.26 |
| Figure 3.1 Quarter-wavelength monopole on an infinite perfect electric conductor .....   | 3.4  |
| Figure 3.2 Vertical plane patterns of a monopole of $\lambda/4$ on infinite ground plane.....  | 3.5  |
| Figure 3.3 Flowchart of Evolutionary Algorithm.....  | 3.7  |
| Figure 3.4 Software flowchart showing the link between NEC and MATLAB in this thesis .....   | 3.13 |
| Figure 3. 5 Detailed process flowchart for the GA.....   | 3.14 |
| Figure 3.6 CAD design of linear wire antenna.....  | 3.15 |
| Figure 3.7 Antenna geometries.....   | 3.18 |
| Figure 3.8 Geometrical model (physical) of the wire antenna designs.....   | 3.25 |
| Figure 3.9 Simulated $S_{11}$ results of linear wire antenna sample in CST and NEC2.....   | 3.26 |
| Figure 3.10(a) GA-optimised solutions after 100 generations.....   | 3.27 |
| Figure 3.10(b) GA-optimised solutions after 100 generations.....   | 3.28 |
| Figure 3.11 Wire antennas on Shirt front pocket design.....  | 3.29 |
| Figure 3.12 Geometry of pocket antennas.....   | 3.31 |
| Figure 3.13 Simulated $S_{11}$ of Pocket A.....  | 3.32 |
| Figure 3.14 Simulated $S_{11}$ of Pocket B.....  | 3.32 |
| Figure 3.15 Simulated $S_{11}$ of Pocket C.....  | 3.33 |
| Figure 3.16 Simulated $S_{11}$ of Pocket D.....  | 3.33 |
| Figure 3.17 Diagram of the antenna in a shirt collar showing.....  | 3.34 |
| Figure 3.18 Geometry of collar antennas.....   | 3.35 |
| Figure 3.19 Simulated $S_{11}$ of Collar A.....  | 3.36 |
| Figure 3.20 Simulated $S_{11}$ of Collar B.....  | 3.36 |
| Figure 3.21 Simulated $S_{11}$ of Collar C.....  | 3.39 |
| Figure 3.22 Simulated $S_{11}$ of Collar D.....  | 3.39 |
| Figure 4.1 Measurement set up with Anritsu 37397D Vector Network Analyser.....   | 4.2  |
| Figure 4.2 Measured result $S_{11}$ compared to simulation of linear wire monopole.....  | 4.3  |
| Figure 4.3 Comparison of measured $S_{11}$ of linear and pocket B.....   | 4.4  |
| Figure 4.4 Far field gain pattern (E-plane) of pocket A antenna.....   | 4.4  |

|   |      |
|---|------|
| Figure 4.5 Far field gain pattern (H-plane) of pocket A antenna.....  | 4.5  |
| Figure 4.6 A photograph of pocket antenna.....  | 4.6  |
| Figure 4.7 Simulated and measured $S_{11}$ of the Pocket A.....   | 4.7  |
| Figure 4.8 Simulated and measured $S_{11}$ of the Pocket B.....   | 4.8  |
| Figure 4.9 Simulated and measured $S_{11}$ of the Pocket C.....   | 4.8  |
| Figure 4.10 Simulated and measured $S_{11}$ of the Pocket D.....  | 4.9  |
| Figure 4.11 Measured $S_{11}$ of pocket antennas.....   | 4.9  |
| Figure 4.12 Linear wire antennas (Pocket B) in the anechoic chamber.....  | 4.10 |
| Figure 4.13 Measured radiation pattern of linear wire antenna.....  | 4.11 |
| Figure 4.14 Planar version linear wire design in CST.....   | 4.12 |
| Figure 4.15 Measurement set up for the etched planar antenna.....   | 4.13 |
| Figure 4.16 Measured and simulated $S_{11}$ against frequency for planar antennas.....  | 4.13 |
| Figure 4.17 Radiation Pattern of Planar antennas (Width 10 mm) .....  | 4.14 |
| Figure 4.18 Measurement setup for dielectric parameters of textile samples.....   | 4.16 |
| Figure 4.19 Embroidery machine creating a pocket antenna.....   | 4.17 |
| Figure 4.20 Measured $S_{11}$ results for three identical fabric antennas with different ground plane width.....  | 4.18 |
| Figure 4.21 Photograph of Pocket antennas.....  | 4.18 |
| Figure 4.22 $S_{11}$ results of the Pocket A in three different profiles: linear wire, planar and fabric antennas.....  | 4.21 |
| Figure 4.23 Measurement setup for stitched antenna in anechoic chamber.....   | 4.22 |
| Figure 4.24 Measurement setup Pocket A under bending condition.....   | 4.24 |
| Figure 4.25 Measured $S_{11}$ of Pocket A on curved surface.....  | 4.24 |
| Figure 4.26 Pocket antenna mounted on the flat body phantom of the human body.....  | 4.25 |
| Figure 4.27 Measurement set-ups for on-body test.....   | 4.26 |
| Figure 4.28 Measured $S_{11}$ of Pocket A the on body and Off body.....   | 4.27 |
| Figure 4.29 Far field directive pattern of pocket A antenna without the body.....   | 4.28 |
| Figure 4.30 Far field directive pattern of pocket A antenna on flat body Phantom.....   | 4.29 |
| Figure 4.31 Specific absorption rate (SAR) at 870MHz on human phantom model with input power of 0.25W (a) SAR distribution for 1g and (b) SAR distribution for 10g..... | 4.30 |
| Figure 4.32 Specific absorption rate (SAR) at 870MHz on human phantom model with input power of 0.5W (a) SAR distribution for 1g and (b) SAR distribution for 10g.....  | 4.31 |

|  |      |
|--|------|
| Figure 4.33 Specific absorption rate (SAR) at 870MHz on human phantom model with input power of 1W (a) SAR distribution for 1g and (b) SAR distribution for 10g..... | 4.31 |
| Figure 4.34 Meshed monopole antenna layouts.....   | 4.33 |
| Figure 4.35 Meshed monopole antenna sample.....  | 4.34 |
| Figure 4.36 $S_{11}$ plot of meshed and unmeshed monopole antenna see Table 4.5 for detail of antennas.....  | 4.35 |
| Figure 4.37 Measured $S_{11}$ of two size meshed monopole antennas with different mesh parameters on FR4 see Table 4.5 for detail of antennas.....                   | 4.36 |
| Figure 4.38 Simulated surface current for antenna sample 21.....   | 4.38 |
| Figure 4.39 Stitching patterns.....  | 4.40 |
| Figure 4.40 Triangular stitched pattern of monopole antenna.....   | 4.42 |
| Figure 4.41 $S_{11}$ plot of antenna sample M03 employing denim fabric.....  | 4.43 |
| Figure 4.42 $S_{11}$ plot of measured meshed stitch antenna samples on denim.....  | 4.44 |
| Figure 4.43 $S_{11}$ plot of meshed monopole antenna employing denim and felt fabric.....  | 4.44 |
| Figure 5.1 A square cut from the finite array.....   | 5.2  |
| Figure 5.2 Real part of the normalised resistance to each grid point for a finite array.....   | 5.4  |
| Figure 5.3 Bypassing techniques used for stitch pattern formation.....   | 5.6  |
| Figure 5.4 Three representative stitch patterns.....   | 5.7  |
| Figure 5.5 Mesh stitch problem - no contact made.....  | 5.7  |
| Figure 5.6 Output samples of stitched meshes on felt and denim.....  | 5.9  |
| Figure 5.7 Measurement referenced point of meshed ground plane.....  | 5.10 |
| Figure 5.8 Comparison of measured point with simulation and analytical results of stitched ground plane.....   | 5.13 |
| Figure 5.9 Geometry of proposed inset microstrip fed patch antenna.....  | 5.17 |
| Figure 5.10(a) Antenna geometry of antenna design A and (b) Picture of microstrip patch antenna (Antenna design A) .....   | 5.19 |
| Figure 5.11 The reflection coefficient of Antenna design A with solid ground plane (see Figure 5.10) .....   | 5.20 |
| Figure 5.12 Simulated radiation patterns for microstrip patch (of Fig.5.11-Antenna design A) at 2.45 GHz.....  | 5.21 |
| Figure 5.13 Effect of the linewidth on the resonant frequency of rectangular meshed ground for patch antenna.....  | 5.23 |
| Figure 5.14 Simulated radiation patterns at 2.45 GHz for microstrip antennas.....  | 5.24 |

|  |      |
|--|------|
| Figure 5.15 (a) Simulation model of referenced patch B and (b) Photograph of fabricated microstrip patch (referenced design-inset feed) .....          | 5.25 |
| Figure 5.16 Comparison between simulation and measurement of the proposed microstrip patch (inset feed) of Fig.5.15 by means of the $S_{11}$ plot..... | 5.25 |
| Figure 5.17 Simulated radiation normalised pattern (of Fig 5.15).....  | 5.26 |
| Figure 5.18 $S_{11}$ result for meshed ground plane and conventional patch antenna.....  | 5.29 |
| Figure 5.19 $S_{11}$ Simulation results of horizontal lines ( $N_H = 3$ ) and varying vertical lines ( $N_V$ ) of meshed ground plane.....             | 5.30 |
| Figure 5.20 Simulated radiation patterns for the Gain of antenna design 4, 5, 6, 7 and 8....   | 5.31 |
| Figure 5.21 Simulated surface current on the meshed ground plane at 2.45 GHz.....  | 5.32 |
| Figure 5.22 $S_{11}$ Measured result compared with simulation of solid patch (PA1) with solid ground and meshed patch (MGP1) with meshed ground.....   | 5.36 |
| Figure 5.23 Stimulated radiation pattern of antenna samples MGP1 and PA1.....  | 5.37 |
| Figure 5.24 Simulated and measured $S_{11}$ results of the antenna MGP4 and PA1 (solid patch on meshed and solid ground planes).....                   | 5.38 |
| Figure 5.25 Meshed ground (MPG3) and stitched ground plane (PA2) measured results compared with simulation of PA2.....                                 | 5.39 |
| Figure 5.26 Measured $S_{11}$ results of antennas with different stitched ground plane on different textile substrate.....                             | 5.41 |
| Figure 5.27 Measured $S_{11}$ of antenna sample PA3 off and on body.....   | 5.41 |
| Figure 5.28 Stimulated radiation patterns of antenna samples.....  | 5.42 |
| Figure 5.29 Simulated surface current on meshed ground plane for microstrip patch antenna at 5 Hz .....  | 5.43 |

## List of Tables

|   |      |
|---|------|
| Table 2.1 Review of a selection of wearable antenna found in the literature ..... | 2.10 |
| Table 2.2 Dielectric properties of human body tissues at 900MHz.....              | 2.14 |
| Table 2.3 Dielectric properties of human body tissues at 2.45GHz.....             | 2.15 |
| Table 3.1 Comparison of numerical methods.....                                    | 3.3  |
| Table 3.2 Format of antenna geometry.....   | 3.16 |
| Table 3.3 Genetic Algorithm parameters.....                                       | 3.19 |

|   |      |
|---|------|
| Table 3.4 Optimised samples of wire antennas for shirt pocket.....  | 3.30 |
| Table 3.5 Optimised samples of wire antennas for collar.....  | 3.38 |
| Table 4.1 Results of performance of Pocket antennas.....  | 4.6  |
| Table 4.2 Comparison of different version of Pocket A antenna.....  | 4.19 |
| Table 4.3 Geometry of meshed monopole antennas on FR-4.....   | 4.34 |
| Table 4.4 Parameters of stitched monopole antennas.....   | 4.36 |
| Table 4.5 Measured results for stitched monopole antennas same nominal dimensions in all cases.....   | 4.38 |
| Table 5.1 Finite numerical simulation of the real part of normalised resistance one quarter of a finite array.....                              | 5.4  |
| Table 5.1 Measured mesh point values normalised data for an 8×8 stitched ground plane.....  | 5.11 |
| Table 5.3 Resistances $R_{m,n}$ between node $(0,0)$ and node $(m,n)$ in units of R of infinite array (analytical data adapted from [5.4])..... | 5.12 |
| Table 5.4 Simulated results of patch antenna with meshed ground plane.....  | 5.21 |
| Table 5.5 Simulated and measured result of representative examples for meshed ground plane.....   | 5.28 |
| Table 5.6 Microstrip antenna dimensions and parameters.....   | 5.34 |
| Table 5.7 Simulated and measured parameters of representative examples of meshed and stitched ground planes for microstrip antennas.....        | 5.35 |

# Contents

|   |             |
|---|-------------|
| <b>Summary.....</b>   | <b>i</b>    |
| <b>Acknowledgements.....</b>                                    | <b>ii</b>   |
| <b>Dedication.....</b>  | <b>iii</b>  |
| <b>List of abbreviations.....</b>                               | <b>iv</b>   |
| <b>List of symbols.....</b>                                     | <b>iv-v</b> |
| <b>List of Figures.....</b>                                     | <b>v-ix</b> |
| <b>List of Tables.....</b>                                      | <b>ix-x</b> |
| <br>  |             |
| <b>Chapter 1: Introduction.....</b>                             | <b>1.1</b>  |
| 1.1. Background.....  | 1.1         |
| 1.2. Area of Research.....                                      | 1.2         |
| 1.3. Wearable / Textile Technology.....                         | 1.3 -1.5    |
| 1.4. Motivation for Thesis Application.....                     | 1.5-1.7     |
| 1.5. Research Objectives.....                                   | 1.7         |
| 1.6. Primary contribution of the Thesis.....                    | 1.8         |
| 1.7. Structure of the Thesis.....                               | 1.8-1.9     |
| References.....   | 1.10-1.12   |
| <br>  |             |
| <b>Chapter 2: Textile Wearables Antennas.....</b>               | <b>2.1</b>  |
| 2.1. Introduction.....  | 2.1         |
| 2.2. Desirable properties of an antenna.....                    | 2.2-2.3     |
| 2.3. Antenna measurements.....                                  | 2.3-2.5     |
| 2.4. Wearable Antennas.....                                     | 2.6-2.7     |
| 2.4.1. Antenna types for wearable applications.....             | 2.7-2.10    |
| 2.4.2. Textiles wearable antennas for on-body applications..... | 2.11-2.13   |
| 2.4.3. Antenna properties on flat-body Phantom.....             | 2.14        |
| 2.5. Challenges of wearable antennas.....                       | 2.15        |
| 2.6. Methods of implementing stitched antennas.....             | 2.15        |
| 2.6.1. Embroidery techniques.....                               | 2.15-2.17   |
| 2.6.2. Weaving and Knitting.....                                | 2.18-2.19   |
| 2.6.3. Printing a conductive layer fabric.....                  | 2.19        |
| 2.7. Fabrication of conductive threads.....                     | 2.20        |



|  |           |
|--|-----------|
| 2.7.1. Conductive fibres.....                            | 2.20-2.21 |
| 2.7.2. Conductive fabrics.....                           | 2.21-2.22 |
| 2.8. Electrical properties of the conductive thread..... | 2.23-2.24 |
| 2.9. Review on Optimisation techniques.....              | 2.24-2.26 |
| Conclusion.....  | 2.27      |
| References.....  | 2.28-2.33 |

### **Chapter 3: Optimisation of a Linear Wire Antenna on a Garment .....3.1**

|  |           |
|--|-----------|
| 3.1. Introduction.....   | 3.1       |
| 3.2. Antenna Optimisation.....   | 3.1       |
| 3.3. Numerical Modelling.....  | 3.2-3.3   |
| 3.3.1. Theoretical analysis of basic monopole antenna.....   | 3.3-3.5   |
| 3.3.2. Summary.....  | 3.5       |
| 3.4. Optimisation Methods.....   | 3.6-3.7   |
| 3.4.1. Swarm Intelligence.....   | 3.8       |
| 3.4.2. Genetic Algorithms.....   | 3.8-3.9   |
| 3.4.3. Summary.....  | 3.9       |
| 3.5. General properties of Genetic Algorithms.....   | 3.9-3.10  |
| 3.6. Application of GA in Electromagnetics.....  | 3.10-3.11 |
| 3.7. Implementation of a genetic Algorithm using MATLAB and NEC2 for<br>simulation/Antenna Design Procedure..... | 3.11-3.14 |
| 3.7.1. Antenna Parameterisation for Genetic Algorithm.....   | 3.15      |
| 3.7.2. Implementation details.....   | 3.16-3.20 |
| 3.7.3. Model implementation of the wire antenna.....   | 3.20-3.21 |
| 3.7.4. Reproduction Operations.....  | 3.21      |
| 3.7.5. Fitness function.....   | 3.22      |
| 3.7.6. Fitness weighted selection.....   | 3.22      |
| 3.7.7. Heuristic Crossover.....  | 3.23      |
| 3.7.8. Mutation.....   | 3.23-3.24 |
| 3.8. Procedure for the proposed method.....  | 3.24      |
| 3.9. Novel wearable antennas based on the linear wire .....  | 3.24-3.28 |
| 3.9.1. Pocket antennas.....  | 3.28-3.33 |
| 3.9.2. Collar antennas.....  | 3.34-3.38 |
| 3.9.3. Summary.....  | 3.38      |

|                 |           |
|-----------------|-----------|
| Conclusion..... | 3.39      |
| References..... | 3.40-3.43 |

## **Chapter 4: Implementation and Validation of the Optimised Antennas.....4.1**

|   |           |
|---|-----------|
| 4.1. Introduction.....  | 4.1       |
| 4.2. Optimised linear wire antennas design.....   | 4.1       |
| 4.3. Measurement of linear wire antennas design .....                                       | 4.2-4.6   |
| 4.3.1. Radiation pattern.....   | 4.5       |
| 4.3.2. Effect of Linear wire antenna parameters on Resonant Frequency and<br>Bandwidth..... | 4.6-4.9   |
| 4.3.3. Radiation patterns.....  | 4.9-4.11  |
| 4.4. Planar version of linear wire antenna design.....                                      | 4.11-4.12 |
| 4.4.1. Measurement of planar antennas.....  | 4.13-4.15 |
| 4.4.2. Radiation patterns.....  | 4.15-4.16 |
| 4.5. Characterisation of fabric for antenna .....   | 4.16-4.17 |
| 4.6. Manufacture of fabric antennas.....  | 4.18-4.18 |
| 4.7. Effect of ground plane width on the fabric antenna.....                                | 4.19-4.21 |
| 4.8. Discussion of comparison of simulated, planar and stitched antennas.....               | 4.22-4.23 |
| 4.8.1. Measurements of antenna on curved surface .....                                      | 4.24-4.25 |
| 4.8.2. Human body effects.....  | 4.26-4.28 |
| 4.8.3. Radiation patterns and Specific absorption rate (SAR).....                           | 4.28-4.31 |
| 4.8.4. Summary.....   | 4.32      |
| 4.9. Simulated and measured performance characteristics of meshed monopole<br>antennas..... | 4.32      |
| 4.9.1. Antennas layouts.....  | 4.32-4.36 |
| 4.9.2. Surface current distributions.....   | 4.37-4.38 |
| 4.9.3. Stitched meshed monopole.....  | 4.37-4.44 |
| 4.9.4. Summary.....   | 4.45      |
| Conclusion.....   | 4.46      |
| References.....   | 4.47-4.48 |

## **Chapter 5: Optimisation of antenna meshing.....5.1**

|   |         |
|---|---------|
| 5.1. Introduction to Meshed Ground plane for microstrip patch antennas..... | 5.1-5.2 |
| 5.2. Development of designs: Theory of infinite array of resistors.....     | 5.2-5.3 |
| 5.3. Simulation of finite array.....  | 5.3-5.4 |

|   |           |
|---|-----------|
| 5.4. Bypass method for stitched pattern designs.....  | 5.4-5.9   |
| 5.5. Measurements of Meshed resistive network.....  | 5.10-5.13 |
| 5.6. Modelling and Design of Microstrip Patch antenna with Meshed ground<br>plane.....                                | 5.14-5.17 |
| 5.6.1. Investigation of line width of meshed patch antenna .....  | 5.18-5.19 |
| 5.6.2. Simulated and measured reflection coefficient and simulated radiation<br>patterns.....                         | 5.20-5.21 |
| 5.6.3 Meshed ground plane .....   | 5.21-5.23 |
| 5.6.4. Simulated Radiation pattern of a Patch antenna with solid and meshed<br>ground plane (Realised Gain/dBi) ..... | 5.24      |
| 5.6.5. Microstrip Patch (Inset feed) at 2.45 GHz.....   | 5.25-5.31 |
| 5.6.6. Simulated surface current for meshed ground plane.....   | 5.33-5.33 |
| 5.7. Microstrip patch at 5 GHz for evaluation of meshed ground plane.....   | 5.34      |
| 5.7.1. Production of textile meshed ground plane.....   | 5.35-5.36 |
| 5.7.2. Solid patch with solid ground (PA1) and meshed patch with<br>meshed ground.....                                | 5.36-5.38 |
| 5.7.3. Comparison of patches with meshed and solid ground planes .....  | 5.38-5.40 |
| 5.7.4. Stitched ground plane on fabric substrate .....  | 5.40-5.42 |
| 5.7.5. Simulated surface current for meshed ground plane.....   | 5.43      |
| 5.7.6. Summary.....   | 5.43      |
| Conclusion.....   | 5.44      |
| References.....   | 5.45-5.46 |

## **Chapter 6: Conclusion and Future Work.....6.1-6.5**

### Appendix

|                                      |         |
|--------------------------------------|---------|
| A. Numerical Methods.....            | A1-A6   |
| B. Results from designs.....         | A7-A10  |
| C. optimisation codes.....           | A11-A26 |
| D. creating the stitch patterns..... | A27-A31 |
| E. infinite array.....               | A32-A36 |
| References.....                      | A37     |

# **Chapter 1**

## **Introduction**

### **1.1. Background**

In today's technology advancement, wearable antennas are becoming a major part in our daily paraphernalia. Wearable electronics is a fast-growing industry across both civilian and military markets. Textile antennas have been designed to be body worn while in use for various applications. These textile antennas are used in systems, since they are flexible, for detecting body motion during exercise activity, monitoring heart rate and blood pressure. The basic requirements for wearable electronics include portability during operation, operation consistency, controllability and robustness that guarantee a good fitness of the electronic to the human body application. Many commercial wearable devices are currently fitness watches and heart rate monitors, but stitched antennas are designed to be integrated into garments. Garment integrated wearables are more challenging due to the unconventional materials used. The stitched antenna consists of a conductive element integrated into a non-conductive material known as the substrate. These stitched antennas are lightweight, flexible, not expensive, easy to produce and can be easily and seamlessly integrated into clothing [1.1-1.2].

Research into the designs and development of flexible textile antennas has continued to receive great attention because of the possibilities of integration of electronics into wearable textile systems that can communicate wirelessly with a base-station. Research has been initiated out of the need to integrate a wire antenna and RF system into garment with a view to reduce the size and shape to fit into existing garments. A cost effective and covert system is being sought. Smart clothing and smart textiles are active research areas. The application of this covert antenna is on humans. This antenna, that is applicable to civilians, is targeted for security applications in Nigeria and needs to be hidden in garments. [1.3].

An optimisation method for positioning of the radiating element within the existing garments was developed. This method considered the need for shape, size, cost and comfort of the wearer. In this thesis, an overview of the optimised linear wire antenna as a representative of pocket and collar antennas design is described along with the experimental results of prototype. The antennas are designed not to be visible and in conspicuous on the wearer by

integration within the garment. These antennas can be used for monitoring and tracking civilians with their consent using GSM900 within the Niger Delta terrain of Nigeria.

## **1.2. Area of Research**

This thesis will focus on antenna design for textile applications. These include the optimisation of wire antennas using GA-NEC2, planar and stitched monopole antennas, stitched mesh ground plane and meshed microstrip antennas. An optimisation inspired wearable textile antennas (that operate in the 850-950 MHz for GSM900 application) has been proposed and designed using the genetic algorithm and Numerical Electromagnetic Codes. A set of compact linear wire antennas containing five segments with a linear ground plane were transformed into planar antennas and fabricated. The antennas were stitched using embroidery. Meshed ground planes have been developed for textile antenna applications. Measurement of resistance across the meshes were compared with the theoretical results.

## **1.3. Wearable / Textile Technology**

Wearable technology has advanced significantly in the last 10-15 years because of the ease of integrating antennas into clothing and garments. The advances in this application are as results of miniaturization, seamless integration, functionality, comfort, data processing and communication [1.4]. The integration of systems in garments creates some different applications for fabric industries because most clothes and garments are for the protection of human body. Systems in garments designed for wireless functionalities can communicate with wearers and their immediate environments.

Figure 1.1 shows a representative example of garments with multifunctional integration of wearable antennas and sensors. A miniaturised antenna followed by an RF rectifying circuit capture the RF waves and convert the RF energy to dc. The 2.45 GHz wireless device band is used since it has vast band for energy harvesting. The purpose is to provide power to electronic devices. [1.5]. The body worn antennas were fabricated by embroidering conductive fibre onto regular fabrics.



Figure 1.1 Multifunctional shirt integrated with wearable antennas, sensors and power harvesting devices to enable body-worn wireless communications (Zhang et al, [1.5])

Textile wearable antennas have rapidly developed into flexible structures used for communication systems. Textile antennas are easily integrated into garments and find applications in wearable devices because of their advantages; lightweight, flexible, low fabrication cost and low maintenance cost. These antennas are made of two-parts textile conductive element integrated into a non-conductive textile material as the substrate. Textile antennas have been fabricated using conductive fibre (E-fibre) for GSM and Wi-Fi application for communications. A dual-band flare dipole was developed with two arms connected by a loop cover the two bands 830 – 993 MHz and 1710 – 2210MHz [1.6].

Short range and long-range wireless communications play important role in mobile wearable system. In wearable systems different subparts may be connected to each other via a wireless link, e.g. headset usually needs a wire connection, that could be replaced by a wireless link. Covert antennas could be implemented for civilian applications by either wearable electronics-based consumer devices or integrating electronics intelligence into clothes. Electronic devices are implemented into textiles not only as wearable but has the capabilities of monitoring, computation and wireless communicating [1.7-1.8]. There are numerous and increasing applications for textile electronics including:

- **Sport monitoring**  
Wearable system for measuring performance of baseball players were exploited using an array of wearable sensors, synchronous Inertia Measurement Unit (IMU) with digital magnetometer application in analysing human motion. This network of compact sensor devices has a wireless data system that is worn on the wrists and ankle [1.9-1.10].
- **Health monitoring**  
Ambulatory cardio monitoring was designed and implemented using sensor at 2.4GHz Doppler circuit integrated patch antenna with microcontroller with 12-bit ADC converter as a sampling technique [1.11]. The biomedical application uses smart sensors and processors as interface, to analyse and interpret chronic disease data between patient and health care provider [1.12]
- **Communication systems**  
In the body area network (BAN) used for proposed frequency bands is accomplished with wirelessly connected sensor node and actuators node around, in and on the body. The wireless personal device (PD) for acquiring information and supporting devices are employed for various BAN applications in emergency services, patient monitoring, defence, computer games, emotion detection, sport and fitness etc. Sensor integrated in clothes are applied for continuous health monitoring [1.13-1.14].
- **Wearable computers**  
The wearable Motherboard is a wearable computer that monitors vital signals of an individual using an interface of clothing or garments. This universal interface provides functionalities where a wireless communication system could be integrated with wearable Motherboard for different application in fields such as public safety, sport training performance monitoring, battlefield by soldier, space experiments, hazardous/emergency services and personalized information processing [1.15-1.16].

The antenna plays a vital role in the optimal design of wearable or hand-held unit in this application [1.17]. In designing these antennas, wearable or hand-held units the

electromagnetic interaction among the antennas and the human operator is an important factor to be considered.

Some applications where wearable antennas have found use are:

A textile antenna was designed using fabric for rescue workers [1.18-1.20]. The antenna was inserted into the protective garment. Interactions between the wearer and the surrounding environment were achieved using wearable sensors. Wearable antenna designs not only consider the effect of the lossy body on the wearer, but the antenna can equally be used in a harsh environment. The environments may be cold, rain, heat, smoke, dirt or gases. This wearable antenna has been used in services such as police, paramedics, fire fighters and rescue operations

Medical monitoring the application textile antennas with sensors for data transmission to monitor the inpatient in and out of hospital environments. Miniature wireless sensors are enclosed in patch antenna and bandages for the purpose of collecting and transmitting data. These antennas are very compact and comfortable for the wearer because of their flexibility. A flexible patch antenna was designed to monitor athlete pulse rate during sports events having a sufficient maximum gain and sufficient range coverage of the area of application [1.21].

#### **1.4. Motivation for Thesis Application**

Currently limited work has been reported or published in the area of covert antennas, this work looks at some odd shapes on garments (e.g. pocket,) and designs wire antennas that could fit into or be hidden in the available areas. The purpose of this thesis is to propose an optimisation procedure and to explore other design spaces to create novel linear wire antennas for textile application. This process is optimised by automating the design using genetic algorithms with an electromagnetic simulator to produce the design. The research not only looks at linear wire antennas but creates a novel stitched monopole antenna. The designs were produced using embroidery.

The concept involves wire antennas (seven elements) to produce a conformal antenna, that can be hidden in a garment. Some of the locations on the garments to hide an antenna are



shown in Fig.1.2. Considering the space available the straight monopole ( $\lambda/4$ ) is non conformal or covert [1.22]. These constraints were applied to the design so that the optimisation is governed partly by the space available on the garment (for example using the space around a shirt pocket, collar, and shirt label, top (or front) of a hat, and school children's bags). This wire antenna was optimised to make use of whatever space is available.

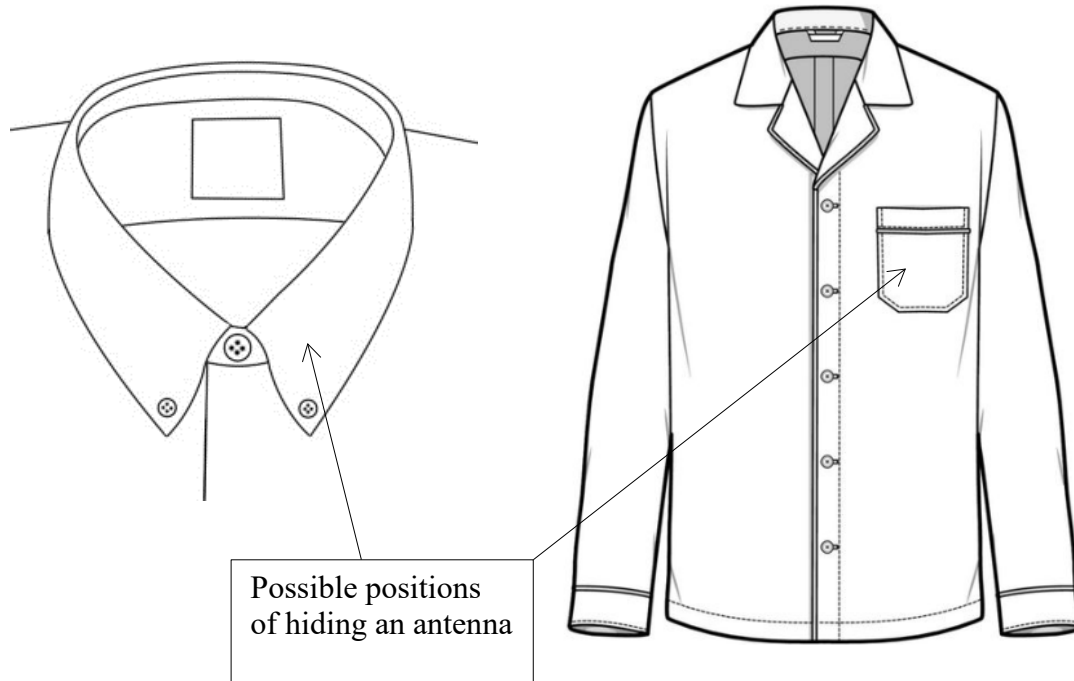


Figure 1.2 Candidate space for hiding an antenna on garments.

Recently much research has been carried out on the design of textile antennas using monopole antennas, dipoles and microstrip patch antennas for wearable applications [1.23-1.24]. The developments of a linear wire antenna using a genetic algorithm has been explored by research based on the open literature [1.25-1.29]. In a designs of linear wire antennas using genetic algorithms with Numerical Electromagnetic Code the MiniNec ground plane was used. In this study, a linear ground plane is proposed. The transformation of the linear wire antenna into planar linear wire antennas was achieved by etching the antenna on an FR4 substrate. Stitched versions of the linear wire antennas were fabricated using embroidery techniques.

The original drive for this research is born out of the challenges faced in Nigeria. These include incidents like kidnapping of school children, killing of farmers, herdsmen and suicide bombing within cities. Wearable textile antennas with an acceptable performance can be

potentially placed on schoolchildren's bags and on body. While Nigeria is very large country (923,768 km<sup>2</sup>) every part is covered by mobile communications systems. GSM base stations are not sparsely spaced within the Niger Delta terrain. Textile wearable antenna at GSM900 for communications could be used by herdsman since people measured their wealth in cattle. The herdsman carry cattle from place to place, of that they need active communication due to civilian challenges. The design solution will reduce the civilian challenges in Nigeria by application of wearable textile antennas using local fabric materials.

## **1.5. Research Objectives**

This research is both numerical and experimental based. In order to achieve the primary focus of this study the following goals were required to be accomplished:

- Explore covert wearable antennas made using very low technology manufacturing techniques such as embroidery stitching.
- Consider the constraints of optimising in specific wearable situations like pocket and collar of a shirt.
- Analyse techniques for achieving stitched ground planes and radiating elements
- Implement an optimization technique for developing novel shaped antennas using a Genetic Algorithm.
- Design automated wearable their wire-based antennas that are suitable for textile devices.
- Explore and select suitable optimisation techniques for linear wire antennas design.
- Investigate the possibility of integrating conductive materials and components into a textile material and develop a stitched ground plane for wearable applications.
- Reduce the material cost of the production of stitched antenna by minimizing usage of embroidery thread.

## **1.6. Primary contribution of the Thesis**

The primary contributions to this thesis are:

- (1) The method of using MATLAB to aid the modelling of wire antennas is proposed using an EM simulation software package (NEC2) built on the application of genetic algorithms.

- (2) The exploration of the design of stitched antennas in both linear and planar form for textile devices
- (3) A method to optimise the stitch patterns with conductive thread for antenna ground plane for 900 MHz global system for mobile communications (GSM) that is common in rural areas in Nigeria, 2.45 Hz industrial, scientific, and medical (ISM) band and 5 Hz wearable wireless local area networks (WLAN) frequencies.
- (4) A theoretical and measurement study on stitched and continuous ground plane.
- (5) A practical confirmation of (4) and validation of the methods of the thesis.

## **1.7. Structure of the Thesis**

Chapter 1 gives a description of introduction to the thesis, that includes textile and wearable technology. It offers an overview of the application of textile antennas used in wearable applications. A brief summary of the area of research, objectives, purpose and primary contribution of the thesis were also presented.

Chapter 2 begins with an overview of wire antenna. An outline of textile antenna technology along with methods of implementing stitched antennas showing the embroidery technology used in the fabrication of stitched antennas is also given. A brief introduction to the theory of linear wire antenna employed in the design is contained in this part. Antenna measurements in a full wave (anechoic) chamber are also presented in this section.

Chapter 3 describes the research procedure and method used for Wire and Planar Antenna design. The numerical method and optimisation techniques are described. Genetic algorithm advantages and applications in electromagnetism are summarised in this section. The steps for the implementation of a genetic algorithm with the electromagnetic simulator are discussed.

Chapter 4 details optimised linear wire antennas design and fabrication of wire, planar and stitched wire antennas. Measurements of linear wire antennas design for reflection coefficient and radiation patterns are presented. Also presented are results on the effect of the ground plane on different antenna samples based on the  $S_{11}$  response. Stitched mesh monopole

antennas and the possibility of integrating these antennas into fabric are also included in this chapter.

Chapter 5 introduces experimental measurement of stitched antenna components. It also provides the design of meshed ground plane using an infinite resistive array study. This part discusses the possible way to incorporate the designs into microstrip patch antennas.

Lastly, Chapter 6 outlines the main contributions of the study and gives suggestions for future work.

## References

- 1.1. M. Chedid, I. Belov, and P. Leisner, "Experimental analysis and modelling of textile transmission line for wearable applications," *Int. J. Cloth. Sci. Technol.*, 19(1), pp. 59–71, 2007.
- 1.2. D. Ferreira, P. Pires, R. Rodrigues and R.F. Caldeirinha, "Wearable Textile Antennas: Examining the effect of bending on their performance," *IEEE Antennas and Propagation Magazine*, 59(3), pp.54-59, 2017.
- 1.3. I. Kazani, F. Declercq, M.L. Scarpello, C. Hertleer, H. Rogier, D.V. Ginste, G. De Mey, G. Guxho and L. Van Langenhove. "Performance study of screen-printed textile antennas after repeated washing," *Autex Research Journal*, 14(2), pp.47-54. 2014.
- 1.4. A. Lymberis, and R. Paradiso, "A Smart fabrics and interactive textile enabling wearable personal applications: R&D state of the art and future challenges," In 2008 30th Annual International Conference of the IEEE Engineering in Medicine and Biology Society, pp. 5270-5273, 2008.
- 1.5. L. Zhang, Z.Wang, D. Psychoudakis and J.L.Volakis, "E-fiber electronics for body-worn devices," *Proc. 6th Eur. Conf. Antennas Propagation, EuCAP*, pp. 760–761, 2012.
- 1.6. Z. Wang, L. Zhang, D. Psychoudakis and Volakis, J.L, "GSM and Wi-Fi textile antenna for high data rate communications", *IEEE Antennas Propag. Soc. AP-S Int. Symp.*, 3, pp. 3–4, 2012.
- 1.7. B. Burchard, S. Jung, A. Ullsperger and W.D. Hartmann, "Devices, software, their applications and requirements for wearable electronics." In *ICCE. International Conference on Consumer Electronics (IEEE Cat. No. 01CH37182)* pp. 224-225, 2001.
- 1.8. D. Marculescu, R. Marculescu, N.H. Zamora, P. Stanley-Marbell, P.K. Khosla, S. Park, S. Jayaraman, S. Jung, C. Lauterbach, W. Weber and T. Kirstein, 2003. "Electronic textiles: A platform for pervasive computing". *Proceedings of the IEEE*, 91(12), pp.1995-2018, 2003.
- 1.9. M. Lapinski, M. Feldmeier and J.A. Paradiso, "Wearable wireless sensing for sports and ubiquitous interactivity." In *SENSORS*, pp. 1425-1428, 2011.
- 1.10. R. Aylward and J.A. Paradiso, "A compact, high-speed, wearable sensor network for biomotion capture and interactive media." In 2007 6th International Symposium on Information Processing in Sensor Networks, pp. 380-389, 2007.

- 1.11. R. R. Fletcher and S. Kulkarni, "A Clip-on wireless wearable microwave sensor for ambulatory cardiac monitoring". Annual International Conference of the IEEE Engineering in Medicine and Biology, pp. 365-369, 2010.
- 1.12. B.J. Agarwal and S. Agarwal, Integrated performance textiles designed for biomedical applications. In 2011 International Conference on Biomedical Engineering and Technology (IPCBEE), 2011.
- 1.13. M. Patel and J. Wang, "Applications, challenges, and prospective in emerging body area networking technologies." IEEE Wireless communications, 17(1), pp.80-88, 2010.
- 1.14. S. Ullah, H. Higgins, B. Braem, B. Latre, C. Blondia, I. Moerman, S. Saleem, Z. Rahman and K.S. Kwak, K.S, "A comprehensive survey of wireless body area networks." *Journal of medical systems*, 36(3), pp.1065-1094, 2012.
- 1.15. C. Gopalsamy, S. Park, R. Rajamanickam and S. Jayaraman, "The Wearable Motherboard™: The first generation of adaptive and responsive textile structures (ARTS) for medical applications." *Virtual Reality*, 4(3), pp.152-168, 1999.
- 1.16. S. Park, K. Mackenzie and S. Jayaraman, "The wearable motherboard: a framework for personalized mobile information processing (PMIP)." In Proceedings 2002 Design Automation Conference (IEEE Cat. No. 02CH37324), pp. 170-174. 2002.
- 1.17. P. Salonen, L. Sydanheimo, M. Keskilampi and M. Kivikoski, "A small planar Inverted-F antenna for wearable applications," In *Wearable Computers, Digest of Papers. The Third International Symposium on* pp. 95-100, 1999.
- 1.18. L. Vallozzi, W. Vandendriessche, H. Rogier, C. Hertleer and M.L. Scarpello, "Wearable textile GPS antenna for integration in protective garments," *Antennas Propag. (EuCAP), 2010 Proc. Fourth Eur. Conf.*, pp. 1–4, 2010.
- 1.19. J. Roh, Y. Chi, and T. J. Kang, "Wearable textile antennas," [Online Accessed: 04-April-2016]. Available from: <http://dx.doi.org/10.1080/17543266.2010.521194>
- 1.20. C. Hertleer, H. Rogier, L. Vallozzi and L. Van Langenhove, "A textile antenna for off-body communication integrated into protective clothing for firefighters," *IEEE Trans. Antennas Propag.*, 57(4), pp. 919–925, 2009.
- 1.21. J. DicCbshfsE, M.K. Abd Rahim, N.A. Samsuri, H.A.M. Salim and M.F. Ali, "Embroidered Fully Textile Wearable Antenna for Medical Monitoring Applications," *Prog. Electromagn. Res.*, 117, pp. 321–337, 2011.

- 1.22. P.S. Hall, Y.I. Nechayev, C.C. Constantinou, Y. Hao, A. Alomainy, R. Dubrovka and C.G. Parini, "Antennas and propagation for on-body communication systems," IEEE Antennas Propagation Magazine, 49(3), pp. 41–58, 2007.
- 1.23. M. Klemm, I. Locher and G.Troster "A novel circularly polarized textile antenna for wearable applications," 7th European Conference on Wireless Technology, pp. 285-288, 2004.
- 1.24. M. Tanaka and J. Jang, "Wearable microstrip antenna," IEEE Antennas and Propagation Society International Symposium, Columbus, Ohio, USA, 2, pp. 704 - 707, 2003.
- 1.25. E. E. Altshuler and D. S. Linden, "Wire-Antenna Designs Using Genetic Algorithms," IEEE Antennas Propagation Magazine, 39(2), pp. 33–43, 1997.
- 1.26. G. A. Casula, G. Mazzarella, and N. Sirena, "Genetic programming design of wire antennas," in IEEE Antennas and Propagation Society, AP-S International Symposium (Digest), 2009.
- 1.27. Y. Yang, S. Zeng, H. Long, Z. Yan, D. Yu and L. Kang, L, "Automated Wire Antennas Design using Dynamic Dominance Evolutionary Algorithm," NASA/ESA Conference on Adaptive Hardware and Systems, pp. 257–262, 2009.
- 1.28. D. S. Linden and E. E. Altshuler, "Evolving Wire Antennas Using Genetic Algorithms: A Review," In: 1st NASA Workshop on evolvable hardware, pp. 225–232. IEEE Computer Society, 1999.
- 1.29. E.E. Altshuler, "Electrically small self-resonant wire antennas optimized using a genetic algorithm," IEEE Transactions on Antennas and Propagation, 50(3), pp.297-300, 2002.

## **Chapter 2**

### **Textile Wearable Antennas**

#### **2.1. Introduction**

An antenna is defined by (IEEE standard definition 145-1983) as a means of radiating or receiving radio waves. In addition, the antenna is the transitional structure between free-space and a guiding devices or transmission lines which may take the form of a coaxial cable, microstrip or waveguide. The guiding device transports electromagnetic energy from the transmitting source to the antenna or from the antenna to the receiver [2.1].

Since F. Braun proposed the first wire antenna in 1898, different types of wire antennas have emerged such as dipole, monopole over a ground plane, rhombic, Beverage, Yagi, log periodic, helix and spiral antennas. In late 1920 Prof Yagi and his student S. Uda designed the series of parallel wires where one element is driven, one element is behind the driven element and is referred to as the reflector, other elements are the directors [2.2]. These antennas have been applied in communication, radar and remote sensing systems. The earlier designs were undertaken using Maxwell's equations to formulate an equation for current distribution of each part of the antenna, and the electromagnetic properties of the antenna are then evaluated. Antenna structures that are complex or simulated with a computer program to closely approximate the designs [2.3].

Antennas are amongst the most essential components in any wireless system, as they transform a signal that flows through wires into an electromagnetic wave that propagates through free space. A good design of antenna improves the overall system performance [2.1]. Antenna design is performed either empirically or via simulator using a numerical method. These are broadly classified into those based on the integral or differential form of Maxwell's equations. The former typically produce frequency domain solution and the latter time domain. Once the antenna properties are known the parameters are optimized using guides such as intuition, experience, simplified equations or empirical studies. An alternative is to use an optimisation method such as a genetic algorithm combined with electromagnetic simulation. Typically, there are several parameters such as a dimension, making it difficult to do an exhaustive search for the best solution.



## 2.2. Desirable properties of an antenna.

### 2.2.1. Radiation Pattern, Antenna Efficiency, Directivity, and Gain

The Radiation pattern is a graphical representation of far-field region as a function of the spherical directional angles  $\theta, \phi$ . The parameters plotted are amplitude, polarisation and directivity.

Radiation Efficiency ( $\eta_r$ ) is the total power radiated ( $P_r$ ) by the antenna to the net power accepted an antenna from the transmitting source. The power dissipated in the form of heat in the antenna is called the ( $P_l$ ) [2.1, 2.4].

$$\eta_r = \frac{P_r}{P_r + P_l} = \frac{R_r}{R_r + R_l} \quad (2.1)$$

where  $R_r$  is the radiation resistance,  $R_l$  is loss resistance.

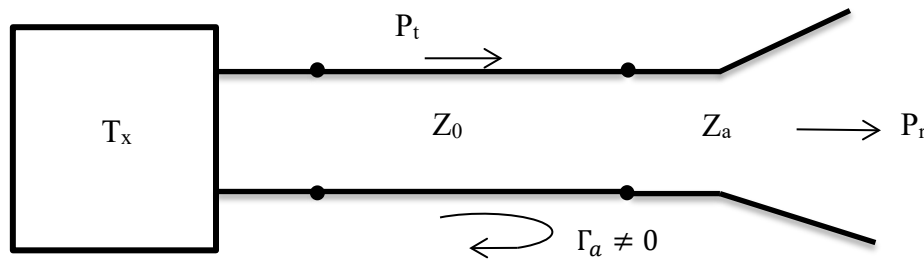


Figure 2.1 Antenna system

The antenna Efficiency ( $\eta_a$ ) take into account the mismatch at the antenna terminals and

$\eta_a \leq \eta_r$  in all cases.

$$\eta_a = \frac{P_r}{P_a} = \frac{P_r}{(1 - |\Gamma_a|^2)P_r} \quad (2.2)$$

$P_a$  includes dielectric losses, conduction loss and reflection (mismatch) loss,  $(1 - |\Gamma_a|^2)$  is the reflection (mismatch) efficiency at antenna,  $\Gamma_a$  is the reflection coefficient at the antenna ( $\Gamma_a = (Z_{in} - Z_0)/(Z_{in} + Z_0)$  where  $Z_{in}$  = antenna input impedance and  $Z_0$  = characteristic impedance of the transmission line).

Antenna Directivity is the intensity function in a given direction from the antenna to the average value of radiation intensity in all direction.

$$D(\theta, \phi) = \frac{U(\theta, \phi)}{U_0} = \frac{4\pi U(\theta, \phi)}{P_r} = \frac{\text{radiation intensity of antenna}}{\text{radiation intensity average over all direction}} \quad (2.3)$$

Where  $U(\theta, \phi)$  is the radiation intensity in the direction  $\theta, \phi$  and  $P_r$  is the radiated power.

Antenna Gain (G) of an antenna is ratio of the intensity in a direction to radiation intensity over power accepted for antenna isotopically radiated. It is expressed as

$$G = 4\pi \frac{\text{radiation intensity}}{\text{total input (accepted) power}} = \frac{U(\theta, \phi)}{U_a} = \frac{4\pi U(\theta, \phi)}{P_a} \quad (2.4)$$

Where  $P_a$  is the accepted input power to the antenna.

## 2.3. Antenna measurements (Reflection coefficient and Radiation pattern in anechoic chamber)

### 2.3.1. Reflection coefficient

The reflection coefficient ( $\Gamma$ ) is the ratio of the electrical field strength E of the reflected wave over the incident travelling wave at an interface port.  $S_{11}$  of an antenna is a measure of the reflection on the circuit side of the antenna. The reflection coefficient gives the operating bandwidth of the antenna. Antenna bandwidth is the frequency band over which the magnitude of the reflection coefficient is below  $-10$  dB.

$$\Gamma = \frac{\text{Electrical field strength E of reflected wave}}{\text{Electrical field strength E of incident travelling wave}} \quad (2.5)$$

### 2.3.2. Radiation pattern in anechoic chamber

The radiation pattern is an antenna characteristic measured using far field or near field techniques. A rectangular anechoic chamber is typically used to measure the radiation pattern and far-field gain of antenna under test (AUT). An anechoic chamber is a controlled environment free of unwanted reflections and designed to minimise electromagnetic interference. It operates in certain range of frequency. The concept of their design is based on geometrical optics techniques which intend to reduce or to minimise specular reflections [2.7]. Chamber wall, floor and ceiling are shield with RF absorbing material, specular reflections can occur from their surfaces in the case of large angles of incident [2.7].

The radiation pattern is a full 3-D measurement. Often radiation patterns are plotted over two principle plane cuts. As shown in Fig. 2.2, these are the  $xy$  plane (azimuth plane) and the  $xz$  plane (the elevation plane). Measurement at the chamber is performed by rolling the phi axis while the theta stepping per “Great Circle cut System.” The theta axis is disc spinner or azimuth control. Phi axis controls the elevation or the roll positioner. Subsequent interpretation of the radiation pattern and two planes will be based on the configuration of (Fig.2.2 and Fig. 2.3).

The positional axis measurement for the anechoic chamber used is shown in Figure 2.3. This guide is used for understanding the radiation pattern from the chamber setting. A typical software setup for a positioning movement involves the following steps (1) Initialise positioner (2) Positioner control (3) Analyser control (4) Antenna gain calibration file and (5) Measure. Two polarisations are used in the chamber, the reference antenna (horn antenna) is vertical ( $E_\phi$ ) and when the horn antenna is horizontal, ( $E_\theta$ ). A reference horn antenna is used because its radiation patterns have minimum side lobe levels [2.7].

Taper anechoic chamber are designed in the form of a pyramidal horn that lights from a small illuminating end to a larger rectangular section. Different transitional shape of the tapered chamber has evolved across the years from square to cone and octagonal transformed into cylindrical launch sections [2.8]. The design principle could be explained numerically from the ray tracing techniques. There a little difference in phase between the direct path and reflected ray at any test point within the tapered chamber. This chamber is used for low frequencies because the antennas are physically very large.

Tapered chamber experiences two effects: deviation from the  $1/R^2$  dependence and a decrease or increase in signal when compared with free space transmission. These two effects limit the performance of tapered chamber when used within the indoor range. At low frequencies where low directivity antenna is used, there is significant variation between the transmission loss and free space loss [2.8]. The transmitting antenna is usually placed at the small distance from the apex. The tapered chamber experiences multipath effects compared to the rectangular anechoic chamber. The change in phase difference between the direct and the reflected rays across the chamber is small as smoother amplitude illumination is obtained compared to rectangular chamber [2.9].

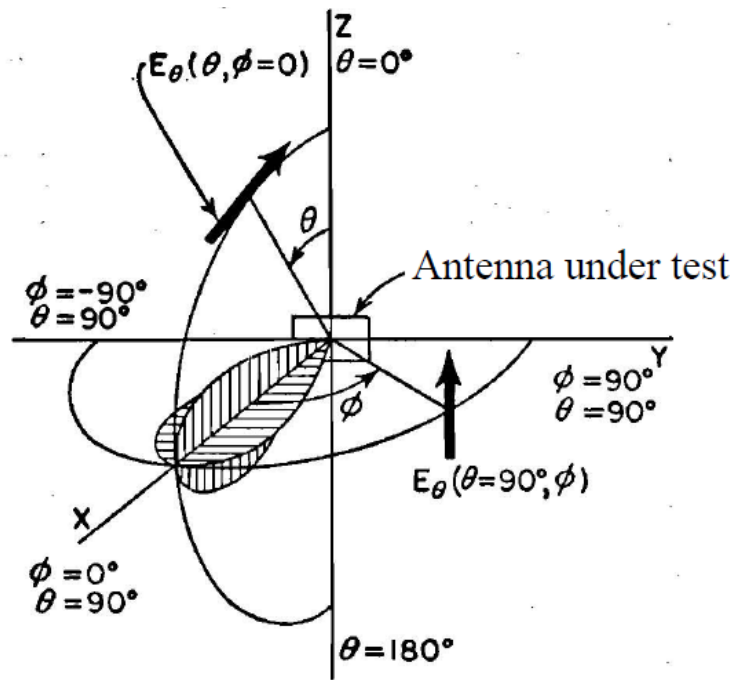


Figure 2.2 Standard spherical coordinate system used in antenna measurements [2.7].

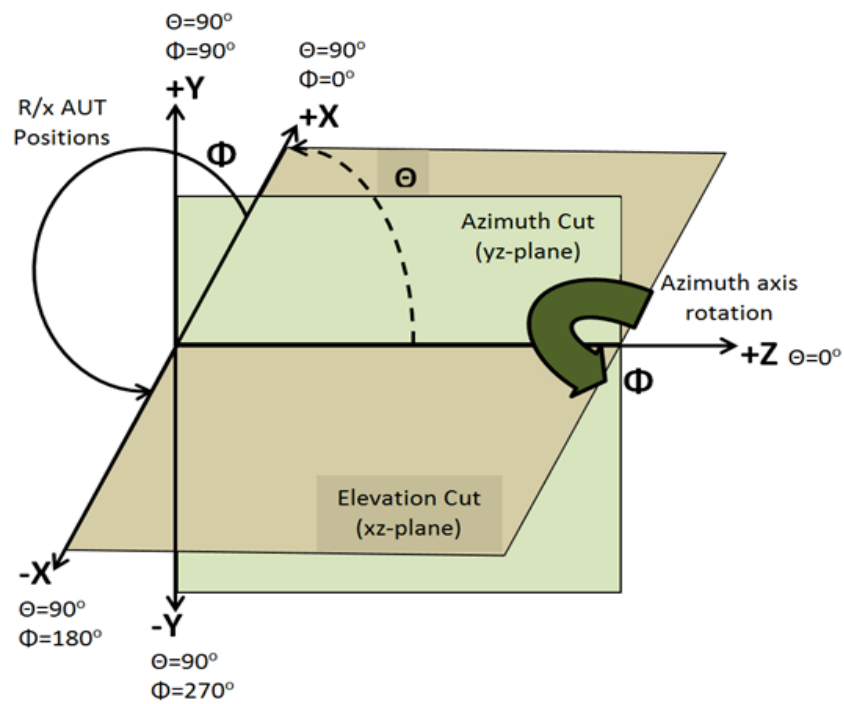


Figure 2.3 Positional axis for chamber measurements

## 2.4. Wearable Antennas

Wearable antennas are designed and meant to be part of clothing for application on the human body or animal. Wearables have attracted industry interest due their applications and increasing demands in the wireless world. Wearables are devices worn on the body that use advanced circuitry and have independent processing potential. Wearables are part of daily functionalities for data analysis and communication between smartphone and body. These devices make use of a combination of sensors, machine learning and data analysis to provide information to consumer's body. The commercial market has various types of wearables devices including fitness trackers, smartwatches, smart glasses wearable cameras, gesture devices, location trackers, body sensors and smart clothing. The devices are used for various applications ranging from healthcare to sporting notifications [2.10-2.18].

Wearables offer portability during operation by allowing hands-free or hands-limited use; attract the user attention even when not in use. Numerous ranges of form factors have been evolved from wearable computers since the early 1990s. The early form factor of wearable computers includes, belt mounted configuration called Vumen, Vest and jacket configuration to blend with fabric and IBM Smart Watch [2.10]. Figure 2.4 (a) Half keyboard. Edgar Matias and his colleagues developed this system in 1994. Systems using the half-keyboard approach are available from the Matias Corporation ([www.matias.ca](http://www.matias.ca)) and Fig.2.4 (b) Wearable system that overlays computer information on the wearer's view were introduced by the University of South Australia in 2003.

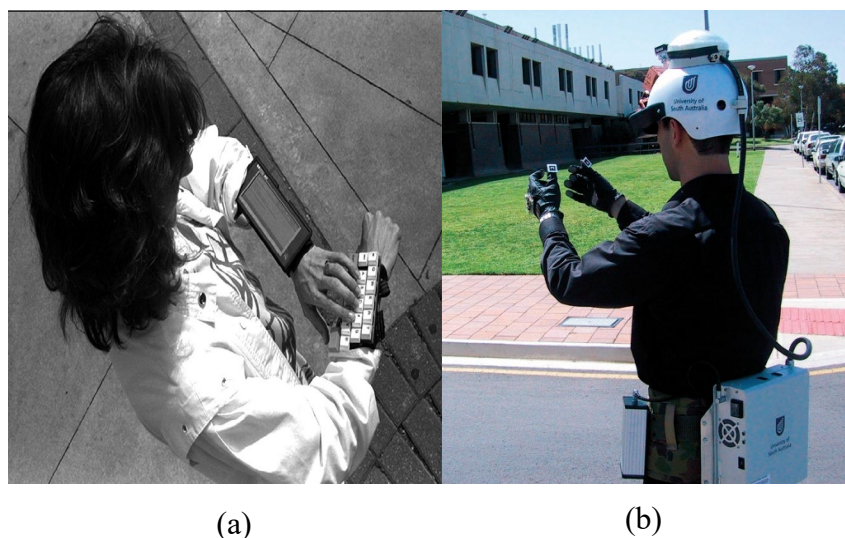


Figure 2.4 Examples of early wearable applications [2.10]

A textile-based circuitry was constructed using e-broidery (electronic embroidery) for creating computation active textile. The examples of these applications include, an electrical dress and a musical jacket using an e-broidered keypad and fabric buses. A musical jacket was turned into a wearable musical instrument and the wearer plays notes, chords and rhythms. Figure 2.5 (a) is the Musical Jacket, comprising a fabric keypad on one side, a MIDI synthesizer “boat” on the other side, speakers behind speaker grills in the pockets, and fabric buses visible inside the jacket. Fig.2.5 (b) is a composite image of both sides of the circuit board attached to the back of the fabric keypad [2.11].

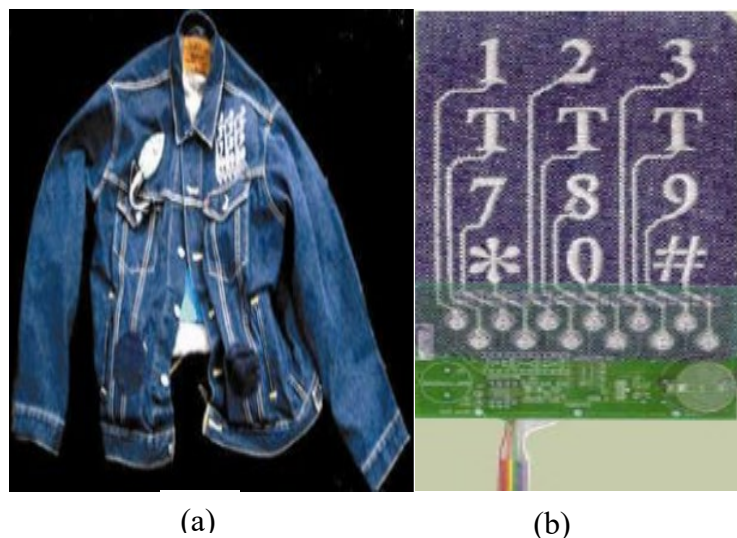


Figure 2.5. Functional chording keyboard embroidered into a jacket [2.11]

Textile antenna designs have received great attention from many researchers using flexible fabrics and conductive materials for various applications (see Table 2.1). For the design of wearable textile antenna three aspects are important for an improved performance: evaluation of the dielectric constant of fabric materials, the conductivity of the conductive threads and methods for optimising the fabrication process.

### 2.4.1. Antennas types for wearable applications

Antenna designs can be classified into two types which include conventional solid antennas and flexible antennas. The conventional antennas are based on rigid substrates. Flexible antennas may be of the form of wearable or textile antenna. The wearables textile antennas include planar dipole [2.12-2.13], monopole [2.14], planar inverted-F (PIFAs) [2.15] and Microstrip patch antennas [2.16]. These antennas appear in most literature for the design of wearable and textile antennas. Most of the research work on wearable antennas are centred on

patch antennas (rectangular microstrip antenna) because their advantages of miniaturisation, ease of integration and good radiation patterns.

Wearable antennas must be biocompatible and compliant with health and safety requirements. Some basic antennas are of textile a patch antenna that is made of three conductive layers: upper and lower conductive layers, a middle of dielectric substrate. The mesh ground plane has low sheet resistivity ( $\leq 1\Omega/\text{square}$ ), same resistivity over the fabric area, flexibility and stretchability [2.16].

Most of the research for fabric antenna is carried out using microstrip antennas due to the advantages of miniaturization, ease of integration and good radiation pattern. Microstrip antennas seem to find more application in wearable or textile antennas than wire or whip antennas because of their radiation pattern. Conventional wire antennas are more efficient than patches. When antennas are placed close to the human body, there is a reduction in radiation efficiency of the antennas radio link failure [2.17].

Wearable antennas designed and constructed from non-fibrous materials such in the inverted-F antenna in which U-shaped slot etched to form for dual band operation were made of non fibrous material [2.15]. The dual band antenna was developed for GSM1900 and WLAN application using fleece fabric material. Conductive material is copper tape while the antenna substrate may be in fabric. These conducting elements give the antenna a flexible form, low profile and low weight [2.18].

In [2.13] a comparison was made between the silver fabric and embroidered dipole textile antenna to determine their performance using different conductors. Seven different dipole antenna structures were studied. The embroidered antennas were achieved through two strategies, single layer or dual layer using conductive thread. Their experiment suggested that using the double layer embroidery gives a gain of 1.5 dB over the single layer. Alignment of the stitched lines was along direction of the current flow in the structure.

In [2.19] a high conductive metalized Nylon fabric-Dell Nora is used as the conductor for fabrication of a textile UWB antenna for WLANs. The dielectric substrate, an acrylic fabric of 0.5 mm thickness is used. The substrate has the advantages of being light with good drapability and stable in height. A design of a Leaf-shaped dual band textile antenna was reported [2.20] for 1.8 GHz and 2.6 GHz. A denim substrate of  $\epsilon_r$  of 1.67 and loss tangent ( $\tan\delta$ ) = 0.025 was used since the material is robust, flexible and lightweight. Two

different conductive materials were used for this design: Copper tape with a thickness of 0.035 mm and conductivity ( $\sigma$ ) of  $5.8 \times 10^7 \text{ S/m}$  and ShieldIT fabric with thickness of 0.17 mm and  $\sigma = 6.5 \times 10^4 \text{ S/m}$ . The Zip based monopole antenna design at 2.5GHz used felt fabric of relative dielectric permittivity ( $\epsilon_r$ ) of 1.22 and loss tangent ( $\tan\delta$ ) of 0.016. The thickness of the dielectric substrate was 2 mm. The radiating element of this antenna the Shieldit electrotexile [3.36]. Using low loss tangent and relative permittivity materials tends to reduce the surface wave loss and gives an improved bandwidth for textile antennas [2.16].

The feeding method is important for determining characteristics of the textile antennas specifically the impedance bandwidth. The stitched ground patch antennas were fed using a microstrip line inset from the radiating edge. The input impedance of the patch antenna depends on the connection between the feedline and patch, and also on the thickness and permittivity of the substrate. To attach the connector to the antenna, two ways were used: soldering the embroidered circuit under low temperature or conductive adhesive layer is used to glue the connector to embroidered circuit. These processes produce good electrical connections and flexibility between the 50 $\Omega$  SMA connector and wire antennas. Feeding the stitched antenna using this method is efficient and comfortable for wearable applications [2.21-2.23].



Table 2.1 Review of a selection of wearable antenna found in the literature

| Antenna                      | Conductive layers  | Dielectric layer  | Antenna gain (dBi)  | Frequency Band              | Antenna Efficiency (%)   |
|------------------------------|--|---|---|-----------------------------|--|
| Patch [2.24]                 | embroidered using silver coated Amberstrand yarn   | Taconic RF – 45<br>$\epsilon_r = 4.5$ and $\tan\delta = 0.0037$   | -   | 2GHz                        | 31-53  |
| Patch [2.25]                 | silver-plated copper threads, Cordura® fibres yarns woven fabric, conductive electro textile | Rogers Duroid® 5880<br>$\epsilon_r = 2.2$ , $\tan\delta = 0.0009$<br>polyester fabric $\epsilon_r = 1.9$ , $\tan\delta = 0.0045$                          | 1. Copper patch antenna=7.42<br>2.E-textile patch (metal) =6.59 dB<br>3.E-textile patch Antenna (fabric)=7.09 | 2.44 GHz, WLAN applications | 1.copper patch antenna as reference measured 95%<br>2. E-textile patch (metal) 78.5%<br>3. E-textile patch Antenna (fabric)=88.1 % |
| Patch [2.25]                 | Flectron (patch and ground plane)  | Substrate material: protective closed-cell foam, $\epsilon_r = 1.12$<br>$\tan\delta = 0.003$  | 8.4   | 1.4-1.8 GHz                 |  |
| Patch [2.26]                 | Materials used for ground plane and patch: Copper  | Insulating fabric material employed: Polyester and polyester combined cotton curtain cotton fabric<br>$\epsilon_r=1.44-1.51$ , $\tan\delta = 0.01 - 0.02$ | 7.2-9.6   | 2.-3GHz                     | 61-70 % Measured   |
| Textile Patch [2.27]         | 1.Copper foil<br>2.Knitted Fabric  | a permittivity $\epsilon_r=1.45 \pm 0.02$ for the felt<br>$\tan\delta = 0.02$ for felt<br>$\epsilon_r=1.14 \pm 0.025$ for spacer fabric                   | 9.0<br>5.5  | 2-3GHz                      | 99.0%<br>44.9%   |
| E-Fibre Based antenna [2.28] | Flexible silver coated Amberstrand fibers,   | Polydimethylsiloxane (PDMS) substrate<br>$\epsilon_r=3.0$ and $\tan\delta = 0.02$   | 5.6 dB Planar surface<br>3.0 dB Curvilinear surface   | 2.2 GHz                     |  |
| Textile antenna [2.29]       | Conductive yarn  | Fleece $\epsilon_r = 1.17$  | 5.0   | 2.4GHz<br>1.5-3.5 GHz       |  |

### **2.4.2. Textiles wearable antennas for on-body applications.**

Textile antenna design for wearability focuses on two aspects; the shape of the wearable and the active relationship or position with human form. Textile antennas are designed to work at different frequency bands for various applications and placed on different locations on the human body. The implementation of a covert wire antenna in textile introduces some additional constraints. Compared to conventional antennas, the issue of the space to attach the antenna is fixed and the antenna must be hidden. In the work [2.30] multiple arrays around the body give omnidirectional radiation pattern.

Antennas have been stitched on a fabric or integrated into personal accessory (such as shoes, glasses, buttons, helmets and vests) [2.31-2.33]. High impedance surface (HIS) for wearable dipole antennas designed to operate at frequencies 0.1 – 1.5 Hz and used in body armour vest [2.32]. The armour has a relative substrate permittivity ( $\epsilon_r = 2$ ) and conducting layers. In [2.33], where two wearable antenna systems were integrated into a floating life jacket and connected to personal Locator Beacons (PLBs) of the Cospas-Sarsat systems. The antennas operate at 406 MHz installed in two possible placements; in the front/ chest part and head/neck of a life jacket.

An antenna placed on the body experiences de-tuning which cause the RF power radiated from the antenna to be reduced. These effects could be reduced by isolating the antenna from the human body using separation and selective shielding as shown in [2.33]. The separation can be achieved using EBG surfaces. Impedance bandwidth can be increased for any proposed antennas. These antennas have been placed in various positions on the body, front, back and shoulder of garments.

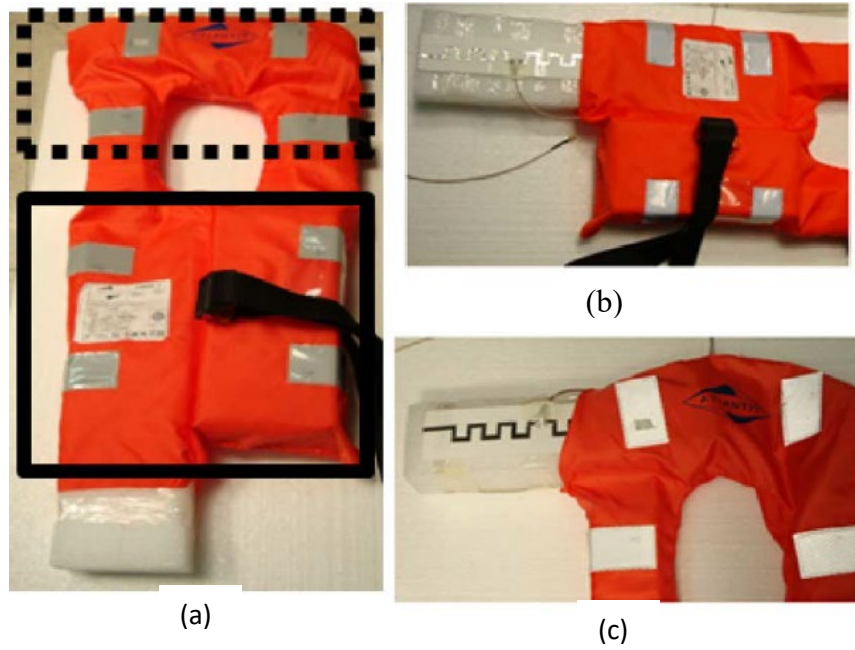


Figure 2.6 Commercial floating lifejacket: (a) front view, (b)-(c) two possible placements for the meandered dipole antennas developed in [2.33], to enlarge antenna coverage of the personal locator beacon for satellite-based search-and-rescue systems at 406MHz.

Embroidered radio frequency identification (RFID) antennas with a wireless link were placed on human arm for on-body measurement. The measurement was done considering by separation between antenna and arm to be 0.7 mm. When antennas are placed on the body, the effects on the body is prominent if the antenna to body isolation is small and absorption dominates. This leads to reduction of efficiency. When the between the body and the antenna is increased, the body could be modelled as a reflector [2.34].

Wire antennas and planar antenna printed on substrate experiences change in wavelength and change in the resonance frequency when operating in a stand-alone mode. Antenna design with ground or reflectors (microstrip patch antenna) experience less effect when placed on the human body. Figure 2.7 shows a textile patch antenna placed on the human chest and conformal on the human arm. The effect of changing positions on body, which degrade the performance by detuning the frequency and leading to pattern deformation at resonance [2.35].



Figure 2.7 Fabricated textile patch antenna placed conformal on the human arm for experimental analysis of the body effect on antenna performance [2.36]

In the work [2.37] where eight element e-textile antenna array, shown in Fig. 2.8(a), operate at 2.45 Hz . The patch antenna is linearly polarised with a conductive fabric. A Nomex (Shieldex Trading, Palmyra, NY) felt fabric ( $\epsilon_r = 1.18$ ,  $\tan\delta = 0.004$ ) is attach using conductive threads. These antennas are made of e-textiles and integrated into astronaut systems. The Nora-Dell conductor textile ( $0.03 \Omega/\text{sq}$ ) is used for several different antennas. Figure 2.8 (b) shows six complementary -8 antenna elements is placed periphery of an astronaut suit. Pattern diversity is used and implemented by rotating antenna element through  $90^\circ$  increase polarisation.

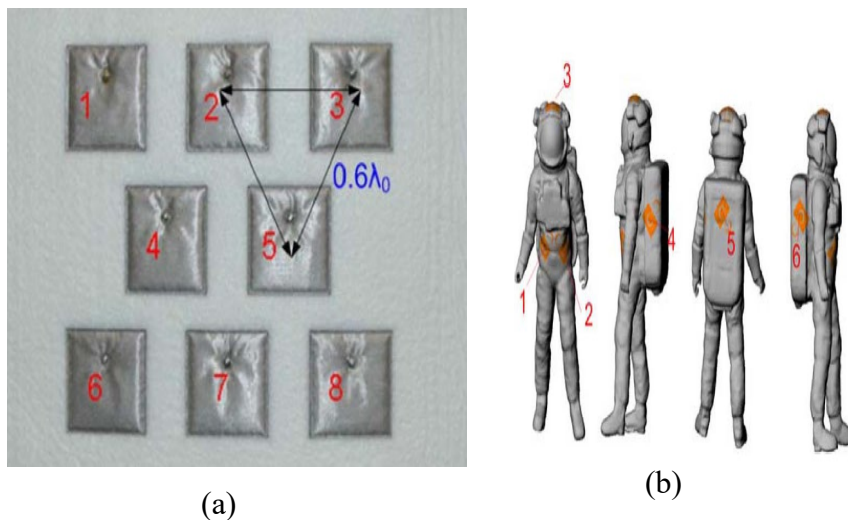


Figure 2.8 Six e-textile complementary-8 antennas placement on astronaut suit [2.37]

### 2.4.3. Antenna properties on Flat-body Phantom

When the EM field penetrates a lossy dielectric power is dissipated. The EM fields decay in the material and there is a heating effect. Usually this is an extremely small effect where temperature rise is insignificant. However even at nonthermal levels caution is usually exercised and SAR is quantified and limited. Specific Absorption Rate (SAR) is a measure of the rate at which energy is absorbed in a unit mass of tissue when exposed to an EM field [2.38-2.39]. The SAR limit for Europe standard is set maximum level of 2 W/kg for any 10 g of tissue [2.40]. The International Commission on Non-Ionizing Radiation Protection (ICNIRP) guideline defined SAR limit for occupational exposure and general public exposure for frequency range 10 MHz-10 GHz as 0.4 W/kg and 0.08 W/kg (whole-body average SAR) respectively [2.41]. SAR is defined as [2.38]:

$$SAR = \frac{\sigma|E|^2}{2\rho} \quad (2.6)$$

where  $\sigma$  is the conductivity of human tissue ( $S/m$ ),  $E$  is the electric field strength ( $V/m$ ),  $\rho$  is the density of the human tissue ( $kg/m^3$ ). The value of SAR varies from location to location since it depends on tissue density, electric field strength and conductivity. The properties of the human tissues in Table 2.2 and Table 2.3 were used to simulate the interaction with human model and antenna radiation in CST Microwave Studio at 900 MHz and 2.45 GHz.

Table 2.2 Dielectric properties of human body tissues at 900MHz [2.39]

| Tissue | Permittivity<br>$\epsilon_r$ | Conductivity<br>(S/m) | Density<br>(kg/m <sup>3</sup> ) |
|--------|------------------------------|-----------------------|---------------------------------|
| Skin   | 39.59                        | 0.693                 | 1126                            |
| Muscle | 60.73                        | 1.198                 | 1059                            |
| Fat    | 4.786                        | 0.053                 | 943                             |
| Bone   | 12.61                        | 0.172                 | 1850                            |

Table 2.3 Dielectric properties of human body tissues [2.40] at 2.45GHz

| Tissue | Permittivity<br>$\epsilon_r$ | Conductivity<br>(S/m) | Loss<br>Tangent | Density<br>(kg/m <sup>3</sup> ) |
|--------|------------------------------|-----------------------|-----------------|---------------------------------|
| Skin   | 31.29                        | 5.0138                | 0.2835          | 1100                            |
| Fat    | 5.28                         | 0.1                   | 0.19382         | 1100                            |
| Muscle | 52.79                        | 1.705                 | 0.24191         | 1060                            |
| Bone   | 12.661                       | 3.8591                | 0.25244         | 1850                            |

## 2.5. Challenges of wearable antennas

As well as absorbing energy radiated from the wearable antennas worn on the lossy human body tissue experience frequency response changes and radiation efficiency degradation. In order to reduce these, antennas are simulated using human phantom and measured on a real human body or a phantom. The measurement and simulation consider  $S_{11}$ , near field, far field etc. Measurement could be carried out in an anechoic chamber or in a real environment (outdoor or indoor). Measurement is of practical since applications rely on measurement results rather than pure simulations [2.42].

## 2.6. Methods of Implementing stitched antennas

Usually textile antennas take the form of planar structures that conform to the human body or follow underlying shape of the garment (e.g. a hat). Several material properties influence the working of a textile antennas. Permittivity and the thickness of the substrate determine the bandwidth and efficiency of a planar microstrip antenna. The use of textiles in antenna design requires characterisation of their properties. The accurate characterisations of textile substrate properties are fundamental before the antenna design. The conductivity of the ground plane and of the patch is an essential critical factor in determining the efficiency of the antenna [2.30]. Over the years, many techniques and materials have been employed in producing textile antennas. Textile antennas can be fabricated by several methods, but embroidery, weaving and printing are examined in this section.

### 2.6.1 Embroidery Techniques

A digital embroidery machines at Loughborough University is shown in Fig. 2.9. Embroidery was chosen as the method for fabrication of stitched antennas because digital embroidery is fast and flexible in pattern generation and the integration of high frequency systems into clothing [2.43]. Stitch antennas do not require glue or cutting or lamination processes only stitching the design onto fabric. Antenna designs are converted into a format compatible with an embroidery machine for production. In embroidery patterns are superimposed onto an existing fabric and a stitch design is created. This technology provides high speed, ease of manufacturing, accurate and easily modified stitch antennas. Antennas are automatically integrated into fabric through this process which reduces cost of production. Conductive threads are expensive. A sample quantity of Amberstrand silver yarn costs £1 per metre [2.43]. Embroidery uses specialist conducting thread that have a polymer core and coated with a silver / nickel.

A number of authors have addressed the issue of fabricating textile antennas using embroidery [2.12, 2.17, 2.24, and 2.43-2.48]. Embroidery was used to incorporate RF functions into garments and clothes. The more closely the stitch space the better the electrical connectivity between neighbouring stitches and the better the antenna performance.



Figure 2.9 Brother Pr1000e embroidery machine at Loughborough University

Figure 2.10(b) is a sketch of the lock stitch formation comprising; conductive thread (1) and non-conductive thread (2). To create stitch pattern on a substrate material two threads are required. The stitched antennas in this work were embroidered using textile conductive thread (Liberator or Amberstrand) on denim or felt substrate. Conductive thread was set up in the bobbin of the embroidery machine; see Fig.2.10 (b) in the blue in this study as in Fig.2.10 (a) because of tension on the conductive thread. Using the conductive thread in the bobbin allows the thread to be straight. The upper thread was a non-conductive polyester yarn that goes into the substrate material during embroidery. The principle used in creating a lock stitched pattern employed by embroidery is the needle containing the upper thread is sunk through the fabric material into the lower section of the machine where the conductive thread is placed in the bobbin. A hanger hooks onto the upper thread just after the thread goes into the needle. A rotating mechanism loops the upper thread around the bobbin and then a feed dog pulls the extra upper thread available around the bobbin back to the top of the fabric. The conductive thread is then pulled along the bottom of the substrate forming a lock stitch. In the process of embroidery, small portion of oil was applied to Liberator thread and Amberstrand so that the threads would not unravel or break during the stitching process. This makes the thread filament stick together and reducing the unravel loss. Single-layer embroidery was used to realise higher conductive textile surfaces giving a lower DC resistance [2.43-2.44]. In all the fabrications of wire antennas, planar wire antennas and microstrip antennas single layer stitching densities were employed.

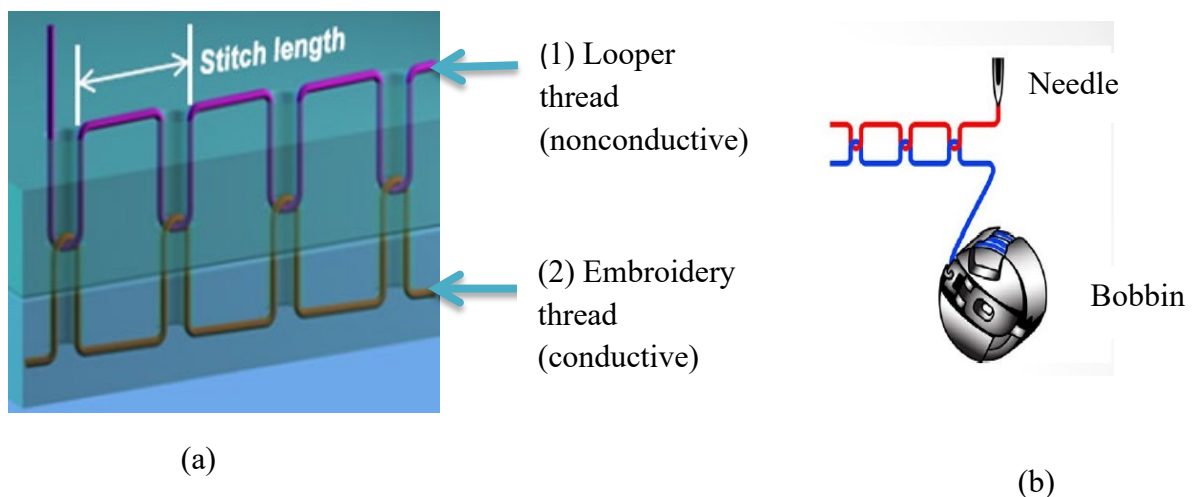


Figure 2.10 (a) Sketch of the lock stitches and (b) Bobbin with top thread and looper thread (from [2.45])



### 2.6.2. Weaving and Knitting

In weaving two different sets of threads or yarn are used called warp (longitudinal) and weft (lateral). The two yarns are interlaced at right angles to form a fabric [2.49]. The warp yarns are chucked and run length wise through the machine. The weft yarn is woven into the warp yarn. The yarn could be arranged into different formations for examples either as conductive thread integrated into fabric in the warp direction or flexible plastic fibre with integrated electronic functionality and contact pads into a fabric material in the weft direction as in Fig. 2.11. This gives an example of an application of weaving. The conductive thread and contact pads on the e-fibre are connected. Embroidery is more flexible when applied to fabric sheet compared with weaving when changing designs. Weaving is suitable for large and customised conductive area like wearable/Textile Frequency Selective Surface (FSS). The wider fibres correspond to plastic fibres with integrated electronics. Four warp yarns are replaced with conductive threads and the black dots symbolize contacts between conductive threads and plastic fibre. Sensor-ICs or more general electronic devices are distributed randomly (black rectangles).

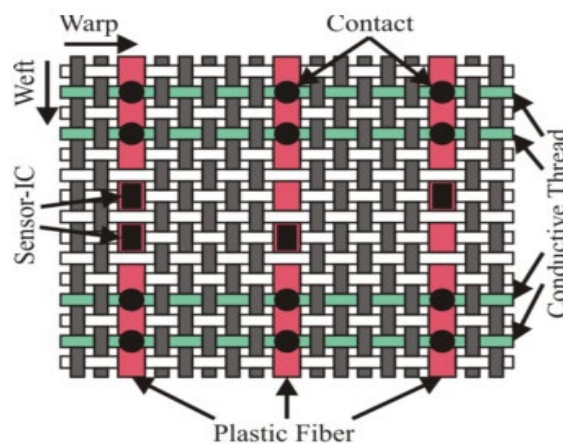


Figure 2.11 Schematic of a woven textile with warp yarns in white and weft yarns in dark grey [2.49].

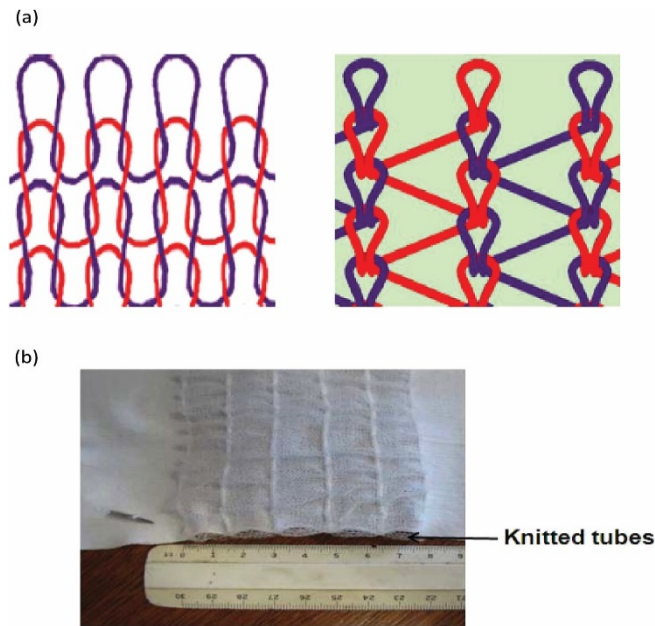


Figure 2.12 (a) Weft knitted (on left) and warp knitted (on right). The blue yarns represent a particular row inside the fabric. (b) A fabric with knitted tubes [2.50].

Knitting is the process of using two or more needles to loop yarn into a series of interconnected loops to create a finished garment or fabric. Knitting creates multiple loops of yarn called stitches, in a line or tube as shown in Fig.2.12. Knitting has multiple active stitches on the needle at one time. A knitted fabric consists of several consecutive rows of interlocking loops [2.50]. Knitting is very versatile but does not produce textiles that is of good pattern resolution.

### 2.6.3. Printing a conductive layer fabric

Conductive ink on fabric is achieved through two processes which include Sheet-based inkjets and screen printing. Inkjet printed interactive electronic textiles are produced using conductive inks. These inks when printed on textile or materials create electrically active patterns. It is one of the most suitable ways of introducing conductive materials onto textile substrate. Screen printing is a technique used to impose design on a screen of fine mesh. The mesh is composed of an area coated with an impermeable substance. The ink is forced through the mesh onto printing surface by moving the squeegee across the mesh [2.51]

## 2.7. Fabrication of Conductive threads

### 2.7.1. Conductive fibres

Textile structures that have some degree of conductivity or are used to supply electronic or computation functionality are often referred to as electro-textiles. The functionality may be for the electromagnetic interference shielding or electronic application. A wire drawing process is applied to produce metal fibres. Figure 2.13 (a-d) shows the various drawing steps, called coarse, medium, fine and carding train [2.42].

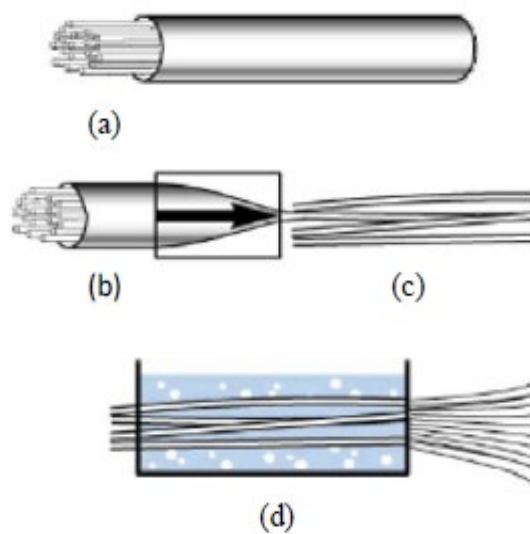


Figure 2.13 (a) Metal coated wire combined in iron tube; (b) Several diameter reductions of tube; (c) Bundling of tubes; (d) Leaching, realizing fibres [2.42]

There are three known techniques for creating conductive threads [2.42]. Filling of fibre with carbon or metal particles, coating of fibres with conductive polymers or metal or the use of fibres that are completely made of conductive materials. Conductive threads are made from single or multiple strands of conductive and non-conductive fibres. Figure 2.14 (a-d) shows a multifilament conductive thread. The multifilament of Fig.2.14 (a) is formed by twisting many thin elastic silver-plated nylon fibres together. Figure 2.14(b) is made of 60 copper fibres and diameter of each of the fibre is  $40\mu\text{m}$ . The composite threads in Fig 2.14(c and d) are formed by spinning  $40\mu\text{m}$  silver plated copper fibres around a nonconductive core, which is composed of multiple nonconductive fibres. Figure 2.14 (e) is monofilament conductive thread. Each of the conductive threads has different electrical properties. Their wearability and reliability characteristics of the conductive thread vary [2.54].

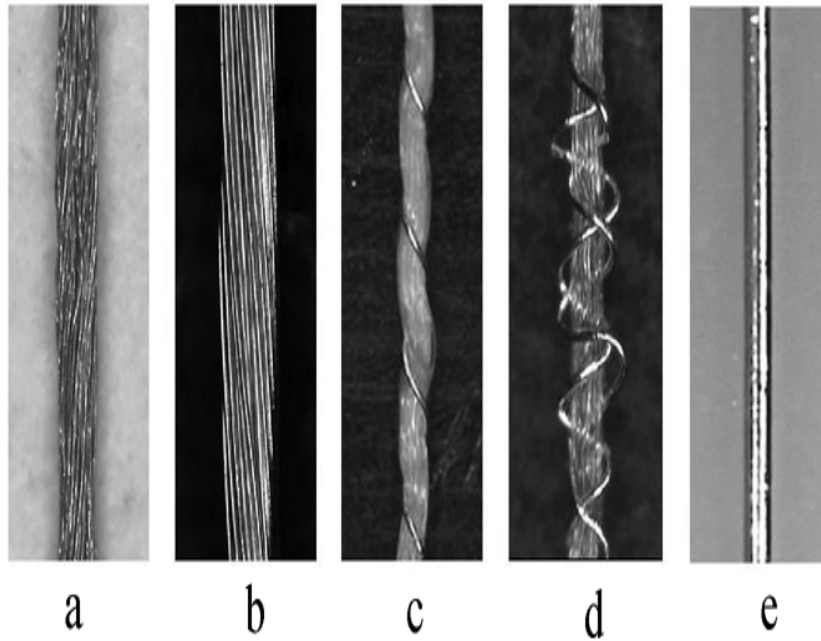
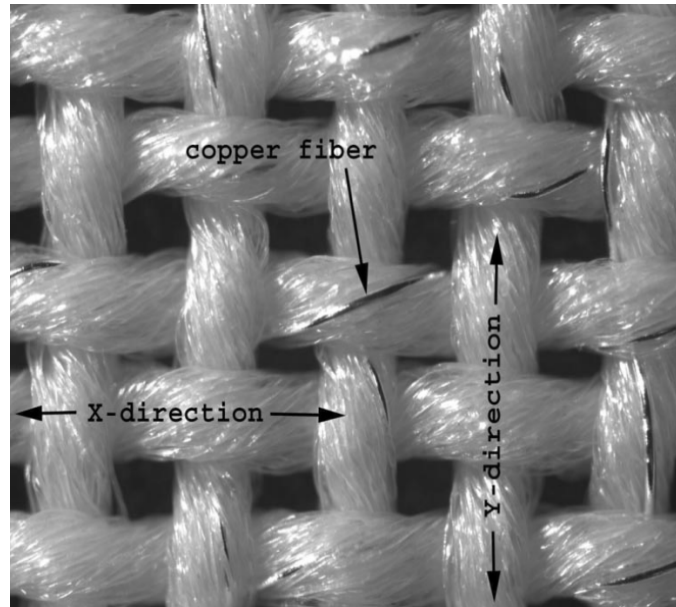


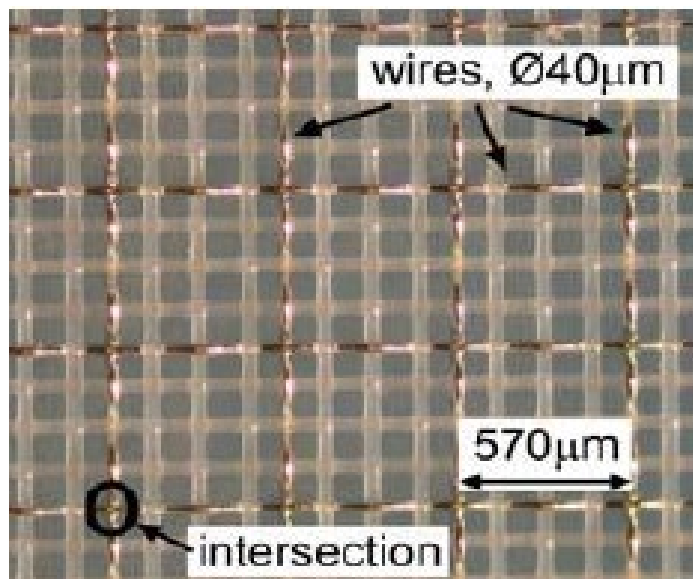
Figure 2.14 Various conductive threads [2.54]

### 2.7.2. Conductive Fabrics

Conductive fabrics may be in the form of fibre, yarn or built structure. The conductivity of the conductive fabrics is enabled either after manufacturing or during manufacturing. This process is achieved through coating or conductive threads. Electrically conductive fabric is produced by integrating conductive yarns into a textile structure by the process called weaving and knitting. A plain-woven textile structure was created by twisting polyester yarns with one copper thread [2.41]. Figure 2.15 (a) is standard design and the hybrid fabric is called (PETEX) in Fig.2.15 (b). Single filament yarns (PET) consist of woven polyester with a diameter of  $40\text{ }\mu\text{m}$  and a copper alloy of diameter  $50 \pm 8\text{ }\mu\text{m}$ . The copper wire is coated with an electrical insulation known as polyurethane varnish. The spacing between the nodes is  $570\text{ }\mu\text{m}$  as indicated.



(a)



(b)

Figure 2.15 (a) Standard design of copper yarn twisted with polyester fibres; (b) PETEX (picture from [2.42])

## 2.8 Electrical properties of the conductive thread

The skin effect is the process whereby at high frequency alternating current and magnetic flux penetrate into the surface of wire only to a limited depth. It is explained in terms of inductive reactance as discovered by Maxwell, that the voltage required to force a changing current through a wire increases more than would be expected. At higher frequencies the magnetic fields within the conductor cause current to concentrate on the outer surface of the conductor in a thin skin. The depth of penetration depends on the frequency, properties of the material, its conductivity or resistivity and its permeability [2.52]. For antenna design, the fabric materials are characterised by the surface resistance to show their electrical properties. The conductivity of the fabric  $\sigma$ , surface resistivity  $\rho_s$  and  $t$  thickness of fabric is defined in equation (2.7) [2.53].

$$\sigma = 1/\rho_s \cdot t \quad (2.7)$$

The DC resistance of a uniform wire having a length  $l$  and cross-sectional area  $A$  is given by equation (2.8)

$$R_{dc} = \frac{1}{\sigma} \frac{L}{A} \quad (2.8)$$

where  $R_{dc}$  is the DC value of a given length of thread, the length of wire sample is  $L$ ,  $\sigma$  is conductivity of the metal (S/m). Skin depth  $\delta$  depends on frequency and conductor dimensions of the conductor radius.

$$\delta = \sqrt{2/\omega\mu\sigma} \quad (2.9)$$

$$\mu = \mu_r \cdot \mu_0 \quad (2.10)$$

$\mu_0$  is the permeability of free space equal to  $4\pi \times 10^{-7}$  H/m,  $\mu_r$  is the relative permeability of the material. The high frequency resistance ( $R_{hf}$ ) of uniform current distribution along the length of the wire is given as [2.49]

$$R_{hf} = \frac{L}{P} R_s = \frac{L}{P} \sqrt{\frac{\omega\mu_0}{2\sigma}} \quad (2.11)$$

where  $\omega = 2\pi f$ ,  $f$  is frequency,  $P$  is the perimeter of the cross section of the rod ( $P = 2\pi a$  for a circular wire of radius  $a$ ) and  $R_s$  is the surface resistance of the conductor.

Equation (2.8) and (2.11) are used to analyse a uniform metal rod for uniform current distribution but the conductive thread does not have a uniform metal structure as Liberator-20 and Amberstrand silver 66 are all made of several filaments. The cross-sectional area normal to the current flow direction of metal in single filament of Amberstrand is approximately  $50 \mu\text{m}^2$ . The total cladding for Amberstrand silver 66 in the entire thread is  $66 \times 50 \mu\text{m}^2 = 3300 \mu\text{m}^2$ . The calculated resistivity of the metallisation is given as  $2.2 \times 10^{-8} \Omega\text{m}$ , while the conductivity which is given as  $1/\rho$  is  $4.5 \times 10^7 \text{S/m}$  is small compared to silver with  $\sigma = 6.2 \times 10^7 \text{S/m}$  and is the value of equivalent conductivity of solid conductor of the same overall dimensions [2.43].

## 2.9. Review on Optimisation techniques

Structures of wire antennas may be simple, but antenna design is complex and achieving the design using an analytical approach to get the optimal solution is not always possible. Search spaces for antenna design are highly multimodal and using a numerical approach or trial and error seems to yield poor results. Antenna designs need a starting point close to the global optimum or they could get trapped in a local minimum. This thesis focuses on GA as an optimisation method, the choice of which will be justified later [2.2-2.3].

Genetic algorithms are used to explore the design domain and automatically discover novel antenna designs that can be more effective than would be developed by other means [2.3]. Genetic algorithms are numerical algorithms modelled on the concepts of natural selection and evolution theory, which modifies and optimise results over several generations. GAs operate on a population of potential solutions applying the principal of survival of the fittest to produce better and better approximations to a solution [2.59-2.60].

Wire antennas have been reported for the WLAN multiband operation (in the literature [2.59-2.65]). The desirable frequency band covered is 2.4-2.484 GHz for British Telecom applications, 2.4GHz and 5GHz for Wi-Fi applications, and 2.4 GHz, 5.2 GHz, and 5.8 GHz for WLAN applications (WLAN IEEE802.11 standard) [2.61]. The wire antenna for WLAN applications is designed using the Structure-based Evolutionary Design (SED) where the antenna is analysed with NEC2 during the evolution process. The folded wire antenna was designed to reduce the interaction between the mobile terminal and the human body. This

antenna structure consists of two open loops, one larger loop and smaller loop providing half-wavelength modes for the GSM900 (880-960 MHz) and DCS1800 (1710-1880 MHz) [2.62]. Genetic Algorithms have been successfully applied to crooked-wire antennas, planar wire antennas, zigzag patterns, meander-line and even fractal geometries [2.2-2.3]. Genetic algorithm has been applied to designed and optimized antenna problems like microstrip spiral antenna with 6 and 10 segments [2.62], wire antennas with 4 segments and crooked-wire genetic antenna with 7 segments [2.2] and small wire antennas with 7 segments [2.63-2.64]. In this study the methods of multi-segment wire structure are used similar to the one applied in [2.2-2.3]. This antenna design is achieved through the unique approach of bending/meandering the antennas to reduce the size and give it a compact design [2.2-2.3 and 2.60-2.65].

This thesis differs from other works by developing an automated generic method for optimisation and simulation of linear wire antennas. Using this application, a set of novel covert antennas which could be attached to pocket and collar area of garments were optimised and fabricated. These covert antennas can be retrofitted to existing garment designs and there is a high level of flexibility. Monopole stitching and stitched mesh ground plane were modelled as wearable and flexible antennas using a novel manufacturing method. This method provides better interconnection between the mesh nodes and reduces the discontinuities of the stitched path. This work also optimises stitched pattern and reduces overstretching of the mesh.

The crooked wire genetic antenna was optimised using both binary and real chromosome. The number of wire segments and connection representation was investigated using 5, 6, 7 and 8 connected wire segments. Results from the investigation indicate that 7-wire genetic antenna give better performance than 5, 6 and 8 segments. All the wire segments are connected in series for simplicity and ease of construction. A singular goal optimisation was to obtain right hand circular polarisation  $10^0$  above the horizon over the hemisphere for the crooked wire genetic antenna at a frequency of 1600 MHz [2.2, 2.65].

Antenna design problems are complex multi-objective optimisation problems. Using traditional methods to solve the problem is difficult and time consuming. NASA's space Technology 5 (ST5) which has a goal to launch multiple miniature spacecraft, to test and demonstrate the technologies by measuring the effect of solar activity on the earth for three months. Each satellite consists of two antennas at the top and the bottom of each of the



spacecraft. The wire antennas with four identical monopole arms, each set  $90^\circ$  from its near neighbours were used. Evolutionary antennas were optimised based on the method used in the crooked wire antenna design. This work creates a new model to solve antenna problems. Feasible solutions to solve the antenna problem were realised and optimal solutions were found [2.3]. Figure 2.16 was evolved for applications in a variety of aerospace applications. Figure 2.16(a) is one of the best antenna designs ST5-3-10 and Fig.2.16 (b) is one of the evolved antennas ST5-33-142-7 successfully launched into space.

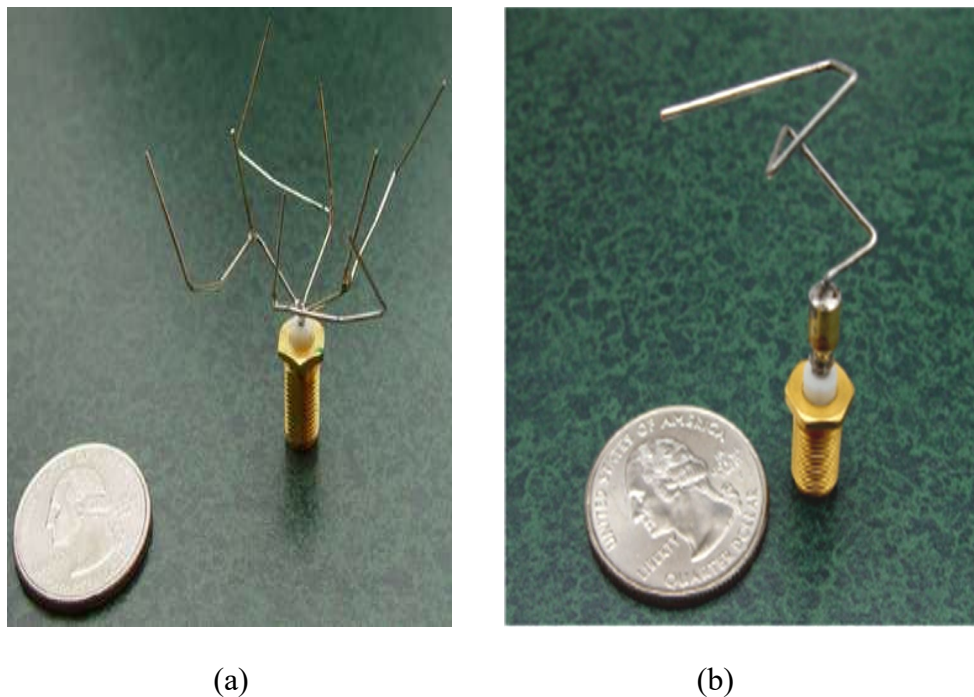


Figure 2.16 Photographs of prototype evolved antennas: (a) the best evolved antenna for the initial gain pattern requirement, ST5-3-10; (b) the best evolved antenna for the revised specifications, ST5-33-142-7 (picture from [2.3])

## Conclusion

This chapter has reviewed the current state of the art in Textile Wearable Antennas. There is a vast array of literature, some of which will be expanded in subsequent chapters. The present thesis narrows the scope to stitched antennas and their optimisation. Even with this narrower focus there are significant areas of research which can be expanded. One specific advantage of stitched antennas is their simplicity of construction. They can be retrofitted to existing garment designs and there is a high level of flexibility. The thesis develops methods for making use of two flexibility by considering a set of problems with many variables and seeking optimal solutions with GA methods.

The study has centred on optimisation inspired wearable wire antennas. A review of a selection of textile antennas was conducted. Several authors for the design of textile antennas used different conductive materials and dielectric substrates. Textile antennas have been fabricated by various methods including weaving, knitting, lamination, printing and embroidery. An embroidery technique was chosen because of the compelling technique for fabrication of stitched antennas in this thesis.

The application of genetic algorithm for the optimisation of crooked-wire antennas, planar wire antennas, zigzag patterns, meander-line and even fractal geometries is briefly discussed. Chapter 3 presents methods and optimisation technique for the realisation of the designs.

## References

- 2.1. C.A. Balanis, “Antenna theory: analysis and design,” John Wiley & Sons. 2016.
- 2.2. D. S. Linden and E. E. Altshuler, “Evolving Wire Antennas Using Genetic Algorithms: A Review,” Proceedings of the First NASA Workshop on Evolvable Hardware, Pasadena, CA, U.S.A., IEEE Computer Society, Los Alamitos, CA, U.S.A., pp. 225-232, 1999.
- 2.3. G. Hornby, A. Globus, D. Linden, and J. Lohn, “Automated Antenna Design with Evolutionary Algorithms,” In Space. pp. 7242. 2006.
- 2.4. W. L. Stutzman and G. A. Thiele, Antenna Theory and Design,” Wiley, New York, 1998.
- 2.5. B. Aswoyo, O. Makino, Y. Shimoshio and Tokuda, M B. “A measurement method for reflection coefficient of anechoic chamber using standing wave techniques,” Asia-Pacific Conf. Circuits Syst., 1, pp. 115–119, 2003
- 2.6. W. H. Kummer and E. S. Gillespie. “Antenna measurements,” Proc. IEEE, 66. pp. 483-507. 1978. (See also: P. H. Napier and R. H. T. Bates, Proc. IEEE, 32, pp. 164-165. 1971; Int. J. Eng., 9. pp. 1107-1112, 1103-1208, 1971)
- 2.7. D. Mandaris, N. Moonen, S. Van de Beek, F. Buesink and F. Leferink, “Validation of a Fully Anechoic Chamber,” Asia-Pacific Int. Symp. Electromagn. Compat. APEMC, 2, pp. 865–868, 2016
- 2.8. H. E. King, F. I. Shimabukuro, and J. L. Wong, “Characteristics of a Tapered Anechoic Chamber,” IEEE Trans. Antennas Propag., AP-15(3), pp. 488–490, 1967.
- 2.9. R. B. Dybdal and C. O. Yowell, “VHF to EHF Performance of a 90-FT Quasi-Tapered Anechoic Chamber,” IEEE Trans. Antennas Propag., 21(4), pp. 579–581, 1973.
- 2.10. O. Amft and P. Lukowicz, “From Backpacks, to Smartphones: Past, Present, and Future of Wearable Computers,” IEEE Pervasive Computing, 8(3), pp.8-13. pp. 8–13, 2009.
- 2.11. E.R. Post., M. Orth., P.R. Russo and N. Gershenfeld., “E-broidery: Design and fabrication of textile-based computing,” IBM Systems journal, 39(34), pp. 840–860, 2000.
- 2.12. T. Acti, A. Chauraya, S. Zhang, W.G. Whittow, R. Seager, J.C. Vardaxoglou, and T. Dias, “Embroidered wire dipole antennas using novel copper yarns,” IEEE Antennas and Wireless Propagation Letters, 14, pp.638-641, 2015.

- 2.13. T. Kaufmann, I. Fumeaux, and C. Fumeaux, "Comparison of fabric and embroidered dipole antennas," *Antennas Propag. (EuCAP)*, 7th Eur. Conf., pp. 3252–3255, 2013.
- 2.14. M. Mantash, A. C. Tarot, S. Collardey, and K. Mahdjoubi, "Wearable monopole zip antenna," *Electronics Lett.*, 47(23), pp.1266–1267, 2011.
- 2.15. P. Salonen., L. Sydanheimo., M. Keskilammi and M. Kivikoski., "A Small Planar Inverted-F Antenna for Wearable Applications," *The Third International Symposium on Wearable Computers*, pp. 95 - 100, 1999.
- 2.16. W. Zeng., L. Shu., O. Li, S. Chen., F. Wang. and X.M. Tao, X.M., "Fiber-based wearable electronics: a review of materials, fabrication, devices, and applications," *Advanced materials*, 26(31), pp.5310-5336, 2014.
- 2.17. A. Tsolis, W. Whittow, A. Alexandridis and J.Vardaxoglou, "Embroidery and Related Manufacturing Techniques for Wearable Antennas: Challenges and Opportunities," *Electronics*, 3(2), 2014
- 2.18. P. Salonen., Y. Rahmat-Samii., H. Hurme, H. and M. Kivikoski., "Dual-band wearable textile antenna," *Antennas and Propagation Society International Symposium IEEE*, 1, pp. 463- 466, 2004
- 2.19. M. Klemm and G. Troester, "Textile UWB Antennas for Wireless Body Area Networks," *IEEE Trans. Antennas Propag.*, 54(11), pp. 3192–3197, 2006.
- 2.20. N.J. Ramly, M.K.A. Rahim., N. Samsuri., M.E. Jalil, M.A.A. Majid., N.A.Elias and R. Dewan., "Leaf-shaped dual band antenna textile performance for on-body application," *IEEE Asia-Pacific Conf. Appl. Electromagn. APACE Proceeding*, pp. 257–260, 2015.
- 2.21. T. Maleszka and P. Kabacik, "Bandwidth properties of embroidered loop antenna for wearable applications," *Proceedings of the 3rd European Wireless Technology Conference (EuMA) 2010*.
- 2.22. N. H. M. Rais., P.J. Soh., F. Malek., S, Ahmed., N.B.M. Hashim and P.S. Hall., "A Review of Wearable Antenna," *Loughborough Antennas & Propagation Conference, LAPC 2009 Progress in Electromagnetics Research B*, 27, 307-325, 2011
- 2.23. D. H. Schaubert, "Microstrip antennas," *Electromagnetics*, 12, pp. 381-401, 1992.
- 2.24. R. Seager, S. Zhang, A. Chauraya, W. Whittow, Y. Vardaxoglou, T. Acti and T. Dias, "Effect of the fabrication parameters on the performance of embroidered antennas," *In 2014 IEEE Asia-Pacific Conference on Applied Electromagnetics (APACE)*, pp. 257-260. IEEE 2013

- 2.25. N. Liu, Y. Lu, S. Qiu and P. Li, “Electromagnetic properties of electro-textiles for wearable antennas applications,” *Frontiers of Electrical and Electronic Engineering in China*, 6(4), pp. 563–566, 2011
- 2.26. L. Vallozzi, W. Vandendriessche, H. Rogier, C. Hertleer and M.L. Scarpello., “Wearable textile GPS antenna for integration in protective garments,” *Antennas Propag. (EuCAP), Proc. Fourth Eur. Conf.*, pp. 1–4, 2010.
- 2.27. S. Sankaralingam and B. Gupta, “Development of textile antennas for body wearable applications and investigations on their performance under bent conditions,” *Prog. Electromagn. Res. B*, 22, pp. 53–71, 2010
- 2.28. I. Locher., M. Klemm., T.Kirstein and G. Trster, G “Design and characterization of purely textile patch antennas,” *IEEE Transactions on advanced packaging*, 29(4), pp.777-788.2006.
- 2.29. Z. Wang, L. Zhang, Y. Bayram, and J. L. Volakis, “Embroidered conductive fibers on polymer composite for conformal antennas,” *IEEE Trans. Antennas Propag.*, 60(9), pp. 4141–4147, 2012
- 2.30. P. Nepa and H. Rogier, “Wearable antennas for off-body radio links at VHF and UHF bands (below 1 GHz): Challenges, state-of-the-art and future trends,” *IEEE Antennas Propag. Mag.*, 57(5), pp. 1–23, 2015
- 2.31. D. Psychoudakis, G.Y. Lee, C.C. Chen and J.L. Volakis, “Military UHF body-worn antennas for armoured vests,” in *Proc. European Conf. Antennas Propagation*, Barcelona, Spain, pp. 1–4, 2010.
- 2.32. B. Sanz-Izquierdo, E.A. Parker, J.C. Batchelor and J.A. Miller, “Body armour with integral high impedance surface,” in *Proc. European Conf. Antennas Propagation*, Rome, Italy, pp. 1061–1064, 2011.
- 2.33. A. A. Serra, P. Nepa, and G. Manara, “A wearable two-antenna system on a life jacket for Cospas-Sarsat personal locator beacons,” *IEEE Trans. Antennas Propag.*, 60(2), pp. 1035–1042, 2012.
- 2.34. K. Koski, E. Moradi, M. Hasani, J. Virkki, T. Björninen, L. Ukkonen and Y. Rahmat-Samii, “Electro-textiles – The Enabling Technology for Wearable Antennas in Wireless Body-centric Systems,” In *2015 IEEE International Symposium on Antennas and Propagation & National Radio Science Meeting*, pp. 1203-1204, IEEE pp. 1203–1204, 2015.
- 2.35. A. Priya, A. Kumar, and B. Chauhan, “A Review of Textile and Cloth Fabric Wearable Antennas,” *Int. J. Comput. Appl.*, 116(17), pp. 1–5, 2015.

- 2.36. J. G. Santas, A. Alomainy, and Y. Hao, "Textile Antennas for On-Body Communications: Techniques and Properties," In Proceedings of the European Conference on Antennas and Propagation (EuCAP), Edinburgh, Scotland, pp. 1–4, 2007.
- 2.37. T.F. Kennedy, P.W. Fink, A.W. Chu, N.J. Champagne, G.Y. Lin, and M.A. Khayat, "Body-Worn E-Textile Antennas: The Good, the Low-Mass, and the Conformal," IEEE Transactions on Antennas and Propagation, 57(4), pp.910-918. 2009.
- 2.38. J.C. Lin, "Specific absorption rates (SARs) induced in head tissues by microwave radiation from cell phones," IEEE Antennas and Propagation Magazine, 42(5), pp.138-139, 2000.
- 2.39. M.A. Bhat and V. Kumar, "Calculation of SAR and measurement of temperature change of human head due to the mobile phone waves at frequencies 900 MHz and 1800 MHz,". Advances in Physics Theories and Applications, 16, 2013.
- 2.40. U. Ali, S. Ullah, J. Khan, M. Shafi, B. Kamal, A. Basir, J.A. Flint and R. D. Seager, "Design and SAR analysis of wearable antenna on various parts of human body, using conventional and artificial ground planes," Journal of Electrical Engineering and Technology, 12 (1), pp. 317-328, 2017.
- 2.41. International Commission on Non-Ionizing Radiation Protection (ICNIRP), "Guidelines for limiting exposure to time-varying electric, magnetic and electromagnetic fields (up to 300 GHz)," Health Physics, 74 (4), pp 494-522; 1998
- 2.42. M. Stoppa and A. Chiolerio, "Wearable Electronics and Smart Textiles: A Critical Review," Sensors 2014, 14, pp. 11957–11992, 2014.
- 2.43. S. Zhang, "Design Advances of Embroidered Fabric Antennas", PhD dissertation, Loughborough University, Loughborough, 2014.
- 2.44. A. Chauraya, W.G. Whittow, J.Y.C. Vardaxoglou, Y. Li, R. Torah, K. Yang, S. Beeby and J. Tudor, "Inkjet printed dipole antennas on textiles for wearable communications," IET Microwaves, Antennas Propag., 7, 2013
- 2.45. T. Acti, S. Zhang, A. Chauraya, W. Whittow, R. Seager, T. Dias and Y. Vardaxoglou, "High Performance Flexible Fabric Electronics for Megahertz Frequency Communications," Loughborough Antennas & Propagation Conference, pp. 5–8, 2011.
- 2.46. S. Zhang, R. Seager, A. Chauraya, W. Whittow and Y. Vardaxoglou, "Textile manufacturing techniques in RF devices," 2014 Loughborough. Antennas Propag. Conf. (LAPC), pp. 182–186, 2014.

- 2.47. J. S. Roh, Y. S. Chi, and T. J. Kang, "Wearable textile antennas," *International Journal of Fashion Design, Technology and Education*, 3(3), pp. 135–153, 2010.
- 2.48. D. Cottet, J. Grzyb, T. Kirstein and G. Troster, "Electrical Characterisation of Textile Transmission Lines," *IEEE Transaction on Advance Packaging*, 26(2), pp. 182-190, May 2003.
- 2.49. C. Zysset, K. Cherenack, T. Kinkeldei and G. Tröster, "Weaving integrated circuits into textiles," *International Symposium on Wearable Computers (ISWC)*, 2010.
- 2.50. K. Cherenack and L.V. Pieterse, "Smart textiles: challenges and opportunities," *Journal of Applied Physics* 112(091301), 2012. <https://doi.org/10.1063/1.4742728> (Accessed on 25th August 2012)
- 2.51. I. Kazani, C. Hertleer, G. De Mey, A. Schwarz, G. Guxho, and L. Van Langenhove, "Electrical conductive textiles obtained by screen printing," *Fibres & Textiles in Eastern Europe*, 20(1), pp.57-63.2012.
- 2.52. H. A. Wheeler, "Formulas for the skin effect," *PROC. I.R.E.*, 30, pp.412-424, 1942
- 2.53. E. Moradi, T. Björninen, L. Ukkonen and Y. Rahmat-Samii, "Characterization of embroidered dipole-type RFID tag antennas," 2012 *IEEE Int. Conf. RFID-Technologies Appl. RFID-TA*, pp. 248–253, 2012
- 2.54. Y. Ouyang and W. J. Chappell, "High frequency properties of electro-textiles for wearable antenna applications," *IEEE Trans. Antennas Propag.*, 2008.
- 2.55. E. Li, Y.E. Erdemli, J.L.Volakis and P.Y. Papalambros, "Design optimization of conformal antennas by integrating stochastic algorithms with the hybrid finite element method," *IEEE Trans. Antennas Propagat.*, 50, pp. 676–684, 2002
- 2.56. J. M. Johnson and Y. Rahmat-Samii, "Genetic algorithms in engineering electromagnetics," *IEEE Antennas Propag. Mag.*, 1997
- 2.57. S.Y. Lin, "Multiband Folded Planar Monopole Antenna for Mobile Handset," *IEEE Transactions on Antennas and Propagation*, 52(7), pp. 1790-1794, 2004.
- 2.58. M. Mehrparvar, O. H. Izadi and H. Oraizi, "Design of microstrip spiral antenna using Genetic Algorithm," In *Telecommunications (IST), Sixth International Symposium*, pp. 11-14, 2012
- 2.59. D. A. Van Veldhuizen, B.S. Sandlin, R.E. Marmelstein, G.B.Lamont and A.J. Terzuoli. "Finding improved wire-antenna geometries with genetic algorithms," In *Evolutionary Computation Proceedings, IEEE World Congress on Computational Intelligence*, pp. 102-107, 1998.

- 2.60. K. Jagodzinska, M. Wysota, and M. Walkowiak, "Electrically small linear antennas generated with a genetic algorithm," In Information Technology, IT 2008. 1st International Conference, pp. 1-4, 2008.
- 2.61. R. Ghatak, D. R. Poddar, and R. K. Mishra, "Design of sierpinski gasket fractal microstrip antenna using real coded genetic algorithm," IET Microw. Antennas Propag., 3(7), p. 1133, 2009.
- 2.62. R. L. Haupt and D. H. Werner, Genetic Algorithms in Electromagnetics, Hoboken, NJ: Wiley, 2007
- 2.63. K. Jagodzinska, M. Wysota, and M. Walkowiak, "Electrically small linear antennas generated with a genetic algorithm," In Information Technology, IT 2008. 1st International Conference, pp. 1-4, 2008.
- 2.64. R. Ghatak, D. R. Poddar, and R. K. Mishra, "Design of sierpinski gasket fractal microstrip antenna using real coded genetic algorithm," IET Microw. Antennas Propag., 3(7), p. 1133, 2009.
- 2.65. R. L. Haupt and D. H. Werner, Genetic Algorithms in Electromagnetics, Hoboken, NJ: Wiley, 2007



## **Chapter 3**

### **Optimisation of a Linear Wire Antenna on a Garment**

#### **3.1. Introduction**

Antennas are characterised based on frequency, aperture, polarisation and radiation pattern. Polarisation of an antenna is the orientation of the electromagnetic wave radiated by the antenna in each direction, which may normally be in linear (vertical/horizontal/diagonal) or circular polarisation. The radiation pattern of an antenna may be loosely classified in the following shapes: omnidirectional, directional or hemispherical. Antennas are generally placed in one of these groupings: Wire antennas (dipole, monopole, helix and loops), aperture antennas (Horn antenna), reflector (parabolic reflective antenna and Cassegrain antenna) and microstrip antennas (patches) [3.1].

There is a number of options for antenna geometry covered in this chapter. However, some are unsuitable due to size and have limited options for integrating into existing garments. A simple antenna type that can be changed in shape easily is the linear wire monopole. The input impedance and radiation pattern of a monopole antenna changes as the dimensions of the wire element and ground plane vary. The direction of peak radiation of a monopole antenna is assumed to be horizontal relative to the ground plane. The radiation pattern of a monopole is uniform in the azimuthal plane and has an omnidirectional pattern in that plane [3.2].

#### **3.2. Antenna Optimisation**

For complex antenna installations, it is often necessary to change the shape of conventional antennas to make them fit into specific locations. In wearables, it is often the case that the antenna must conform to the body and may be too physically large to fit onto garment features. Therefore, the optimisation task is to ensure best fit for the garment whilst maintaining adequate antenna performance ( $S_{11}$ , pattern, etc.). In order to optimise, it is necessary to make use of a numerical solver, which computes the solution of Maxwell's equations and couple solution this to a mathematical optimisation technique. This chapter aims to produce an optimiser for a particular example garment and select suitable optimisation and EM numerical solvers.

A number of numerical techniques are briefly discussed as background before focussing on the chosen technique. The Numerical Electromagnetic code (NEC2) simulator is used for this research because MoM is designed for wire antennas and considered accurate and reliable for wire antenna structures [3.3]. The numerical optimisation consists of two components namely the evolutionary optimisation and computational electromagnetics. The Genetic algorithm is an example of evolutionary optimisation and is used for this research

### **3.3. Numerical Modelling**

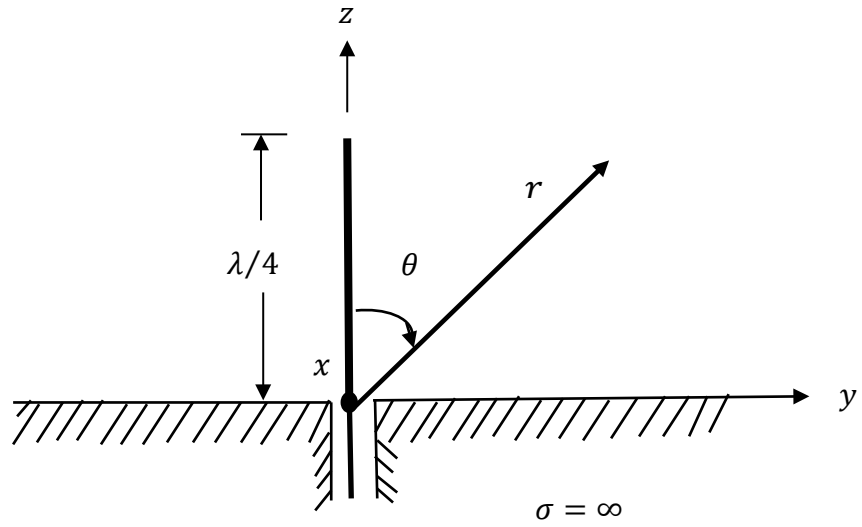
Numerous problems in electromagnetics are analysed in terms of electric and magnetic fields that propagate in space and distribute themselves in various media. Maxwell's equations explain the relationship between electric and magnetic fields and their interactions with boundaries. The concept of numerical solutions of electric and magnetic field is given important consideration in [3.4, 3.5]. Numerical methods are used to solve Maxwell's equations subject to the required boundary conditions. The antenna is treated as a boundary valued problem (usually that the tangential electric-field components vanish at the conducting surface). These methods provide very accurate solutions to well defined problems. Full-wave numerical methods can be subdivided into integral and differential equation-based technique as shown in Table 3.1. These numerical methods are divided into frequency domain method (such as Method of Moments and Finite Element Method) and Time Domain Technique (Finite Difference Time Domain and Transmission Line Matrix (TLM) method).

Table 3.1 Comparison of numerical methods (MoM [ 3.3], FDTD and FIT [3.4-3.5]).

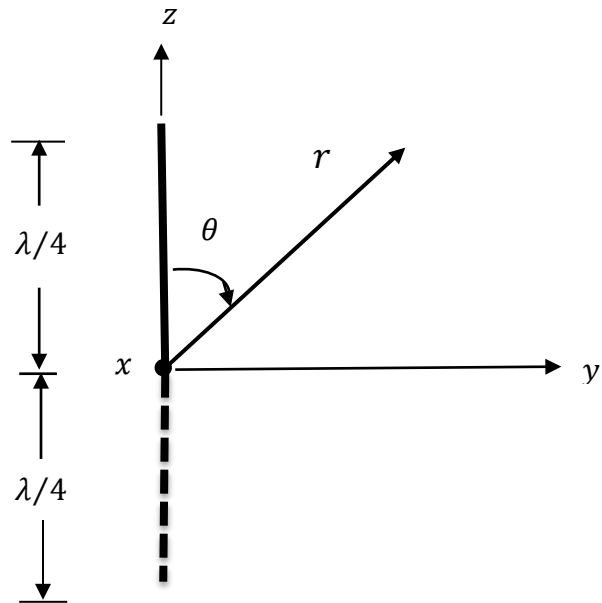
|                            | MoM  | FDTD  | FIT   |
|----------------------------|--|---|---|
| Solution domain            | Frequency domain method  | Time domain method  | Frequency and Time domain method, depending on formulation.                     |
| Method                     | EFIE with MoM is used for curved surfaces  | FDTD uses the differential form of Maxwell's equations and its iterative                                  | FIT uses the integral form of Maxwell's equations                               |
| Example of simulation tool | NEC  | Empire  | CST MWS   |
| Advantages                 | It is simple and efficient for a single frequency Efficiently applied to thin wires/ planar and surfaces | It is an efficient technique to solve complex transient problems giving broadband output at a single run. | The transient and frequency domain solver can give broadband at each simulation |
| Disadvantages              | Dielectric material is challenging to model  | It relies on an absorbing boundary condition which is not efficient.                                      | Ripples in the frequency response   |

### 3.3.1. Theoretical analysis of basic monopole antenna.

Monopole antenna is a form of dipole which is divided into two halves and fed from the midpoint against the ground plane. Figure 3.1 shows a quarter wavelength monopole ( $l = \lambda/4$ ) that is placed above a ground plane and is fed by a coaxial line. The principle of image theory is presented in Figure 3.1(b). To account for reflections where a monopole is  $\lambda/4$ , an image is introduced to form the  $\lambda/2$  equivalent. The input impedance of a quarter wavelength monopole above the ground plane is equal to one-half of a dipole and is given as  $Z_{in}(monopole) = 36.5 + j21.25$ . The quarter wavelength monopole has differing radiation pattern when the ground plane is finite or infinite as shown in Fig. 3.2. The solid line indicates the radiation of infinite ground while the dotted and dashed lines shows the radiation pattern using a finite ground plane. Using finite ground planes, the maximum radiation is not considered with respect to ground but at an angle above the ground  $\alpha$  [3.6].



(a)  $\lambda/4$  monopole on infinite electric conductor



(b) Equivalent of  $\lambda/4$  monopole on infinite electric conductor

Figure 3.1 Quarter-wavelength monopole on an infinite perfect electric conductor [3.1].

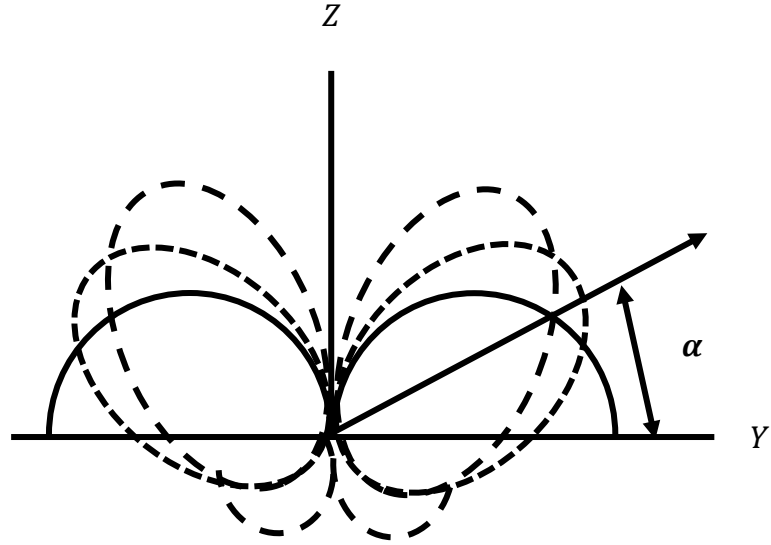


Figure 3.2 Vertical plane patterns of a monopole of  $\lambda/4$  on infinite ground plane (solid) on finite ground plane (dashed and dotted) [3.7].

In Nakano et al. [3.7], a bent dipole antenna was studied as a function of bending angle, if the bending angle is increased the intensity of the radiation in the antenna plane tends to decrease. The antenna characteristics varies with increase in the bending angle.

In this thesis a wire monopole antenna was modified into the 5 segments with a linear ground for textile applications. Monopole antennas were chosen because of ease to design, light weight and omni-directional radiation pattern in the horizontal plane [3.6].

### 3.3.2. Summary

There are many different of numerical techniques. A few have been covered in this chapter These includes FDTD, FIT and MoM. However, MoM chosen for the EM simulation within the optimisation system because the software package works well on wire antenna. NEC is a well-established and extensively validated package, which justifies its use in this thesis.

### 3.4. Optimisation Methods

Optimisation methods are classified into two different distinctions as local or global search techniques. Conjugate gradient methods [3.8], Quasi-Newton methods [3.9] and Simplex method [3.10] are examples of local optimisation while the global optimisation includes Random Search Methods [3.11], Simulated Annealing [3.12], Genetic Algorithms [3.13] and Evolutionary Algorithms (EA) [3.14]. Local techniques are highly dependent on the starting point or initial guess while global optimisers do not need initial conditions. Simplex (Nelder and Meed) is type of linear optimisation techniques that use continuous variables with linear constraints and a single linear objective function. Nonlinear optimisation methods such as quasi-Newton's method and gradient descent approach are categorised as being easily coupled to the solution domain and resulting in fast converge to a local minimum. Local optimisation methods search for best solutions using gradient or random guesses. The gradient method can easily get stuck in local minima since it requires gradient calculations, working on continuous parameters and is limited to few parameters [3.15, 3.16].

Global methods do not require defined starting point and the amount of required information is small compared to other antenna design techniques. These methods use few constraints on the solution domain, due to absence of constraints the global optimisation is more robust in an ill- performed solution space. Gradient type calculations are not used during the search process. Global techniques are employed for broad range of problem optimisation especially in microwave circuits [3.16].

Evolutionary optimisation uses guided random search techniques where added information serves as a guide to the search. Evolutionary algorithms (EA) are numerical techniques based on evolution any concepts and are probabilistic in nature. A flow chart for evolutionary algorithm is shown in Fig. 3.3, defining the processes and variables.

EAs are population based and the entire population of candidate solutions are processed at the same time. Individuals of the population which meet certain criteria reproduce and other individuals die. The population only converges to those that meet the set criteria for the next generation. The computation dynamics of the EA follows the Darwinist evolution theory. The EA is separated into classified categories that include genetic algorithm (GA) genetic

programming (GP), evolutionary strategies (ES), evolutionary programming (EP) and learning classifier systems (LCS) [3.14] - [3.18].

Evolutionary optimisation methods are used to optimise performance of existing antennas and to create new or novel designs of antennas. A genetic algorithm is one of the examples of Evolutionary computation technique. Genetic algorithm works on a set of instructions contained within the chromosome, where instructions are coded into a set of genes. Designs are number of instruction or specifications like length, frequency, diameters, materials or other characteristics. These instructions may be reduced into a series of numbers giving the necessary information. These specifications are arranged into a series that will indicate properties of the designs [3.19].

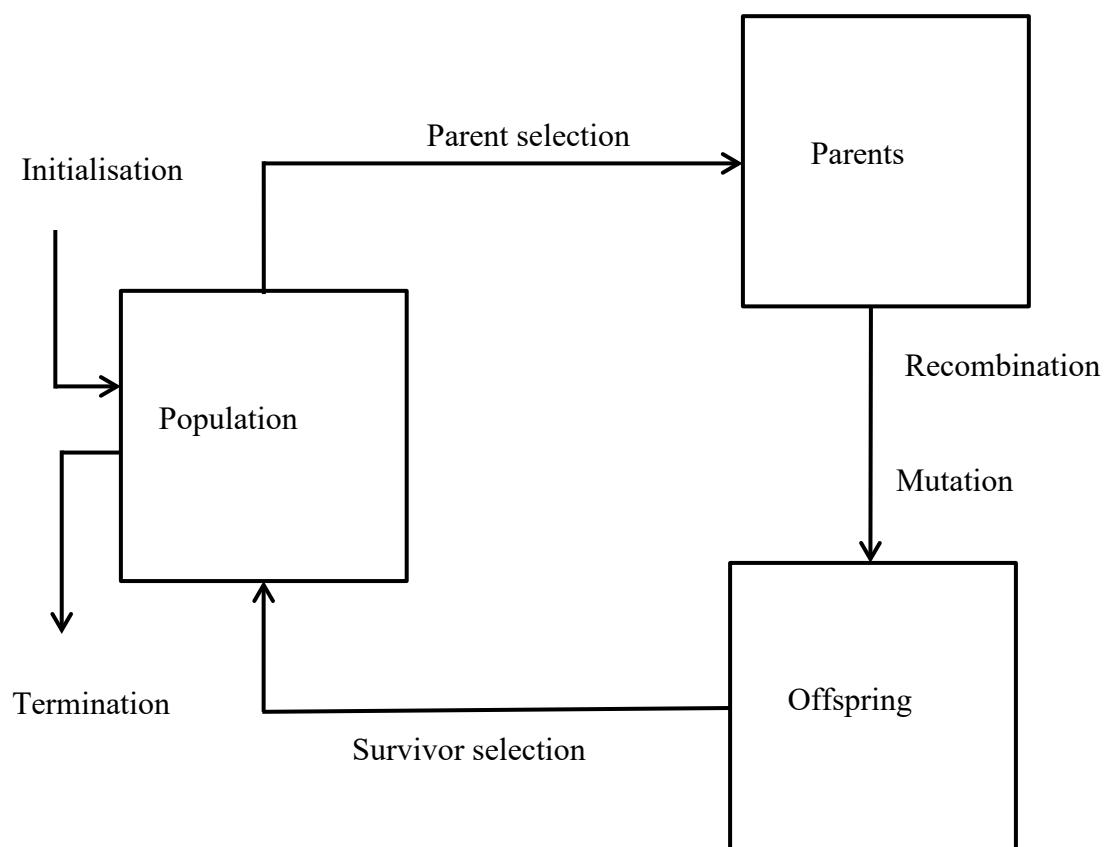


Figure 3.3 Flowchart of Evolutionary Algorithm (adapted from Streichert [3.19])

### **3.4.1. Swarm intelligence**

Swarm Intelligence and Evolutionary algorithms have been applied to antenna design and electromagnetic optimisation in recent years [3.20-3.24]. Global optimisation methods include: Swarm intelligence algorithm, genetic algorithm and differential evolution [3.21]. Examples of Swarm Intelligence Algorithms (SI-based algorithms) includes: Ant Colony Optimisation (ACO) [3.22], Particle Swarm Optimisation (PSO) [3.23], Glow worm Swarm Optimisation (GSO) [3.24] and Cuckoo Search Algorithm (CSA) [3.25]. PSO and GA are commonly algorithms used in antenna synthesis but performs differently in some cases. The two methods traverse the problem they solution space differently [3.20].

Particle swarm optimization (PSO) is a stochastic evolutionary computation technique based on the movement and intelligence of swarms of bees in a field. The swarm theory was inspired by social behaviour of birds flocking to a food source. This behaviour birds are related to an optimisation search for solutions to non-linear equations. Particle swarm is a population-based search method. Each individual has a position called current location in the current solution, a current velocity and a best position prior to the search point. Particle swarm does not use the selection function from its processing but uses two operators: crossover and highly directional mutation. In particle swarm parent information is contained within each particle and evolutionary optimisation is shared among the individuals. Particle swarm optimisation does not implement survival of the fittest, but all particles uses updated velocities. Particle swarm optimisation has been demonstrated to solve different kinds of problems as genetic algorithm [3.20-3.23].

### **3.4.2. Genetic Algorithms**

There are various techniques for optimising the antenna characteristic so that they can meet the design criteria. Complicated problems where the solution cannot be easily solved by analytical methods have been solved by means of numerical optimization algorithms. Among these, genetic algorithm, simulated annealing and particle swarm optimizers have become widely used in electromagnetics. In this design the genetic algorithm optimizer is used because it is a robust, stochastic search method, modelled on the principles and concepts of natural selection and evolution. As an optimizer, the powerful heuristic of the GA is effective at solving complex, combinatorial and related problems. GA Optimizers are particularly effective when the goal is to find an approximate global maximum in a high dimension,



multi-modal function domain in a near-optimal manner. GAs involves three major operations in every generation, which are selection, crossover and mutation. Implementations of the decision variables were encoded as strings of binary alphabets, zero and one [3.27-3.29]. The genetic algorithm was chosen because it has significant advantages over traditional optimization techniques [3.18]:

- It can be applied to a wide range of problems.
- It conducts a universal search in the solution space.
- It does not require previous knowledge of the optimization problem.
- It does not depend on the initial conditions of the search.
- It operates on continuous or discrete variables.
- It does not require derivative information of the cost function.
- Good results are obtained using a large number of parameters.
- It optimizes variables with quite complex cost surfaces.
- It provides a list of best parameters, not just a single solution.

### **3.4.3. Summary**

In this thesis, GA is used because of its advantages of modelling various problems in extensive range of disciplines, such as aerospace, operational research, social science, and quantum physics. Optimising antennas using traditional optimisation techniques such as gradients or random guesses have some drawbacks, which include quick convergence of the algorithm once it reaches the local minimum and being trapped in local minima. In random search methods, gradient calculation is not required but tends to be slow and it can easily become stuck in local minima [3.30-3.33].

### **3.5. General properties of Genetic Algorithms**

The genetic algorithm with Numerical Electromagnetic code is used to search resonant for wire antenna configuration that best defined the linear wire for the desired frequency. This approach has the following properties:

- (1) The principle advantage in using the GA (MATLAB)-NEC2 method is the ability to automate the design of new linear wire antennas. The evolutionary optimisation with

electromagnetic simulation is used to search the design space to create compact and novel antenna designs [3.27-3.29].

- (2) The Genetic Algorithm integrated with Electromagnetic solvers is an efficient procedure for antenna design automation. This approach allows designers to generate an optimal antenna structure based on specified design goals [3.13].
- (3) Programming with GA, the parameters are selected for optimisation and the solver employed runs independently from the user. GA has high degree of freedom to make change in mode of operation of antenna to fit new designs.
- (4) The automated design procedure can search a larger solution space than standard optimisation algorithms [3.29]. Search spaces for antenna design are multimodal. Conventional antenna designs are difficult to optimise and are almost impossible to optimise manually because of the number of variables involved.

Chromosomes are represented in two ways using either binary or real values. Binary coding has  $N$  number of bits. The value of  $N$  is different for each of the parameters. For calculation of the cost function, the chromosome is decoded first. A binary chromosome has  $N_{par}$  parameters that are encoded into  $N_{pbit}$  to give an array of quantised versions of the parameters ( $q_n$ ). The total number of chromosomes is given as  $N_{gbit} = N_{pbit} \times N_{par} \text{ bits}$ . The original values of the solution are recovered through the process of decoding [3.18]. Earlier implementation of GA used the binary codes to represent the search space to avoid local minima, but the computation cost is high. The binary GA representation has some setbacks, which include difficulties when it is applied to problems having a large search spaces and requiring high precision. To overcome the inherent difficulties in using the binary representation, real encoding of chromosomes is used [3.30-3.34].

In real value coding all parameters are represented as real numbers. When a real representation is used the steps of encoding and decoding are not applied in the GA execution process. Large domains are easily explored when real parameters are used [3.34].

### **3.6. Application of GA in Electromagnetics**

Genetic algorithm (GA) methods have been used for the design of electrically loaded wire antenna with stubs or lumped components such as LC, RL or RLC networks. Matching networks, transformers or attenuators were used as part of load wire optimisation. A

monopole loaded with modified dipole for uniform power pattern with six design variables has been designed using a GA [3.15]. Stub-loaded miniature whip antennas find applications in mobile and ground-based communication systems. In [3.16] GA has been quite useful and successfully applied to optimise array pattern, thinning circular arrays, planar arrays with directional elements and scanning planar arrays.

Convoluted wire antennas [3.33] and printed wire structure have been design using GA to select the wire from predefined rectangular grid where all wires joined at their end points. Modelling of the structures through solving the current distribution is performed by electromagnetic solver (NEC2). NEC2 is used in collaboration with the GA solver to evaluate the convoluted structure properties. In this analysis, the convoluted antennas were optimised without dielectric substrate or ground plane.

There are various techniques for optimising the antenna characteristics so that they can meet the design criteria. Complex solutions of electromagnetics are solved by means of numerical optimization algorithms. In this design, genetic algorithm optimisers are used because they are robust, stochastic search methods, modelled on the principles and concepts of natural selection and evolution [3.32].

### **3.7 Implementation of a Genetic Algorithm using MATLAB and NEC2 for simulation**

This thesis develops an implementation of a GA-MoM simulation driven by MATLAB. In this research on linear wire antennas, modelling was the primary focus; NEC2 was used for wire modelling due to its fast computation and accuracy. In linear wire antenna modelling three things are considered; the geometry of the antennas and segment excitation and the properties of the ground. The input file of NEC2 consists of a set of commands (called a card) specifying the geometry of the wire antenna, the excitation and electromagnetic properties of the antenna [3.13].

The MATLAB-NEC2 automated program structure for the design of linear wire antenna combines evolutionary optimisation and a computational electromagnetics method. The former uses a real coded Genetic Algorithm and the later uses NEC2. MATLAB is the control for the optimisation process. The automation cycles begin with a linear wire antenna design in MATLAB, which uses real valued variables. The correct dimensions of the antenna

design at 900 MHz was used and MATLAB was linked to NEC2. The operational frequency ranges from 850 to 950 MHz to cover a mobile frequency band. The GA generates the parameters of each structure of the antenna and sends them to the fitness function module, where the computation of the fitness values of all the structures are calculated. The GA adjusts the antenna structures automatically and communicates with the NEC2 solver to calculate the fitness values. The NEC2 calculates reflection coefficient ( $S_{11}$ ) of each of the antennas and substitutes them into the fitness function module.

Real Coded Genetic algorithms (RVGA) use real values as parameters of the chromosome in the population. In this scheme, no coding and decoding processes are needed before evaluating the fitness value of individuals. However, in optimization problems, it is more natural to represent the gene directly as real numbers since the representations of the solutions are very close to the natural formulation. The RVGA narrows the search space to a much smaller area of the entire search space. Other conventional methods, such as conjugate gradient methods can be used to optimise the parameters of antennas but for this design, the GA is applied because they are very likely to find the global optimum while the conventional methods can be easily trapped in local minimum. Genetic algorithms use an objective value and not the parameters to determine the direction of the search. GA was broken down into several steps, which involved problem definition, problem representation, fitness evaluation, selection method, crossover procedure and mutation scheme to achieve the optimisation process. In the present thesis, the optimisation technique has been implemented using MATLAB as the controlling program for NEC as shown in Fig 3.4. The detailed implementation of the GA itself can be found in Fig.3.5. The combination of this flow chart was built into an automated tool for the fast estimation of the wire antenna geometries. The operations performed by the GA optimiser could be summarised into six main functions:

- (1) Representation of the design variables
- (2) Create a population of individuals.
- (3) Initialise a starting population.
- (4) Evaluate and assign fitness values to everyone in the population.
- (5) Perform reproduction of offspring through the fitness-weighted selection.
- (6) Create a next generation (new population) through the process of crossover and mutation.

The genetic algorithm is used to select random sample of possible solution from a population of all the wire configurations. The GA is also used to specify the number of the population and the number of generations. The performance ( $S_{11}$ ) of wire configurations is computed using NEC2 and ranked in order of fitness. This evolutionary process for the linear wire optimisation proceeds until at optimal wire configuration are achieved.

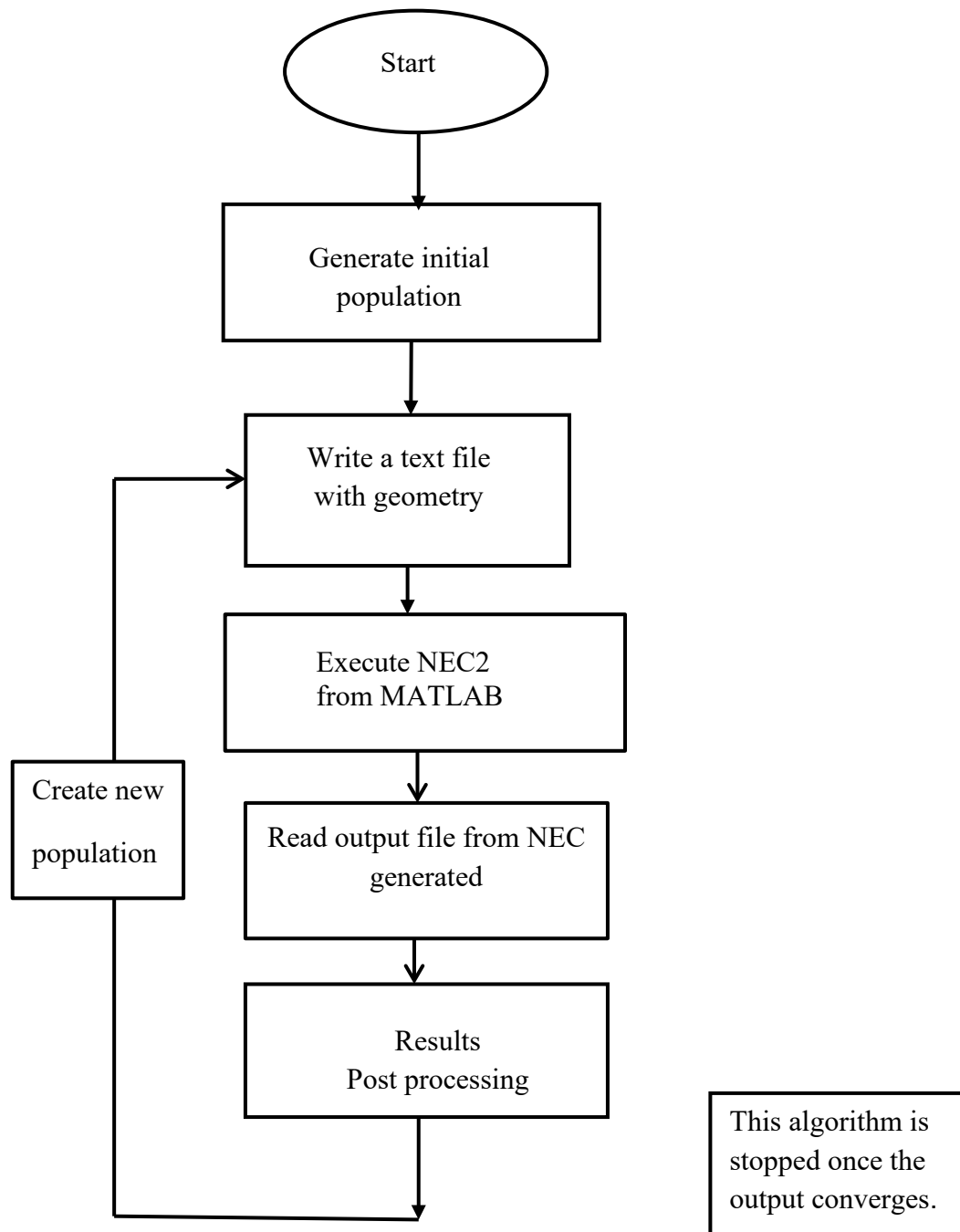


Figure 3.4 Software flowchart showing the link between NEC and MATLAB in this thesis.

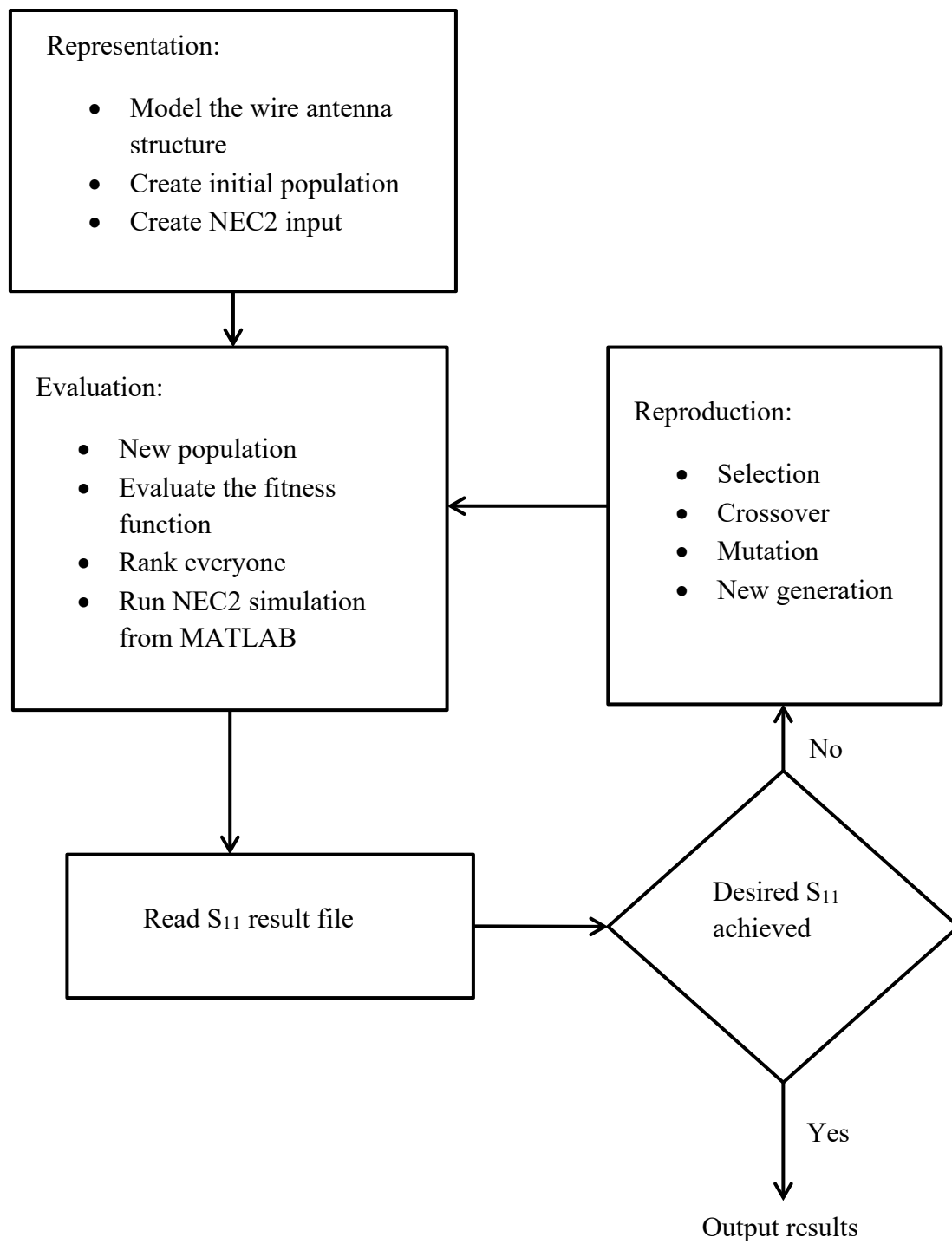


Figure 3.5 Detailed process flowchart for the GA

### 3.7.1. Antenna Parameterisation for Genetic Algorithm

Identifying parameters is the first step in any optimisation procedure for antenna design. In this design of linear wire antennas three parameters were require, namely the segment length, angle between segments and the radius of the wire. The parameters can be varied to obtain the desired frequency of operation for the antenna. A mathematical model was developed and demonstrated with a 7- segment parameterised antenna structure (see Fig.3.6). Each segment of the wire is defined by starting points and endpoints. The antenna configuration has 12 input parameters that create the antenna geometry ( $l_1, \theta_1, l_2, \theta_2, l_3, \theta_3, l_4, \theta_4, l_5, \theta_5, l_6$  and  $l_7$ ). A mathematical model based on coordinate geometry was used to calculate the segments and angles from the equations (3.27) – (3.37). Segments are closely fitted together and follow the path of the conductor. The boundaries of the design variables were determined. The segment of the antenna was defined in the range of  $\lambda/40 \leq \text{segment} \leq \lambda/15$ . The ranges give the GA a boundary for search space. The angles were defined as  $30^\circ \leq \text{angle} \leq 60^\circ$ . The limits of these angles are chosen to avoid segment overlap leading to meaningless results.

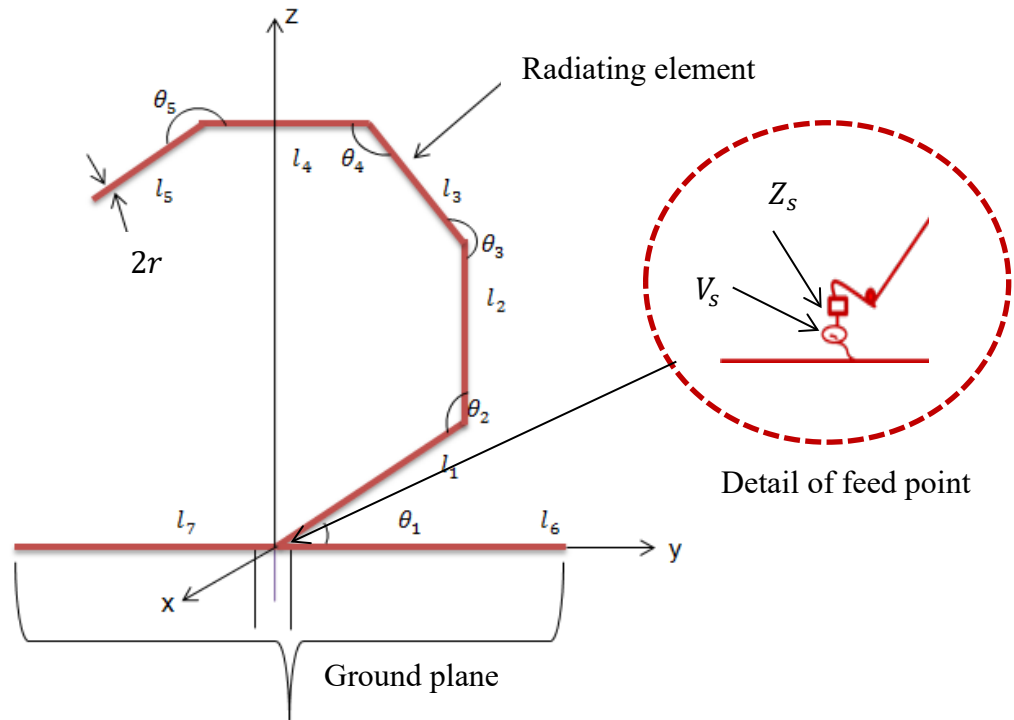


Figure 3.6 CAD design of linear wire antenna

### 3.7.2. Implementation details

In design of the linear wire antennas geometry in NEC2, a card structure is use in writing the input script and consists of the following antenna geometry as shown in Table 3.2. NEC2 has a file interface for input and output that makes it easier to use with optimiser. The writeInput.m script was used to generate the input data. Wire segments are connected in series.

Table 3.2 Format of antenna geometry

|        | Start point  | End point    | Radius |
|--------|--------------|--------------|--------|
| Wire 1 | (0, 0, 0)    | (x1, y1, z1) | r      |
| Wire 2 | (x1, y1, z1) | (x2, y2, z2) | r      |
| Wire 3 | (x2, y2, z2) | (x3, y3, z3) | r      |
| Wire 4 | (x3, y3, z3) | (x4, y4, z4) | r      |
| Wire 5 | (x4, y4, z4) | (x5, y5, z5) | r      |
| Wire 6 | (0, 0, 0)    | (x6, y6, z6) | r      |
| Wire 7 | (0, 0, 0)    | (x7, y7, z7) | r      |

In the pocket antenna its ground plane was symmetrical and was not varied in orientation. The collar antenna ground plane was asymmetrical and not straight. The ground plane remains linear in the plane containing the monopole as the final design is intended to be a planar antenna

MATLAB script, meander new.m, builds the model and checks its integrity: continuity, overlaps etc

Starting from

$$X_0 = (0.0) \text{ and } Y_0 = (0.0)$$

$$A(1, 1, j) = X_0;$$

$$A(2, 1, j) = Y_0; \quad (3.27)$$

First length does not need to be check for intersection.

$$A(1, i, j) = L_1(j) * \text{find}(\theta_1(j)) + A(1, 1, 1);$$



$$A(2, i, j) = L_1(j) * \cosd(\theta_1(j)) + A(2, 1, 1) \quad (3.28)$$

Creating the second line and using the line intersections:

$$\begin{aligned} A(1, i, j) &= L_2(j) * \cosd(\theta_2(j) + \theta_1(j)) + A(1, 2, j); \\ A(2, i, j) &= L_2(j) * \sind(\theta_2(j) + \theta_1(j)) + A(2, 2, j) \end{aligned} \quad (3.29)$$

Line intersection for line line1 and line2

$$\begin{aligned} \text{line1} &= [A(1, 1, j) \quad A(2, 1, j) \quad A(1, 2, j) \quad A(2, 2, j)]; \\ \text{line2} &= [A(1, 2, j) \quad A(2, 2, j) \quad A(1, 3, j) \quad A(2, 3, j)]. \end{aligned} \quad (3.30)$$

Creating the third line and checking if the lines are intersecting.

$$\begin{aligned} A(1, i, j) &= L_3 * \cosd(\theta_3(j) + \theta_2(j) + \theta_1(j)) + A(1, 3, j); \\ A(2, i, j) &= L_3 * \sind(\theta_3(j) + \theta_2(j) + \theta_1(j)) + A(2, 3, j). \end{aligned} \quad (3.31)$$

Checking the line intersection:

$$\begin{aligned} \text{linex} &= [A(1, k, j) \quad A(2, k, j) \quad A(1, k+1, j) \quad A(2, k+1, j)]; \\ \text{line3} &= [A(1, 3, j) \quad A(2, 3, j) \quad A(1, 4, j) \quad A(2, 4, j)] \end{aligned} \quad (3.32)$$

Creating the fourth line:

$$\begin{aligned} A(1, i, j) &= L_4 * \cosd(\theta_4(j) + \theta_3(j) + \theta_2(j) + \theta_1(j)) + A(1, 4, j); \\ A(2, i, j) &= L_4 * \sind(\theta_4(j) + \theta_3(j) + \theta_2(j) + \theta_1(j)) + A(2, 4, j). \end{aligned} \quad (3.33)$$

Plotting and checking the line intersection:

$$\begin{aligned} \text{linex} &= [A(1, k, j) \quad A(2, k, j) \quad A(1, k+1, j) \quad A(2, k+1, j)]; \\ \text{line4} &= [A(1, 4, j) \quad A(2, 4, j) \quad A(1, 5, j) \quad A(2, 5, j)]. \end{aligned} \quad (3.34)$$

Creating the fifth segment:

$$\begin{aligned} A(1, i, j) &= L_5 * \cosd(\theta_5(j) + \theta_4(j) + \theta_3(j) + \theta_2(j) + \theta_1(j)) + A(1, 5, j); \\ A(2, i, j) &= L_5 * \sind(\theta_5(j) + \theta_4(j) + \theta_3(j) + \theta_2(j) + \theta_1(j)) + A(2, 5, j). \end{aligned} \quad (3.35)$$

$$\text{linex} = [A(1, k, j) \quad A(2, k, j) \quad A(1, k+1, j) \quad A(2, k+1, j)];$$

$$\text{line5} = [A(1,5,j) \quad A(2,5,j) \quad A(1,6,j) \quad A(2,6,j)]. \quad (3.36)$$

The wire radius is small compared to wavelength of linear wire antenna. The current on the surface of a wire segment is referred to as a filament of current. Only currents in the axial direction of wire segments are considered as discussed in section 3.3.4. The thin wire structures were subdivided into segments and the currents is assumed to flow along the axis. Segments of the created antennas were designed to be non-intersecting and connected in series. The segments are electrically connected and have coincident ends.

The linear wire antennas with invalid geometries were discarded see for examples of geometries Figure 3.7((a), (b) and (c)). The MATLAB code was written to remove geometries touching the ground, extending below the ground and having intersecting segments. The segments with invalid solutions were excluded from the design. A set of physically feasible linear wire antennas was produced (Figure 3.7(d)).

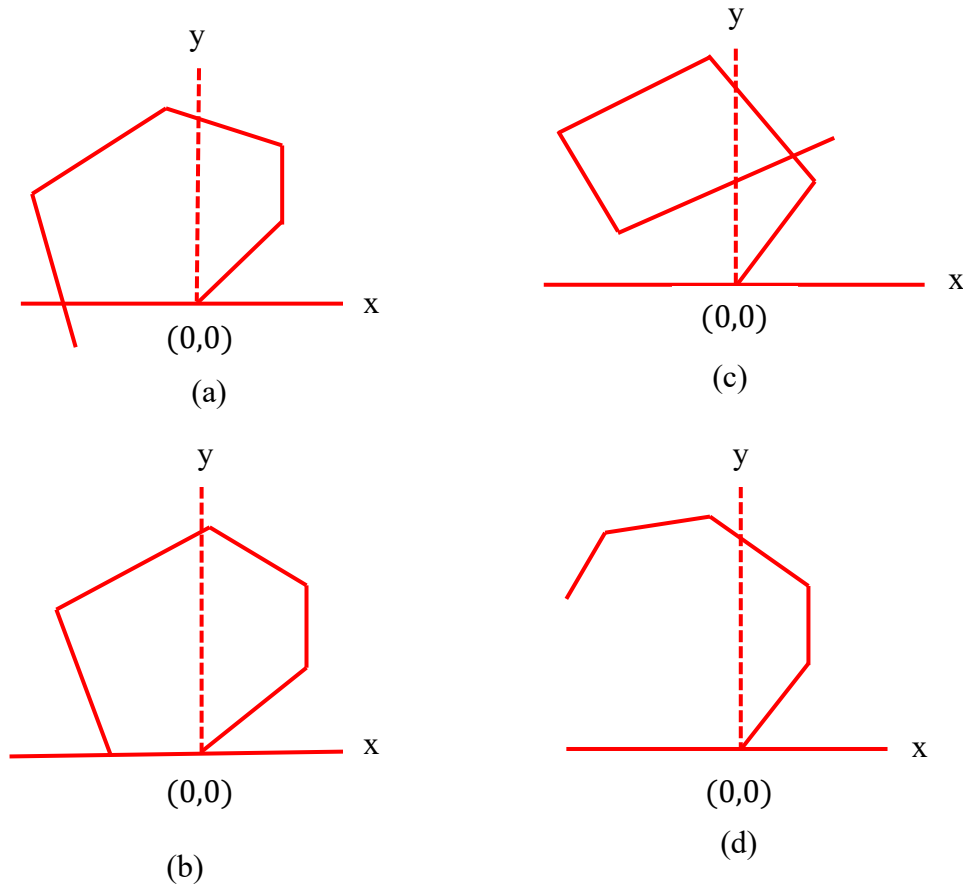


Figure 3.7 Antenna geometries (a), (b) and (c) are invalid geometries (d) Physical feasible antenna

A set of initial populations of linear wire antennas was created and assigned a random value from the domain of each chromosome using a random function generator as in equation (3.38). Randomness was introduced into the GA to move the solution from possible local minima to a near optimal solution. The total size of the chromosomes depends on the wire segments and the angle between the antenna lengths. The population consist of sample of each antenna and all the information about that sample is in chromosome. This information is stored in the chromosome. Each individual is represented by a real variable. The Genetic Algorithm processes starts with the generation of a population of 30 individuals. These were created by using random number generator in MATLAB. The population undergoes evaluation using three operators: selection, recombination and mutation to form a new generation.

$$npv = ll + (ul - ll) * \text{rand}(\text{noantenna}, 1) \quad (3.38)$$

Where  $npv$  is the new parameter value,  $ll$  is the lower limit and  $ul$  is upper limit.  $S_{11}$  (input reflection coefficient) is voltage ratio. In dBs it is a power ratio.

$$\text{Fitness} = \min (S_{11}) \quad (3.39)$$

$$\text{Reflection coefficient } (S_{11}) = \frac{Z_a - Z_l}{Z_a + Z_l} \quad (3.40)$$

$$\text{Return Loss} = -20\log|S_{11}|\text{dB} \quad (3.41)$$

Where the Input impedance ( $Z_a$ ) =  $R_a + jX_a$ ,  $R_a$  is the resistance and  $X_a$  is reactance  $Z_l$  is the characteristic impedance of the transmission line feeding the antenna  $50\Omega$ .  $S_{11}$  and return loss were computed from equations (3.39) – (3.41). The line count command was used to keep track of the line number, get data written, and assign it to line. The line count looks for a specified string in the line. The data of input impedance was obtained from the NEC2 output file and then extracted data.

A summary of GA parameters for the proposed design is listed in Table 3.3. A convergence criterion was used to terminate the genetic algorithm run. At the start of the GA run, the maximum number of generations is defined. GA can equally be stopped when many

generations have passed without achieving a significant improvement in the next generations [3.41],

Table 3.3 Genetic Algorithm parameters

| GA parameters                 | Value                                     |
|-------------------------------|---|
| Number of variables           | 12  |
| Population size               | 30  |
| Maximum number of generations | 500                                       |
| Selection mechanism           | Rank-based fitness weighted               |
| Crossover rate                | 80%                                       |
| Mutation rate                 | 1%  |
| Fitness limit                 | -10dB                                     |
| Cost function                 | $\min\{ S_{11} , f \in [900 \text{ MHz}]$ |

A genetic algorithm was used to explore the design domain efficiently and automatically discover novel antenna designs that can be more effective than might be developed by other methods. Genetic algorithms are numerical algorithms modelled on the concepts of natural selection and evolution theory, which modifies and optimised results among several generations. GAs operates on a population of potential solutions applying the principal of survival of the fittest to produce better and better approximations to a solution. Genetic algorithms are different from conventional calculus-based search algorithms in parallel computation of a population of solution using simple stochastic operators (selection, crossover and mutation) to explore the solution domain in the search of optimal solution and no gradient information.

### 3.7.3. Model implementation of the wire antenna

In this study, several scripts were written in MATLAB to execute this design. Meander\_new.m is for generating the antenna structures, calculating the segments and drawing the segments. This file was used to produce NEC2 input and output files. OutputFile.m contains the initialisation of generation, maximum number of generations to run calculation of the return loss each of the antenna parameters and computation of the objective function.  $S_{11}$  results are displayed as plots and array. Individual  $S_{11}$  and average  $S_{11}$

results are computed. Optimised (GA.m) program calculates the fitness value, the sum objective value and sort fitness values in descending order. These scripts generate a new population. Crossover and mutation parameters are also calculated in these scripts.

In this design, the design parameters are real values. The real numbers are mapped into a chromosome which is a representation of the design. The real valued GA was used in contrast to most works that have use a binary implementation. Binary implementations are described in [3.30].

The NEC2 output scripts consist of several relevant simulation details. The files are in array forms, which include structure specification, wire coordinates, frequency of operation, and distances in wavelength, radiation patterns and input impedance data at the point of excitation. The optimising programs generate an input file and execute the NEC2 solver. All relevant information such as input impedance for the computation of the objective function is output.

#### **3.7.4. Reproduction Operations**

The evolution operators in GA provide a basic search mechanism and create a new population from the existing solutions in the population. The evolution process in GA consists of three basic units, which include reproduction, crossover and mutation as illustrated in Fig. 3.2. According to the flow chart, the first step is to create a model of the design and initiate the population, and then assigns a random value from the domain of each chromosome. The aim of random selection is to ensure that the initial population is uniformly distributed over the entire search space. Each antenna is defined by 12 variables. The population of the antennas are simulated to estimate the cost function. The reproduction process utilises the principle of survival of the fittest. This process evaluates each antenna's fitness and uses fitness-weighted selection to produce the next population. Reproductions consists of the selection of new individual based on probability distribution of the individual in population with respect to current population.

### 3.7.5. Fitness function

The fitness function is designed to identify the frequency at 900 MHz and to get a return loss better than 10 dB. In this linear wire optimisation, the evaluation function computes values for each individual by calculating the difference between its individual  $S_{11}$  and the goal  $S_{11}$ . The evaluation function returns an absolute measure of the individual in the population. These differences give the objective value of each individual, a smaller difference equates to a higher objective value. The average error is given as the summation point errors divided by the number of frequency points. The fitness function is a measure used to define the quality of an individual in a population. The fitness function is designed to provide an assessment of each individual in the current population. The fitness function is also a measure of value of an individual relative to the rest of the population [3.33].

### 3.7.6. Fitness weighted selection

Selection in the GA is in two stages, selection for reproduction and selection for replacement. The latter creates a new generation from the current one while selection for reproduction aims to identify better chromosomes in the population for reproduction. The selection operator performs two functions select fitter individuals and discard inferior individuals based on the fitness value. Everyone in the selection pool has a reproduction probability based on the individual's objective value and the objective value of the rest of the individuals in the pool. Uniform scaling takes place across the population by ranking and this gives an uncomplicated way of controlling the selective pressure. In the ranking method, the selection probability is defined (3.41) [3.34]

$$Probability[Selecting\ the\ ith\ individual] = q(1 - q)^{r-1} / 1 - (1 - q)^P \quad (3.42)$$

Where  $q$  is the probability of selecting the best individual;  $r$  is the rank of the individual after sorting (with 1 is the best after sorting,  $P$  is the population size).

### 3.7.7. Heuristic Crossover

The crossover operator is a method for sharing information between chromosomes; it combines the features of two parent chromosome  $C_1 = \{x_{11}, x_{12}, x_{13}, x_{14}, x_{15}, \dots, x_{1n}\}$  and  $C_2 = \{x_{21}, x_{22}, x_{23}, x_{24}, x_{25}, \dots, x_{2n}\}$  to form an offspring  $H_1$  and  $H_2$ , where the fitness of  $C_2$  is higher than or equal to the fitness of  $C_1$  as in equation (3.43)-(3.45). In practice, not all parents in the mating pool are selected depending on fitness for crossover operation so that some of the good strings may be preserved. This crossover method uses the objective value to define the direction of the search space. Offspring are produced according to the rule [3.37]:

$$\text{Offspring} = \text{parent}_1 + \alpha (\text{parent}_2 - \text{parent}_1) \quad (3.43)$$

$$H_1 = C_1 + \alpha (C_2 - C_1) \quad (3.44)$$

$$H_2 = C_2 - (1 - \alpha)(C_1 - C_2) \quad (3.45)$$

Where  $\alpha$  is the scaling factor chosen uniformly at random over an interval  $[-0.25, 1.25]$  for each variable of a new offspring. The value of the parameter  $d$  defines the size of the area for possible offspring.

### 3.7.8. Mutation

After crossover of parents to produce the offspring, each offspring undergoes the process of mutation. Non-uniform mutation is used in real coded GAs [3.26]. Mutation creates a new individual from only one chromosome by altering one or more genes in the search space. Mutation is achieved, to ensure that the population is not trapped in a local minimum. The two individuals (children) resulting from each crossover operation will now be subjected to the mutation operator in the last step to form the new generation. In this study, the mutation process was evaluated using equations (3.46) – (3.48) and mutation probability occurs at 1% [3.38].

$$X^{\text{old}} = \{x_1, x_2, \dots, x_n\}, \quad (3.46)$$

$$x_k^{\text{new}} = LB_k + r * (UB_k - LB_k), \quad (3.47)$$

$$X^{\text{new}} = \{x_1, x_2, \dots, x_k^{\text{new}}, \dots, x_n\}, \quad (3.48)$$

Where  $n$  the number of parameters and  $r$  is a uniformly distributed random number between 0 and 1. LB and UB are upper and lower bounds of the parameter,  $LB_k$  and  $UB_k$  are the low and upper bound at location  $k$ .  $X^{old}$  is the population before mutation and  $X^{new}$  represent the new population after mutation operation.

### 3.8. Procedure for the proposed method

The procedure for the proposed GA method is summarised based on the Fig. 3.2 and 3.3:

- (1) Define the following; Antenna configuration, GA parameters, type of variable, population size, fitness function, maximum number of generation and convergence criteria.
- (2) Generate the initial population using random number generator.
- (3) Calculate the objective function and evaluation function using NEC2: check the  $S_{11}$  plots.
- (4) Analyse the GA results, the number of generations that were set as the convergence criteria and if satisfied with  $S_{11}$  results terminate the run or if in the GA yields no improvement in fitness value end.
- (5) Generate next generation through reproduction process: selection, crossover and mutation.
- (6) Repeat steps (3) through (5) until.....

### 3.9. Novel wearable antennas based on the linear wire.

The NEC2 was used to evaluate the performance of the linear wire antennas. Finite ground planes were used for the evaluations. All the wire antenna designs had the same diameter of 0.75 mm. Use of larger wire radius changes the wire connections and leads to inaccuracy in NEC2. The initial population consisted of 30 antennas. Each antenna consists of 12 parameters based on the designed antenna structure. A physical model of the optimised wire antenna in Fig.3.8. The wires consist of five for the radiating length and two segments as the linear ground plane.

The theoretical percentage bandwidth of the achieved solution at -10 dB  $S_{11}$  was:

$$\text{Bandwidth} = \frac{f_2 - f_1}{f_c} \times 100 = 11.1\%$$



where:

$$f_1 = 850 \text{ MHz}$$

$$f_2 = 950 \text{ MHz}$$

$$f_c = \frac{f_2 - f_1}{2} + f_1 = 900 \text{ MHz}$$

The percentage bandwidth optimised solution is 3% more than the theoretical solution with an  $S_{11}$  of -27dB.

The NEC2 results were compared to CST simulations, a FIT solver, before fabrication as shown in Fig.3.9. The slight variations in the 4NEC2 to CST simulation were because of the differences the feed points and the differences caused by meshing in CST and choice of Basis Functions inherent in NEC2. The ground plane remains linear in the plane containing the monopole as the final design is intended to be a planar antenna. The only time this not same is for the collar antenna.

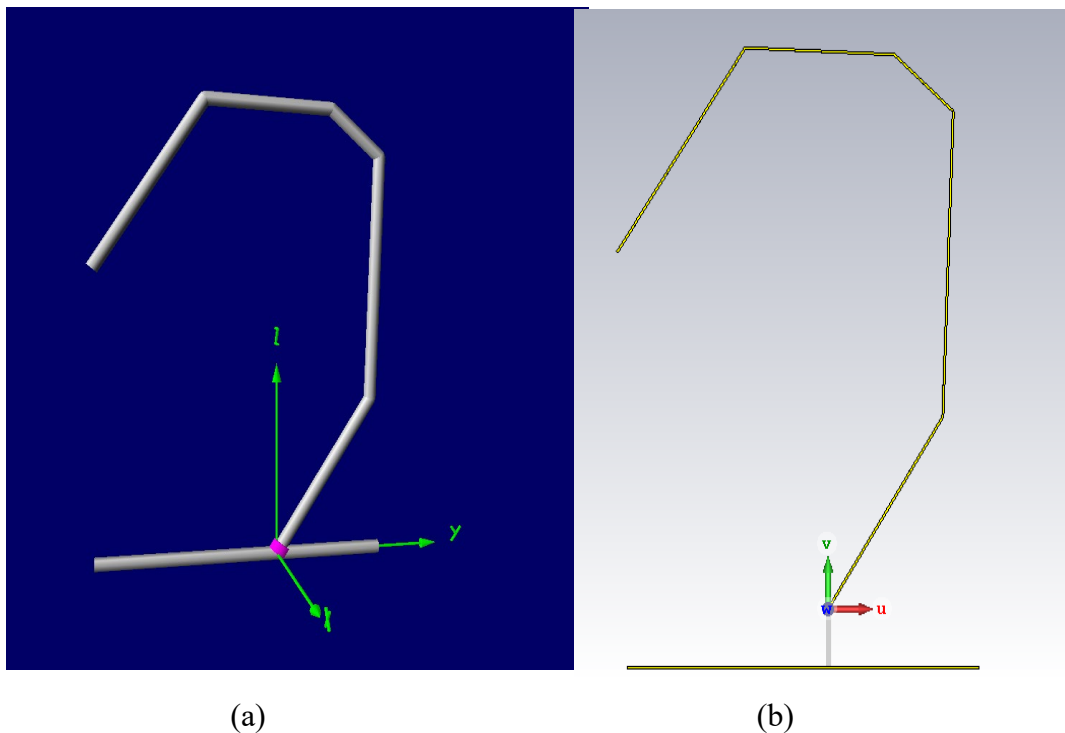


Figure 3.8 Geometrical model (physical) of the wire antenna designs visualised in (a) NEC2 and (b) CST

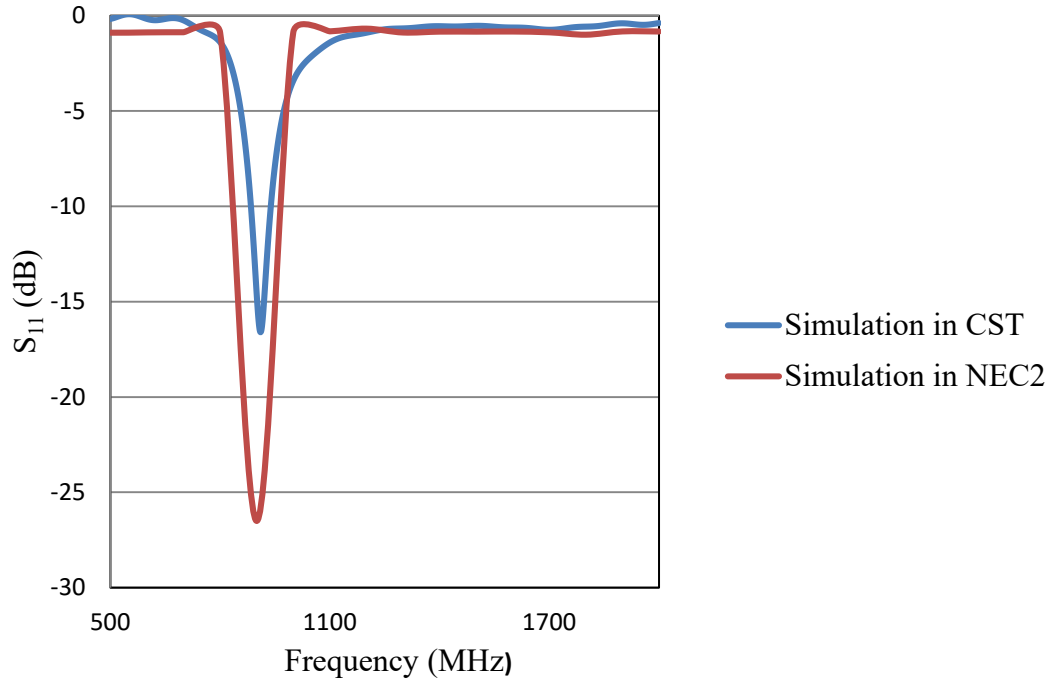


Figure 3.9 Simulated  $S_{11}$  results of linear wire antenna sample in CST and NEC2

It takes 50 minutes to run 100 generations of wire antennas with a population of 30. The specifications of the computer are: Processor Intel(R) core (TM) i5-4460 CPU@ 3.20 GHz 3.20 GHz, System type: 64-bit operating system, x64 based processor.

Population size remains the same across each generation. After each GA run, the data were stored observe see the progression. From the GA history, useful records of the number of simulations are saved for analysis. It is observed during GA runs, that some antennas would shows good fitness but poor  $S_{11}$  results. Each GA runs gives different results either good characteristics or poorer result than anticipated. Sometimes GA can converge to a wrong answer, but the efficiency of the GA improved by beginning with defined coarse searches that leads to a refined search [3.39].

The GA code initialises a sample of 30 individuals with 12 parameters to optimise. The GA evolved a sufficient number of generations that converge toward an optimum as illustrated in Fig. 3.10(a) and (b). Both plots have the same starting point and almost the same average value in used to achieving the desired results. The plots show the best, worst and average objective value of each generation during the runs. The objective value increases to 1.71 at the first generation and between the generation 2 and 16 the objective values were constant at 2.06. From the generation 16 the objective function increases to 2.36 at generation 17. The

fitness value increases from generation to generation making the solution better. At the generation 22 to 23 increases to 2.72, the objective function remains constant to generation 100 there was no improvement in the objective functions (at 2.72). There may be some distortion in generations due population diversity. Similarities and distance between individuals or chromosomes may be the reason. The higher the objective values the small the error in the target.

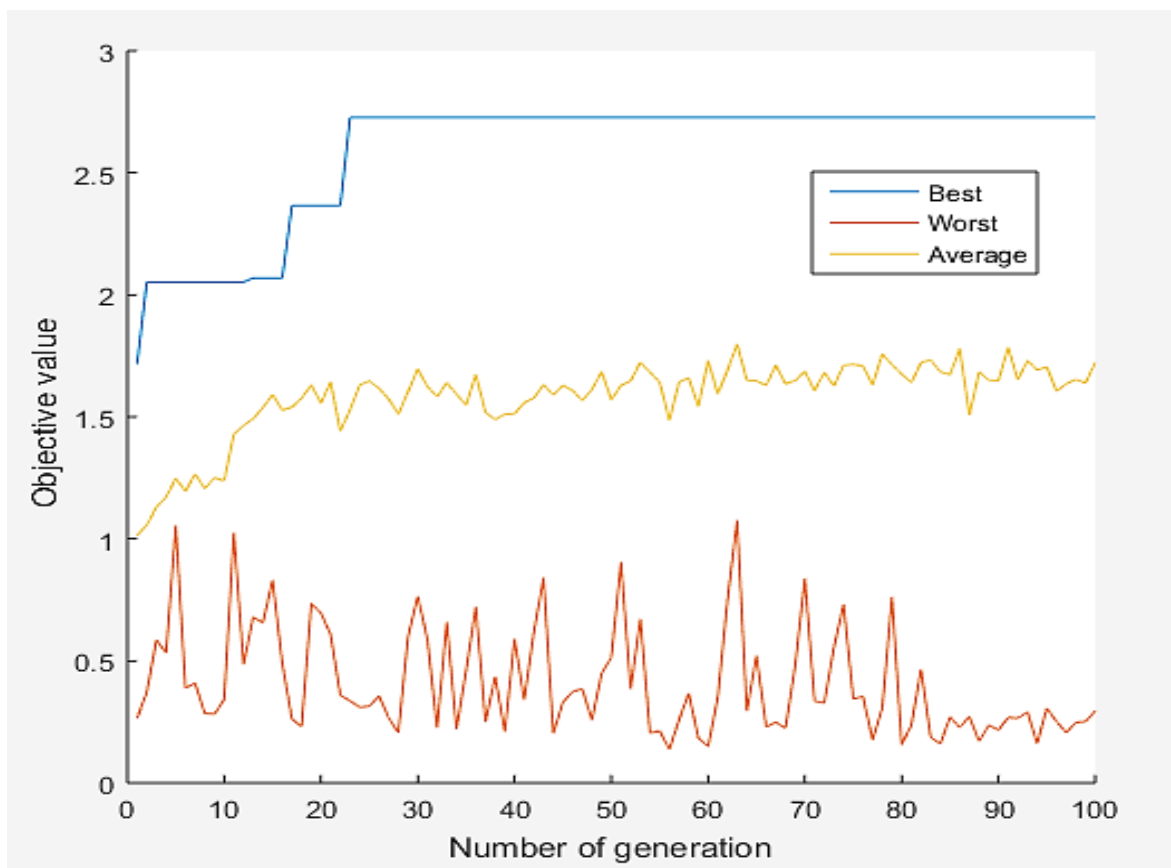


Figure 3.10(a) GA-optimised solutions after 100 generations.

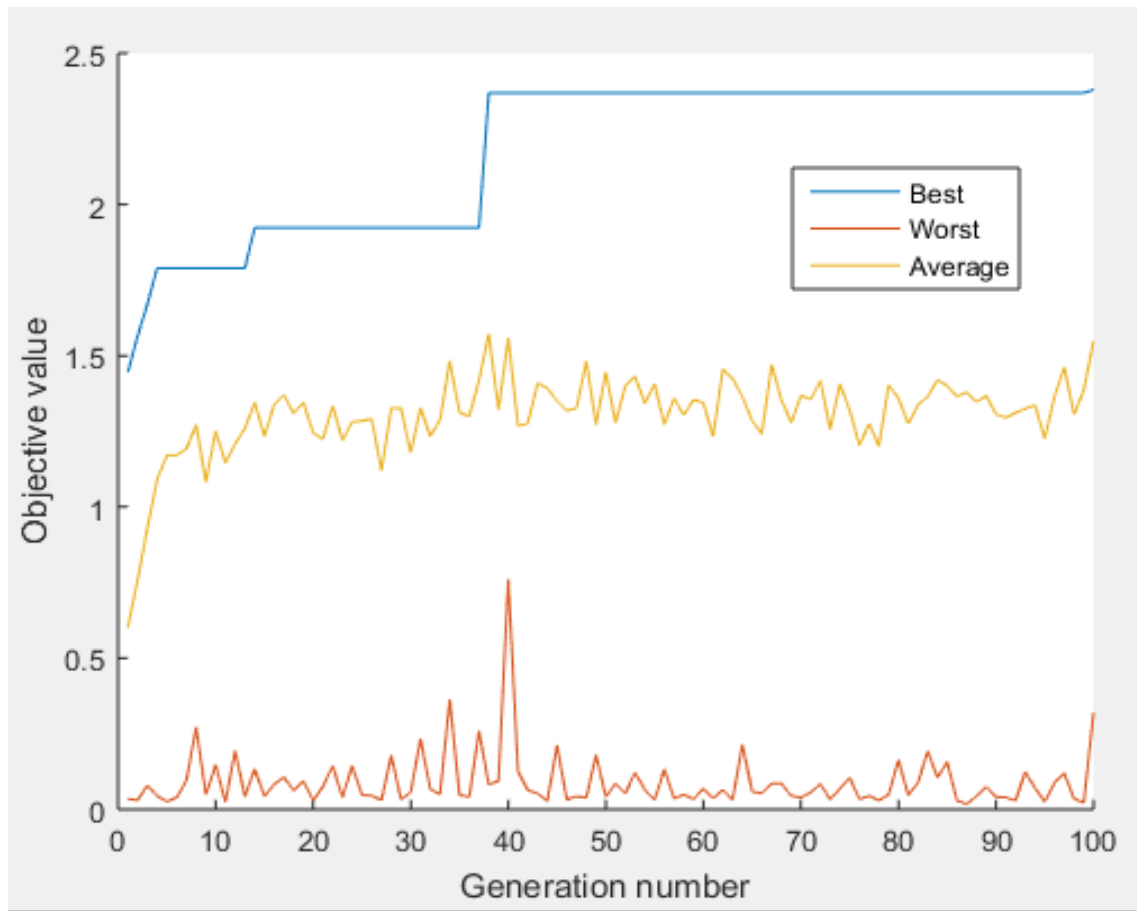


Figure 3.10(b) GA-optimised solutions after 100 generations.

Based on the GA-NEC2 process, a population of thirty individuals has 30 % overlap from generation to generation. The GA runs was stopped after a hundred generations were completed. The GA goal is optimised wire antennas with a centre frequency of 900 MHz at acceptable  $S_{11}$ . Figure (3.12-3.22) represent some selected antenna samples for fabrication. Their dimensions are in Table 3.4 and Table 3.5. The wire antenna dimensions,  $S_{11}$  values, objective function and fitness values are shown based on the GA convergence since no improvement average scores. The probability that there will be significant change if several generations are evolved is low.

### 3.9.1. Pocket antennas

The pocket antenna is visualised as a wire antenna in Fig.3.11. The wire antenna could be stitched on the front pocket of shirt and covered with fabric materials. All the linear wire antennas were design and optimised inside a static boundary using the bounding box

geometry. The bounding box has been created in the shape of shirt front pocket. Intersection point between the wire antennas and the bounding box was determined using line intersect analysis. The possibilities of the both shapes intersecting was eliminated by developing the polygon shape first and connecting the final point and first points.

The data consists of antenna segment, coordinates, ground plane, excitation source, operating frequency of antenna, number of frequencies, radiation pattern, and loading parameter. Antennas were designed within a bounding box as on the front pocket of shirt. In designing wearable antennas, placement is critical because the antennas should be positioned on the areas that have low movement/ flexibility even when the body is in motion.

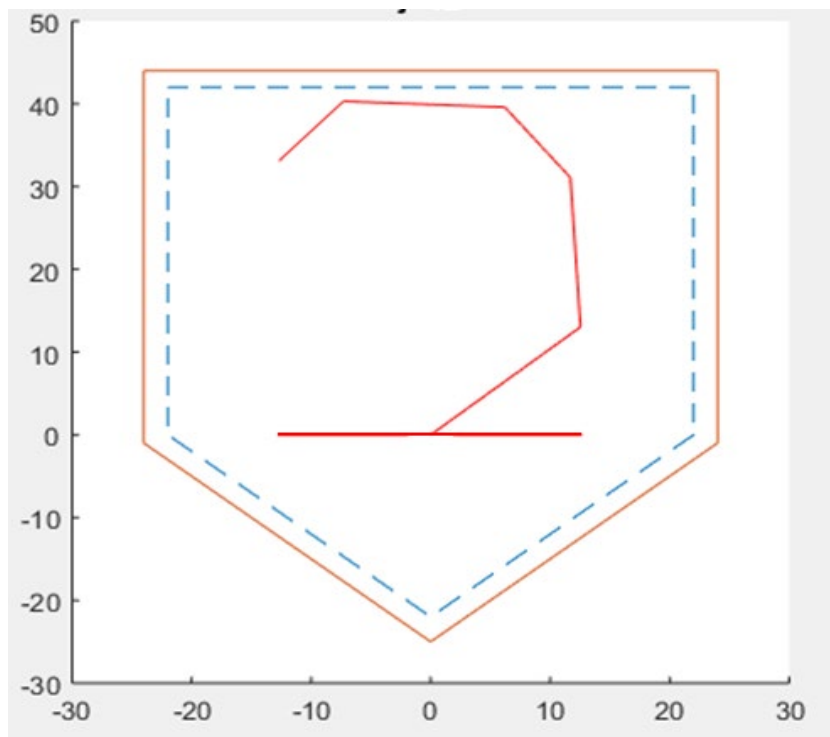
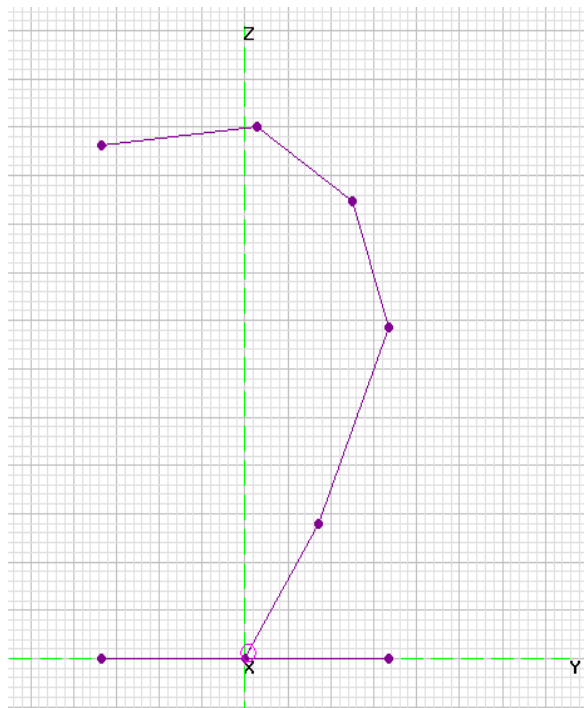


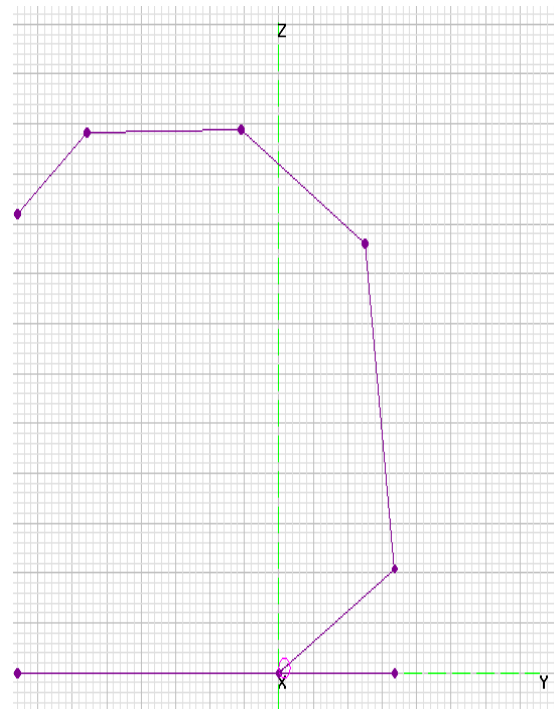
Figure 3.11 Wire antennas on Shirt front pocket design

Table 3.4 Optimised samples of wire antennas for shirt pocket

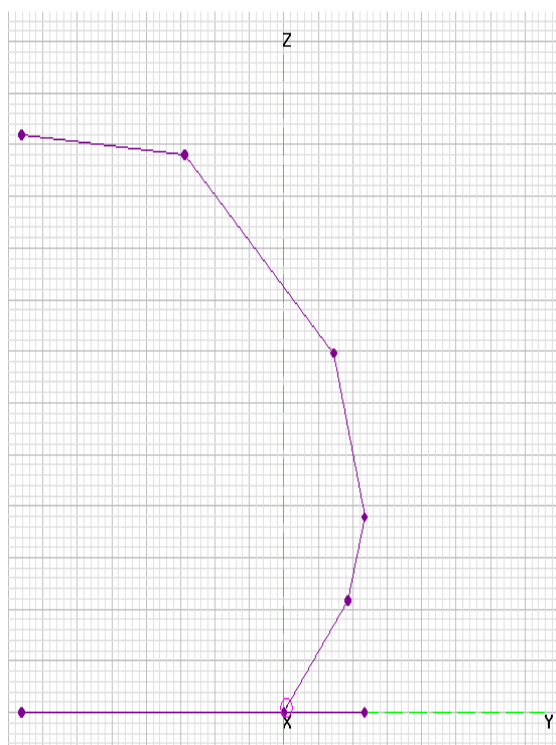
| Antenna samples     | Pocket A | Pocket B | Pocket C | Pocket D |
|---------------------|----------|----------|----------|----------|
| $L_1$ (mm)          | 12.96    | 16.68    | 19.21    | 11.15    |
| $\theta_1$ (degree) | 49.11    | 42.25    | 26.12    | 57.55    |
| $L_2$ (mm)          | 24.09    | 10.86    | 48.90    | 14.93    |
| $\theta_2$ (degree) | 46.68    | 53.67    | 52.00    | 32.50    |
| $L_3$ (mm)          | 9.38     | 16.09    | 17.64    | 29.02    |
| $\theta_3$ (degree) | 42.27    | 35.48    | 50.82    | 35.79    |
| $L_4$ (mm)          | 23.69    | 10.91    | 22.52    | 10.01    |
| $\theta_4$ (degree) | 30.97    | 45.78    | 57.14    | 45.48    |
| $L_5$ (mm)          | 20.52    | 11.99    | 19.06    | 14.90    |
| $\theta_5$ (degree) | 48.00    | 54.66    | 49.54    | 36.89    |
| $L_6$ (mm)          | 16.75    | 12.42    | 11.71    | 16.81    |
| $L_7$ (mm)          | 16.74    | 21.06    | 38.08    | 39.68    |
| $S_{11}$ (dB)       | -22.50   | -17.70   | -19.34   | -24.47   |
| Objvalue            | 2.47     | 2.72     | 2.53     | 2.36     |



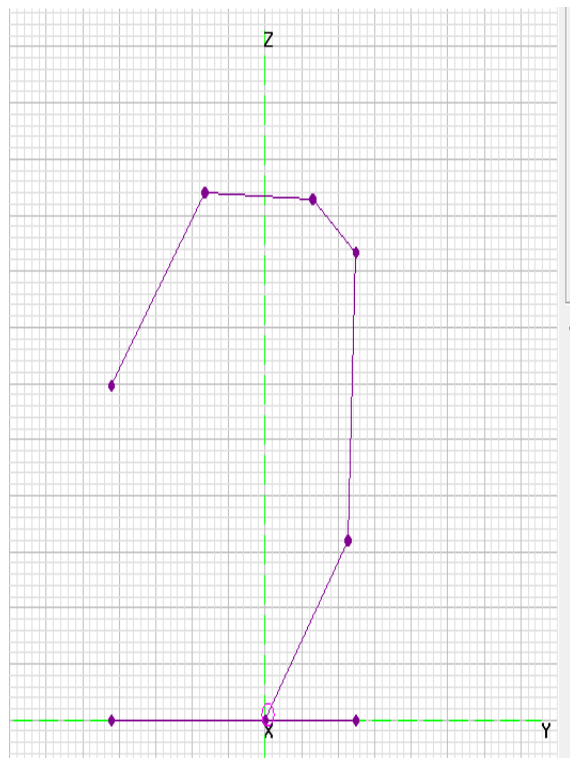
Pocket A



Pocket C



Pocket B



Pocket D

Figure 3.12 Geometry of pocket antennas

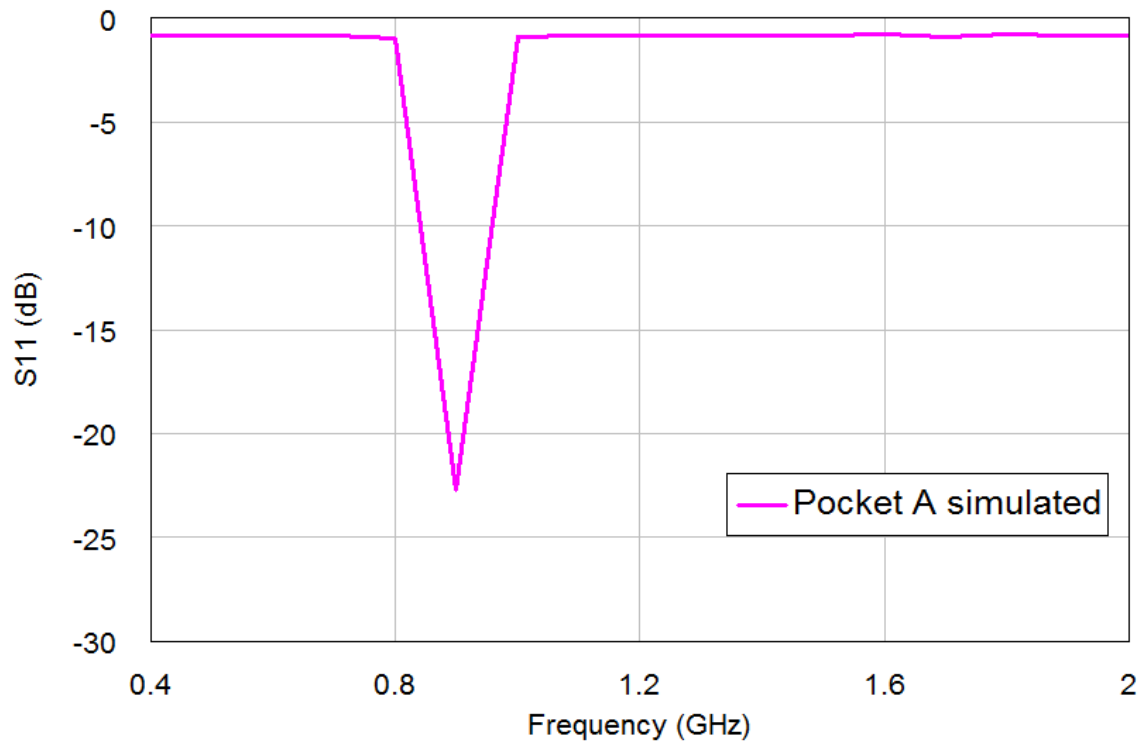


Figure 3.13 Simulated  $S_{11}$  of Pocket A

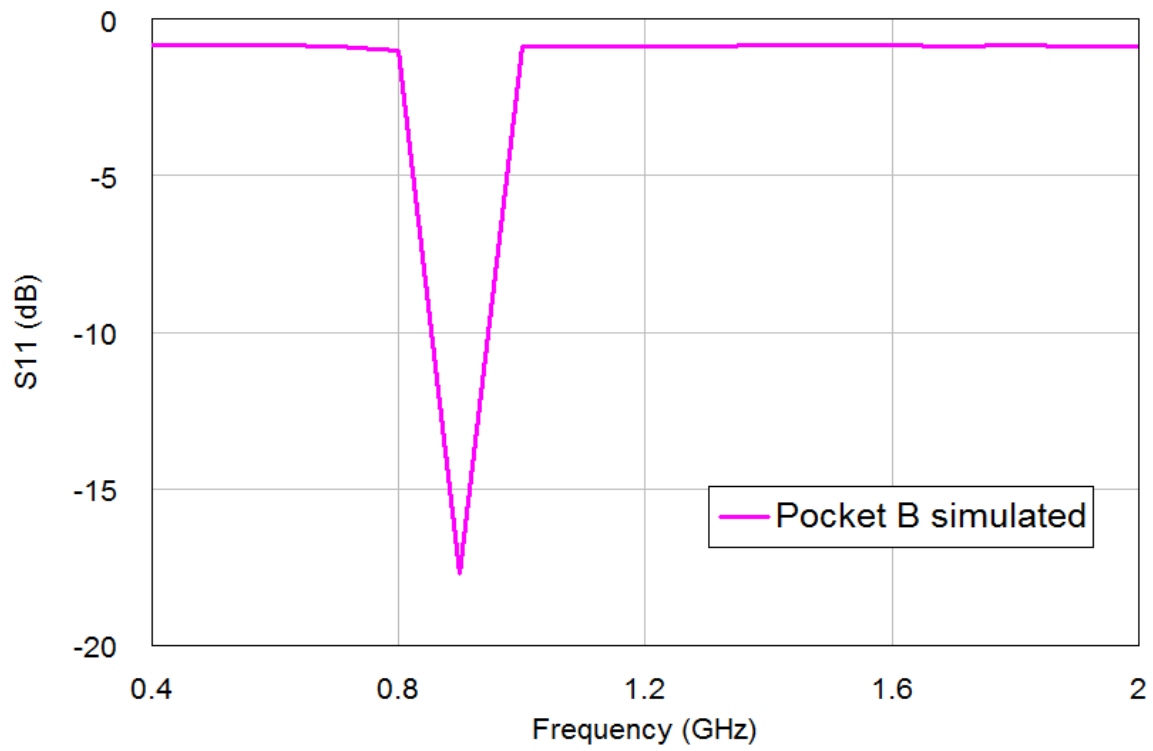


Figure 3.14 Simulated  $S_{11}$  of Pocket B



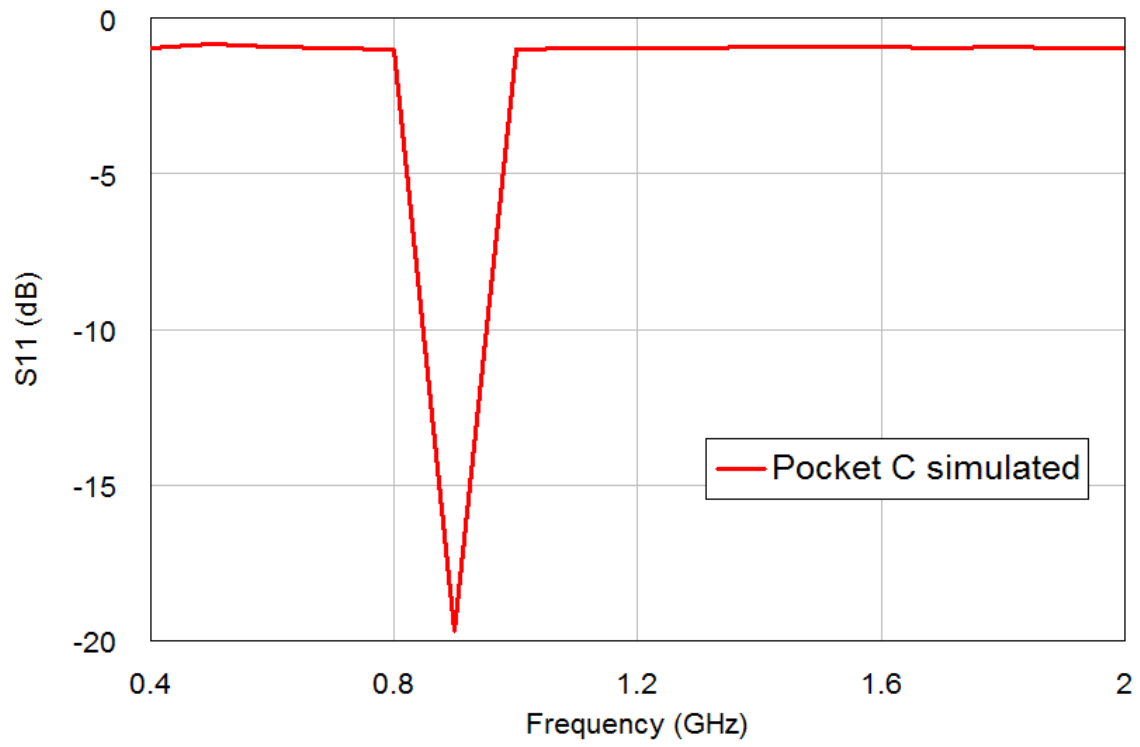


Figure 3.15 Simulated  $S_{11}$  of Pocket C

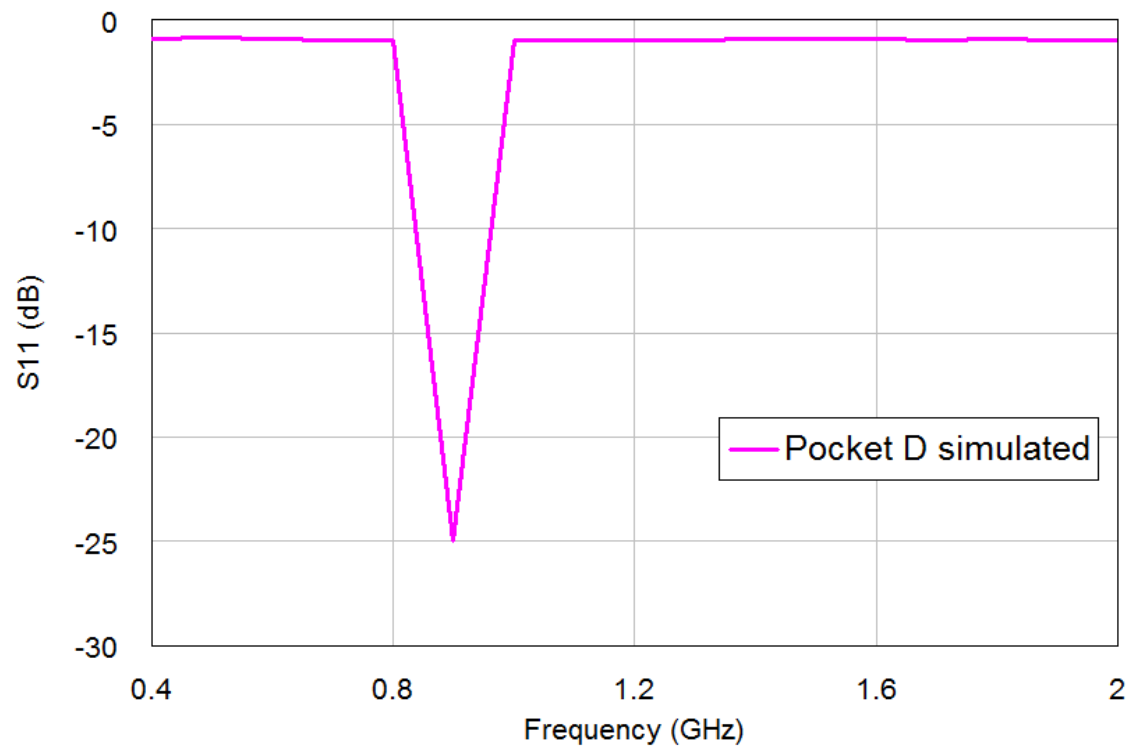


Figure 3.16 Simulated  $S_{11}$  of Pocket D

### 3.9.2. Collar antennas

The wire antennas with a fixed ground plane on the collar were optimised using the genetic algorithm. The collar used the seam around the edges as ground. Figure 3.17 demonstrate how the wire antenna on the collar can be connected to electronics. One advantage to this is that the collar sits further away from the body.

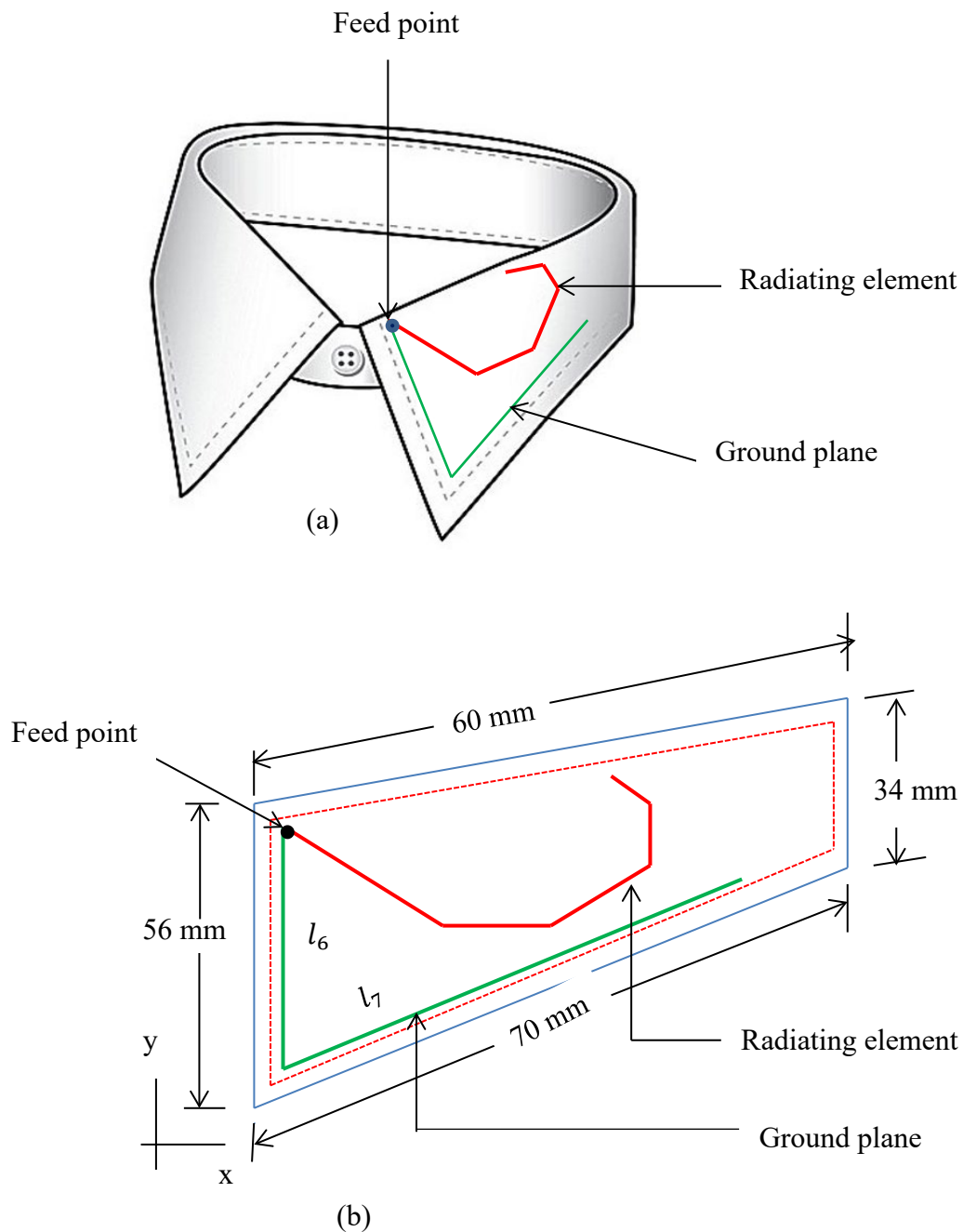
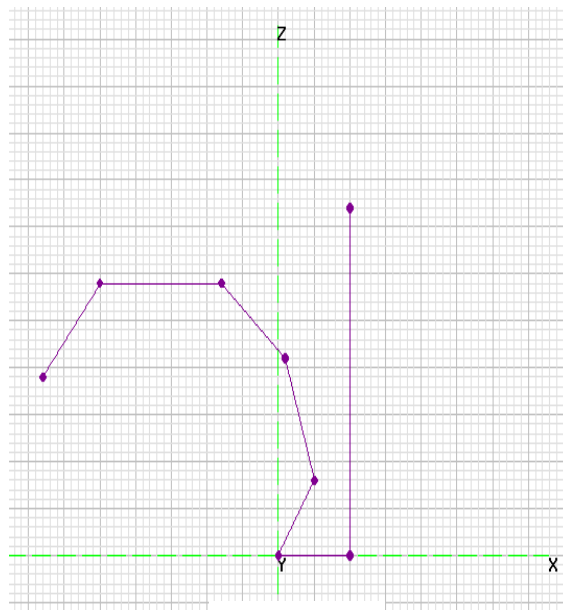
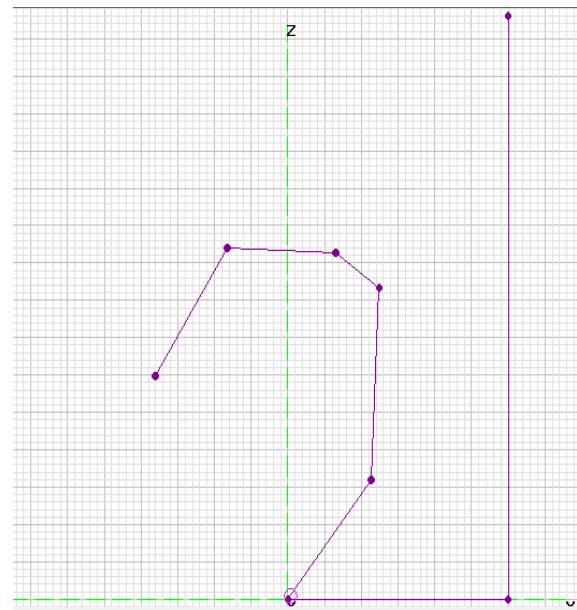


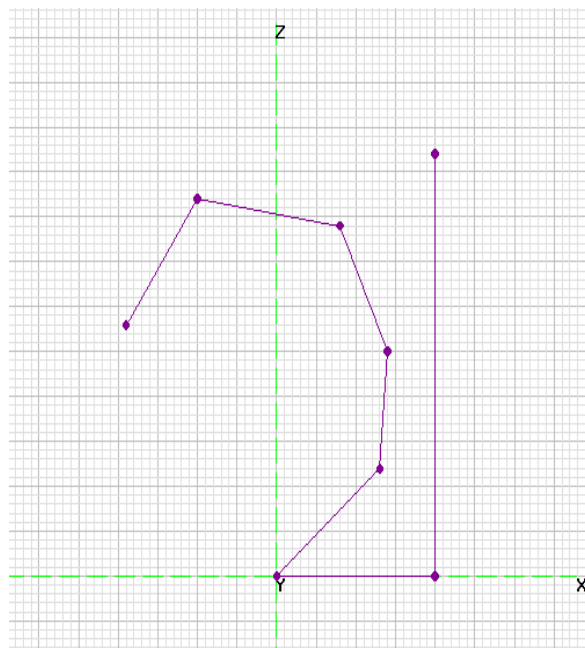
Figure 3.17 Diagram of the antenna in a shirt collar showing (a) the garment in its natural shape (adapted from [3.43]) and (b) the planar implementation.



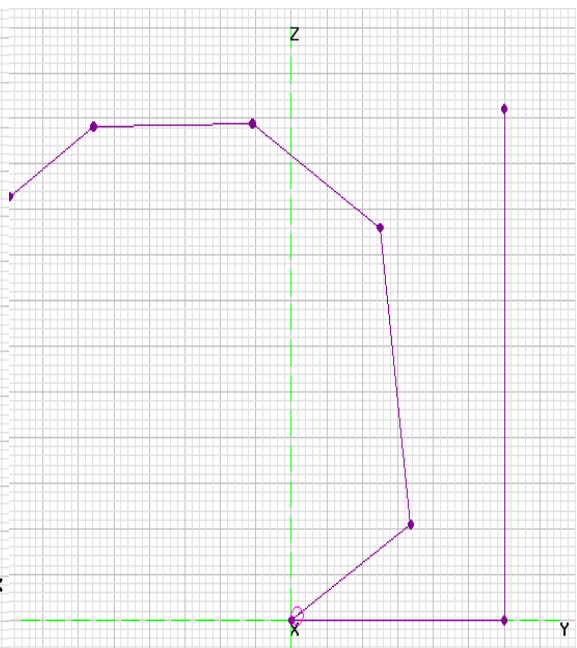
Collar A



Collar C



Collar B



Collar D

Figure 3.18 Geometry of collar antennas

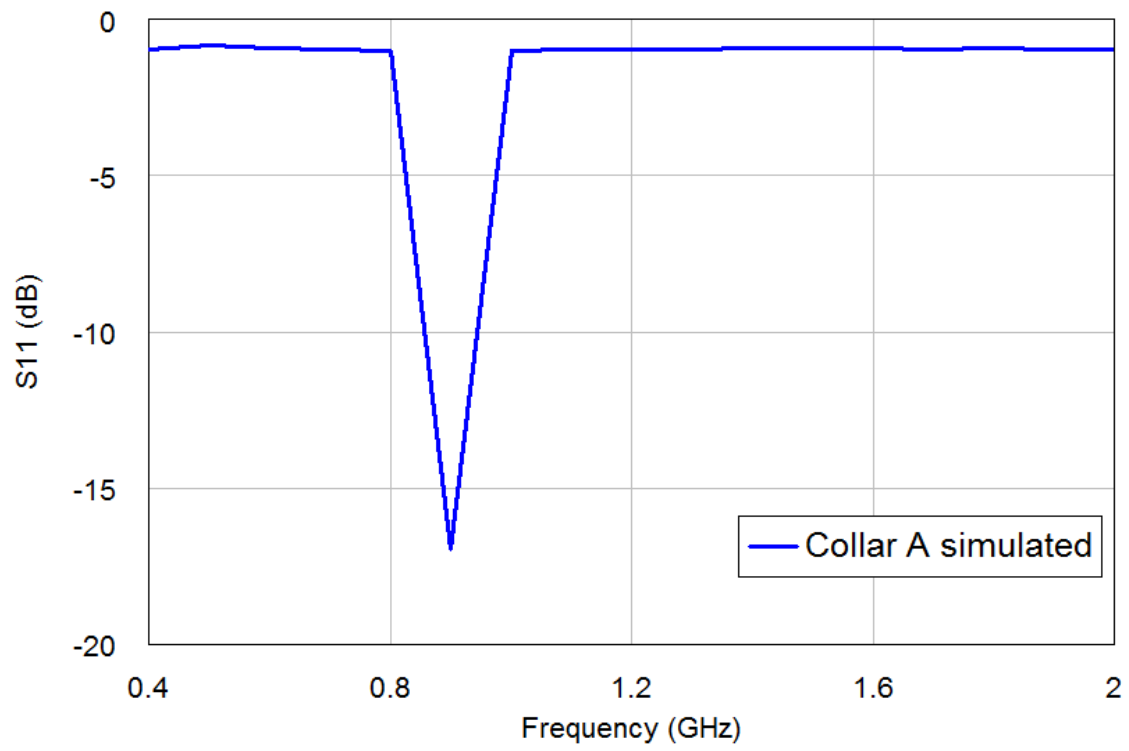


Figure 3.19 Simulated  $S_{11}$  of Collar A

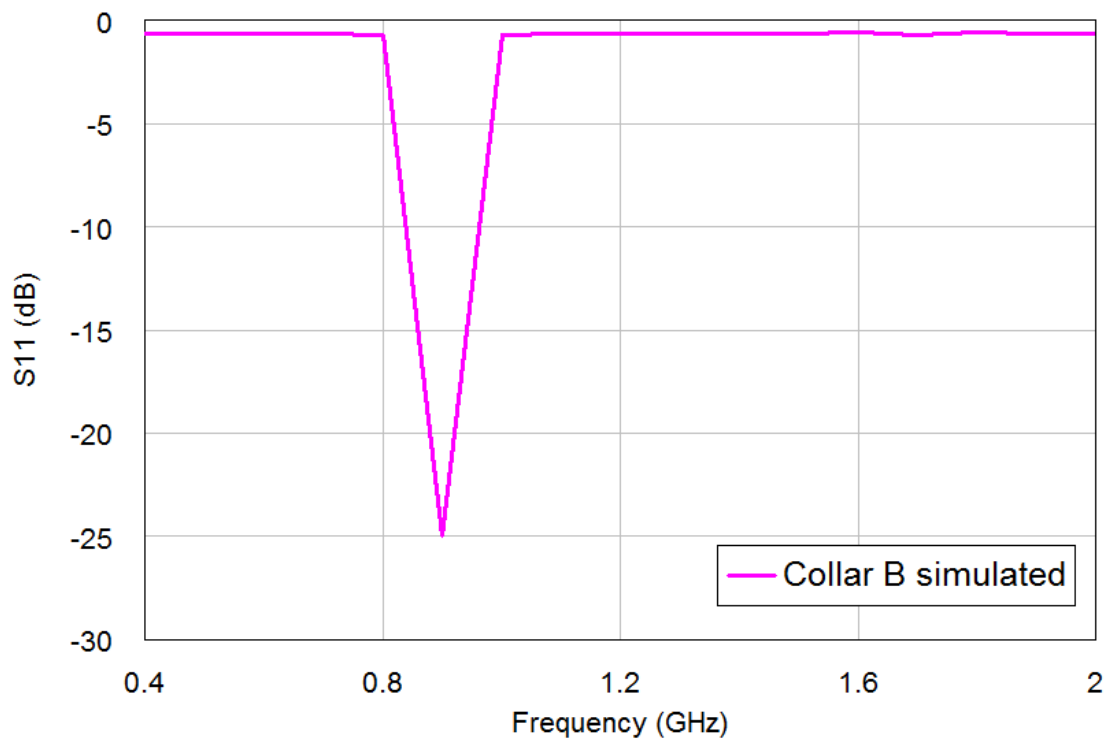


Figure 3.20 Simulated  $S_{11}$  of Collar B

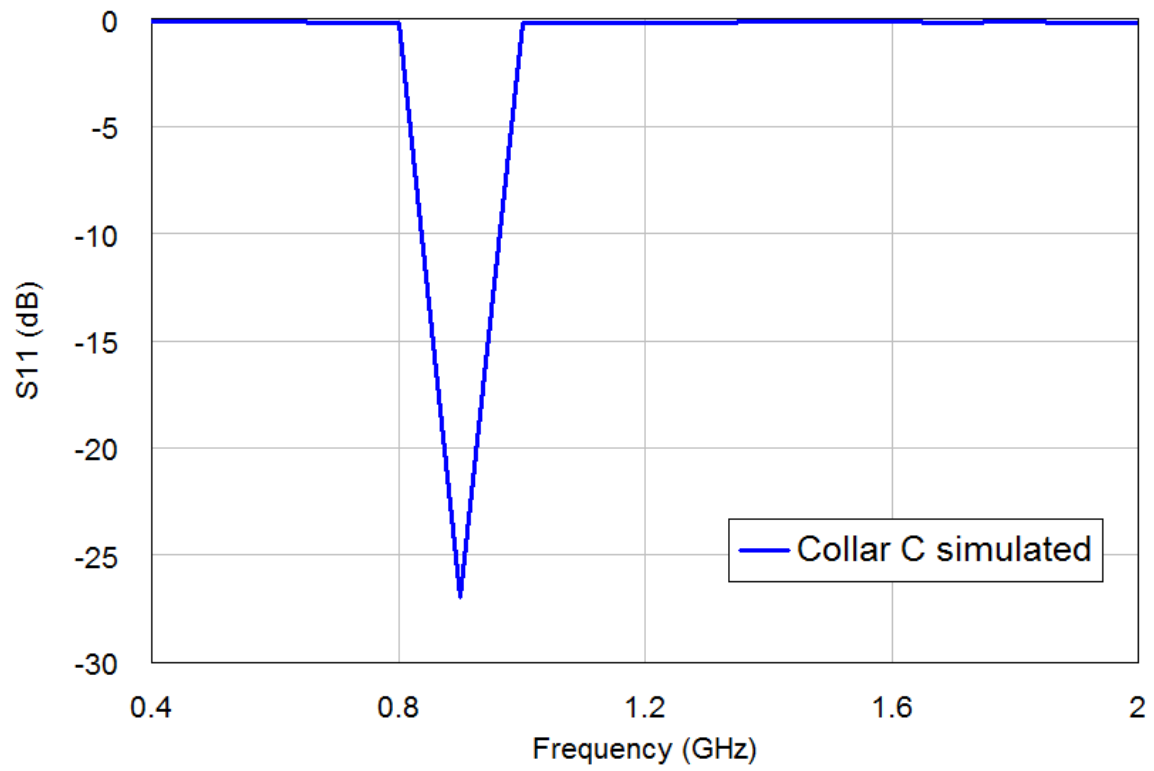


Figure 3.21 Simulated S<sub>11</sub> of Collar C

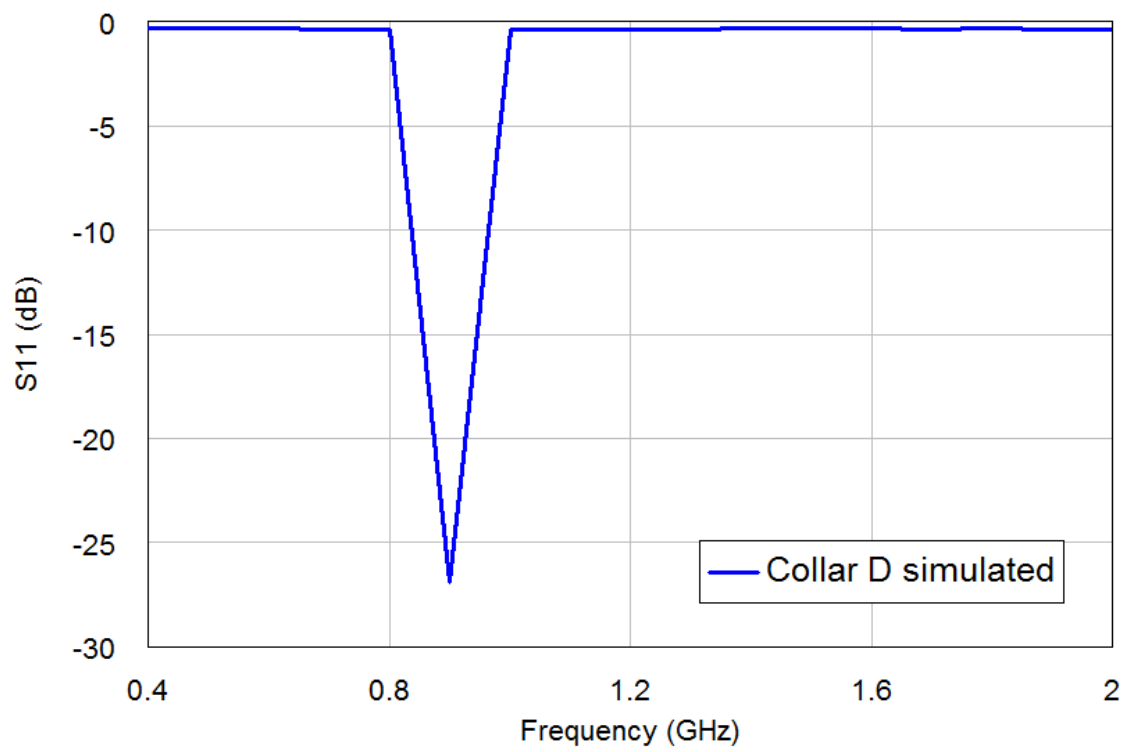


Figure 3.22 Simulated S<sub>11</sub> of collar D

Table 3.5 Optimised samples of wire antennas for collar

| Antenna samples     | Collar A | Collar B | Collar C | Collar D |
|---------------------|----------|----------|----------|----------|
| $L_1$ (mm)          | 28.63    | 23.77    | 17.93    | 16.85    |
| $\theta_1$ (degree) | 43.88    | 43.78    | 36.20    | 44.43    |
| $L_2$ (mm)          | 10.01    | 18.02    | 14.09    | 27.12    |
| $\theta_2$ (degree) | 38.53    | 49.02    | 30.96    | 37.84    |
| $L_3$ (mm)          | 20.10    | 12.51    | 17.07    | 22.54    |
| $\theta_3$ (degree) | 43.02    | 31.77    | 32.53    | 51.14    |
| $L_4$ (mm)          | 15.55    | 17.93    | 13.69    | 13.69    |
| $\theta_4$ (degree) | 58.95    | 32.30    | 35.95    | 39.09    |
| $L_5$ (mm)          | 17.23    | 16.88    | 12.79    | 20.52    |
| $\theta_5$ (degree) | 43.75    | 45.96    | 36.33    | 34.85    |
| $L_6$ (mm)          | 24.82    | 14.77    | 14.24    | 14.07    |
| $L_7$ (mm)          | 53.58    | 55.15    | 45.77    | 38.92    |
| $S_{11}$ (dB)       | -16.73   | -24.81   | -26.88   | -26.77   |
| Objvalve            | 2.23     | 2.73     | 2.68     | 2.24     |

### 3.9.3. Summary

During the GA runs, parameters were evaluated quickly to determine whether they were appropriate for this GA and MoM optimisation. Once started, the process does not require any user input. Results are not always obtained immediately requiring several generations are evaluated. Observing the GA run, the run terminated if results obtained are not acceptable. Several generations are run before achieving the target solution. In the GA optimisation, the use of cross over, mutation and selection improve the fitness function in the next generation. These operators create a necessary variety in the GA runs and thereby facilitate novelty in the use of this optimisation technique. The wire antenna was designed and fabricated in the form of pocket antennas and collar antennas were optimised using the optimised method. For the pocket antenna, a minimum return loss range of 17.70 dB - 24.47dB was realised at 900 MHz and, for the collar antenna, optimised return loss minimum range of 16.73 dB - 26.77 dB was evolved. Pocket and collar antennas are resonant at 900MHz.

## Conclusion

Comparisons were made between NEC and CST for wire antenna designs. The integration of a genetic search engine with an electromagnetic solver method for the design of linear wire antennas was used. Several numerical methods were considered for this design but the NEC2 solver which is designed for wire antennas, coupled with a genetic algorithm was chosen because of its robustness and consistency. In the process of these designs, several MATLAB scripts were written including `Meander_new.m`, `Lineintersect.m`, `writeInput.m`, `OptimisedGA.m`, `Newexecute.m`, and `PlotBoundary.m`. All these scripts were used in executing the automated design. The Genetic algorithm was explained as a means selecting optimal parameters of designed antennas.

One of the major advantages of this novel scheme for designing linear wire antennas is that it works without prior knowledge of any design equations. The method was used for determination of parameters of the antenna namely the segment length, angle, radius of the wire. The fitness function has been defined to optimise magnitude of the reflection coefficient. The controlled parameters of genetic algorithm were selected based on literatures reported in this Thesis. The fitness weighted selection method (based on ranking) was used in selecting the antennas for reproduction.

A real-valued code represents the design variables. In this real valued genetic algorithm, no coding and decoding of the antenna parameters is necessary. This makes the calculation efficient and easy to implement. Several GA generations were evolved in this study. Results was analysed based on the optimisation procedure. In the next chapter the fabrication, the measurement of optimised wire antennas and on body applications are analysed. Compact and novel antennas were selected and built based on their  $S_{11}$  response.

This chapter has presented the numerical results for two novel wearable antennas based on the linear wire. The first is designed for planar implementation on a shirt pocket. The second is for a collar.

## References

- 3.1. C.A. Balanis, "Antenna theory: analysis and design," John Wiley & sons. 2016.
- 3.2. M.M. Weiner, Monopole antennas. CRC Press, 2003.
- 3.3. R. Carter, "The Method of Moments in Electromagnetics, by W.C. Gibson," Contemp. Phys., 51, (2), pp. 183–184, 2010.
- 3.4. P.B. Johns, "A symmetrical condensed Node for the TLM method" IEEE Transactions on theory and techniques, Vol. MTT-35 (4) 1987 pp.370-376
- 3.5. M. Bartsch., "Solution of Maxwell's equations," Comput. Phys. Commun., 73(1–3), pp. 22–39, 1992.
- 3.6. J.D. Kraus and R.J. Marhefka, "Antennas for all applications," 3<sup>rd</sup> Ed. McGraw-Hill Education 2002.
- 3.7. H. Nakano, K. Hirose and J. Yamauchi, "Effects of arm bend on one-wavelength dipole antenna with asymmetric feeding" International Journal of Electronics, 56:1, 121-125, 2007. DOI: 10.1080/00207218408938799
- 3.8. J.R. Shewchuk. "An introduction to the conjugate gradient method without the agonizing pain." 1994 [Online Accessed: 04-October-2019]. Available from: <https://www.cs.cmu.edu/~quake-papers/painless-conjugate-gradient.pdf>
- 3.9. P. Hennig and M. Kiefel, 2013. "Quasi-Newton method: A new direction." Journal of Machine Learning Research, 14(Mar), pp.843-865.
- 3.10. G.B. Dantzig, "Origins of the simplex method." (No. SOL-87-5). Stanford University CA Systems Optimization Lab, 1987.
- 3.11. F.J. Solis and, R.J.B. Wets. "Minimization by random search techniques." Mathematics of operations research, 6(1), pp.19-30,1981.
- 3.12. D. Bertsimas and J. Tsitsiklis. Simulated annealing. Statistical science, 8(1), pp.10-15, 1993. [Online Accessed: 04-October-2019]. Available from: <https://www.mit.edu/~dbertsim/papers/Optimization/Simulated%20annealing.pdf>
- 3.13. E. E. Altshuler and D. S. Linden, "Wire-Antenna Designs Using Genetic Algorithms." IEEE Antennas Propagat. Mag., 39,pp.33-43 Apr.1997.
- 3.14. L. Kumar and N. K. Reddy, "Design of helical antenna using 4NEC2," Int. J. Eng. Res. Gen. Sci., 3 (2).
- 3.15. W. Comisky and J. R. Koza, "Automatic Synthesis of a Wire Antenna Using Genetic Programming," Late Breaking Papers at the 2000 Genetic and Evolutionary



- Computation Conference, Las Vegas, Nevada, pp. 179-186.
- 3.16. J. M. Johnson and Y. Rahmat-Samii, "Genetic algorithms in engineering electromagnetics," *IEEE Antennas Propag. Mag.*, 1997.
  - 3.17. R. L. Haupt and D. H. Werner, "Genetic Algorithms in Electromagnetics," John Wiley & Sons, Upper Saddle River, NJ, USA, 2007
  - 3.18. M. F. Pantoja, A.R. Bretones and R.G. Martin, "Benchmark antenna problems for evolutionary optimization algorithms," *IEEE transactions on antennas and propagation*, 55(4), pp.1111-1121, 2007.
  - 3.19. F. Streichert, "Introduction to Evolutionary Algorithms," *Evol. Algorithms Mol. Des.*, 8, pp. 1–13, 2008
  - 3.20. G. Jones, "Genetic and evolutionary algorithms," *Encycl. Comput. Chem.*, 2, pp. 1127–1136, 1998
  - 3.21. A. E. Eiben and J. E. Smith, "What is an Evolutionary Algorithm? Introduction to Evolutional Computation," pp.15–35, 2003. [Online]. [Accessed: 28-April-2018]. Available from: <https://www.cs.vu.nl/~gusz/ecbook/Eiben-Smith-Intro2EC-Ch2.pdf>
  - 3.22. A. Hoorfar, "Evolutionary programming in electromagnetic optimization: A review," *IEEE Trans. Antennas Propag.*, 55(3), pp. 523–537, 2007.
  - 3.23. B. Liu, H. Aliakbarian, Z. Ma, G.A. Vandenbosch, G. Gielen and P. Excell, "An efficient method for antenna design optimization based on evolutionary computation and machine learning techniques," *IEEE Trans. Antennas Propag.*, 62(1), pp. 7–18, Jan. 2014.
  - 3.24. D. W. Boeringer and D. H. Werner, "Particle Swarm Optimization versus Genetic Algorithms for Phased Array Synthesis," *IEEE Transactions on Antennas and Propagation*, AP-52(3), pp. 771-779, 2004.
  - 3.25. J. Kennedy and R. Eberhart, "Particle Swarm Optimization," *Proceedings of the 1995 IEEE International Conference on Neural Networks (Perth, Australia): IEEE Service Centre, Piscataway, NJ, IV*, pp 1942-1948.
  - 3.26. D. Karaboga, "An Idea Based On Honey Bee Swarm for Numerical Optimization, Technical Report-TR06," Erciyes University, Engineering Faculty, Computer Engineering Department, 2005.
  - 3.27. P. J. Angeline, "Evolutionary Optimization versus Particle Swarm Optimization: Philosophy and Performance Differences, Evolutionary Programming VII," *Lecture Notes in Computer Science*, Springer, 1447, pp. 601–610, 1998.

- 3.28. K.N. Krishnanand and D. Ghose, “Glowworm swarm optimization for searching higher dimensional spaces,” In: C. P. Lim, L. C. Jain, and S. Dehuri (eds.) *Innovations in Swarm Intelligence*. Springer, Heidelberg, 2009.
- 3.29. X. S. Yang and S. Deb., “Cuckoo Search via Levy Flights, ” *Proc. World Congress on nature and biologically inspired computing (NaBIC)*., pp 210–214, 2009
- 3.30. D. S. Linden, (1997). *Automated Design and Optimization of Wire Antennas using Genetic Algorithms* PhD thesis, ( 1997) MIT.
- 3.31. G. Hornby, A. Globus, D. Linden, and J. Lohn, “Automated Antenna Design with Evolutionary Algorithms,” *American Institute of Aeronautics and Astronautics*. vol. 5, pp. 1–8, 2006.
- 3.32. M. Dorica and D. D. Giannacopoulos, “Evolution of wire antennas in three dimensions using a novel growth process,” *IEEE Trans. Magn.*, 43, (4), pp. 1581–1584, 2007.
- 3.33. R.L. Haupt, “Antenna design with a mixed integer genetic algorithm,” *IEEE Transactions on Antennas and Propagation*, 55(3), pp.577-582, 2007
- 3.34. A. D. Chuprin., “Design of convoluted wire antennas using a genetic algorithm,” *IEEE Proc. Microw. Anten. Propag.* 148(5):323–326 2001.
- 3.35. R. Ghatak, D. R. Poddar, and R. K. Mishra, “Design of Sierpinski gasket fractal microstrip antenna using real coded genetic algorithm,” *IET Microwaves, Antennas Propag.*, 3(7), p. 1133, 2009
- 3.36. K. Deep and M. Thakur, “A new crossover operator for real coded genetic algorithms” *Applied Mathematics and Computation* 188, pp. 895–911, 2007.
- 3.37. K. S. N. Ripon, S. Kwong and K.F Man, “A real-coding jumping gene genetic algorithm (RJGGA) for multiobjective optimization,” *Information Sciences*, 177(2), pp.632-654, 2007.
- 3.38. F. Herrera., Lozano, M. and A.M, Sánchez, “A taxonomy for the crossover operator for real-coded genetic algorithms: An experimental study,” *International Journal of Intelligent Systems*, 18(3), pp.309-338, 2003.
- 3.39. D. E. Goldberg, “Real-coded Genetic Algorithms , Virtual Alphabets and Blocking,” *University of Illinois at Urbana-Champaign*, Technical Report No 90001, 1990.
- 3.40. A. H. Wright, “Genetic algorithms for real parameter optimization,” *Foundations. Genetic. Algorithms*, G.J.E. Rawlin(Ed.) (Morgan Kaufmann, Los Altos, CA), 1, pp. 205–220, 1990.

- 3.41. M. Safe, J. Carballido, I. Ponzoni, and N. Brignole, “On Stopping Criteria for Genetic Algorithms,” *Advance. Artif. Intell. – SBIA*, pp. 405–413, 2004.
- 3.42. C. R. Houck and M. G. Kay, “A Genetic Algorithm for Function Optimization : A Matlab Implementation,” *Ncsuie Tr*, 95(919), pp. 1–14, 2008.
- 3.43. Straight collar pattern. <https://www.pinterest.co.uk/pin/430093833134120819/>  
Accessed on 14-March-2018.

## **Chapter 4**

### **Implementation and Validation of the Optimised Antennas**

#### **4.1. Introduction**

The purpose of this chapter is to validate wire antenna and designs from the previous chapter. This will be explained in use of a more complex computational model and in fabrication. Two manufacturing approaches are given, firstly using a conventional planar method with good conductors (substrate base) and secondly using actual stitched devices and fabrics. The chapter also considers the manufacture of wider conductors using multiple stitched lines which becomes the focus of chapter 5.

This section also presents prototype antennas in the form of linear wire, planar and fabric antennas which are built and measured. Results in free space and on body are compared with simulated results. The effects of bending are shown in terms of resonant frequency and bandwidth. The antenna samples were optimised in free space in NEC2 without any dielectric loading. Four optimised linear wire antenna samples were fabricated on a FR-4 substrate of relative permittivity of 4.3 for mechanical support.

A design example is presented that has been optimised at 900 MHz. The method of moment (MoM-NEC2) and FIT (CST Studio Suite 2015) solvers are used for this design. MATLAB is used to as an interface to control NEC2 solvers for antenna design and analysis. The genetic algorithm procedures are written in MATLAB.

#### **4.2. Optimised linear wire antenna design**

Currently there is limited reported work on covert antennas. To make a wearable antenna practically and cost effectively it would be desirable if a stitching method such as embroidery could be used. Some assumptions considered are

- The antenna is intended to be hidden.
- It is not possible to change the space available for the antenna.

A wearable antenna will need consideration of the cost and performance trade off in terms of the amount of conductive yarn used. Using commercially available textile systems will provide a cost-effective production process. The ease of retrofitting antennas through basic embroidery, and ease of inclusion of standard embroidery machines in the projection line, are

the main driving factors. This thesis focuses on these issues as well as the electrical performance.

### 4.3. Measurement of linear wire antenna designs

Experiments were conducted using an Anritsu 37397D VNA for measuring scattering parameters ( $S_{11}$ ) of the designed antennas as shown in Fig. 4.1. The measurements were conducted on a test bench, experiments showed the environment had little influence on the results. The working frequency range from 400MHz to 2000MHz was selected and the VNA was calibrated using the Anritsu 36582KKF autocal module to minimise instrument errors and achieve the best possible results.

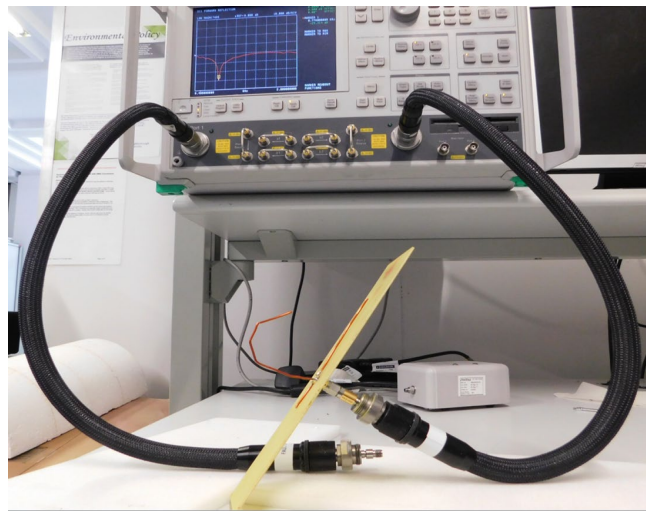


Figure 4.1 Measurement set up with Anritsu 37397D Vector Network Analyser

To meet the design requirements, several generations were evolved, and selection was implemented to get the best antenna design for fabrication and testing. Using the optimised results several prototype antennas were built. An example of the prototype is shown in Chapter 3. The NEC2 results were compared to CST simulations before fabrication. Possible sources of variations in the results can be put down to the CST mesh settings and the variation in the source position. It is shown that all the four antennas were well matched at their resonant frequencies. The return loss of pocket B is 21.29 dB at 900 MHz with 98MHz 10dB bandwidth.

The (pocket B) antenna was compared to the linear wire monopole in terms of  $S_{11}$  since both antennas have the same radiating length  $\lambda/4$  at 900MHz. The linear wire monopole was

simulated in CST and with an  $S_{11}$  result of  $-13.11\text{ dB}$  at  $893\text{ MHz}$ , a  $-10\text{ dB}$  bandwidth of  $51\text{ MHz}$  was produced. The linear wire monopole was designed using a linear wire ground plane of length  $120\text{ mm}$ . Measured  $S_{11}$  is  $-17.16\text{ dB}$  at  $896\text{ MHz}$  and  $-10\text{ dB}$  bandwidth of  $92\text{ MHz}$ . Measured and simulated  $S_{11}$  of the linear wire monopole against frequency is shown in Fig. 4.2. Good agreement was shown in the return loss characteristics. The simulated results give a resonant frequency which agrees with the measured result. Bandwidth is the useful range of operational frequencies of antenna and it is usually expected to be as large as possible. It is expressed in percent as the ratio of the useful span over the nominal operating frequency [4.1]. Figure 4.2 shows the simulation and measurement model of a linear wire monopole. The different in the results is due to the dielectric substrate, which may be affecting the upper resonance differently to the lower. There could also be dielectric resonances. Feed different is also different, as there is a wire attached in the measurement.

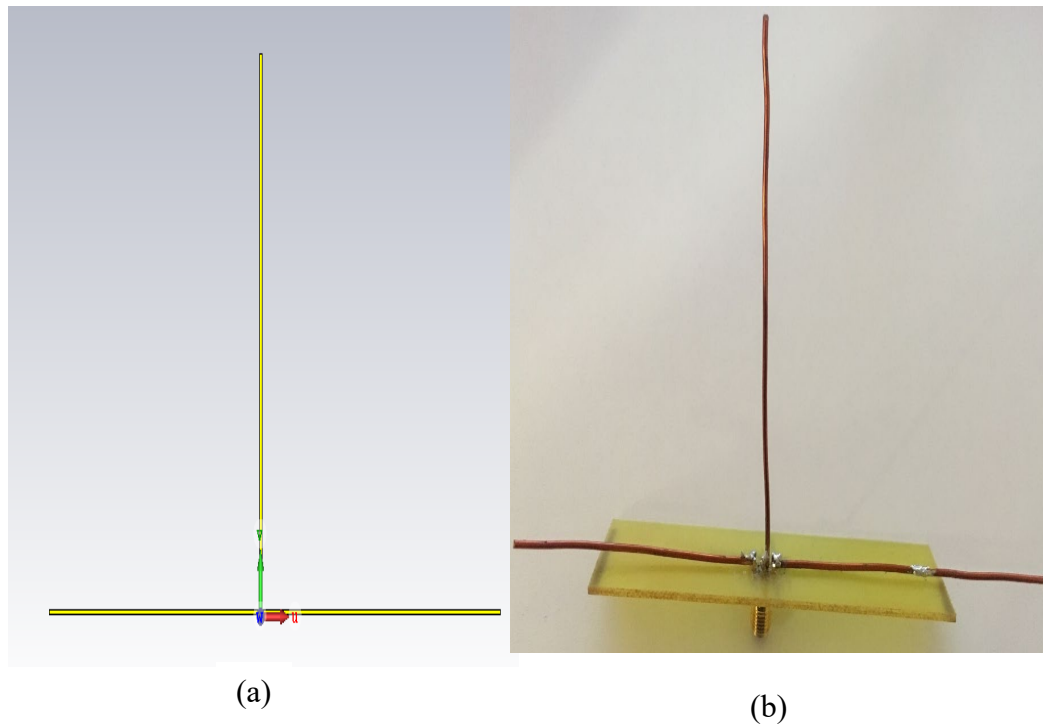


Figure 4.2 Simulation and measurement feeds of linear wire monopole (a) CST model and (b) fabrication model.

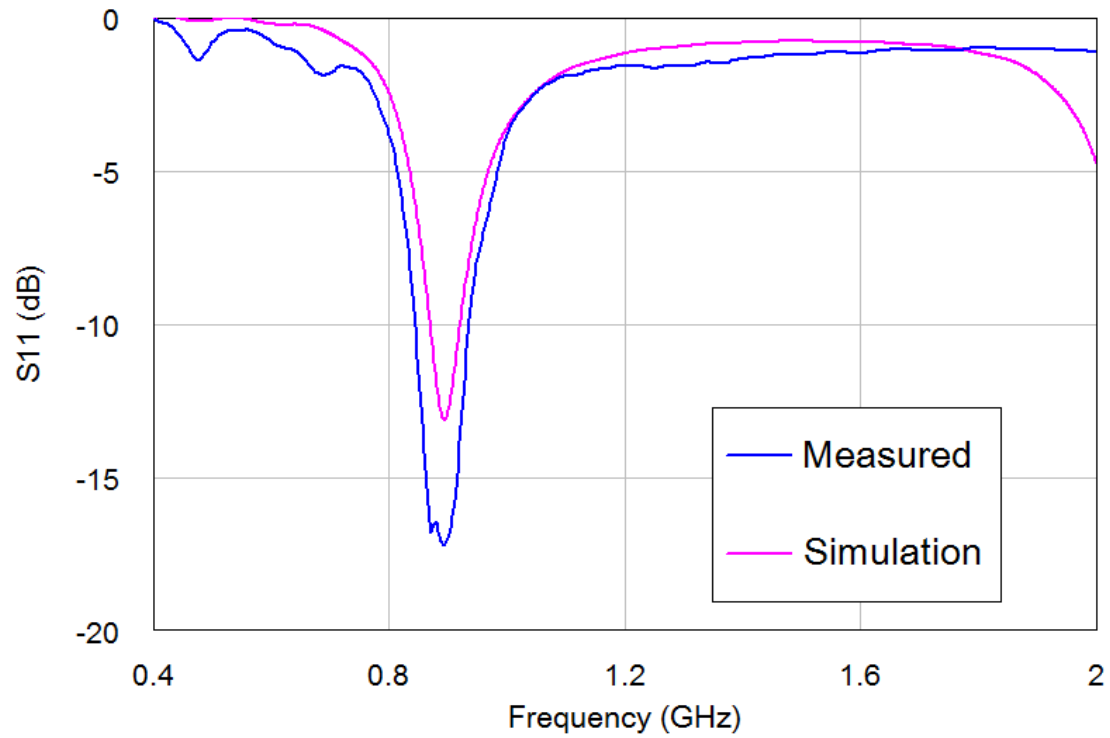


Figure. 4.3 Measured result  $S_{11}$  compared to simulation of linear wire monopole antenna

Figure 4.4 gives a comparison between the measured  $S_{11}$  of linear monopole antenna and pocket B (as one of the samples of the optimised pocket antennas). Measured  $S_{11}$  of pocket B is  $-21.41\text{dB}$  at  $900\text{ MHz}$  with  $-10\text{ dB}$  bandwidth of  $100\text{ MHz}$ . A Pocket B has a bandwidth of  $11.1\%$  while the linear wire monopole has a bandwidth of  $10\%$ . The picture of pocket antenna B is shown in Figure 4.6.

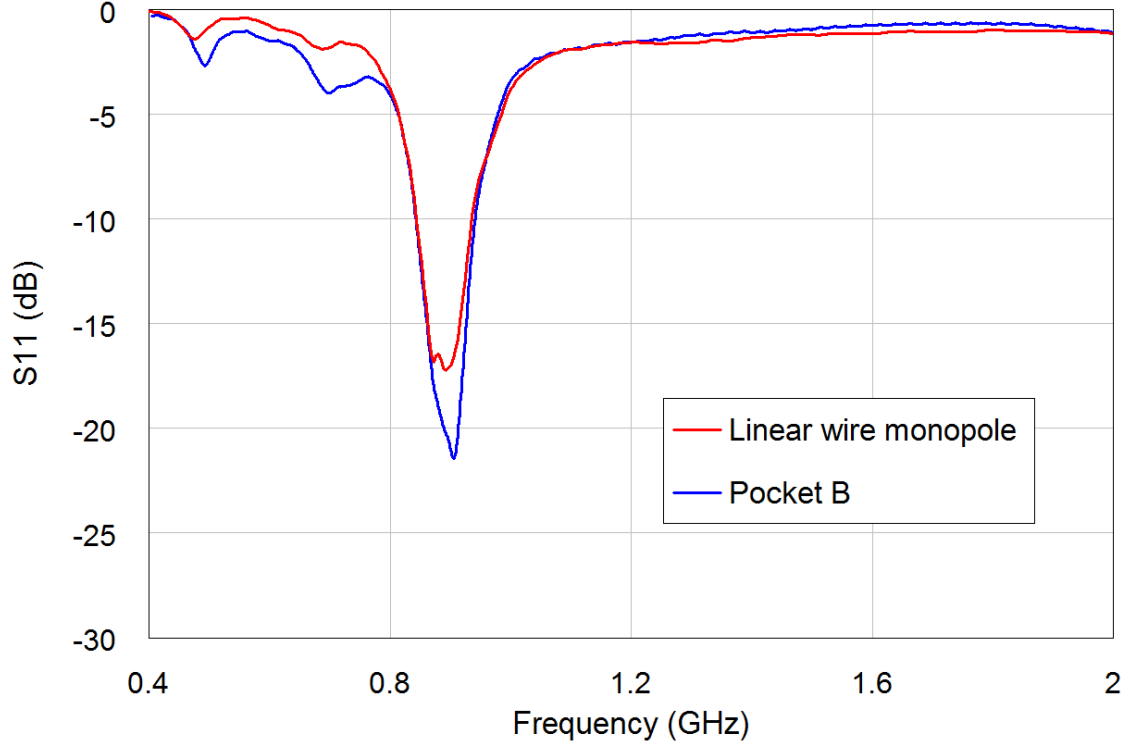


Figure 4.4 Comparison of measured  $S_{11}$  of linear and pocket B antennas

The geometry of the proposed antenna was presented in chapter 3. The antenna consists of 5 segments and 5 angles between the segments. The ground is a linear wire of radius  $r$  and given as  $l_6 + l_7$ . The total length of the antenna  $l_T$  is  $l_1 + l_2 + l_3 + l_4 + l_5$ . The linear wire antenna length  $l_T = \lambda/4$ , where  $\lambda$  is the wavelength corresponding to design frequency of 900MHz. Results were analysed from the GA run and four samples of linear wire antennas was selected based on the  $S_{11}$  parameter. The antenna samples were named Pocket A, Pocket B, Pocket C and Pocket D. The optimisation technique generated the resulting design parameters in Table 4.1 including summary of the total length and ground plane size of all four antennas. All four antennas, with different configurations were referred to as optimised pocket antennas. The antennas were fabricated using copper wire of radius 0.75 mm, based on the simulation results.



### 4.3.1. Radiation pattern

Figure 4.4 is a slight deviation of pocket A antenna from the linear wire monopole in the E-plane. Pocket A wire antenna gives a similar radiation pattern to the conventional linear wire monopole. In the H-plane, pocket A and linear wire antenna give an omnidirectional radiation pattern as shown in Fig. 4.5. Pocket A wire antenna shows a reduced gain only in the H-plane.

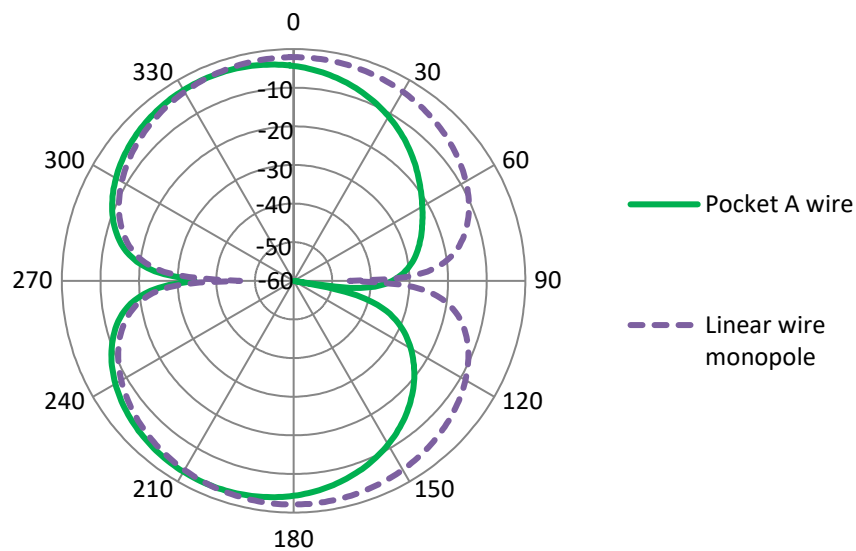


Figure 4.4 Simulated far field gain pattern (E-plane) of pocket A antenna

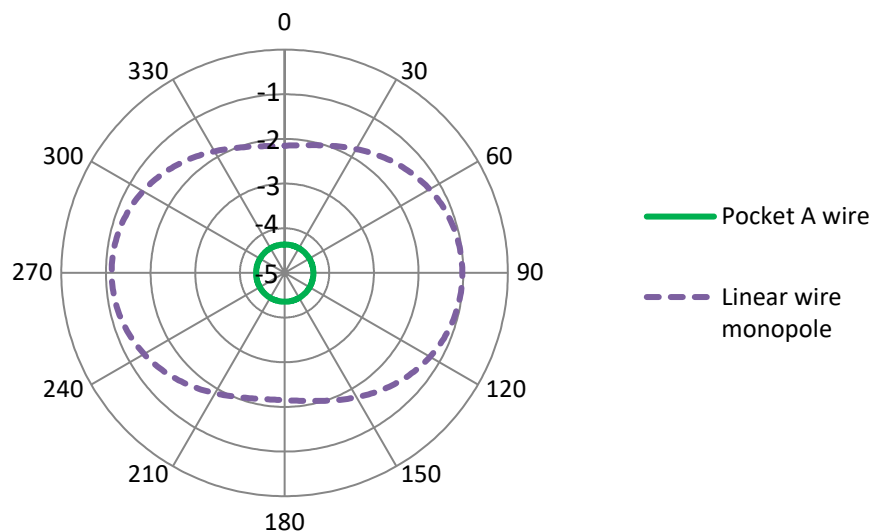
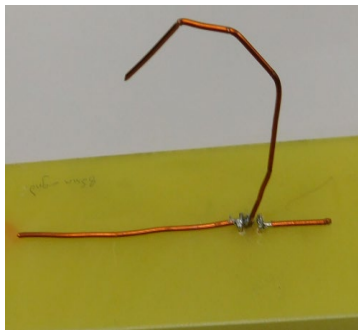


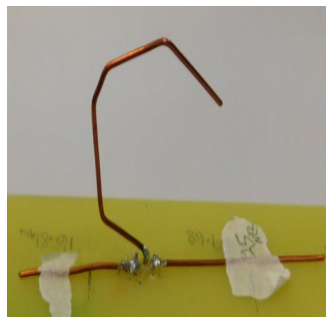
Figure 4.5 Simulated far field gain pattern (H-plane) of pocket A antenna

Table 4.1 Results of performance of Pocket antennas

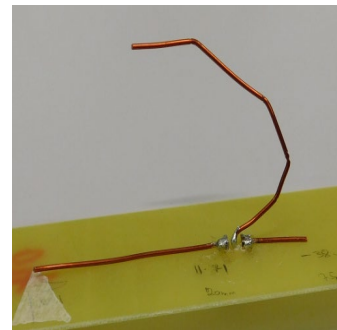
| Antenna number | $l_r$<br>(mm) | $l_6 + l_7$<br>(mm) | Resonant frequency<br>(MHz) | Simulated $S_{11}$ (dB) |        | Measured $S_{11}$ (dB) | -10dB Bandwidth<br>(MHz) | Radiated Gain (dBi) | Radiated Efficiency (%) |
|----------------|---------------|---------------------|-----------------------------|-------------------------|--------|------------------------|--------------------------|---------------------|-------------------------|
|                |               |                     |                             | NEC2                    | CST    |                        |                          |                     |                         |
| Pocket A       | 84            | 84                  | 900                         | -22.50                  | -12.45 | -15.07                 | 70                       | 2.34                | 83                      |
| Pocket B       | 86            | 78                  | 901                         | -17.70                  | 11.70  | -21.29                 | 110                      | 2.63                | 88                      |
| Pocket C       | 83            | 80                  | 897                         | -19.34                  | 14.45  | -22.83                 | 102                      | 2.54                | 87                      |
| Pocket D       | 85            | 78                  | 930                         | -24.47                  | 13.56  | -32.05                 | 127                      | 1.85                | 70                      |



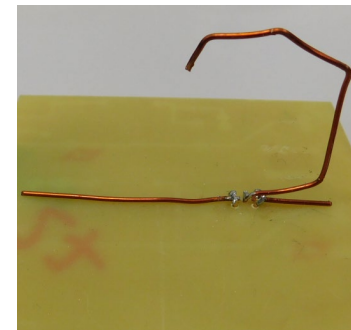
Pocket A



Pocket B



Pocket C



Pocket D

Figure 4.6 Photograph of pocket antennas

### 4.3.2. Effect of Linear wire antenna parameters on Resonant Frequency and Bandwidth

The magnitudes of  $S_{11}$  versus frequency (also known as return loss) for the 4 samples of optimised pocket antennas are shown in Fig. 4.7 – Fig. 4.11. Most of the radiated power of the 4 sample antennas will be within 850-950MHz. The measured return loss of the optimised linear wire antenna shows an impedance bandwidth with referenced to 900 MHz that covers the required bandwidth of the GSM system. These four linear wire antennas exhibit similar resonant ( $\lambda / 4$  in length) properties with centre frequency at 898MHz. Pocket A and Pocket B antennas exhibit similar performance characteristics except that their matched. Pocket A antenna has got the least -10dB bandwidth of 70MHz. The antennas show  $S_{11}$  resonance before the design frequency -1.954dB at 497.50MHz and -4.977dB at 691MHz. The measured  $S_{11}$  of the four linear wire antennas are Pocket A antenna is -15 dB at 903 MHz with 70MHz 10 dB bandwidth, Pocket C antenna has a return loss of 22.83 dB at 897MHz with 10 dB bandwidth of 102 MHz, Pocket B antenna has return loss of 21dB at 901 MHz with 10dB bandwidth of 110MHz while Pocket D antenna with  $S_{11}$  of -30.05 dB at 930 MHz and 10 dB bandwidth of 127 MHz

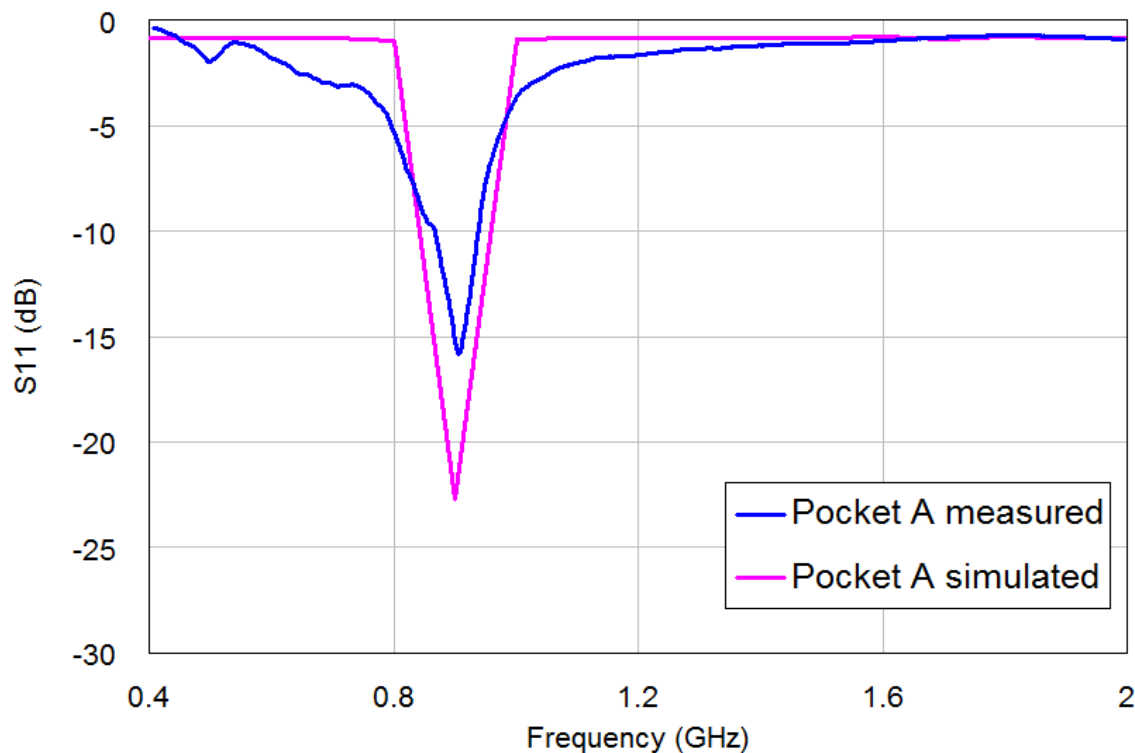


Figure 4.7 Simulated and measured  $S_{11}$  of the Pocket A

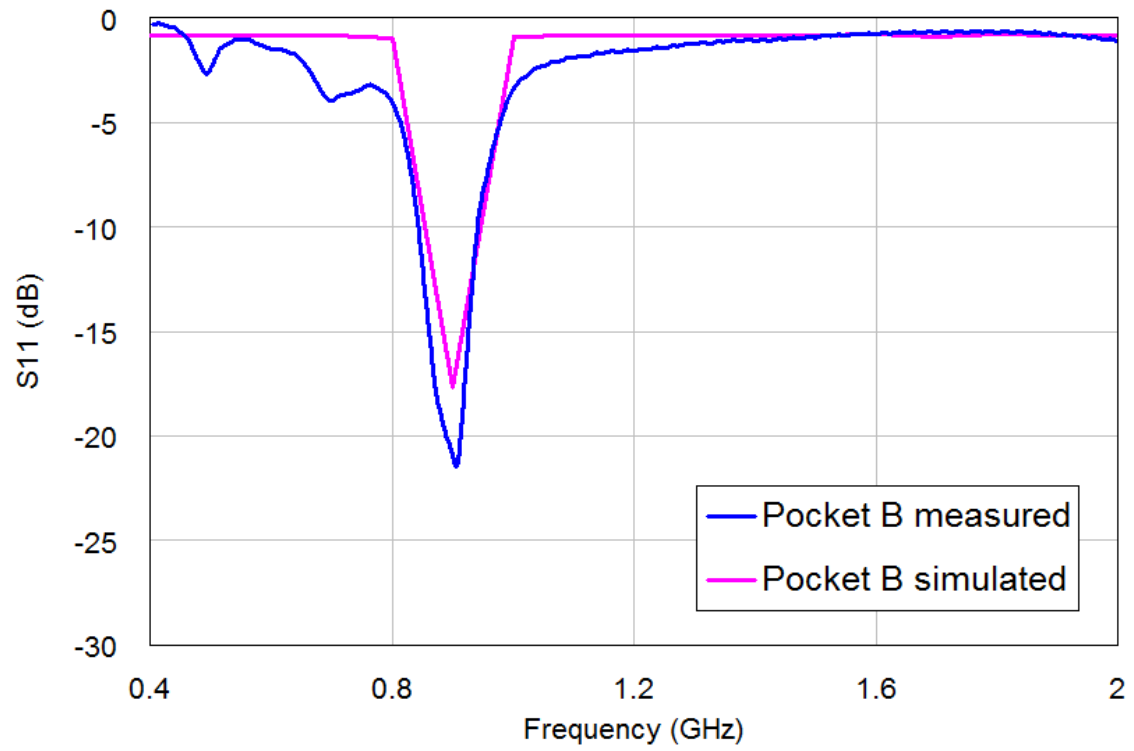


Figure 4.8 Simulated and measured  $S_{11}$  of the Pocket B

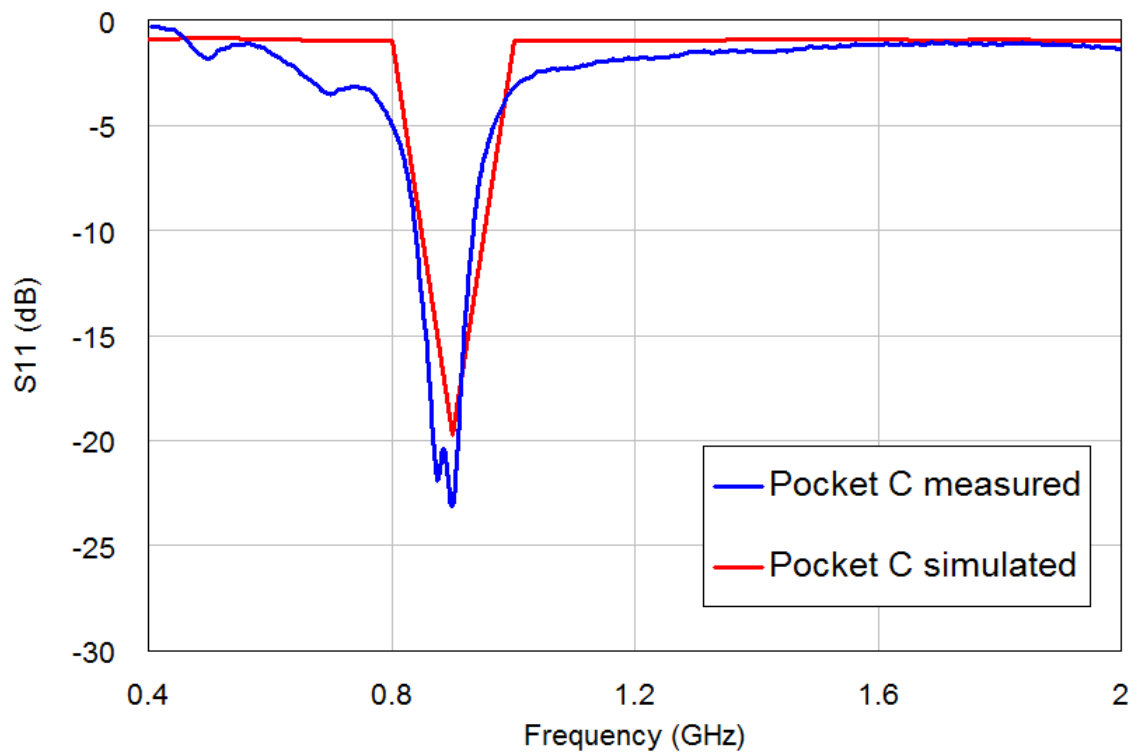


Figure 4.9 Simulated and measured  $S_{11}$  of the Pocket C

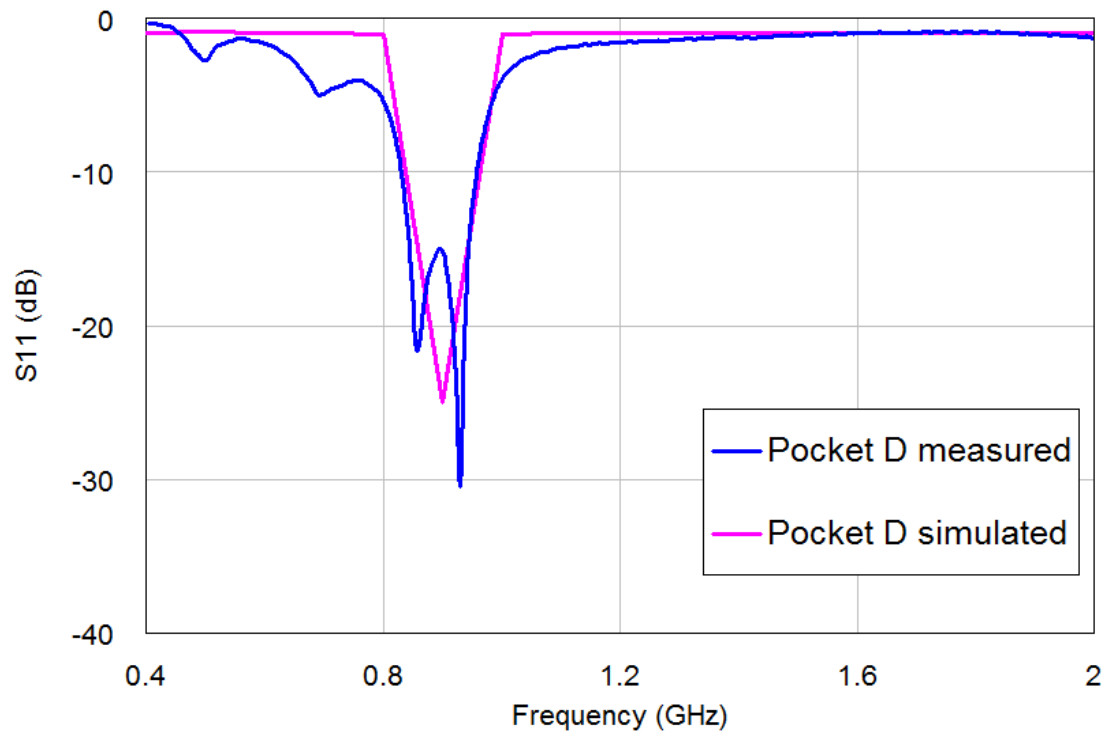


Figure 4.10 Simulated and measured  $S_{11}$  of the Pocket D

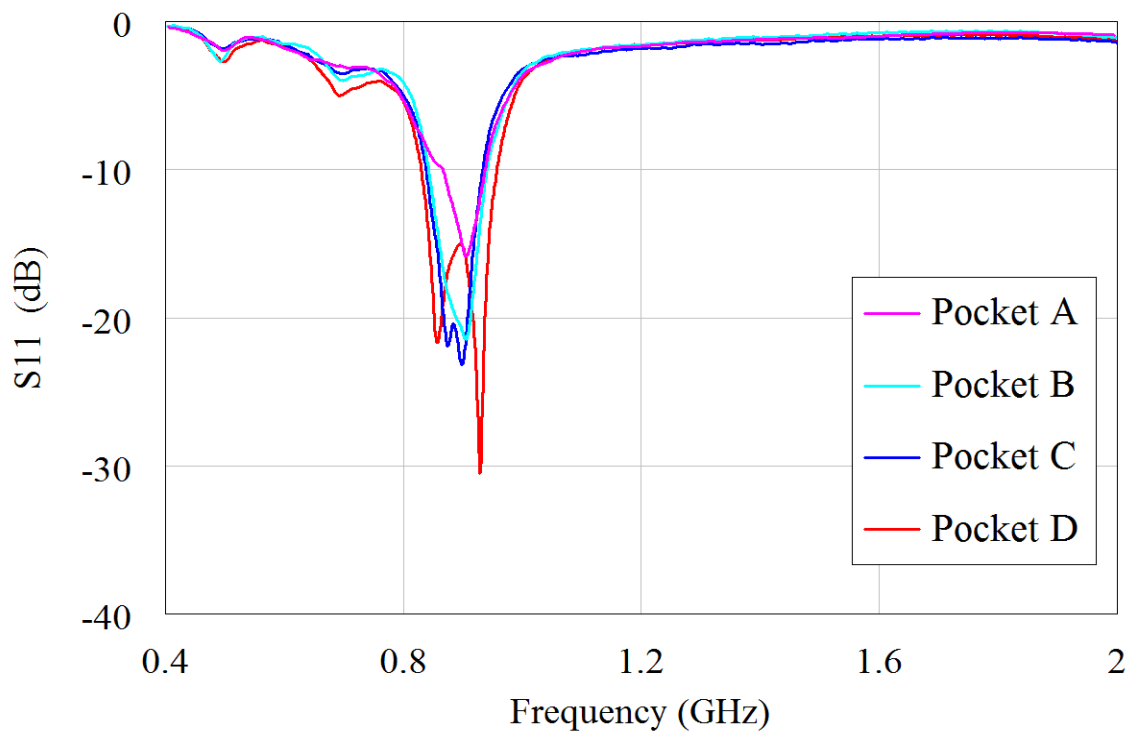


Figure 4.11 Measured  $S_{11}$  of pocket antennas

### 4.3.3. Radiation patterns

The radiation patterns of the optimised linear wire antennas were measured using 11point interpolation for each antenna on the 850 MHz to 950MHz range. The peak gain of antenna (Pocket B) is 2.63 dBi, while simulated peak gain is given as 1.44 dBi. The discrepancies in the results may be due the effects of the linear ground. Both pattern shapes are the same, but the main lobe is reduced because of the linear ground. The efficiency the ratio of the total radiated power to net power accepted by the antenna terminals was measured in the RF anechoic chamber giving 83%, 88%, 87%, and 70% for Pocket A, Pocket B, Pocket C and Pocket D respectively.

The elevation cut and azimuth cut were defined in section 2.3.2 from antenna radiation patterns. Four pocket antennas pattern were measured in the chamber. The antenna under test (AUT) was mounted on the positioner in horizontal plane as shown in Fig. 4.12. The AUT axis was aligned with the axis of the rotation for easy tracking from the transmitter. The  $y$ - $z$  plane (azimuthal plane) is more directive than the  $y$ - $x$  plane (elevation plane). From plots of the measured radiation patterns in Fig. 4.13, it is observed that pattern is stable but not completely Omni-directional but does give the antenna good coverage. The pattern includes a back lobe and minor lobes that may be due the effects of the linear ground plane. Ground plane is not perfectly conducting. The linear ground will resonate and radiate at certain frequencies.

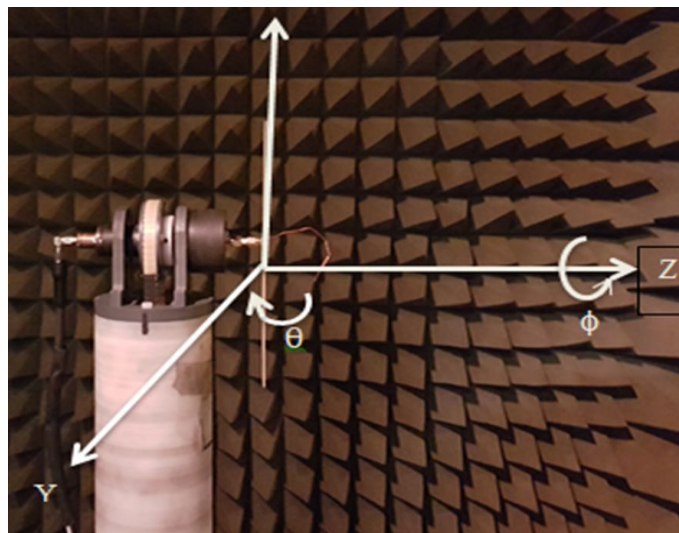
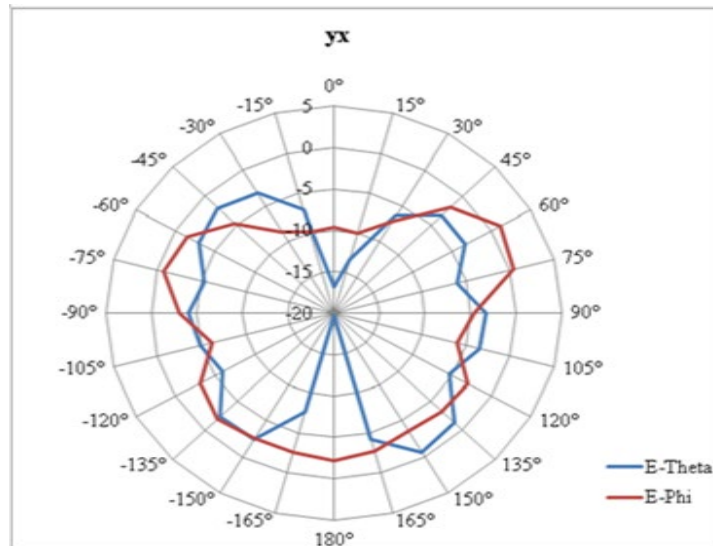
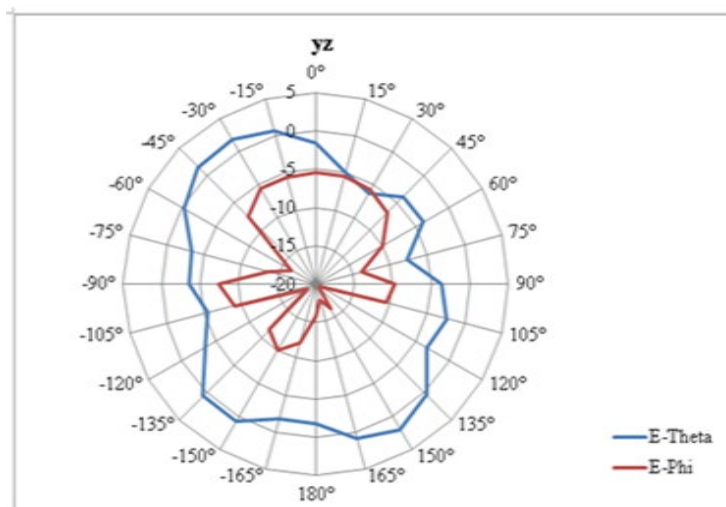


Figure 4.12 Linear wire antennas (Pocket B) in the anechoic chamber.

The ground planes of the wire monopole antennas were designed with an appropriate wire-grid model [4.2]. According to multipole expansion any current source that has a dimension smaller than the wavelength is close to an electric dipole for far field analysis. This basic reason gives the monopole antenna an omnidirectional radiation pattern.



(a)



(b)

Figure 4.13 Measured radiation pattern of linear wire antenna (Pocket B) at

(a)  $\Phi = 0^\circ$  (b)  $\Phi = 90^\circ$

#### 4.4. Planar version of linear wire antenna design

A planar wire antenna may be realised by replacing the radiating and linear ground elements of optimised linear wire antenna with a planar element. The planar version of the linear wire

antennas was designed and simulated in CST Studio Suite. The configuration of the linear wire antenna used for this planar design is shown in Fig. 4.14. This antenna has radiating length of  $\lambda/4$ . The top radiating section has five segments. The planar antenna was made of copper element. Planar antennas were produced through the etching process on a PCB. The electrical length is 84 mm with strip line width of 2 mm. The ground plane is 58 mm by 2 mm and antenna height of 56 mm. The ground plane dimensions are  $L_g$  of 58 mm and  $W_g$  of 10 mm. The PCB dielectric material used below the ground is FR4 thickness of 1.6 mm and a relative permittivity of 4.3.

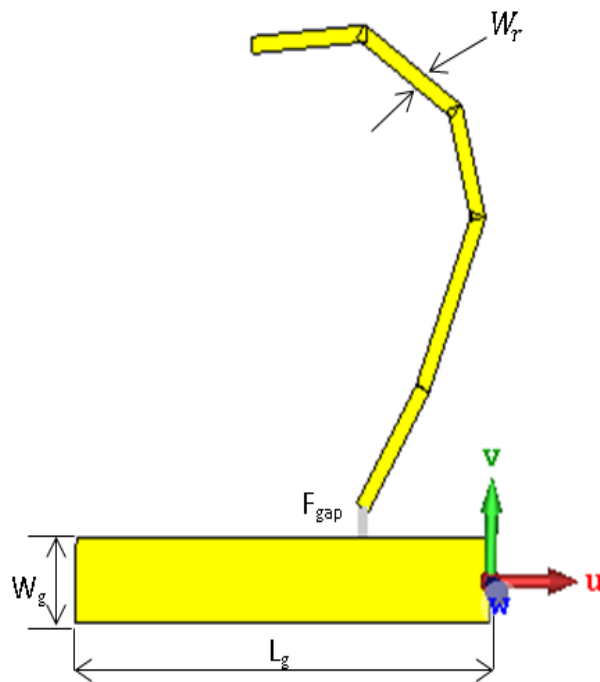


Figure 4.14 Planar version linear wire design in CST

#### 4.4.1. Measurement of planar antennas

To validate the planar antenna design, the fabricated antennas were measured. The calibration of the VNA was performed manually using the SOLT (short-open-load-through) method. Connecting the calibration standards to each of the port and each port are physically connected to each other. Verification of its validity of the calibration was carried out by measuring a matched load ( $50\Omega$ ) connected to each port of the VNA. The measurement set up is shown in Fig.4.15.



Figure 4.16 shows the simulated and measured  $S_{11}$  of the planar version of linear wire antenna etched on FR4 substrate. The measured results have some multiple harmonic— $-3.393\text{ dB}$  at  $492\text{ MHz}$ ,  $-9.406\text{ dB}$  at  $690.3\text{ MHz}$  which is due the effects of the ground plane. The three measured antenna samples exhibit similar characteristics all resonating at  $849\text{ MHz}$ ,  $845\text{ MHz}$  and  $832\text{ MHz}$ . Measurements were made in a laboratory. It became clear that the metal frames of the bench affected the response as the antenna was raised higher above the bench. The measurement did not use a balanced feed and it was obvious that the coaxial feed was contributing to the radiation. The ripple on the plot is because the measurement was carried out outside the anechoic chamber. There are more measured resonances, probably caused by the difference in feeds and the lack of a balun.



Figure 4.15 Measurement set up for the etched pocket A antenna

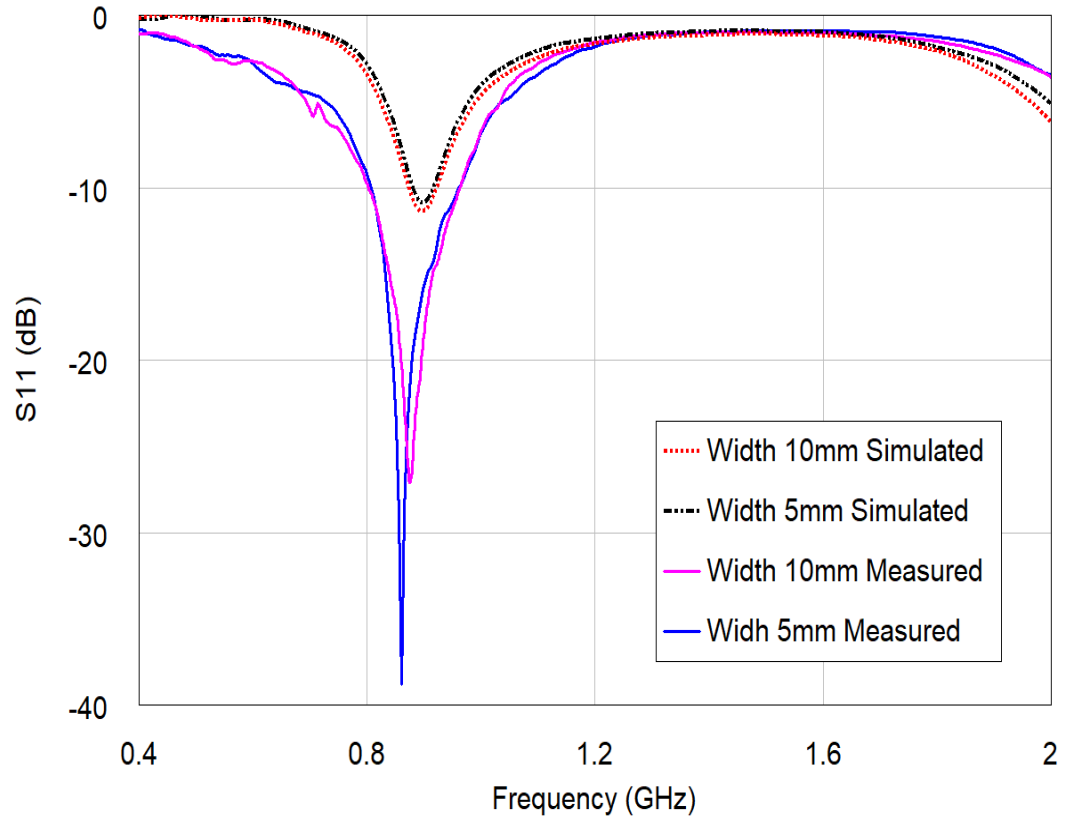
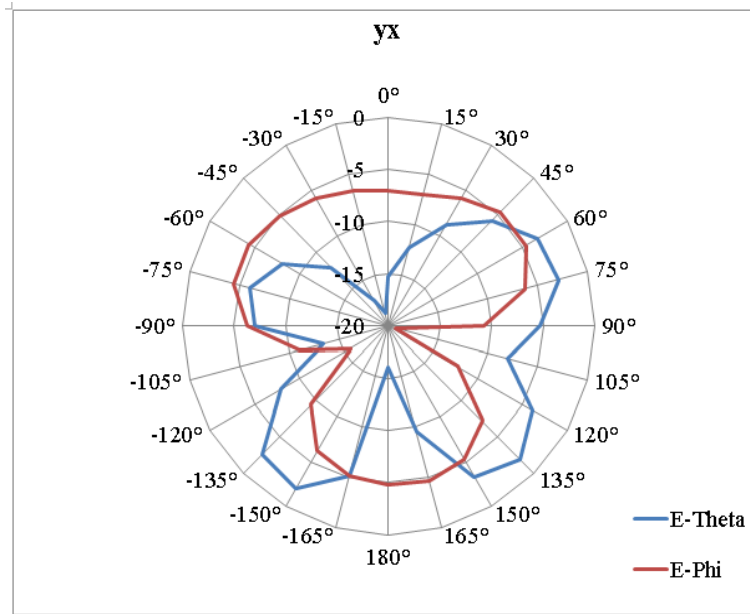


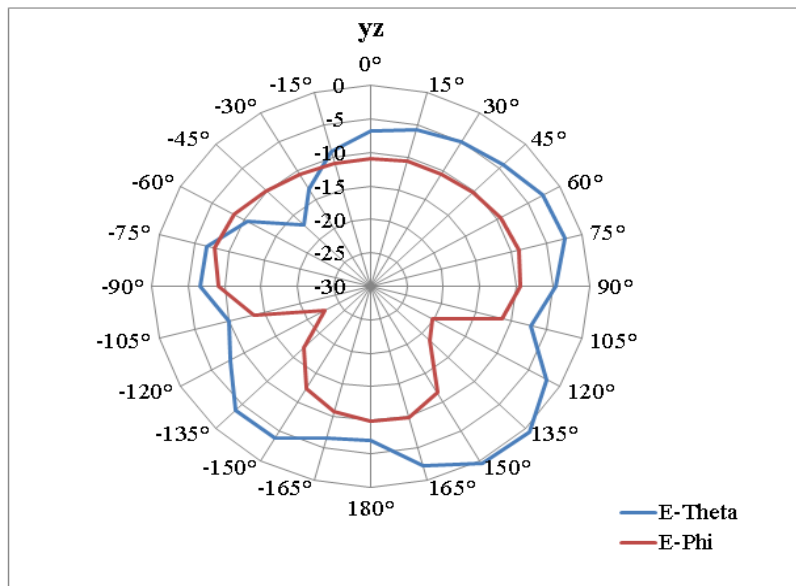
Figure 4.16 Measured and simulated  $S_{11}$  against frequency for planar antennas

#### 4.4.2 Radiation Patterns

The radiation pattern of pocket A etched antenna is shown in Figure 4.17. The radiation characteristics of the pocket A etched antenna were measured in the anechoic chamber. The standard horn antenna was used as reference to measure the gain and radiation pattern of the antenna. The y-x plane and y-z plane patterns are similar.



(a)



(b)

Figure 4.17 Measured radiation pattern of planar antennas (Width 10 mm)

#### 4.5. Characterisation of fabric for antenna

The dielectric properties of the textiles (denim and felt) used in this study were characterised using a split post dielectric resonator at 1101 MHz (closest frequency to 900 MHz in terms of measurement equipment). It is possible to evaluate the MUT using either a VNA or Q meter connected to the SPDR. This study uses the Q meter. The Q meter measures the  $S_{21}$

results using split post dielectric resonator without a vector network analyser. The measurement setup as shown in Figure 4. 18. The Q factor was calculated using.

$$Q = \frac{f_r}{f_{h_{3dB}} - f_{l_{3dB}}} \quad (4.1)$$

Where  $f_r$  is the resonant frequency while  $f_{h_{3dB}} - f_{l_{3dB}}$  is the  $-3dB$  bandwidth.

The fabric materials under test (MUT) were cut according the dimension of cavity which was  $13cm \times 13cm$ . The thickness of each textile samples was measured. The Q was measured when the resonator was empty, then the MUT was placed in the resonator and the Q measured. A commercial software was used to calculate the dielectric parameters from the two Q measurements and the sample thickness. Results for the single layer denim are thickness 0.85 mm  $\epsilon_r = 1.97$   $\tan\delta = 0.07$ . For felt fabric results are thickness 1 mm,  $\epsilon_r = 1.2$  and  $(\tan\delta) = 0.0013$ . From the measurement, it is observed that the two fabric samples have low permittivity. Fabric samples are porous in structure.

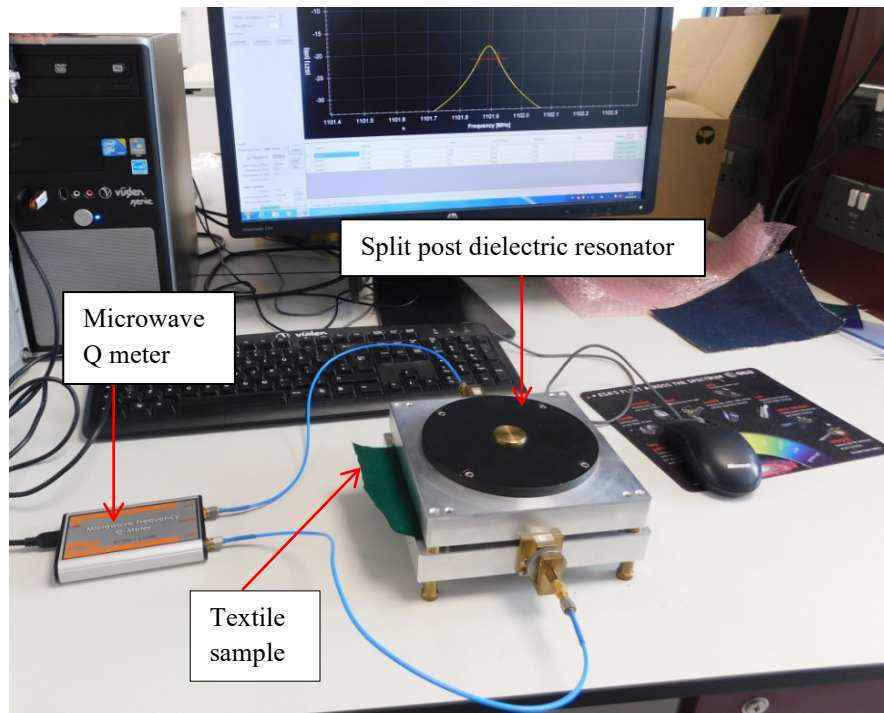


Figure 4.18 Measurement setup for dielectric parameters of textile samples

## 4.6. Manufacture of fabric antennas

Embroidery model of the stitched antenna is based on are fast and flexible generating stitch patterns. This model allows easy integration of high frequency systems into clothing [4.4]. Embroidery was chosen as a method of production of this design. This method provides high speed and easily modified embroidered designs

The fabric antenna design was exported as a graphic format on a drive and sent to the digital embroidery machine (Fig. 4.19). The antenna is embroidered using a multi strand conducting Liberator<sup>TM</sup> with a conductor of silver. The yarn has 66 polymer threads with  $1\mu\text{m}$  silver coating on each thread. Computerised embroidery is used to fabricate all antennas in this study. A denim substrate with thickness of  $0.85\text{ mm}$  was used for the embroidered antenna production. The fabric antennas were sewn using the computerised embroidery machine that has ten needles. This embroidery machine has several stitching patterns and different threads are used based on the design. Threads are selected automatically with designs and needles. The threads and needles can be swapped.

Different stitches such as zigzag stitch, fill stitch, running stitch, and spiral stitch are some of the stitching pattern. Running stitches were used for the fabrication. To achieve a better conduction and lower loss the stitching threads is in a direction parallel to the current flow [4.6]. The fabrication process is fast and accurate depending on stitching patterns. The fabric antenna has two parts the radiating elements 605 stitches and ground plane 556 stitches for Pocket A antenna. A coaxial cable was soldered to the antenna at the lower end of the antenna to obtain a good connection. The solder was used as connection between coaxial cable and antenna because it is easy to remove. Several antennas were made in this design. The fabric pocket A antennas having a ground plane of widths 10 mm, 5 mm and 2 mm parameters are summarised in Table 4.2.

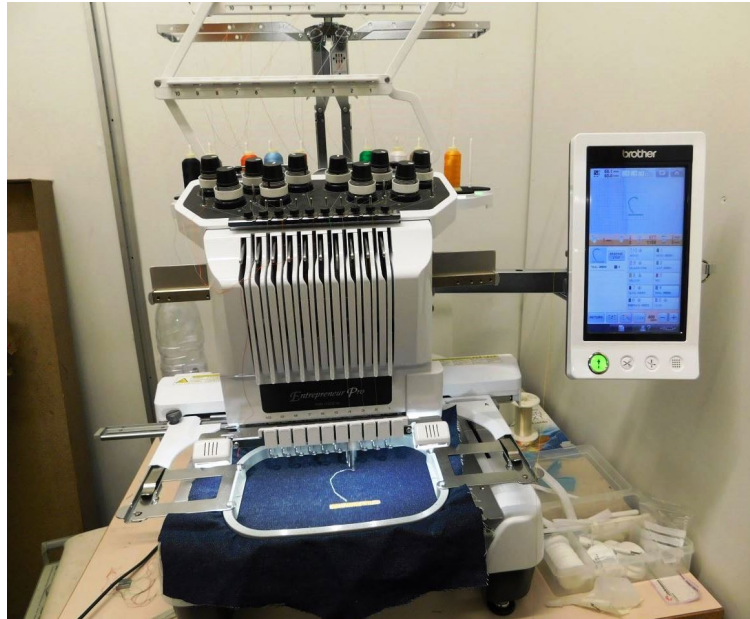


Figure 4.19 Embroidery machine creating a pocket antenna

#### 4.7. Effect of ground plane width on the fabric antenna

The length of the ground plane,  $L_g$ , and ground plane width,  $W_g$ , were varied. It was observed that the centre frequency of the three antennas shifted. Figure 4.20 shows the measured return loss for three fabric antenna samples with ground plane widths of  $2\text{ mm}$ ,  $5\text{ mm}$  and  $10\text{ mm}$ . The  $S_{11}$  parameter of Pocket A antenna (see Fig.4.21) with these different ground widths antennas show significant resonances at  $932\text{MHz}$  at  $-21.19\text{dB}$ ,  $907.30\text{MHz}$  at  $-19.6\text{dB}$  and  $900\text{MHz}$  at  $-33.98\text{dB}$ . The ground plane of fabric antenna acts as a radiating element and its parameter influences the  $S_{11}$  response. For monopole antennas with a finite ground, ideally the ground should have no effect on performance of antenna. Current distribution on the ground plane affect the impedance bandwidth, gain and the radiation pattern of the antenna [4.7]-[4.8]. The radiated efficiency increases as the width of the ground plane is increased. The increased in length of the ground plane also gives a better resonant frequency the antenna. The ground plane controls the efficiency of the fabric antenna. The gains of the fabric antenna increase as the ground plane width get larger.

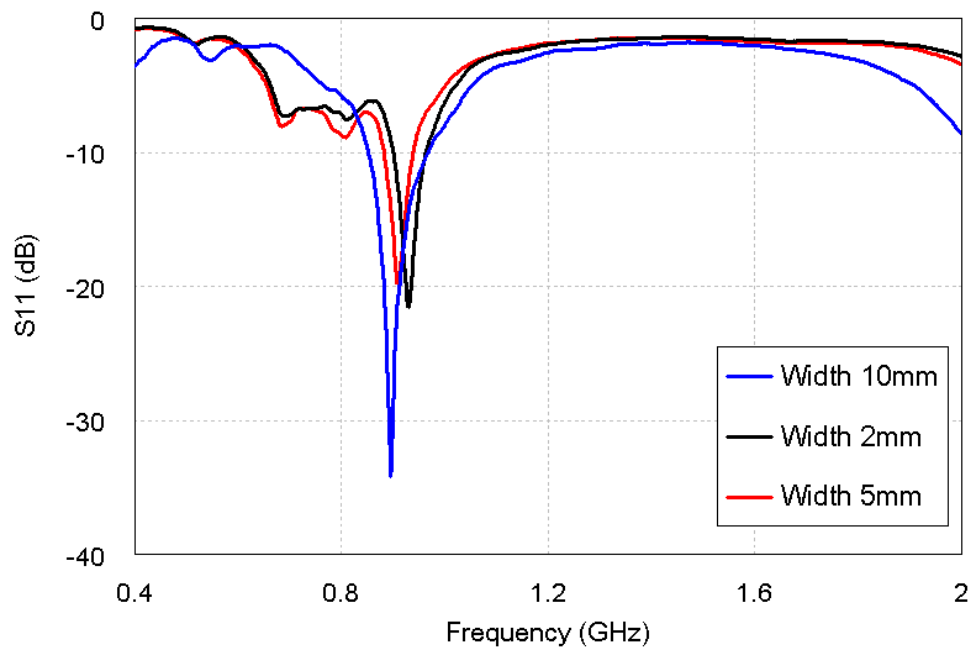


Figure 4.20 Measured  $S_{11}$  results for three identical fabric antennas with different ground plane width.

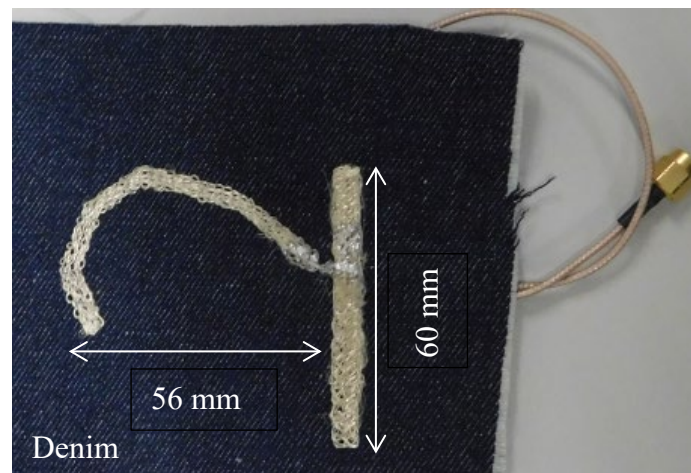


Figure 4.21 Photograph of Pocket antennas

Table 4.2 Comparison of different version of Pocket A antenna.

| Antenna sample<br>(see Note below) | Antenna length<br>(mm) | Width of radiating element<br>(mm) | Ground plane<br>(mm <sup>2</sup> ) | Measured $f_0$ (MHz) | Measured $S_{11}$ (dB) | -10dB Bandwidth (%) | Radiated Efficiency (%) | Peak gain (dBi) |
|------------------------------------|------------------------|------------------------------------|------------------------------------|----------------------|------------------------|---------------------|-------------------------|-----------------|
| 1                                  | 84                     | 4                                  | $60 \times 10$                     | 900                  | -33.99                 | 12.2                | 60                      | 2.08            |
| 2                                  | 84                     | 4                                  | $60 \times 5$                      | 907                  | -19.68                 | 6                   | 57                      | 1.15            |
| 3                                  | 84                     | 4                                  | $78 \times 2$                      | 929                  | -21.12                 | 6.8                 | 53                      | 1.4             |
| 4                                  | 84                     | 4                                  | $60 \times *$                      | 900                  | -15.1                  | 7                   | 87                      | 2.34            |
| 5                                  | 84                     | 4                                  | $58 \times 10$                     | 843                  | -21.0                  | 19.3                | 80                      | 2.5             |

Note:

- (1) Fabric version of Pocket A antenna with 10mm ground plane
- (2) Fabric version of Pocket A antenna with 5mm ground plane
- (3) Fabric version of Pocket A with antenna 2mm ground plane
- (4) Wire sample of Pocket A antenna
- (5) Planar version of Pocket A antenna

\* Ground plane thickness of wire diameter (0.75mm)



#### 4.8. Discussion of comparison of the simulated, planar and stitched antenna

An important feature in this study was comparing the operating bandwidth of the different antennas. Table 4.2 shows a comparison result of the measured for measured of linear wire, planar and fabric antennas. The five antennas have good impedance matching that gives wide bandwidth. The bandwidth is calculated from  $S_{11}$  and referenced to the centre frequency  $f_c = (f_u + f_l)/2$  where  $f_u$  the upper  $-10$  dB frequency and  $f_l$  is the lower edge frequency at  $-10$  dB. The antenna sample 1 has a broad bandwidth but almost 80 % radiated efficiency may likely due some errors in the setting the chamber for measurements and is less likely to be the true resonance frequency.

The measured result and simulated reflection coefficient ( $S_{11}$ ) are shown in Fig. 4.22. Antenna sample 5 has a resonant frequencies of 846.3 MHz at -20.99dB while that of the antenna sample 1 resonates 900 MHz at -33.98dB. Simulated  $S_{11}$  resonated at -11.31dB at 899MHz that of antenna sample 4 the resonant frequency is at -15.1dB at 903MHz. Based on the  $-10$ dB bandwidth antenna sample 5 has a bandwidth of 174MHz but low gain, better performance than the other antennas have good return loss of 21.06dB. The fabric antenna has a low gain and bandwidth of 115MHz which covers the desired frequency band for the envisaged applications There are variation between the fabric and planar antenna because the substrate denim permittivity is 1.9 used for the embroidery while planar FR4 substrate was 4.3. The variation in the substrate will explain the differences in antenna performances. Fabrication inaccuracies and measurement errors are some of also likely causes. The planar antenna made of copper strip has a better performance than fabric antennas in terms of usable frequency. The fabric antenna is flexible, it can be easily integrated into clothing and is wearable.

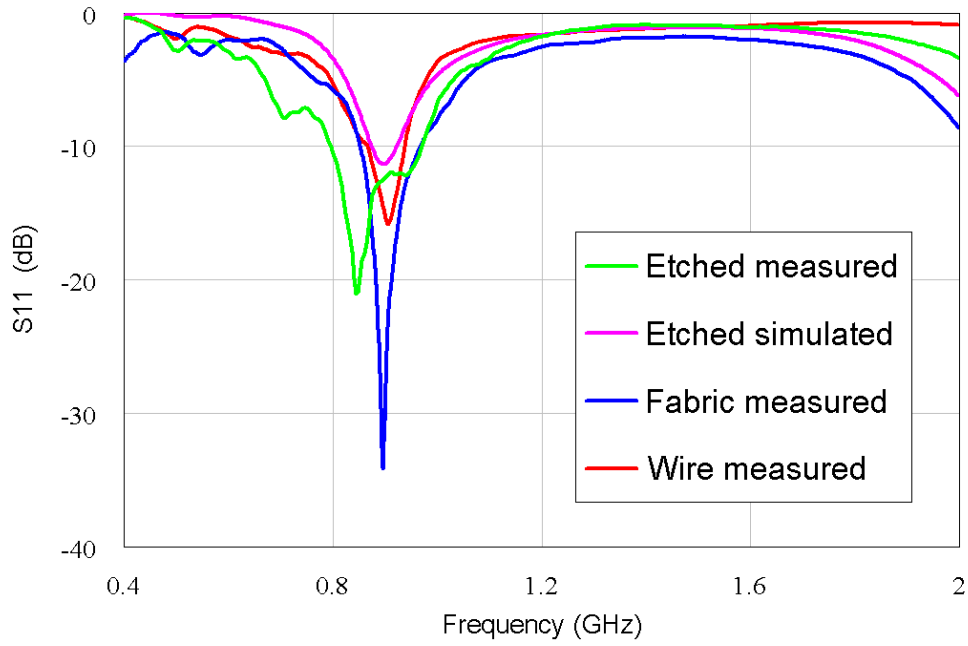


Figure 4.22  $S_{11}$  results of the Pocket A in three different profile: linear wire, planar and fabric antennas.

Radiation characteristics were also studied. The measurement set-up for the fabric antennas is depicted in Fig.4.23. The radiation patterns were measured for all the constructed fabric antennas (900 MHz). Measurements were performed using standard horn antenna (RS100250) as reference. The gain, efficiency and radiation pattern were measured. The antennas were measured in the  $E_\theta$  and  $E_\phi$  plane

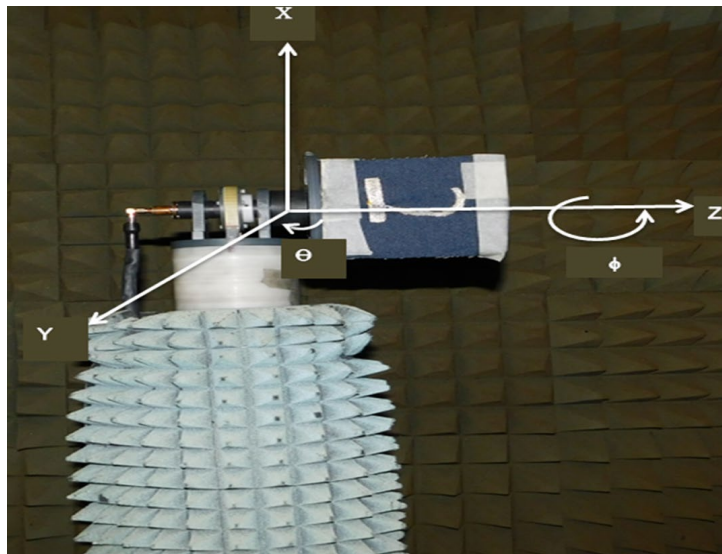


Figure 4.23 Measurement setup for stitched antenna in anechoic chamber.

The gain of the antenna is  $1.57\text{ dBi}$  with a maximum gain of  $2.08\text{ dBi}$  for the operating frequency at GSM band ( $900\text{ MHz}$ ). The fabric antenna has a low gain possibly due to the lossy material. The radiation efficiency the antenna is  $60\%$  at  $900\text{ MHz}$ .

#### **4.8.1. Measurements of antenna on curved surface**

A fabric antenna was measured in free space, on a human body and a human body with isolating layer. The various distances from the human body were considered during  $S_{11}$  measurements to study the antenna performance. When antennas are operating on some parts of the human body, certain factors must be considered for flexible and wearable antennas. These include bending, crumpling and twisting actions [4.10]. The antenna was placed on a curved surface, a polystyrene foam cylinder of  $120\text{ mm}$  diameter similar to that of human leg to examine the antenna performance. The polystyrene form has a relative permittivity close to that of free space.

Figure 4.24 shows the setup of antenna measurement on curved.  $S_{11}$  measurements were carried out on the bent. fabric pocket A antenna and  $S_{11}$  results are shown in Figure 4.25. The resonant frequency and reflection coefficients from the plots are: curved surface  $935\text{ MHz}$  at  $-28.35\text{ dB} - 10\text{ dB}$  bandwidth  $102\text{ MHz}$  and free space  $900\text{ MHz}$  at  $31.09\text{ dB} - 10\text{ dB}$  bandwidth  $108\text{ MHz}$ . Based on the analysis, the reflection coefficient and resonant frequency shift reduces to the  $935\text{ MHz}$  at  $-28.35\text{ dB}$  and  $-10\text{ dB}$  bandwidth reduces to  $102\text{ MHz}$  from  $108\text{ MHz}$ . The antenna resonant frequency shift is most likely due to the curve on the antenna as well as the fact that the flat antenna was lying on a wooden table. The reflection coefficient has changed slightly,  $10\text{ dB}$  bandwidth has also changed. This is most likely caused by a change in impedance match. The fabric antenna still operates within the desired frequency range.

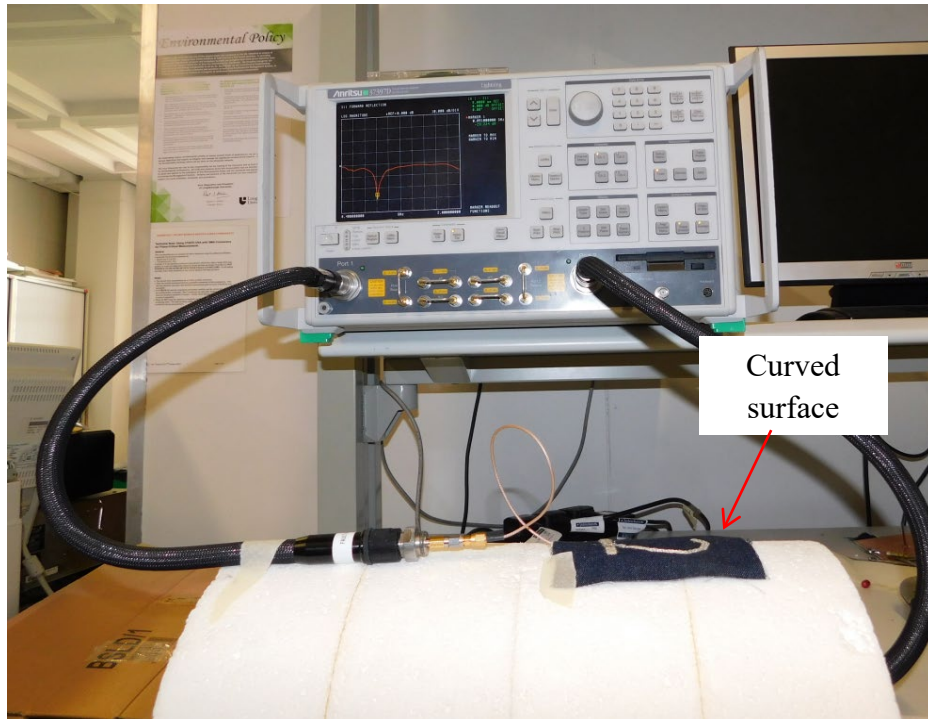


Figure 4.24 Measurement set Pocket A under bending condition

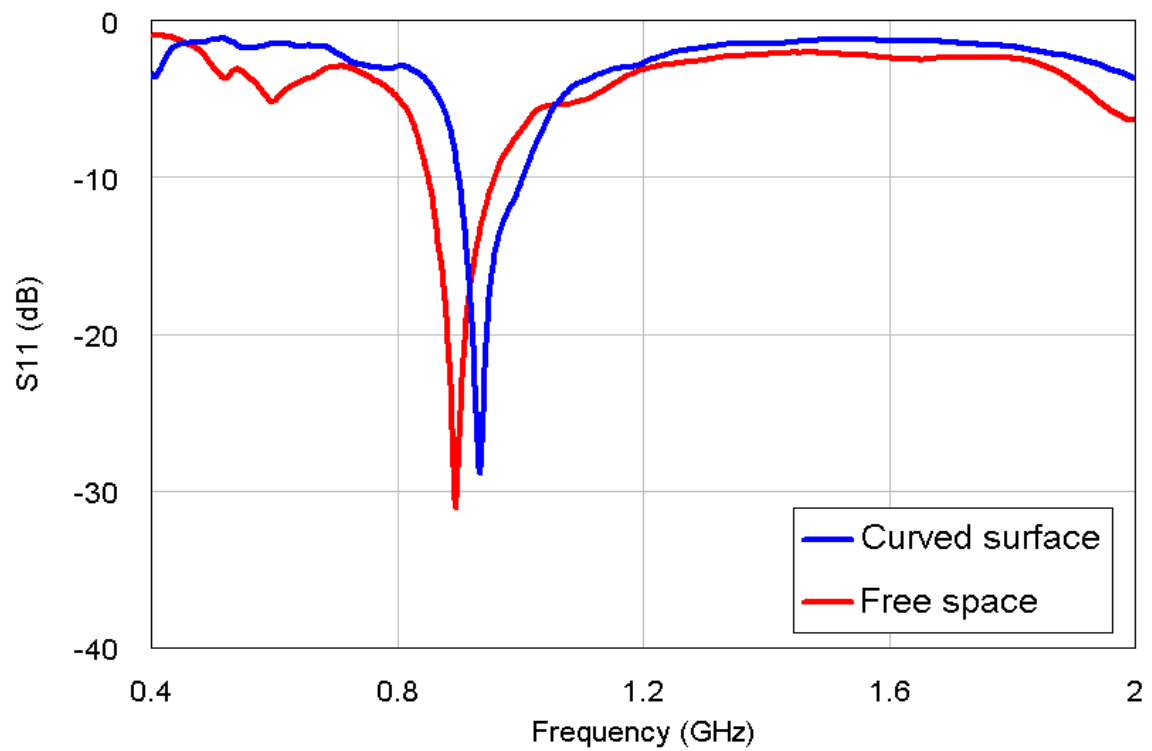


Figure 4.25 Measured  $S_{11}$  of Pocket A on curved surface.

## 4.8.2 Human body effects

Textile antennas have been used over recent years as wearable antennas due to flexibility and structural elasticity to ensure comfort to users. This antenna can be fully integrated into intelligent garments called wearable electronic systems [4.11]. The concept of wearability requires the antennas to be measured on-body. The human body has a frequency dependent conductivity and permittivity. The body tissue has a high permittivity and is also a lossy medium that cause the resonant frequencies to change.

The designed antennas are to operate in proximity to the human body, when they are placed on layers of a garment. The antenna has been simulated in CST Microwave Studio using a flat body Phantom (Figure 4.26) with a separation distances from the human body. The antenna was simulated in free space. For this pocket antenna simulation an average clothing thickness of 2 mm was considered. The air gap between the felt fabric substrate and the human body was small (1mm). The properties and parameters of the flat body Phantom are: Muscle ( $\epsilon_r = 52.79$ ;  $\sigma = 1.705$ , *thickness* = 23mm). Skin ( $\epsilon_r = 31.29$ ;  $\sigma = 5.0138$ , *thickness* = 2mm) and Fat ( $\epsilon_r = 5.28$ ;  $\sigma = 0.1$ , *thickness* = 8mm) [4.13].

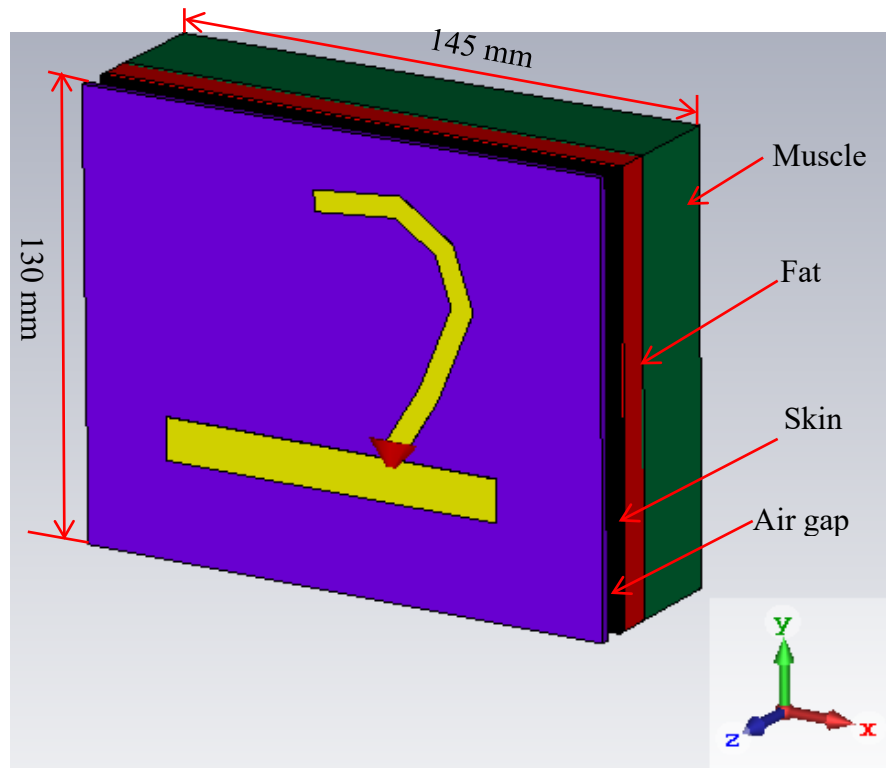


Figure 4.26 Pocket antenna mounted on the flat body phantom of the human body

Fabric antenna measurements were performed when worn on human body and off body indicated in set-up in Figure 4.27. The effect of body on input match characteristic of fabric antenna was measured by placing the antenna on the chest.



Figure 4.27 Measurement set-ups for on-body test.

Simulated and measured reflection coefficients ( $S_{11}$ ) for the pocket antenna both with and without the presence of flat body Phantom are shown in Figure 4.28. For the results without the body  $S_{11}$  is 900 MHz at  $-32.31$  dB, and bandwidth is 13.78 % (841 – 965MHz). The results with body resonant frequency of 858 MHz at  $-43.4$  dB and bandwidth is 15.26 % (805 – 936MHz). Simulated results without flat Phantom gives a resonant frequency of 907 MHz at  $-16.94$  and a bandwidth 10.8% (858MHz – 956MHz) while simulations with the flat Phantom gives a resonant frequency of 868 MHz at  $-22.52$  dB and a bandwidth 11.8% (805MHz – 907MHz).

For the chest measurements; the antenna is mounted directly on the shirt of thickness about 3mm (measured). This may account to detuning effects because of the lossy nature of human body. When the antenna was worn on the body from the  $S_{11}$  response plot, comparing the

results of the detuning effect when the antenna is in Off-body and On-body, there is a downward shift in frequency. The results show that the pocket antenna is suitable and efficient over the 120 MHz band from 805 MHz to 936 MHz. Over this band the pocket antenna achieved a gain of 1.9 dBi and  $-5.61$  dBi without and with flat body Phantom. Human body lowers the resonant frequency of the wearer [4.14].

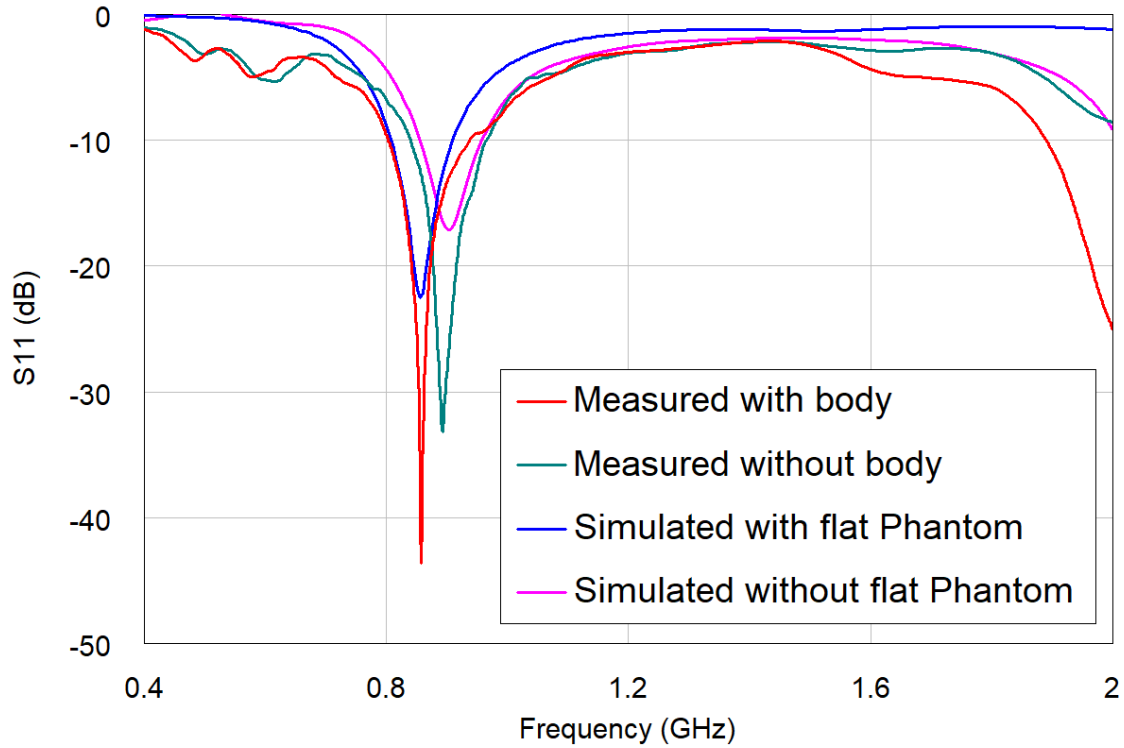


Figure 4.28 Measured  $S_{11}$  of Pocket A the on-body and Off body

### 4.8.3. Radiation patterns

The simulated 3-D far field pattern is shown in Figure 4.29 antenna radiation pattern without the body. The region with the highest gain 1.9 dBi which is coming from the radiating element. When the pocket A antenna is placed on the body the radiation pattern is shown in Figure 4.30 with the antenna gain of  $-5.61$  dBi. The gain of the antenna reduced from 1.9 dBi to  $-5.61$  dBi when the antenna pattern changes because of dielectric constant property of the body phantom. From Fig. 4.30 the antenna was simulated without the human model; the radiation efficiency is 83 % but when the simulated on a human phantom there is a drop in the radiation efficiency to 15.8 % as shown in Fig. 4.30. The change is due to separation distance

of 3 mm-gap used in the simulation between antenna and human phantom. This gives a proximity to the body because the gap is small.

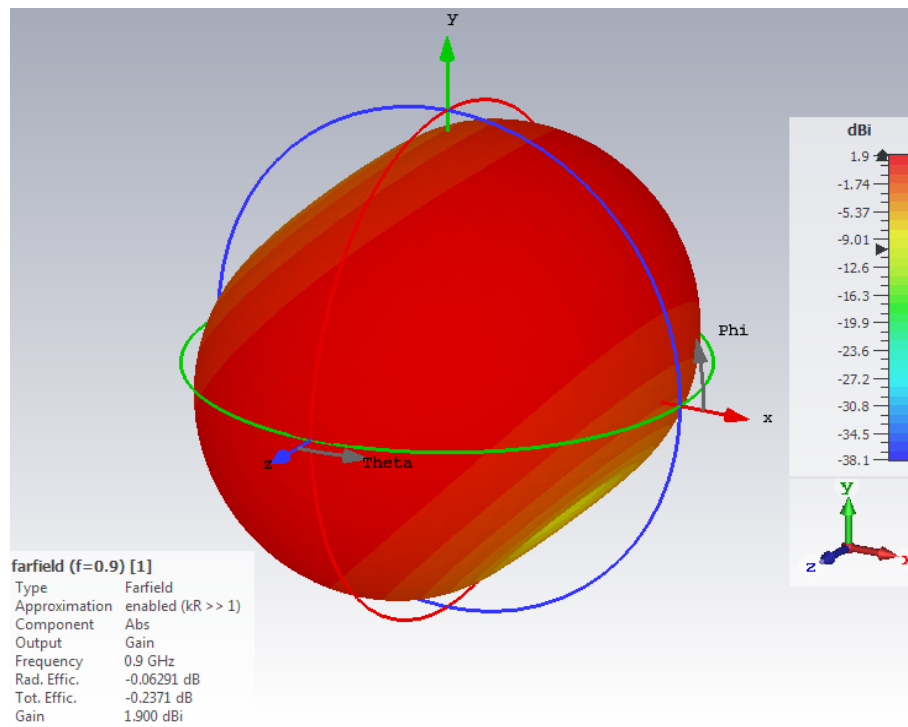


Figure 4.29 Far field directive pattern of pocket A antenna without the body

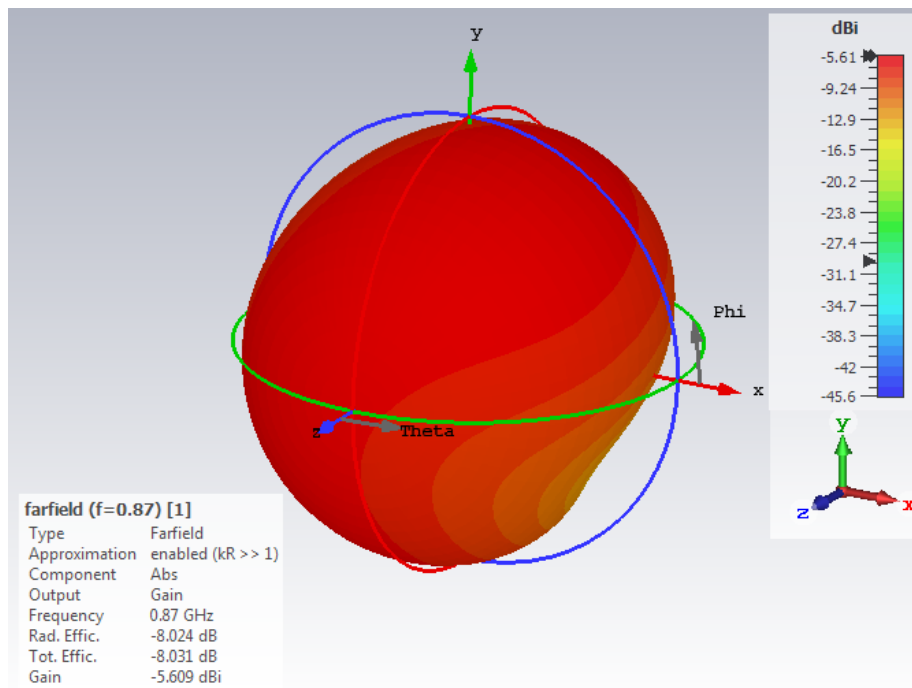


Figure 4.30 Far field directive pattern of pocket A antenna on flat body Phantom



The simulation of pocket A antenna was performed on the human phantom using CST Microwave Studio. The CST uses the IEEE C95.3 standard averaging method. The dielectric properties of the human body tissues in section 2.4.3 were used. The referenced input power of  $0.25\text{ W}$  gives a SAR distribution of Fig.4.31. The simulated results are  $2.38\text{ W/kg}$  for  $1\text{g}$  of tissue and  $1.55\text{ W/kg}$  for  $10\text{g}$  of tissue. Figure 4.32 shows the simulated results at input power of  $0.5\text{ W}$ ; ( $1\text{g}$  SAR) averaging gives  $4.757\text{ W/kg}$  and ( $10\text{g}$  SAR) is  $3.102\text{ W/kg}$ . Using a referenced input power for the SAR averaging is shown in Fig.3.33. The maximum level of  $9.515\text{ W/kg}$  for  $1\text{g}$  of tissue and  $6.205\text{ W/kg}$  for  $10\text{g}$  of tissue. The lossy nature of human body causes energy to get absorbed when electromagnetic waves are propagating. At the lower input power, the SAR limit is within the acceptable limit. The high SAR value could be reduced by using a reflector on the ground plane.

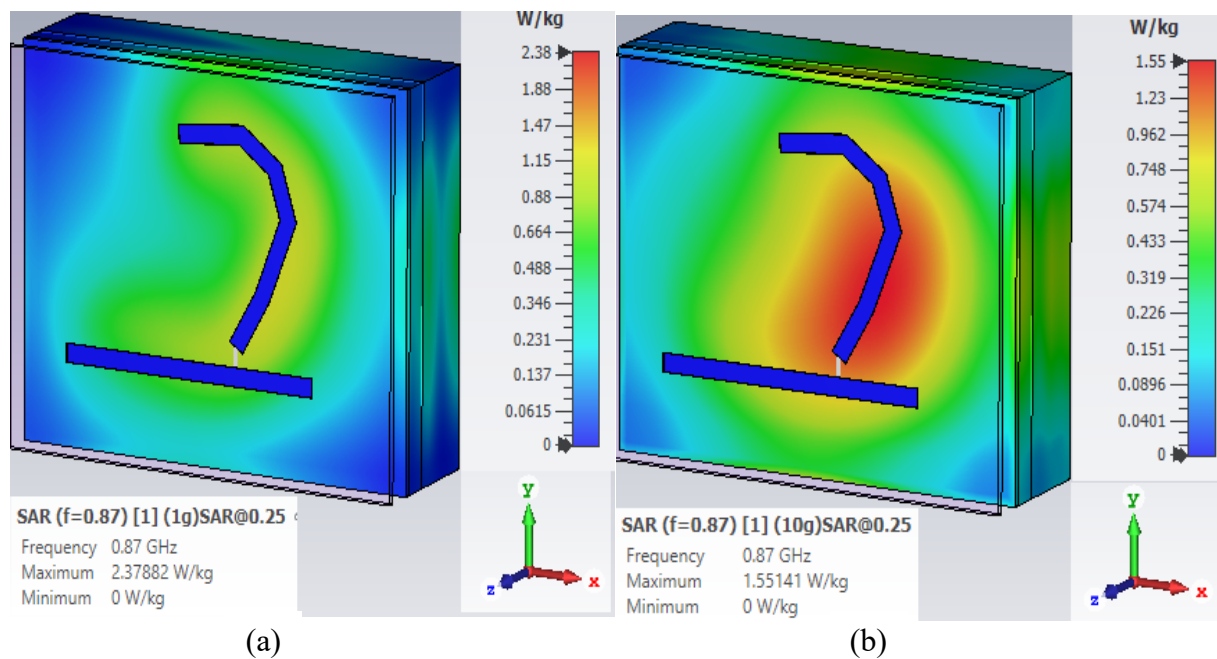


Figure 4.31 Specific absorption rate (SAR) at 870MHz on human phantom model with input power of  $0.25\text{ W}$  (a) SAR distribution for  $1\text{g}$  and (b) SAR distribution for  $10\text{g}$

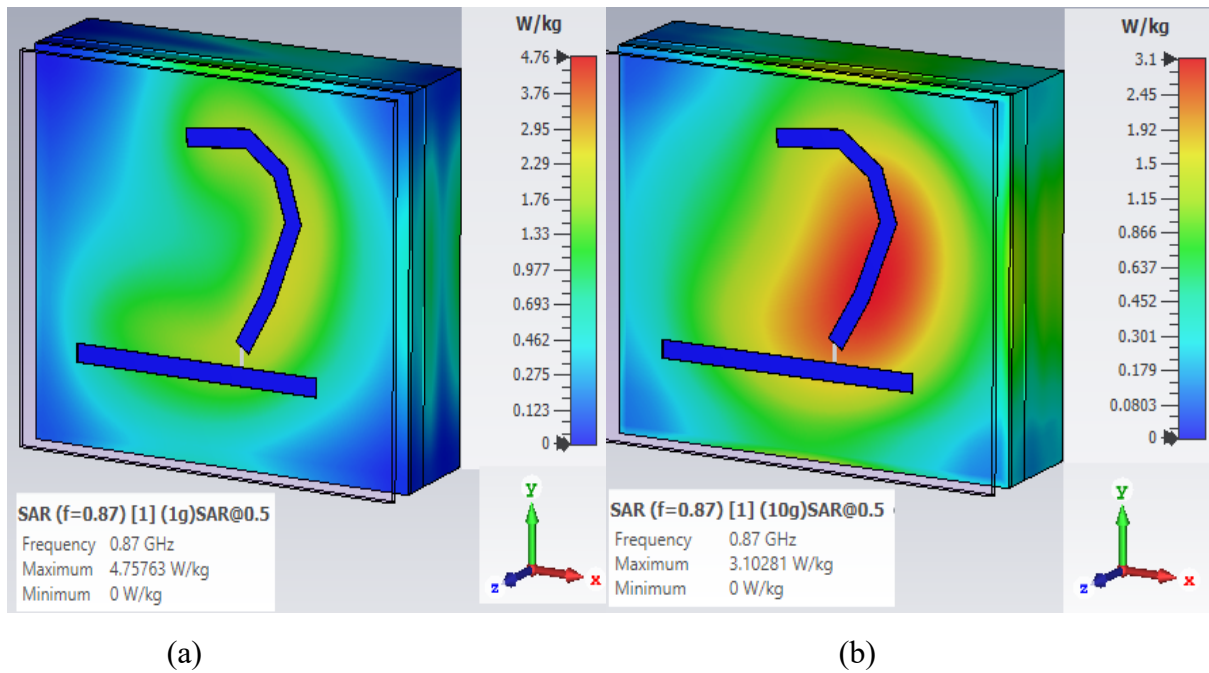


Figure 4.32 Specific absorption rate (SAR) at 870MHz on human phantom model with input power of 0.5W (a) SAR distribution for 1g and (b) SAR distribution for 10g

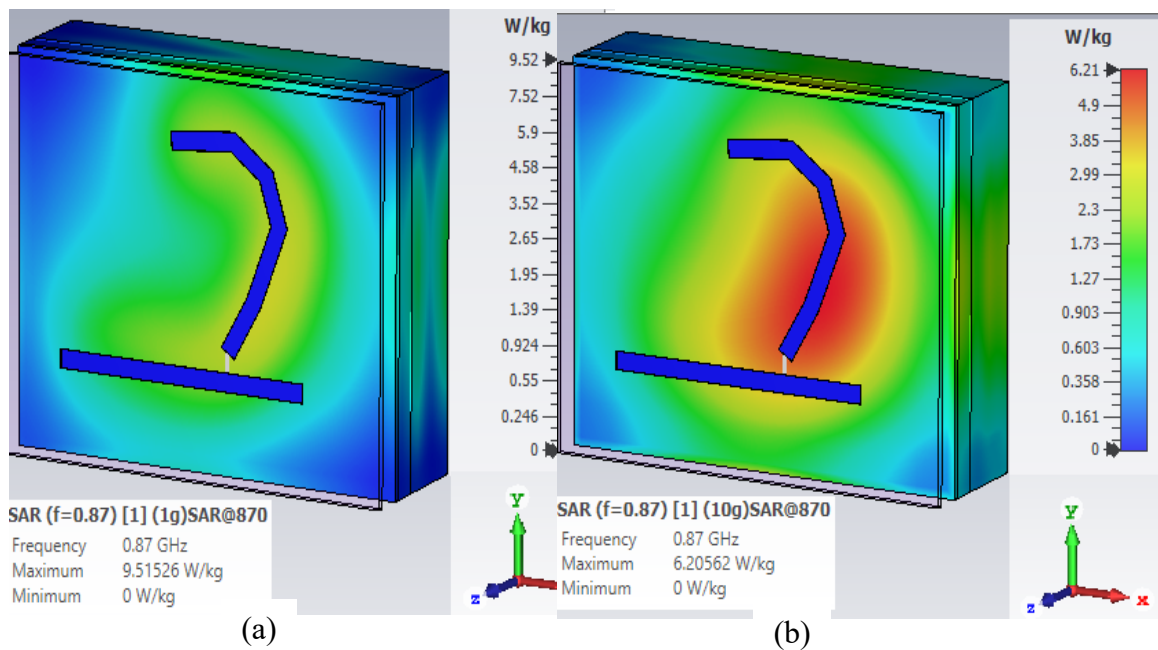


Figure 4.33 Specific absorption rate (SAR) at 870MHz on human phantom model with input power of 1W (a) SAR distribution for 1g and (b) SAR distribution for 10g

#### 4.8.4. Summary

Pocket antennas designed and fabricated with 10 mm ground plane width shows better antenna performances compared to 2mm and 5mm ground plane width antennas. The 10 mm ground plane width gives a resonant frequency and reflection coefficient of 900 MHz at -33.99 dB with a 12.2% bandwidth compared to 2mm, 929 MHz at -21.12 dB and 5mm, 907 MHz at -19.68 dB which are 6% and 6.8 % respectively.

It is demonstrated that from the results of Figure 4.28 that when the Pocket A antenna is placed on human body a flat phantom, the resonant frequency shifted downward but still covered -10 dB bandwidth for GSM 900. Placing the antenna directly on the human body worsens the antenna performance because of lossy nature of human tissues but the pocket antenna was tested on body considering separation gap of 3 mm.

### 4.9. Simulated and measured performance characteristics of meshed monopole antennas

#### 4.9.1. Antennas Layouts

The investigation of meshed monopole antenna properties was carried out using CST Microwave Studio. The interaction of the parallel and orthogonal lines in  $TM_{010}$  current path was examined. The structure of proposed meshed monopole antenna is shown in Fig.4.34. Meshed monopoles consist of two sets of mesh lines. The radiating element of the monopole antenna is meshed and represented by a length of  $\lambda/4$  with strip width of the radiating element  $W_s$ . A coaxial cable with an impedance of 50  $\Omega$  is used to feed the antennas. Meshed ground plane is defined by  $W \times L_g$ . The distance  $d_L$  and  $d_W$  between the strip can be calculated by  $(L - L_w)/(N_{v,h} - 1)$ . The line width  $L_w$  of the strip is taken as 0.2 mm and variables  $N_v$  and  $N_h$  represents the number of vertical lines and horizontal lines respectively. The transparency  $T_{Monopole}$  is given as the ratio between the non-metal area and the total area of the solid structure (4.2) [4.12]. The total number of vertical lines are fixed to five and length ( $L$ ) of the radiating segment is fixed to  $\lambda_g/4$ .

$$T_{transparency} = \frac{L.W - L_w.N_h.L - L_w.N_v.W + L_w^2.N_v.N_h}{L.W} \quad (4.2)$$

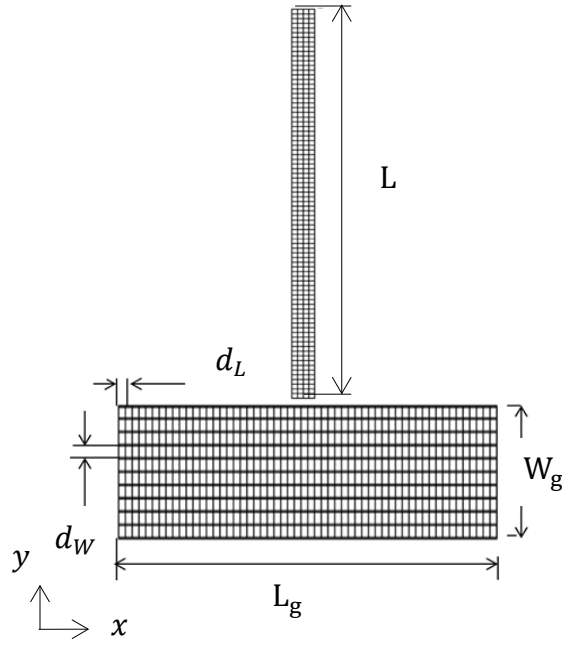


Figure 4.34 Meshed monopole antenna layouts

The monopole is meshed and printed on FR4. The meshed monopole antenna has no ground plane behind the radiating element. The printed meshed monopole was designed using equation (4.3). The meshed monopole antenna samples were constructed with 1.6 mm thickness on an FR4 substrate with relative dielectric constant of 4.3 and loss tangent of 0.018. The meshed lines were etched on a PCB substrates.

$$\lambda = \lambda_g = \frac{\lambda_0}{\sqrt{\epsilon_{eff}}} \quad (4.3)$$

Where  $\lambda_0 = c/f$  free space wavelength,  $\lambda_g$  guided wavelength in FR4 substrate and  $\epsilon_{ff}$  is the effective dielectric constant which is applied to microstrip transmission line. Equation (4.4) [4.15] was used to roughly computed as approximately 1.6783.

$$\epsilon_{eff} = 1 + \frac{\epsilon_{FR4}-1}{2} \left\{ 1 - \left[ \frac{w_s/h}{1+w_s/h} \right] \right\} \quad (4.4)$$

Pure copper of thickness 0.035mm was used with a line width of 0.2 mm. The meshed monopole antennas were placed on solid ground plane of 60 mm × 10 mm as shown in Fig.4.35. The meshed monopole consist of vertical ( $N_v$ ) = 5 and horizontal lines ( $N_h$ ) = 68 width a radiating length 68 mm. In this study a line width of 0.2 mm was used but the line width affects the transparency of the meshed monopole antennas.

The reflection coefficient ( $S_{11}$ ) response of antenna sample 20 (uniform meshed monopole) was simulated and measured and compared with the unmeshed monopole antenna. The spacing between the uniform mesh is 1mm both with ground plane and radiating element.

Figure 4.36 shows the  $S_{11}$  of the simulated and measured meshed and unmeshed monopole antenna sample. The resonant frequency of uniform meshed monopole 20 (measured) is 921 MHz at  $-32.86\text{ dB}$ ,  $-10\text{ dB}$  bandwidth 283 MHz while the simulated result is 905 MHz at  $-16.52\text{ dB}$ ,  $-10\text{ dB}$  bandwidth 100 MHz. The impedance bandwidth increased from 11 % (simulated) to 30 % (measured) for the uniform meshed antenna. The unmeshed monopole antenna resonated is 866 MHz at  $-28.17\text{ dB}$ ,  $-10\text{ dB}$  bandwidth 237 MHz for the measurement and at 900 MHz at  $-14.77\text{ dB}$ ,  $-10\text{ dB}$  bandwidth 85 MHz for the simulation. A discrete port was placed between the ground plane and the radiating element. Meshing an unmeshed monopole antenna increased the resonant frequency suggesting a reduction in current path length.

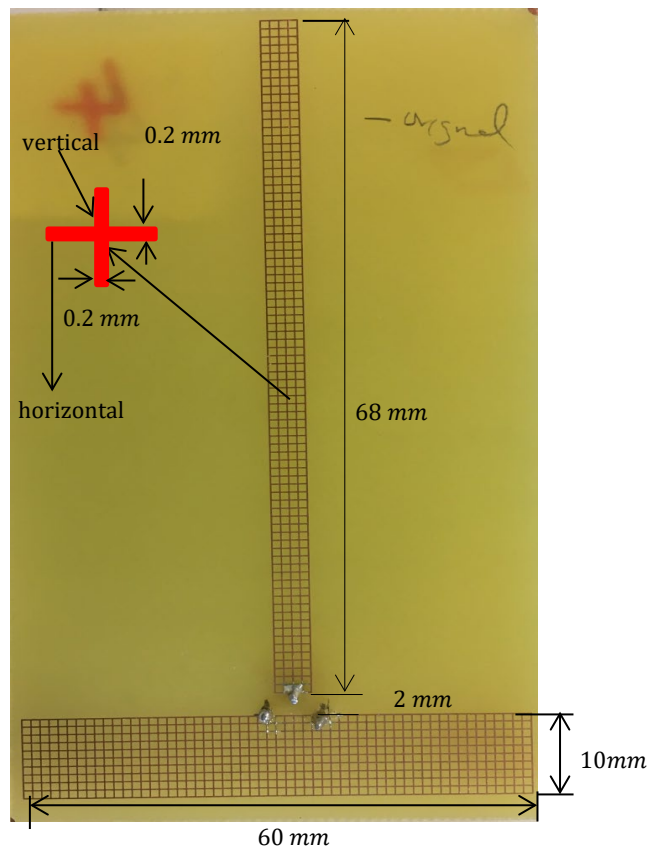


Figure 4.35 Meshed monopole antenna sample 20

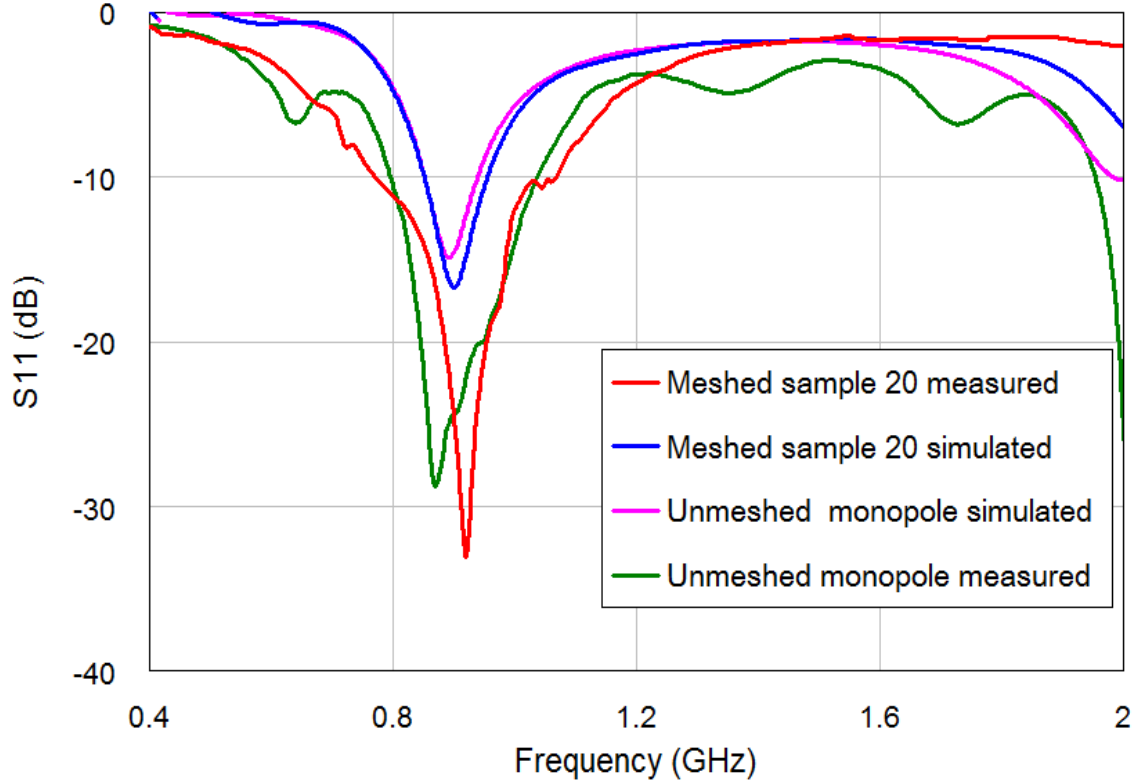


Figure 4.36  $S_{11}$  plot of meshed and unmeshed monopole antenna see Table 4.5 for detail of antennas

Antenna sample 21 is meshed monopole consisting of  $N_h = 8$  horizontal lines and  $N_v = 5$  vertical lines. Antenna height ( $H_L$ ) is 68 mm, width a radiating width of 4 mm, with  $d_L = 1\text{ mm}$  and  $d_w = 10\text{ mm}$ , ground plane length ( $L_g$ ) = 60 mm and width of the ground plane ( $W_g$ ) = 5 mm. Antenna sample 24 is meshed having the following dimensions of  $N_v = 5$  and  $N_h = 17$ ,  $d_L = 1\text{ mm}$ ,  $d_w = 5\text{ mm}$ ,  $H_L = 84\text{ mm}$ ,  $L_g = 60\text{ mm}$  and  $W_g = 5\text{ mm}$ . The line width is 0.2 mm and radiating width of 4 mm.

$S_{11}$  plots of samples of meshed monopole are shown in Figure 4.37. Antenna sample 21 (measured) 894 MHz at  $-52.32\text{ dB}$  and  $-10\text{ dB}$  bandwidth (862 – 942 MHz) while the simulated  $S_{11}$  is 899 MHz at  $-11.22\text{ dB}$ ,  $-10\text{ dB}$  bandwidth (878 – 926 MHz). The measured and simulated  $S_{11}$  of antenna sample 24 are 885 MHz at  $-57.25\text{ dB}$ ,  $-10\text{ dB}$  bandwidth (861 – 927 MHz) while simulated value is 892 MHz at  $-16.62\text{ dB}$ ,  $-10\text{ dB}$  bandwidth (852 – 949 MHz).

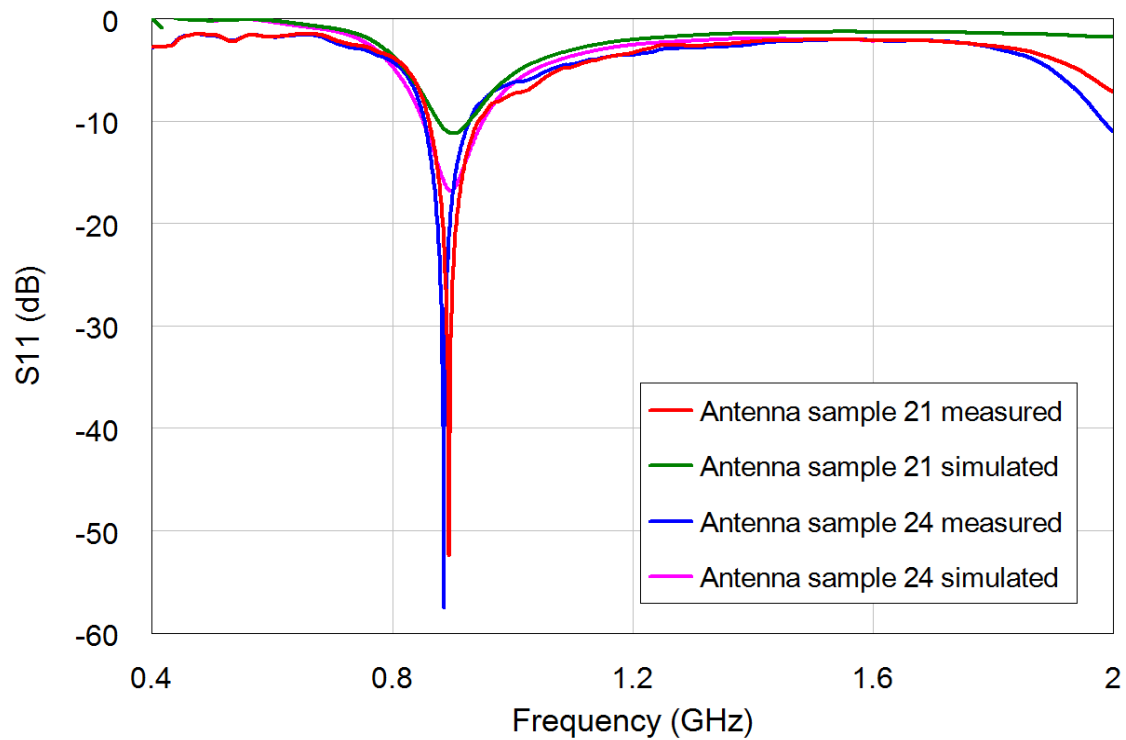


Figure 4.37 Measured  $S_{11}$  of two size meshed monopole antennas with different mesh parameters on FR4 see Table 4.5 for detail of antennas

The details of the geometries of the meshed monopole are shown in Table 4.5. The unmeshed monopole and uniformly meshed monopole exhibit similar resonant frequencies and -10dB bandwidth. The mesh material used was a copper conductor. The linewidth was fixed at  $0.2\text{ mm}$  while the number of vertical lines is 5 and the number of horizontal lines varied from 41 to 3. The transparency ranged from 64.57% to 73.55%. Reducing the horizontal lines of the meshed monopole does not change the antenna performance. Meshing is carried out to reduce the material used in fabrication of the meshed monopole whilst maintaining acceptable antenna performance.

Table 4.3 Geometry of meshed monopole antennas on FR-4

| Meshed monopole type | Meshed monopole dimensions $L \times W$ (mm) | Measured $f_0$ (MHz) | Measured $S_{11}$ (dB) | -10 dB Bandwidth (MHz) | $N_h$             | $N_v$ | $T_{monopole}$ (%) |
|----------------------|--|----------------------|------------------------|------------------------|-------------------|-------|--------------------|
| Unmeshed monopole    | 68 by 4                                      | 864                  | -28.14                 | 238                    | unmeshed          |       | 100                |
| Sample 20            | 68 by 4                                      | 920                  | -32.86                 | 282                    | 41                | 5     | 67.59              |
| Sample 21            | 84 by 4                                      | 894                  | -52.19                 | 71                     | 10                | 5     | 73.55              |
| Sample 24            | 84 by 4                                      | 884                  | -56.40                 | 73                     | 18                | 5     | 71.74              |
| Sample 25            | 84 by 4                                      | 721                  | -27.05                 | 96                     | 3                 | 3     | 64.57              |
| Sample 26            | 84 by 4                                      | 901                  | -47.71                 | 80                     | 41                | 5     | 67.59              |
| Sample 27            | 84 by 3                                      | 904                  | -42.20                 | 138                    | Triangular meshed |       |                    |

#### 4.9.2. Surface current distribution

Figure 4.38 shows the currents on the vertical and horizontal line of a meshed monopole antenna. A detailed analysis of the surface current show that current flows along the vertical and horizontal lines. There is more current flow along the vertical lines showing that the main current flows in that direction. The horizontal lines causes meandering in the current path and the vertical lines decreasing surface current leading to lengthened current path. The fundamental resonant frequency is lowered due to more meandering sections. Current flows along the surface within antenna vertical length because of the number of paths but mesh paths are two dimensional. The meshed monopole forces a slight offset on the source position.



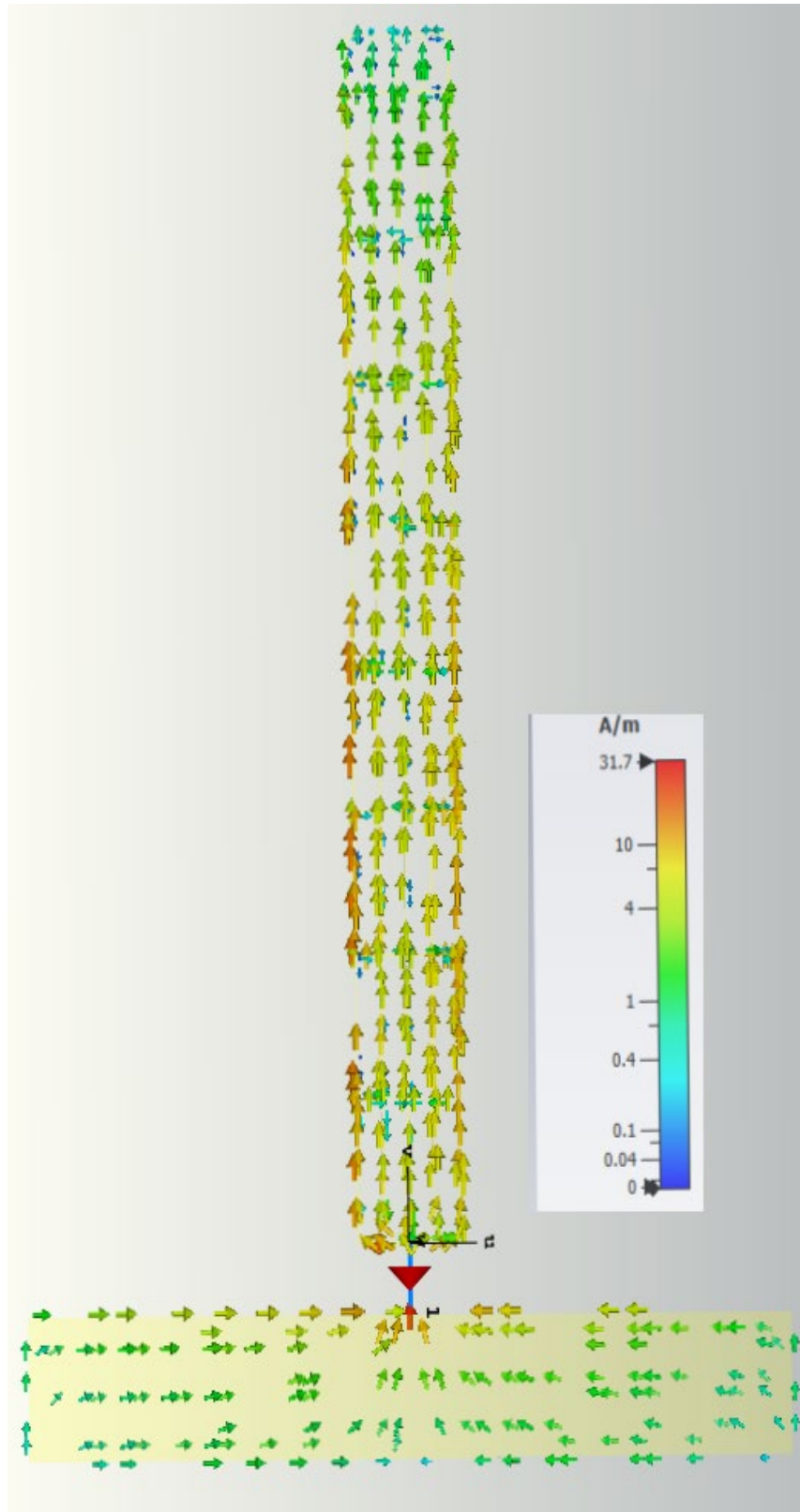


Figure 4.38 Simulated surface current for antenna sample 21 at 900 MHz.

### 4.9.3. Stitched meshed monopole

The meshed monopole antenna samples were named as shown in Table 4.4 Figure 4.39(a), (b), (d) and (f) are of the dimensions. Antennas have different stitching designs. Figure 4.39(c) and (e) uses the different square stitched configurations with same dimensions.

Table 4.4 Parameters of stitched monopole antennas

| S/No | Antenna samples (Dimensions in mm)                                 | Stitched pattern     | Fabric |
|------|--|----------------------|--------|
| 1    | M01: ground ( $70 \times 10$ ) radiating element ( $84 \times 4$ ) | Cross stitch         | Felt   |
| 2    | M04: ground ( $70 \times 10$ ) radiating element ( $84 \times 4$ ) | Square stitch        | Denim  |
| 3    | M05: ground ( $70 \times 10$ ) radiating element ( $84 \times 4$ ) | Cross stitch         | Denim  |
| 4    | M4: ground ( $70 \times 10$ ) radiating element ( $84 \times 4$ )  | Cross stitch         | Felt   |
| 5    | M1: ground ( $68 \times 10$ ) radiating element ( $83 \times 4$ )  | Triangular           | Felt   |
| 6    | M03: ground ( $65 \times 5$ ) radiating element ( $84 \times 4$ )  | Square with diagonal | Denim  |
| 7    | M3: ground ( $68 \times 10$ ) radiating element ( $84 \times 4$ )  | Square stitch        | Denim  |
| 8    | M02: ground ( $70 \times 10$ ) radiating element ( $84 \times 4$ ) | Running stitch       | Denim  |
| 9    | M5: ground ( $70 \times 10$ ) radiating element ( $84 \times 4$ )  | Fill stitch          | Denim  |
| 10   | M6: ground ( $70 \times 10$ ) radiating element ( $84 \times 4$ )  | Fill stitch          | Felt   |

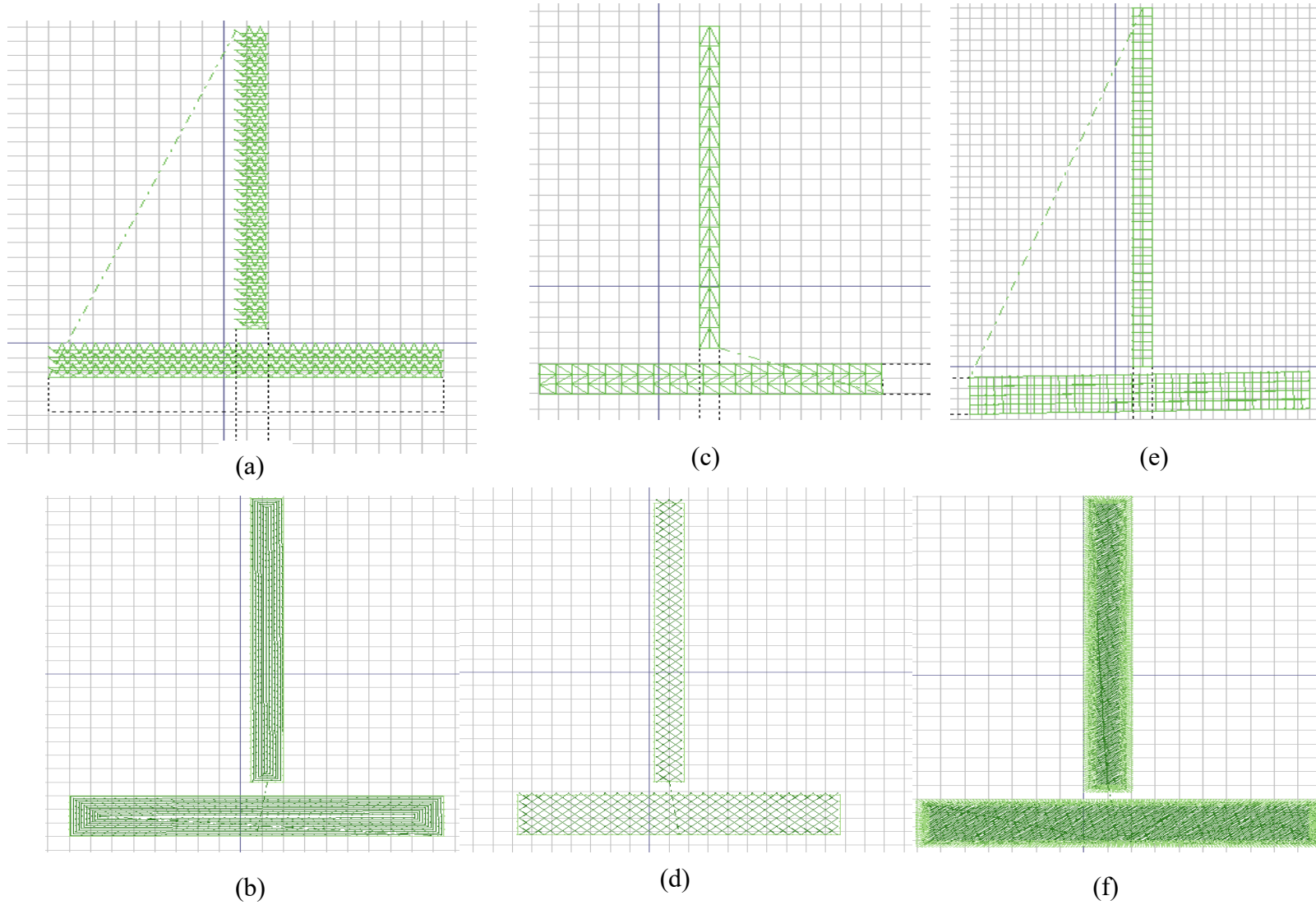


Figure 4.39 Stitching patterns (a) triangular stitch (b) running stitch (c) square with diagonal stitch (d) cross stitch (e) square stitch (f) fill stitch

Table 4.5 Measured results for stitched monopole antennas same nominal dimensions in all cases

| Antenna design                          | Running (Denim) M2 | Square with diagonal (Denim) M3 | Fill stitch (Denim) M5 | Square (Denim) M03 | Triangular (Felt) M1 | Fill stitch (Felt) M4 | Cross stitch (Felt) M01 |
|---|--------------------|---------------------------------|------------------------|--------------------|----------------------|-----------------------|-------------------------|
| Measured $f_0$ (MHz)                    | 935                | 880                             | 937                    | 909                | 919                  | 937                   | 951                     |
| Measured $S_{11}$ (dB)                  | -26.81             | -31.71                          | -31.39                 | -28.96             | -23.29               | -31.39                | -20.56                  |
| -10dB Bandwidth (MHz)                   | 114                | 81                              | 120                    | 57                 | 85                   | 122                   | 83                      |
| Number of stitches                      | 1254               | 390                             | 1254                   | 1280               | 1254                 | 1254                  | 1547                    |
| Antenna length (mm) $\times$ width(mm). | $84 \times 4$      | $84 \times 4$                   | $84 \times 4$          | $84 \times 4$      | $84 \times 4$        | $84 \times 4$         | $84 \times 4$           |

The stitched patterns were created using the Bypass stitching method that is explained in chapter 5. The monopole antenna was embroidered onto a felt layer as shown in Fig.4.40. The Stitch pattern is triangular. Due to nature of the Amberstrand thread which has protruding broken strands, edges of the triangle are not smooth. Figure 4.39 shows the five different stitching patterns for embroidery software used in this study. The parameters are shown in Table 4.4. The fabricated geometry is stitched with a better than 1mm precision and the lengths are different due to nature of pattern realisations. Using the monopole dimensions, five different types of stitch were considered: running stitch, cross stitch and fill stitch, square and triangular stitched design. Simulation and measurement were carried out over the frequency range of (0.4 – 2.0 GHz) in each case. Measured  $S_{11}$  results are shown in Fig.4.41, It is shown monopole antenna (M03) is well matched resonant frequencies;  $S_{11}$  of M03 is  $-28.9\text{ dB}$  at 909 MHz, with 57 MHz – 10 dB bandwidth. The antenna M03 has two resonances at 909 MHz and 1804 MHz at  $-13.3\text{ dB}$  width 100 MHz – 10 dB bandwidth.

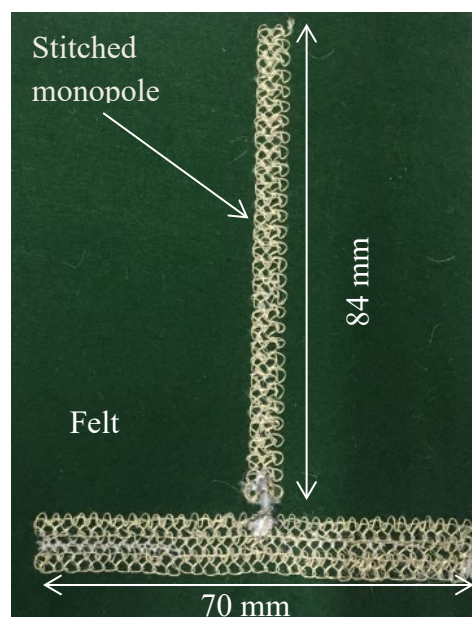


Figure 4.40 Triangular stitched pattern of monopole antenna

Some stitched antenna parameters for both ground and radiating element, M3 is 390: Total antenna height of 84.20 mm, radiating element of monopole 83 mm and width of ground plane of 10 mm, length of ground plane of 68 mm. Sample M03 uses a total number of stitch 1280 but a square stitch pattern design with MATLAB. Parameters for embroidered

monopole antennas height of 84mm and width of the ground of 70mm. As shown in Figure 4.42 measured  $S_{11}$  of  $M1$  of  $-23.3\text{ dB}$  at  $919\text{ MHz}$  and a  $-10\text{ dB}$  bandwidth  $77\text{ MHz}$  ranging from  $888\text{ MHz}$  to  $966\text{ MHz}$  while  $M2$  presented  $S_{11}$  of  $-26.75\text{ dB}$  at  $937\text{ MHz}$  and  $-10\text{ dB}$  bandwidth of  $128\text{ MHz}$  ranging from  $888\text{ MHz}$  to  $1016\text{ MHz}$ .  $M2$  and  $M1$  are all fully textile monopole antennas.  $M2$  has a larger bandwidth than  $M1$  because larger ground plane and the stitched pattern. In both designs, the bandwidth is larger to cover the entire GSM 900.

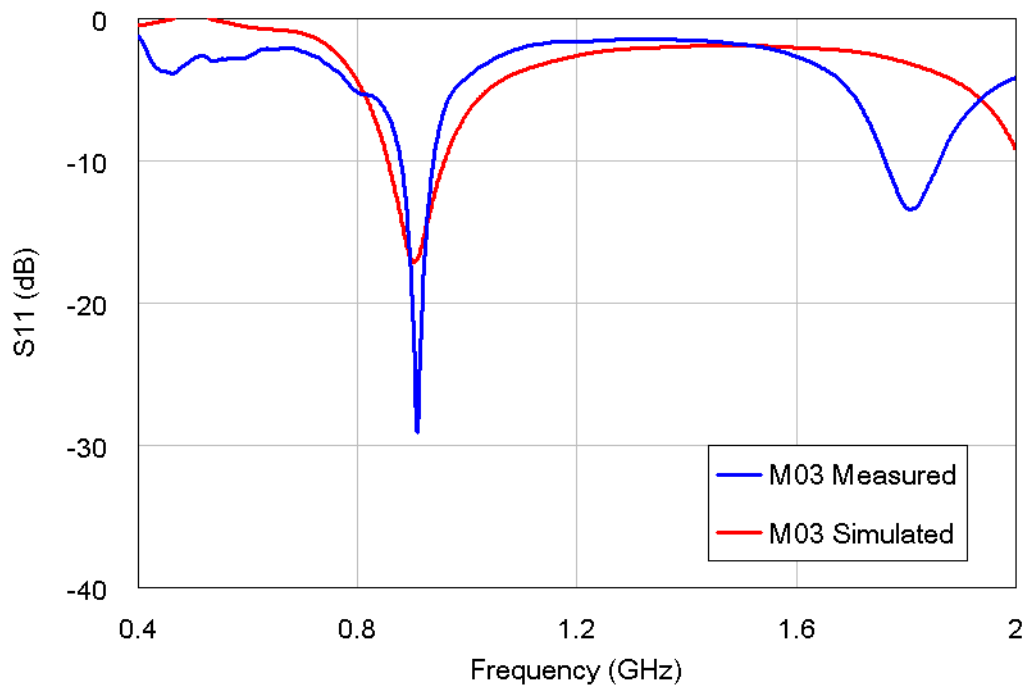


Figure 4.41  $S_{11}$  plot of antenna sample  $M03$  employing denim fabric

The meshed monopole antenna ( $M6$ ) employing the fill stitch in realisation has a stitch count of 1254 with an antenna height of 84 mm and ground plane antenna width of 70 mm. The simulated and measured  $S_{11}$  results are shown in Fig. 4.43.  $S_{11}$  of  $M5$  (simulated) is  $-16.96\text{ dB}$  at  $906\text{ MHz}$  with  $-10\text{ dB}$  bandwidth of  $93\text{ MHz}$  ranging from  $856\text{ MHz}$  to  $953\text{ MHz}$  while measured  $S_{11}$  given as  $-34.57\text{ dB}$  at  $918\text{ MHz}$ ,  $-10\text{ dB}$  bandwidth  $120\text{ MHz}$  ( $871\text{ MHz} - 991\text{ MHz}$ ). Simulated and measured  $S_{11}$  of  $M6$  are  $-14.48\text{ dB}$  at  $906\text{ MHz}$  with a  $-10\text{ dB}$  bandwidth of  $135\text{ MHz}$  ( $856\text{ MHz} - 991\text{ MHz}$ ) while measured  $S_{11}$  of  $-30.28\text{ dB}$  at  $940\text{ MHz}$ ,  $-10\text{ dB}$  bandwidth of  $124\text{ MHz}$  ( $890\text{ MHz} - 1014\text{ MHz}$ ). Both fully textile monopole antennas cover the GSM900 band. The differences between simulation and measurement results of  $S_{11}$  and resonant frequencies may be attributed to fabrication error as results of flexible coaxial SMA positions.

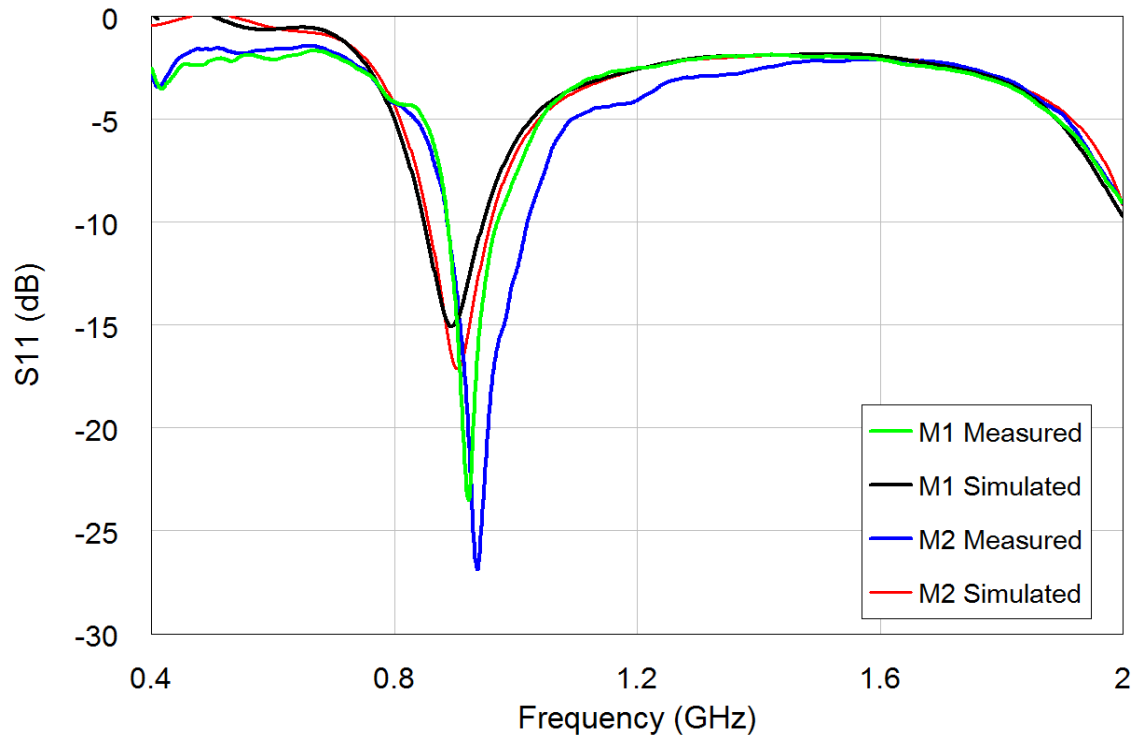


Figure 4.42  $S_{11}$  plot of measured meshed stitch antenna samples on denim

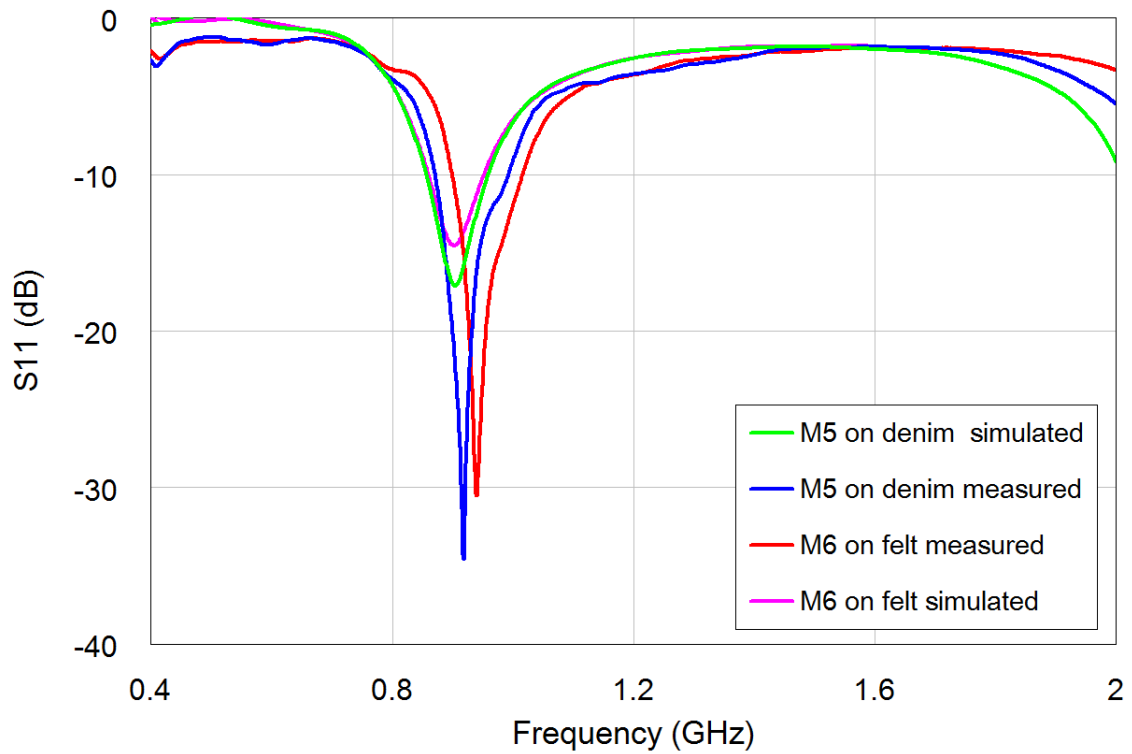


Figure 4.43  $S_{11}$  plot of meshed monopole antenna employing denim and felt fabric

#### **4.9.4. Summary**

The fabric samples were measured using the split post dielectric resonator to determine dielectric properties. The wearable monopole and pocket antennas were simulated using CST Microwave Studio using the denim and felt fabric as substrate with permittivity of 1.97 and 1.2 respectively. A set of fully textile pocket and collar antennas were developed making flexibility and automation of the production process easier using the embroidery machine. Based on the results, the bandwidth of meshed monopole antenna is proportional to number of stitches. The greater the number of stitches the better impedance bandwidth at -10 dB see as Table 4.5. Using the same dimensions of the antenna but different stitch patterns gives different impedance bandwidth.

The stitched pocket and collar antennas with fabric substrate can replaced the rigid antenna of same configurations. The antennas are seamlessly integrated onto felt and denim substrate which could be placed on a garment and address the requirement of unobtrusiveness of wearable antennas.



## Conclusion

A range of test antennas were constructed and fabricated on fabric and FR4. The stitched triangular pattern is a valid alternative to solid conductors. The stitched antennas using Bypass design yields comparable results to antennas stitched using cross stitch or running stitch of the same dimensions. The measured  $S_{11}$  results and simulated samples of the embroidered and meshed monopole antennas exhibits similar resonant frequencies for the same dimensions.

This chapter reports the validation of a numerical optimisation method for the design of linear wire antennas using GA (MATLAB)-NEC2 through experimental measurements. Results from the automated methods were compared with CST models, showing good agreement. Results of the pocket antennas were fabricated. Measurements of antenna return loss were performed with 37397D VNA. Radiation patterns of optimised linear wire antenna, planar and fabric antennas were measured in H-plane and E-plane in the anechoic chamber.

This procedure of using the GA coupled with NEC2 to optimise parameters of antenna yields good designs, showing remarkable performance in terms of bandwidth and return loss ( $S_{11}$ ). There were good agreements between simulated and measured  $S_{11}$  of the optimised linear wire antennas. The proposed antenna designs were well matched as the bandwidth covers the GSM 900MHz. It is observed that as ground plane width of the fabric antennas increased, the gain and radiated efficiency improved. On-body measurement and simulation have been validated. The antenna shows some detuning effects when placed on the body with a resonance frequency shift as in the  $S_{11}$  plots. The distance in which the on-body antenna was placed on the body during the test show some deviation to the free space because of additional layers of clothing as the expected results.

## References

- 4.1. R. Ghatak, D. R. Poddar, and R. K. Mishra, "Design of Sierpinski gasket fractal microstrip antenna using real coded genetic algorithm," *IET Microwaves, Antennas Propag.*, 3(7), pp. 1133, 2009.
- 4.2. E. E. Altshuler and D. S. Linden, "Wire-antenna designs using genetic algorithms," *IEEE Antennas Propagation Mag.*, 39(2), pp. 33–43, 1997.
- 4.3. A. J. Kerkhoff, R. L. Rogers, S. Member, and H. Ling, "Design and Analysis of Planar Monopole Antennas Using a Genetic Algorithm Approach," *IEEE Antennas Propag. Mag.*, 52(10), pp. 2709–2718, 2004.
- 4.4. D. S. Linden and E. E. Altshuler, "Evolving Wire Antennas Using Genetic Algorithms: A Review," in, A. Stocia, D. Keymeulen and J. Lohn, *Proc. of 1st NAS/DoD Workshop on Evolvable Hardware*, IEEE Computer Soc. Press, pp 225-232, 1999.
- 4.5. S. Zhang, "Design Advances of Embroidered Fabric Antennas," PhD, dissertation Loughborough University, Loughborough, April 2014.
- 4.6. R. Seager, S. Zhang, A. Chauraya, W. Whittow, Y. Vardaxoglou, T. Acti, and T. Dias, "Effect of the fabrication parameters on the performance of embroidered antennas," *IET Microwaves, Antennas Propag* 7, pp. 1174–1181, 2013.
- 4.7. S. Zhang, A. Chauraya, W. Whittow, R. Seager, T. Acti, T. Dias, and Y. Vardaxoglou, "Embroidered Wearable Antennas Using Conductive Threads with Different Stitch Spacings," *Loughborough Antennas and Propagation Conference*, pp. 6–9, 2012.
- 4.8. A. Chauraya, R. Seager, W. Whittow, S. Zhang, and Y. Vardaxoglou, "Embroidered Frequency Selective Surfaces on Textiles for Wearable Applications," in *Loughborough Antennas & Propagation Conference (LAPAC)*, pp. 388–391, 2013.
- 4.9. Y.F. Weng, S.W. Cheung and T.I. Yuk, "Effects of Ground-Plane Size on Planar UWB Monopole Antenna," in *TENCON 2010-2010 IEEE Region 10 Conference*, pp. 422-425, 2010.
- 4.10. S. Virdee, "Miniature microstrip-fed ultra-wideband printed monopole antenna with a partial ground plane structure," *IET Microwaves, Antennas Propag.*, pp. 1683–1689, 2011.
- 4.11. N. H. M. Rais, P. J. Soh, F. Malek, S. Ahmad, N. B. M. Hashim, and P. S. Hall, "A Review of Wearable Antenna," in *Proc. LAPC. Loughborough, U.K.*, pp. 225-228, 2009.

- 4.12. T. Yasin, R. Baktur, T. Turpin, and J. Arellano, “Analysis and Design of Highly Transparent Meshed Patch Antenna Backed by a Solid Ground Plane,” *Prog. Electromagn. Res. M*, 56, pp. 133–144, 2017.
- 4.13. U. Ali, S. Ullah, J. Khan, M. Shafi, B. Kamal, A. Basir, J.A. Flint and R. D. Seager. “Design and SAR analysis of wearable antenna on various parts of human body, using conventional and artificial ground planes,” *Journal of Electrical Engineering and Technology*, 12 (1), pp. 317-328, 2017.
- 4.14. T. Kellomaki, J. Heikkinen and M. Kivikoski, “Wearable antennas for FM reception,” In 2006 First European Conference on Antennas and Propagation, pp. 1-6, IEEE, 2006.
- 4.15. C.A. Balanis, “Antenna theory: analysis and design,” John Wiley & sons. 2016.

## **Chapter 5**

### **Optimisation of antenna meshing**

So far, in this thesis some results have been presented for meshed copper and textile monopoles. This chapter explores the optimal mesh structure, density and production techniques. This chapter starts by looking at meshed ground planes for patch antennas as a generic problem. The ground plane of the bent wire and linear monopole is a line. Using a microstrip ground plane provides a proper surface to look at the resistances between meshes. The primary focus of this section is to design a ground plane for microstrip patch antennas using textile materials and standard textile manufacturing techniques of computerised embroidering of conductive thread into fabric.

#### **5.1. Introduction to Meshed Ground plane for microstrip patch antennas**

Textile structures are used for wearable antennas because they are light weight, long-lasting, flexible and conformable. This structure is also soft, deformable, breathable, durable, and washable. Textile antennas have recently been studied by different researchers because of a number of possible applications (i.e. personal communications, health monitoring, sport training, wearable sensors, location tracking, biomedical, antimicrobial textiles ) as well as relative low cost [5.1]-[5.2].

This study is in two parts, measurement on the proposed stitched ground plane compared with an infinite resistive network and using embroidery techniques to increase the stitch density to achieve the same as high stitch density antenna designs. Fabrication of the antennas is by embroidery on fabric performance and etching on FR4 substrate. For comparison, fabrication techniques are important when determining the characteristics, cost, and stability of fibre-based flexible and wearable antennas.

Solid patch antennas with meshed ground are presented as a reference showing the effects on the resonance frequency. Different stitch patterns and densities on the proposed antennas are examined in this chapter. A stitch pattern is developed for the proposed antenna using the microstrip patch antenna as the basis for evaluating the performance.

Meshing renders antenna metallisation transparent and a transparency is evaluated based on the mesh geometry. In [5.3] meshed patch antennas have similar properties to normal microstrip patch antenna since they use less metal making them optically transparent. Meshed monopole antennas are designed and embroidered to show metal coverage using CST

Microwave Studio. All fabricated textile antennas have been designed to function within the 2.45 GHz industrial, scientific, and medical (ISM) band and 5 GHz wearable wireless local area networks (WLAN) frequencies.

## 5.2. Development of designs: Theory of infinite arrays of resistors

It is possible to relate the embroidered mesh structure to the electrical resistance of a resistive network helping to define a sheet or surface resistance. The theory of electrical networks was formulated by Kirchhoff based on linear analysis. This entailed computation of the resistance between nodes in a resistive network considering their potentials. Figure 5.1 gives an illustration of infinite number resistors of resistance ( $R$ ) connected in the form of either a rectangular or square grid. The current that entered a node will be equal to the current leaving and each of the four resistors connected to a node carries a current of  $I/4$ . The resulting voltage drop between the two nodes will be equal  $\left(\frac{I}{4}\right) R$  [5.4-5.6].

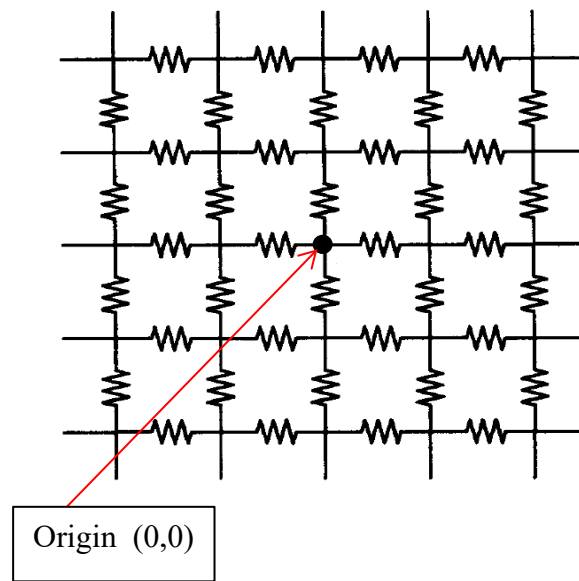


Figure 5.1 A square cut from the infinite array

The node number is represented by  $n$  and  $m$  for the calculation of an equivalent resistance between two arbitrary nodes. The grid is a two dimensional  $m \times n$  square resistance network as shown in Figure 5.1. Applying Kirchhoff's current law at node  $(m, n)$ , the external current entering the node must be equal to the current leaving the node through four resistors that is attached to a node. This concept is given as [5.4]

$$I_{m,n} = (V_{m,n} - V_{m,n+1})/R + (V_{m,n} - V_{m,n-1})/R$$

$$+ (V_{m,n} - V_{m+1,n})/R + (V_{m,n} - V_{m-1,n})/R. \quad (5.1)$$

At a node where  $I_{m,n}$  is zero, this expression (5.1) reduces to

$$4V_{m,n} = V_{m,n+1} + V_{m,n-1} + V_{m+1,n} + V_{m-1,n}. \quad (5.2)$$

The equations (5.1) and (5.2) are finite difference equivalents of Poisson's and Laplace's equations respectively. The resistance between (0,0) and (m,n) could be obtained directly from the solution of the problem in which the current I enters at (0,0) and leaves at infinity and given in terms of the nodes voltages, the resistance is  $R_{m,n} = 2(V_{0,0} - V_{m,n})/I$ ,

$$R_{m,n} = (R/2\pi) \int_0^\pi (2 - e^{-|m|\alpha} \cos(n\beta) - e^{-|n|\alpha} \cos(m\beta)) / \sinh(\alpha\beta) d\beta, \quad (5.3)$$

where  $\alpha$  and  $\beta$  is given as  $\cosh(\alpha) + \cos(\beta) = 2$  and equation (5.4) is expressed as

$$\begin{aligned} R_{m,n} &= (R/\pi) \int_0^\pi (1 - e^{-|m|\alpha} \cos(n\beta)) / \sinh(\alpha\beta) d\beta, \\ &= (R/\pi) \int_0^\pi (1 - e^{-|n|\alpha} \cos(m\beta)) / \sinh(\alpha\beta) d\beta \end{aligned} \quad (5.4)$$

Equations (5.1-5.4) may be summarised as giving resistance [5.4]:

$$R_{0,0} = 0; R_{1,0} = R/2; R_{1,1} = 2R/\pi.$$

### 5.3. Simulation of finite array

A code was developed for calculating the resistance from the centre of a finite grid of resistors to every point in the grid, nodal analysis is used to do the calculation. Assuming that the nodal voltage at each point is  $V(i,j)$ . A finite grid of resistors were created and defects were then introduced into the grid. This is the fraction of the available branches or nodes that have a defect; if a resistor does not connect to a node it is deleted from the netlist completely. There need to be 4 branches before this defect can occur. This is why the ones on the edge are always connected and it goes to the same value.

Figure 5.1 shows the real part of normalised impedance in a finite array. The most defective part of the grid is at the edge where the nodes are connecting. The numerical simulation data is depicted in Table 5.1. The approach used for find the resistance that would be measured between spaced nodes is same with the result obtained.

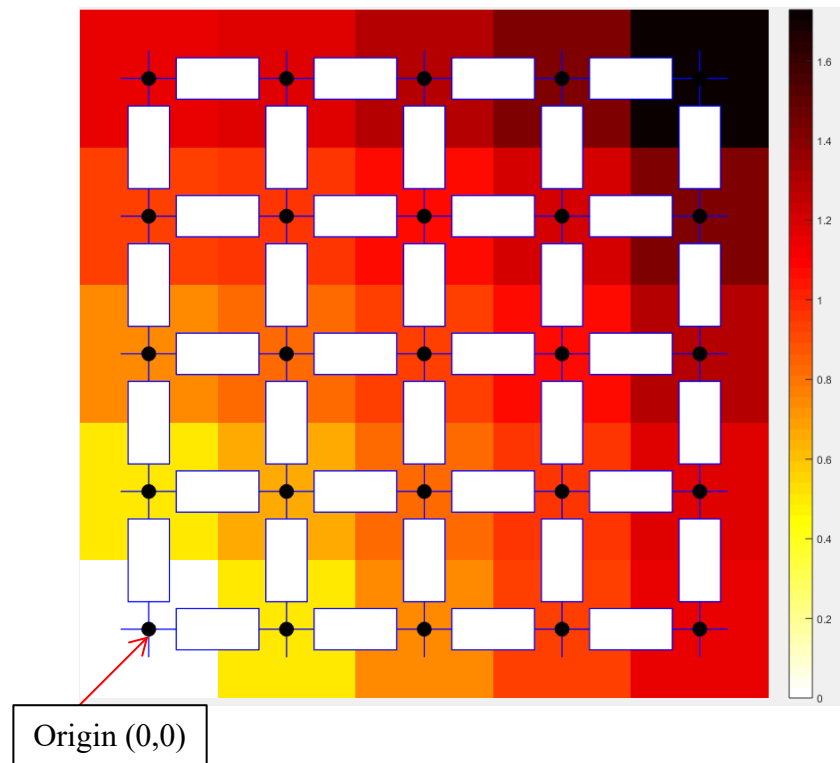


Figure 5.2 Real part of the normalised resistance to each grid point for a  $(4 \times 4)$  array

Table 5.1 Finite numerical simulation of the real part of normalised resistance one quarter of a finite array.

|         |         |         |         |         |
|---------|---------|---------|---------|---------|
| 1.1502  | 1.1882  | 1.2734  | 1.4268  | 1.7288  |
| node 20 | node 21 | node 22 | node 23 | node 24 |
| 0.9367  | 0.9735  | 1.0546  | 1.1940  | 1.4268  |
| node 15 | node 16 | node 17 | node 18 | node 19 |
| 0.7562  | 0.8129  | 0.9199  | 1.0546  | 1.2734  |
| node 10 | node 11 | node 12 | node 13 | node 14 |
| 0.5069  | 0.6513  | 0.8129  | 0.9635  | 1.1892  |
| node 5  | node 6  | node 7  | node 8  | node 9  |
| 0       | 0.5069  | 0.7562  | 0.9366  | 1.1592  |
| node 0  | node 1  | node 2  | node 3  | node 4  |

Origin (0,0)

In the next section a method for constructing textile meshes is developed for MATLAB. This was used to construct physical prototypes.

## 5.4. Bypass method for stitched pattern designs

The stitch pattern for the antennas were created using MATLAB. The MATLAB code is written to reproduce the required stitch pattern proposed. Personal embroidery machine (PE-NEXT) file format is in a .pes file and the instructions for creating pattern commands are 'end', 'stop', 'jump' and 'trim.' The embroidermodder 2.00 software allows one to edit, scale and convert embroidery files to other formats using the libembroidery library. This library supports writing and reading CSV (comma separated values) format files. The file format can be viewed in microsoft excel or Notepad since it is in a spreadsheet. The process conversion from .csv to .pes for the embroidery machine is shown in Fig.5.3. Once the conversion is successful, the pattern is viewed in the embroidery software to check how the pattern looks. The designed pattern is exported to the embroidery machine via a USB port.

When manufacturing a meshed conductive surface the embroidery machine is, ideally to traverse each branch of the mesh only once. This gives gains in terms of production time as well as economy of yarn use. Figure 5.4 shows three possible mesh patterns, two of which meet the criterion of stitching each path only once. The mathematical solution to the problem is not trivial, requiring the evaluation of the euler path. The patterns were created using a set of coordinates geometry and linear equation to actualised the patterns. Stitches are formed by interlocking an upper and a lower yarn (looper).

The size of the squares is in millimetres. The horizontal stitches were created before vertical stitches by making the full length of the line to maximum  $(x, y)$ . Vertical lines were formed from left to right and the last line on  $+y$  before reaching  $x = 0$ . The next full length of line to min  $y$  to one over and make the horizontal lines top to bottom. Figure 5.4 (c) is triangular stitch formations where using the  $x$  and  $y$  coordinates. Create a base for the  $x$  and  $y$  as the  $size_x$  and  $size_y$ . The triangle is created in equilateral shape.

The study of different stitch pattern and sewing type for meshed patch antennas results in different effects on embroidery accuracy and RF performances. Embroidery designs use several sewing types such as zigzag stitch, fill stitch, and spiral stitch. The automated embroidery machines in Loughborough University is used to transform the antenna designs into a stitching pattern for all the stitched antennas [5.7-5.8]. Three different stitching types were created and generated using MATLAB as indicated in Figure 5.4



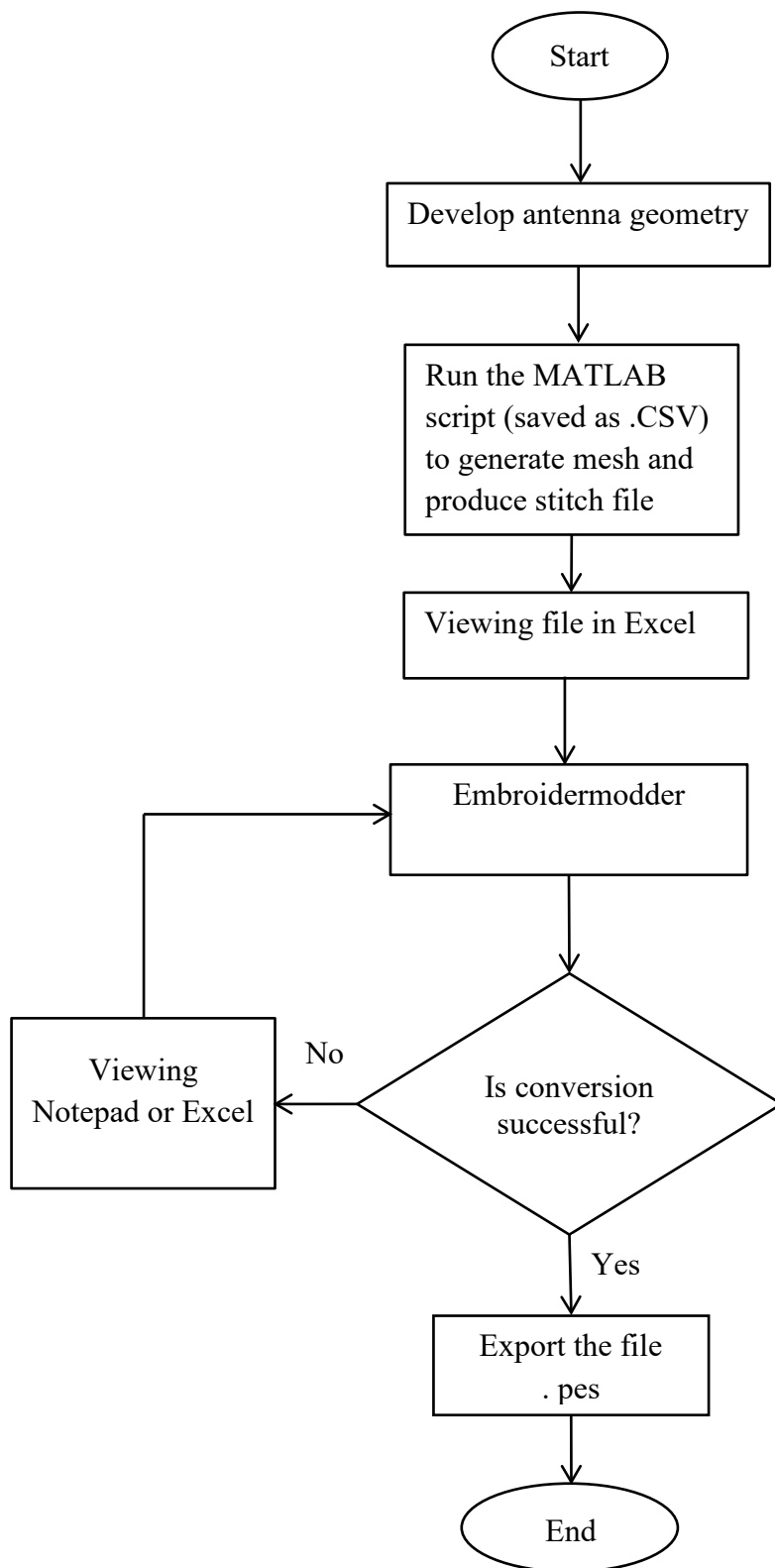
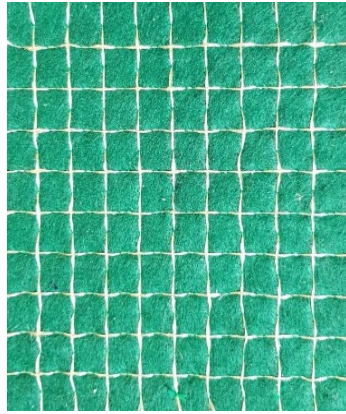


Figure 5.3 Bypassing techniques used for stitch pattern formation



Where  $R = 6.54 \Omega\text{m}^{-1}$  and  $R\Delta L$  is the equivalent resistance of one cell width. From the format in Fig.5.5 all the nodes seem to be connected but this is not so because of the varying tension of the yarn. The major challenges were find out if the nodes are electrically connected. It is observed that the stitches were not always connected at each node, the four threads go through the same hole but there is no electrical contacts. The pattern was created to improved electrical connections across the horizontal and vertical sections. It is a square meshed of size  $8 \times 8$ , with an off-set threads were created of  $\frac{1}{2}$  a grid distance. The nodes are interconnected when checked with a multimeter.

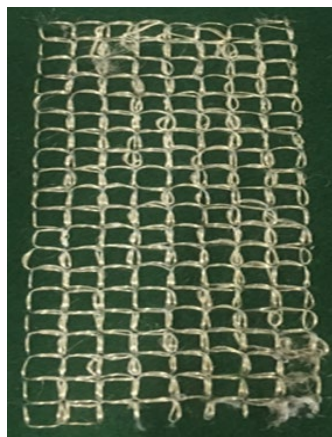
The output sample of the stitched meshes on felt and denim is shown in Fig.5.6(a-f). All the output samples were designed and fabricated using the Bypass method. Samples (a) and(d) are the same offset designs but on different materials. Samples (b) and (d) are rectangular design of the stitched ground plane on felt substrate. The triangular stitched mesh developed and fabricated on a felt substrate (Fig.5.6(c)). The diagonally cross rectangular stitched mesh is shown in Fig.5.6(f).



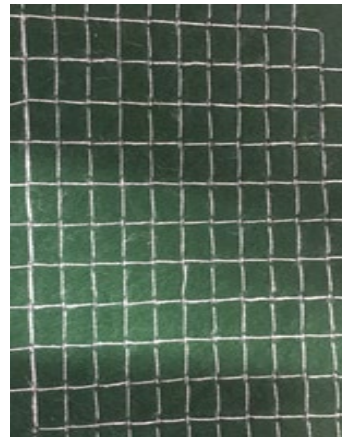
(a)



(d)



(b)



(e)



(c)



(f)

Figure 5.6 Output samples of stitched meshes on felt and denim

## 5.5. Measurements of Meshed resistive network

There are various methods for determining the electrical resistance of electroconductive fabric which include two-electrode method, constant voltage, constant current method, Wheatstone-bridge method and Thomson-bridge method [5.10]. The two-wire used by the ohmmeter measurement is not reliable for measuring low resistances because the resistance of the leads, which may be of the same size as the resistance you are measuring. The four-point probe method is used to overcome the problem of the two-point probe method. This approach gives the function at relationship between the resistance and the voltage and current readings for the various geometries [5.11]. In this measurement the standard 4-wire Kelvin bridge method (separate voltage and current sense probes) was used to obtain the highest accuracy since measuring a low resistance across the grid.

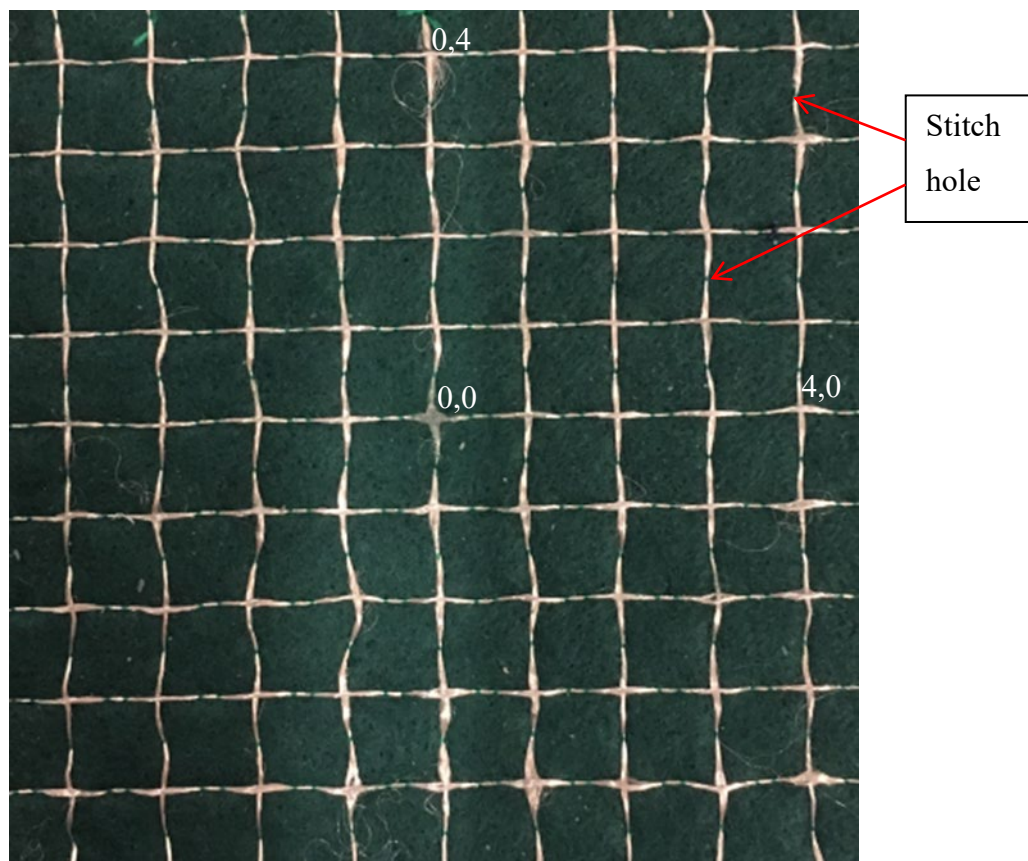


Figure 5.7 Measurement referenced point of meshed ground plane

The measurements were carried using the point (0,0) indicated on the Fig. 5.7 as the referenced node. Analogue meter (HP4328A milliohmmeter) was used but had its precision augmented by connecting a high impedance digital meter in parallel with the moving coil

panel meter in the instrument. The digital meter was calibrated however due to the normalisation this effect was cancelled out. The theoretical value for Amberstrand (R) =  $2\Omega/\text{foot} = 6.54 \Omega\text{m}^{-1}$ . For example the distance between two nodes of 7mm = 46.04 m $\Omega$ . This value is an approximation because across the meshes the distances look equal. Pressing down the probe of the multimeter gives a better results when measuring between nodes across a meshed on fabric material. The measured results from the node points are shown in Table 5.2.

Note the edge effect on the measurements, which are on smaller array than the modelled mesh.

Table 5.2 Measured mesh point values normalised data for an  $8 \times 8$  stitched ground plane

|    | -4     | -3     | -2     | -1     | 0      | 1      | 2      | 3      | 4      |
|----|--------|--------|--------|--------|--------|--------|--------|--------|--------|
| 4  | 1.5443 | 1.3357 | 1.1815 | 1.1424 | 1.0968 | 1.1750 | 1.3466 | 1.4270 | 1.5638 |
|    |        |        |        |        | node20 | node21 | node22 | node23 | node24 |
| 3  | 1.3357 | 1.1880 | 1.1685 | 1.0099 | 0.9470 | 0.9231 | 1.0143 | 1.1012 | 1.3119 |
|    |        |        |        |        | node15 | node16 | node17 | node18 | node19 |
| 2  | 1.1707 | 1.0056 | 1.0143 | 0.8601 | 0.7384 | 0.7558 | 0.8622 | 1.0512 | 1.1316 |
|    |        |        |        |        | node10 | node11 | node12 | node13 | node14 |
| 1  | 1.1055 | 0.8709 | 0.7493 | 0.6993 | 0.4973 | 0.7775 | 0.7037 | 0.8014 | 1.0143 |
|    |        |        |        |        | node 5 | node 6 | node 7 | node 8 | node 9 |
| 0  | 0.9708 | 0.8318 | 0.6972 | 0.5125 | 0      | 0.4973 | 0.7428 | 0.8731 | 0.9600 |
|    |        |        |        |        | node 0 | node 1 | node 2 | node 3 | node 4 |
| -1 | 1.0686 | 0.8622 | 0.7341 | 0.6841 | 0.5582 | 0.7145 | 0.8166 | 0.8644 | 1.0078 |
| -2 | 1.1403 | 0.9622 | 0.9860 | 0.8796 | 0.7645 | 0.8601 | 0.9817 | 0.9730 | 1.0403 |
| -3 | 1.3598 | 1.1576 | 1.1598 | 1.1012 | 1.0317 | 0.9795 | 1.1272 | 1.2098 | 1.2554 |
| -4 | 1.5399 | 1.4487 | 1.3705 | 1.1989 | 1.1989 | 1.3227 | 1.2836 | 1.4183 | 1.5551 |

Origin (0,0)

Table 5.3. Resistances  $R_{(m,n)}$  between node (0,0) and node (m,n) in units of R of infinite array (analytical data adapted from [5.4]).

| n/m | 0      | 1      | 2      | 3      | 4      | 5     | 6     | 7     | 8     | 9     | 10    |
|-----|--------|--------|--------|--------|--------|-------|-------|-------|-------|-------|-------|
| 10  | 1.247  | 1.248  | 1.253  | 1.261  | 1.271  | 1.283 | 1.296 | 1.311 | 1.326 | 1.342 | 1.358 |
| 9   | 1.214  | 1.215  | 1.221  | 1.230  | 1.242  | 1.257 | 1.272 | 1.289 | 1.306 | 1.324 | 1.342 |
| 8   | 1.176  | 1.178  | 1.186  | 1.197  | 1.212  | 1.229 | 1.247 | 1.267 | 1.287 | 1.306 | 1.326 |
| 7   | 1.133  | 1.136  | 1.146  | 1.160  | 1.179  | 1.200 | 1.222 | 1.244 | 1.267 | 1.289 | 1.311 |
| 6   | 1.084  | 1.088  | 1.101  | 1.120  | 1.144  | 1.169 | 1.195 | 1.222 | 1.247 | 1.272 | 1.296 |
| 5   | 1.026  | 1.032  | 1.050  | 1.076  | 1.106  | 1.317 | 1.169 | 1.200 | 1.229 | 1.257 | 1.283 |
| 4   | 0.954  | 0.964  | 0.992  | 1.028  | 1.067  | 1.106 | 1.144 | 1.179 | 1.212 | 1.242 | 1.271 |
|     | node20 | node21 | node22 | node23 | node24 |       |       |       |       |       |       |
| 3   | 0.860  | 0.880  | 0.924  | 0.976  | 1.028  | 1.076 | 1.120 | 1.160 | 1.197 | 1.230 | 1.261 |
|     | node15 | node16 | node17 | node18 | node19 |       |       |       |       |       |       |
| 2   | 0.727  | 0.773  | 0.849  | 0.924  | 0.992  | 1.050 | 1.101 | 1.146 | 1.186 | 1.221 | 1.253 |
|     | node10 | node11 | node12 | node13 | node14 |       |       |       |       |       |       |
| 1   | 0.500  | 0.636  | 0.773  | 0.880  | 0.964  | 1.032 | 1.088 | 1.136 | 1.178 | 1.215 | 1.248 |
|     | node 5 | node 6 | node 7 | node 8 | node 9 |       |       |       |       |       |       |
| 0   | 0.000  | 0.500  | 0.727  | 0.860  | 0.954  | 1.026 | 1.084 | 1.133 | 1.176 | 1.214 | 1.247 |
|     | node 0 | node 1 | node 2 | node 3 | node 4 |       |       |       |       |       |       |

Origin (0,0)

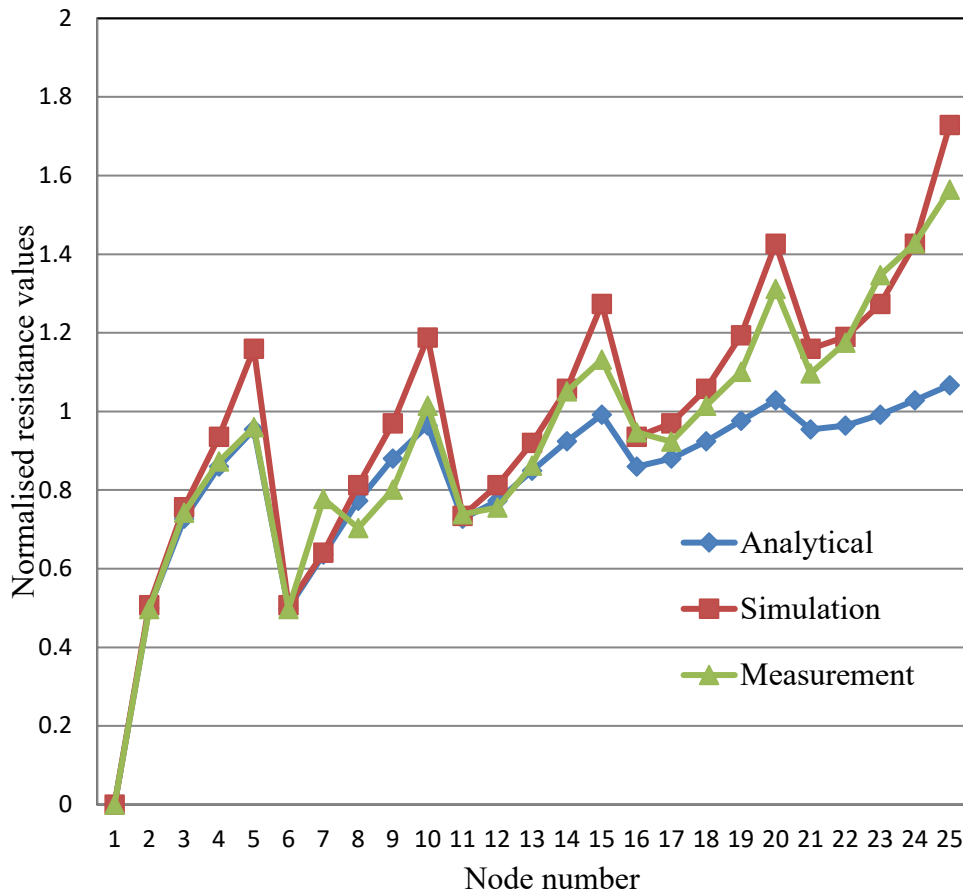


Figure 5.8 Comparison of measured point with simulation and analytical results of stitched ground plane.

The analytical, simulation and measured result of the meshed ground plane are shown in Fig.5.8. The data are plotted from Table 5.1, Table 5.2 and Table 5.3. The meshed grid is simulated with a uniform conductor while the fabrication or embroidery is carried out with a non-uniform conductor. The meshed grid point in the measurement across the points varies due to expansion of Amberstrand conductors. The difference in the results is a result of the distances between meshed and the uniformity of the conductors across the the grid. The separation between two nodes are not equal because of manufacturing tolerance. The simulation considering 7 points gives: 0.9869, 1.0002, 1.0606, 1.0871, 1.0361, 1.0871, 1.5638 and the measurement gives a 1.0968, 1.175, 1.3466, 1.427, 1.1316, 1.3119, 1.1487. The average error across the grid nodes ( $8 \times 8$ ) is about 23.51%. Once the mesh is larger the measured result the resistances across the mesh will be similar to the infinite meshed network.



## 5.6. Modelling and Design of Microstrip Patch antenna with Meshed ground plane

The majority of the research work carried out on fabric antennas in the literature is centred around microstrip patch antennas as a result of its advantages of miniaturisation, low profile, compactness, ease of integration in clothing materials and good radiation patterns. Fabric antennas consist of upper and lower conductive layers of antenna patches and ground plane and a middle layer of dielectric substrate [5.1,5.9]. A planar structure is a basic requirement for wearable textile antenna. A microstrip line-fed rectangular (square) patch as shown in Fig.5.9, was designed using the transmission line model considering the dielectric constant ( $\epsilon_r$ ), resonant frequency ( $f_r$ ) and height of substrate ( $h_s$ ) for calculating the physical dimensions of the patch using equations (5.5)-(5.8) [5.12 -5.14]. The dielectric constant is of a lower value to enhance fringing and radiation. The bandwidth of the patch is a function of substrate height. Patch antenna dimension is  $W_p$  in mm and  $L_p$  in mm where  $\lambda$  is the free space wavelength at 2.45 Hz and 5 Hz wireless networking bands. The dimensions of the feed line are  $L_f \times W_f$  and feed line inset ( $y_0$ ) for impedance matching. The dimension of substrate and ground plane is given as ( $W_s \times L_s$  and  $h_s$ ) and ( $W_g \times L_g$  and  $t_{gs}$ ) all in mm respectively. The microstrip patch antenna has been designed for two applications.

The embroidery technique is used to place a conductive yarn onto Denim or felt substrate for the ground plane of patch antennas operating at 2.45 GHz and 5 GHz frequencies. The substrate dielectric constant and loss tangent are determined by measurement using split post dielectric resonators (SPDR) for the fabric samples. The patch antenna is constructed on a two layer substrate having a FR4 of relative permittivity  $\epsilon_r$  of 4.3 loss tangent ( $\tan\delta$ ) of 0.018 and relative permittivity of Denim fabric of 0.7 mm,  $\epsilon_r$  of 1.97 and loss tangent ( $\tan\delta$ ) of 0.0707 and and for a felt fabric of 1 mm,  $\epsilon_r$  of 1.2 and ( $\tan\delta$ ) of 0.0013. A copper layer of thickness of 0.035mm was used on the reference antenna.

Two types of conductive thread materials were used for the fabrication of the prototype stitched antennas: Liberator-20 and Amberstrand 66 (metal clad polymer) [5.9]. Liberator 20 consists of a yarn of 20 strands of diameter 0.22 mm. Each strands has a Vectran fiber core

with silver coating. The DC resistance of Liberator-20 is  $2\Omega/\text{ft}$  which gives an effective conductivity of  $4.5 \times 10^7 \text{ S/m}$ . Liberator-20 is created by Syscom Advanced Materials. The following formulae for the antenna design are taken from Balanis [5.13]

$$\text{Effective dielectric constant } \epsilon_{\text{reff}} = \frac{\epsilon_r + 1}{2} + \frac{\epsilon_r - 1}{2} \left[ 1 + 12 \frac{h}{W} \right]^{-1/2} \quad (5.5)$$

$$\epsilon_{\text{reff}} \left( \frac{W}{h} \gg 1 \right)$$

$$\text{Effective length } L_{\text{eff}} = L + 2\Delta L \quad (5.6)$$

$$\text{Normised extension length } \frac{\Delta L}{h} = 0.412 \frac{(\epsilon_{\text{reff}} + 0.3) \left[ \frac{W}{h} + 0.264 \right]}{(\epsilon_{\text{reff}} - 0.258) \left[ \frac{W}{h} + 0.8 \right]} \quad (5.7)$$

$$\text{Resonant frequency } (f_r)_{010} = \frac{1}{2L\sqrt{\epsilon_r}\sqrt{\epsilon_r\mu_0}} \quad (5.8)$$

There are various way of feeding the microstrip patch antenna which include coaxial probe feed, microstrip line, inset fed, aperture coupling and proximity coupling. Most designs of microstrip antenna are fed by simple coaxial probe because of ease of fabrication. In this study the rectangular microstrip patch antennas are fed by a microstrip line with inset feed. The inset feed is used for microstrip patch antenna to improve the impedance match with planar feed configuration. The input impedance of microstrip patch antenna depends on the feed position for probe feed or the microstrip feed inset [5.15]-[5.16] .

The transmission-line model represent the patch as a low-impedance line whereby the width of the patch determines the impedance and the effective dielectric constant. A microstrip patch consists of parallel plate radiation conductance and capacitive susceptance that loads both the radiating edges of the patch Thomas Milligan [5.14 ] gives the radiation conductance for a parallel-plate radiator as

$$= \frac{\pi W}{\eta \lambda_0} \left[ 1 - \frac{(kH)^2}{24} \right] \quad (5.9)$$

$$R_e = \frac{1}{2G} \quad (5.10)$$

The computed value of  $G$  was  $2.49\text{m}\Omega$  and  $R_e$  the input resistance at the edge, is  $200\Omega$  with  $y_0$  inset distance. The capacitive susceptance in relation to the effective strip extension is given as

$$B = 0.01668 \frac{\Delta}{H} \frac{W}{\lambda} \epsilon_{\text{eff}} \quad (5.11)$$

Microstrip antenna is fed from the edge using an inset line where the gap on either side of strip line is equal to its width. The feed location  $y_0$  was computed from equation (5.9-5.13) using a radian angle measure.

$$R_i = R_e \sin^4 \frac{\pi y_0}{L} \quad 0 \leq y_0 \leq \frac{L}{2} \quad (5.12)$$

$$y_0 = \frac{L}{\pi} \sin^{-1} \left( \frac{R_i}{R_e} \right)^{1/4} \quad (5.13)$$

Computed values of  $50\Omega$  feed inset,  $y_0$  for 5 Hz was 3.5mm and for 2.45 Hz the value is given as 7.5mm. The values were compared to the computed values in [5.13]

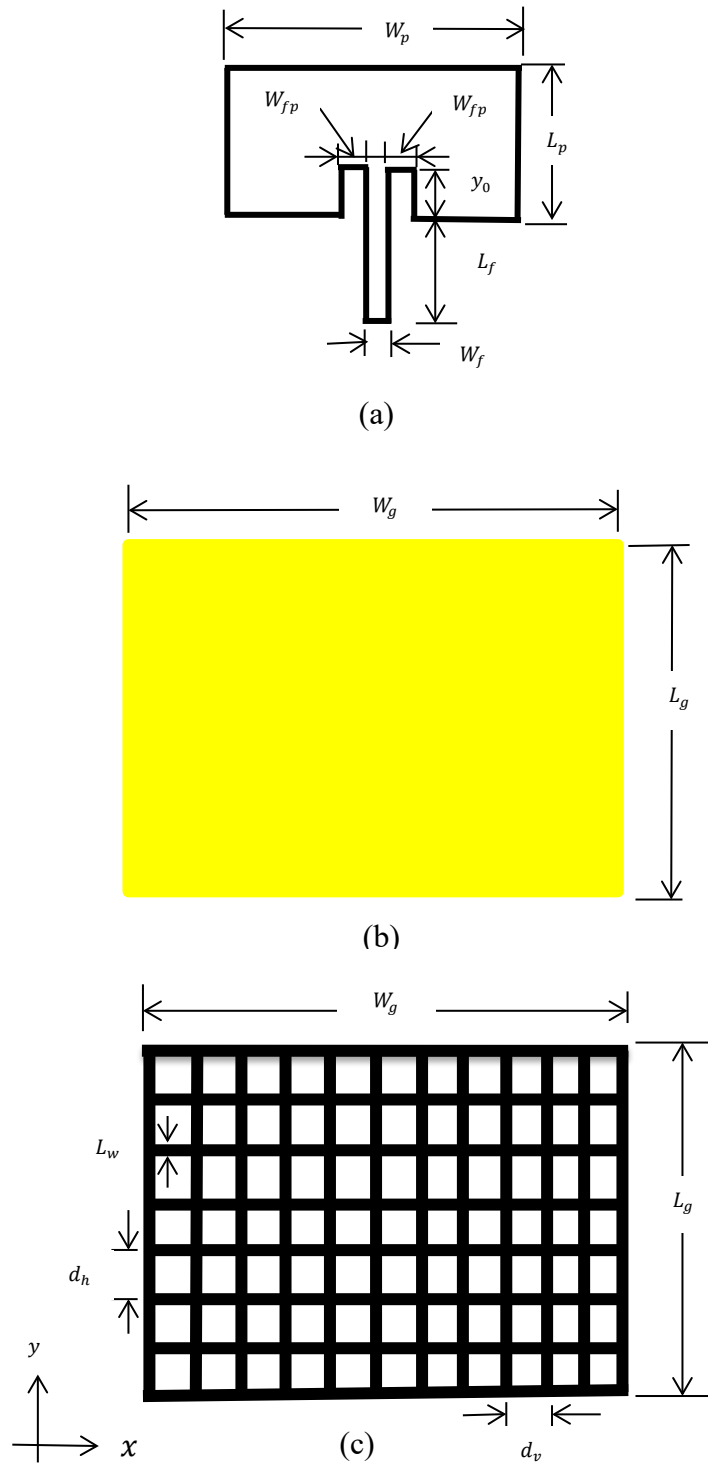
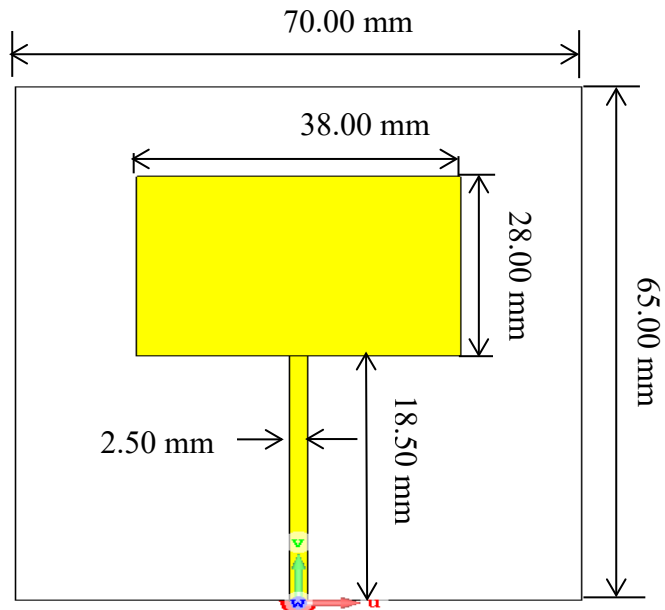


Figure 5.9 Geometry of proposed inset microstrip fed patch antenna (a) Top conductor (b) Solid ground (c) Meshed ground

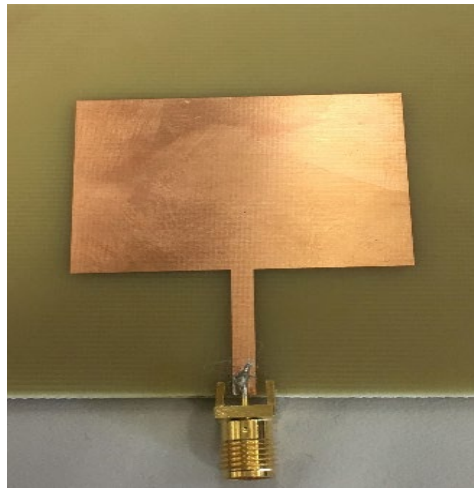
### 5.6.1. Investigation of mesh width of meshed patch antenna

Microstrip patch antennas have a wide range of applications including printing on or within glass areas of vehicles for intelligent and telematics systems providing a cost effective solution. Rectangular printed patch antennas made from conducting mesh have improved bandwidth but have low gain [5.3]. To examine the effect of meshing on the antenna performance and to normalise the meshed antenna to a reference, a solid patch antenna was designed, fabricated from FR4 substrate and tuned to the same frequency as the meshed antennas.

Meshed patch antennas have been studied by Clasen and Langley [5.3] considering mesh lines with fixed line width. In their study they examined meshed patch antenna with solid ground plane and meshed ground plane but the effects of the line width ( $L_w$ ) and the mesh spacing on the resonant frequency and the gain were compared with using a reference patch antenna see Figure 5.10 (a) and (b). The patch antenna has two radiating slots of length  $W_p$ . The microstrip antenna is either fed with a microstrip line or cable. Many modal waves are excited. In this study the antenna was fed with a microstrip line. The antenna design frequency  $f_c = \frac{c}{2L\sqrt{\epsilon_r}} = 2.45 \text{ GHz}$ . The resonant length from the theoretical calculation  $L = \lambda_{eff}/2$  gives 29.5 mm but the actual physical length is set to 28 mm. The rectangular patch antenna had a length  $L_p = 28 \text{ mm}$ , width of the patch  $W_p = 38 \text{ mm}$ , relative permittivity  $\epsilon_r = 4.3$ , thickness of the dielectric substrate is 1.6 mm and the loss tangent  $\tan\delta = 0.018$ . The theoretical length is slight longer than the physical length as expected due to fringing effect.



(a)



(b)

Figure 5.10(a) Antenna geometry of antenna design A and (b) Picture of microstrip patch antenna (Antenna design A)

### 5.6.2. Simulated and measured reflection coefficient and simulated radiation patterns.

The resonant frequency and reflection coefficient of all the designed samples of antennas were measured using a 37397D Vector Network Analyser to verify the theoretical analysis, The simulated and the measured  $S_{11}$  of the antenna sample is shown in Fig. 5.11. The measured result  $S_{11} -11.87\text{dB}$  at  $2.45\text{ Hz}$  with bandwidth of  $70\text{ MHz}$  compared with the simulation  $S_{11}$  of  $-13.87\text{dB}$  at  $2.45\text{ Hz}$  and  $-10\text{ dB}$  bandwidth of  $64\text{ MHz}$ .

Two patterns in two plane  $yz$  and  $xz$  were defined in chapter 2. Figure 5.12 is the simulated pattern of reference antenna A (Fig. 5.10). The maximum directivity is  $7.1\text{ dBi}$ . The E-plane and H-plane at boresight is the same. The front to back ratio of the solid patch  $FBR_{dB} = 15\text{ dB}$ . There are no side lobes but back lobes as a result of the finite ground plane. A larger ground plane or use of EBG materials will reduce the backlobe.

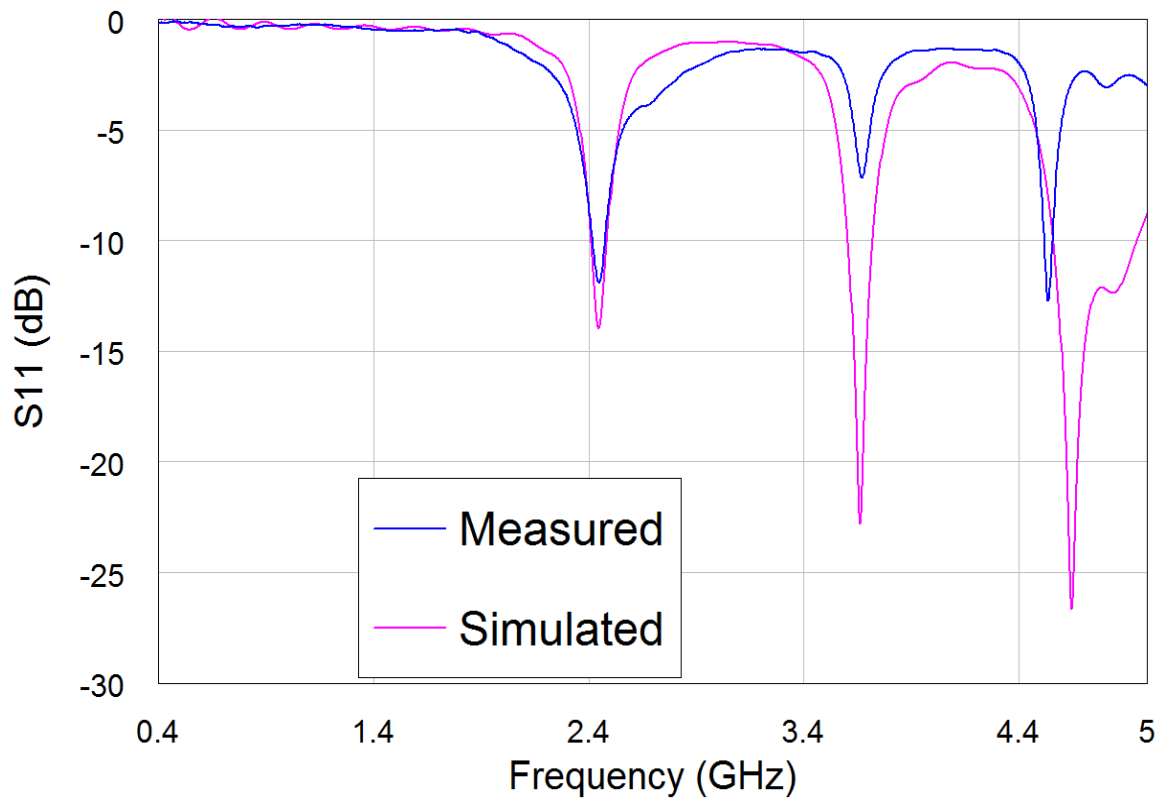


Figure 5.11 The reflection coefficient of Antenna design A with solid ground plane (see Figure 5.10)

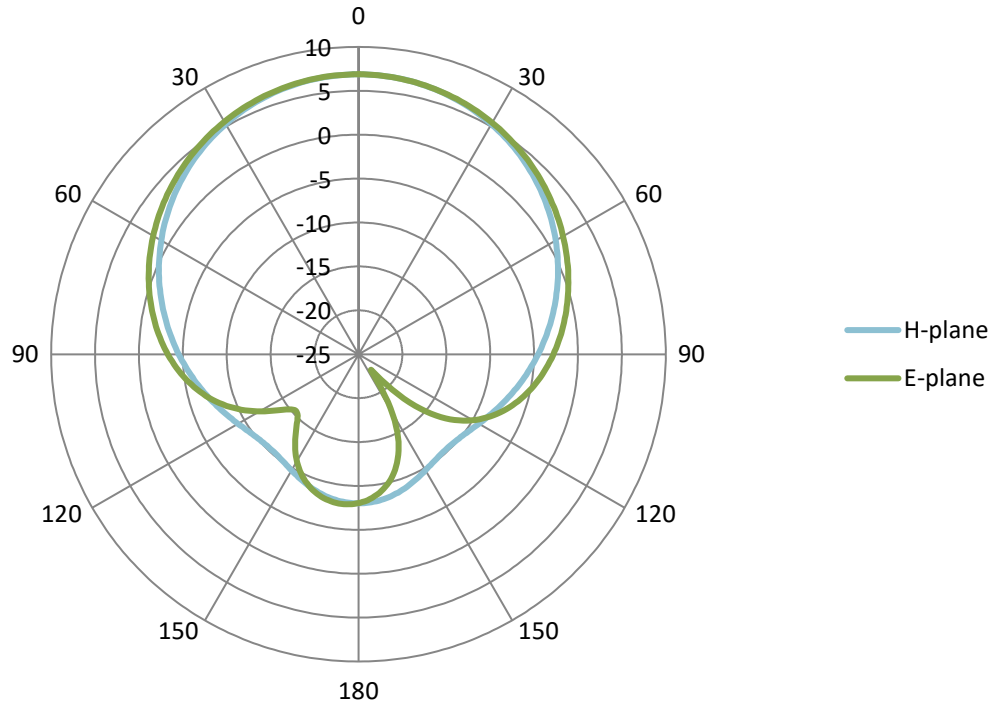


Figure 5.12 Simulated radiation patterns for microstrip patch (of Fig.5.11-Antenna design A) at 2.45 GHz.

### 5.6.3. Meshed ground plane

Table 5.4 shows the parameters of four simulated solid patch antennas with meshed ground planes.  $N_H$  and  $N_V$  are the number of horizontal and vertical lines of the meshed ground plane. The horizontal lines are perpendicular to the resonant length of the patch. The number of horizontal lines is 14 and number of vertical lines is 15 for all the antenna referred to as antenna design A – E. Line width,  $L_w$ , is 0.2 mm and thickness of copper layer is 0.035 mm. These antennas were excited by a 50  $\Omega$  microstrip line in CST Microwave Studio.



Table 5.4 Simulated results of patch antenna with meshed ground plane

| Antennas design        | Simulated $f_0$ (GHz) | Simulated $S_{11}$ (dB) | -10 dB Bandwidth (MHz) | Simulated Directivity (dBi) | Simulated Gain (dB) | Simulated Radiated Efficiency (%) |
|------------------------|-----------------------|-------------------------|------------------------|-----------------------------|---------------------|-----------------------------------|
| A.                     | 2.44                  | -13.97                  | 60                     | 7.1                         | 6.31                | 88                                |
| B.<br>$L_w$<br>= 0.2mm | 2.24                  | -16.05                  | 70                     | 5.66                        | 5.25                | 93                                |
| C.<br>$L_w$<br>= 0.4mm | 2.28                  | -13.07                  | 70                     | 5.81                        | 5.5                 | 93                                |
| D.<br>$L_w$<br>= 0.6mm | 2.31                  | -32.9                   | 80                     | 6.08                        | 5.74                | 92                                |
| E.<br>$L_w$<br>= 0.8mm | 2.37                  | -14.78                  | 90                     | 6.48                        | 6.05                | 90                                |

In [5.19] the resonant frequency, gain and efficiency of the meshed patch antennas decrease when the transparency of the patch antenna is increased. The number of horizontal line and vertical lines were kept constant, changing the line width to examined the transparency The transparency of the meshed ground was computed using equation (5.14) but the parameters are defined in section 4.9.1. From the study its was observed that  $L_w = 0.2 \text{ mm}$  the transparency is 91.5%,  $L_w = 0.4 \text{ mm}$  gives a transparency of 83.4%,  $L_w = 0.6 \text{ mm}$  the transparency is 75.8 % and  $L_w = 0.8 \text{ mm}$  the transparency is 68.4%. Meshed patch antenna design with thin lines produces more transparent antennas but with gain loss of the antenna.

$$T_{\text{transparency}} = \frac{L.W - L_w.N_h.L - L_w.N_v.W + L_w^2.N_v.N_h}{L.W} \quad (5.14)$$

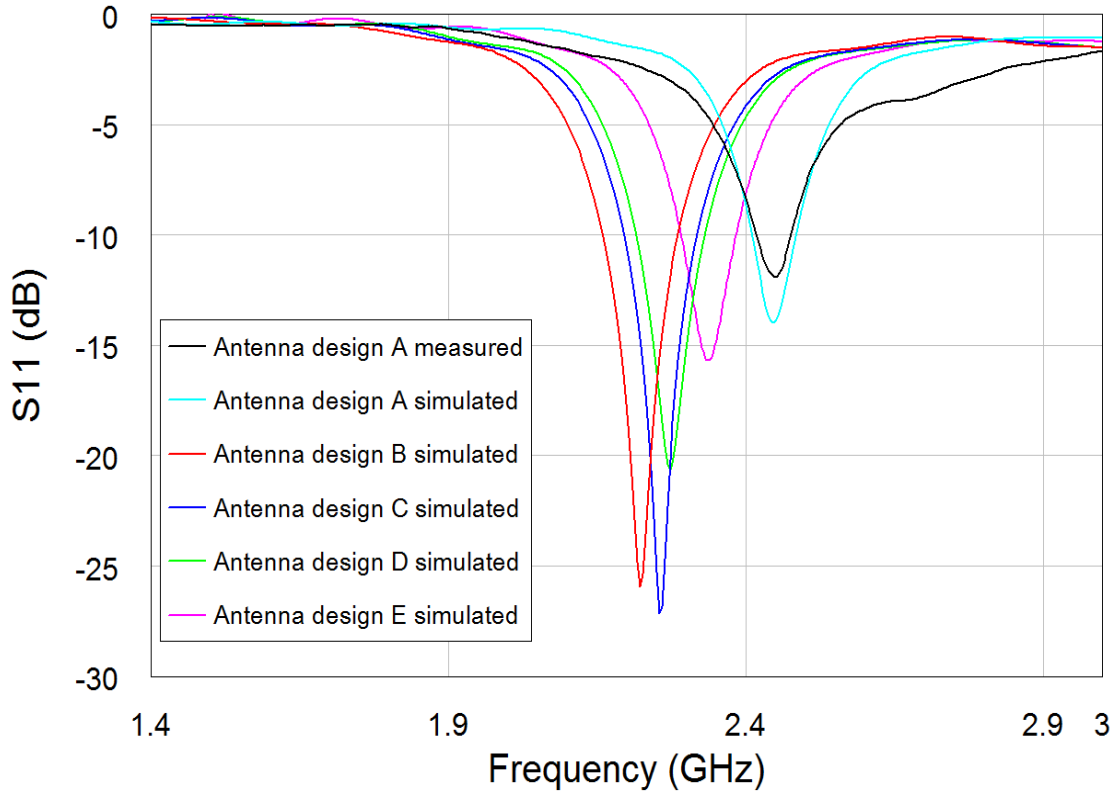


Figure 5.13 Effect of the linewidth on the resonant frequency of rectangular meshed ground for patch antenna.

Increasing the linewidth from 0.2 mm to 0.8 mm increases the impedance bandwidth and shifts the resonant frequencies from 2.44 GHz to of 2.22 GHz as shown in Fig.5.13. The bandwidth of microstrip antennas is proportional to the thickness of the substrate. The FR4 substrates are very thin in terms of the wavelength (thickness  $\ll \lambda_0/4$  making the bandwidth narrow as shown in Table 5.3. The gain and the resonant frequency decrease with a decrease in the line width while the mesh spacing increases. Meshing of the ground causes gain loss of the antenna.

#### 5.6.4. Simulated Radiation pattern of a Patch antenna with solid and meshed ground plane (Realised Gain/dBi)

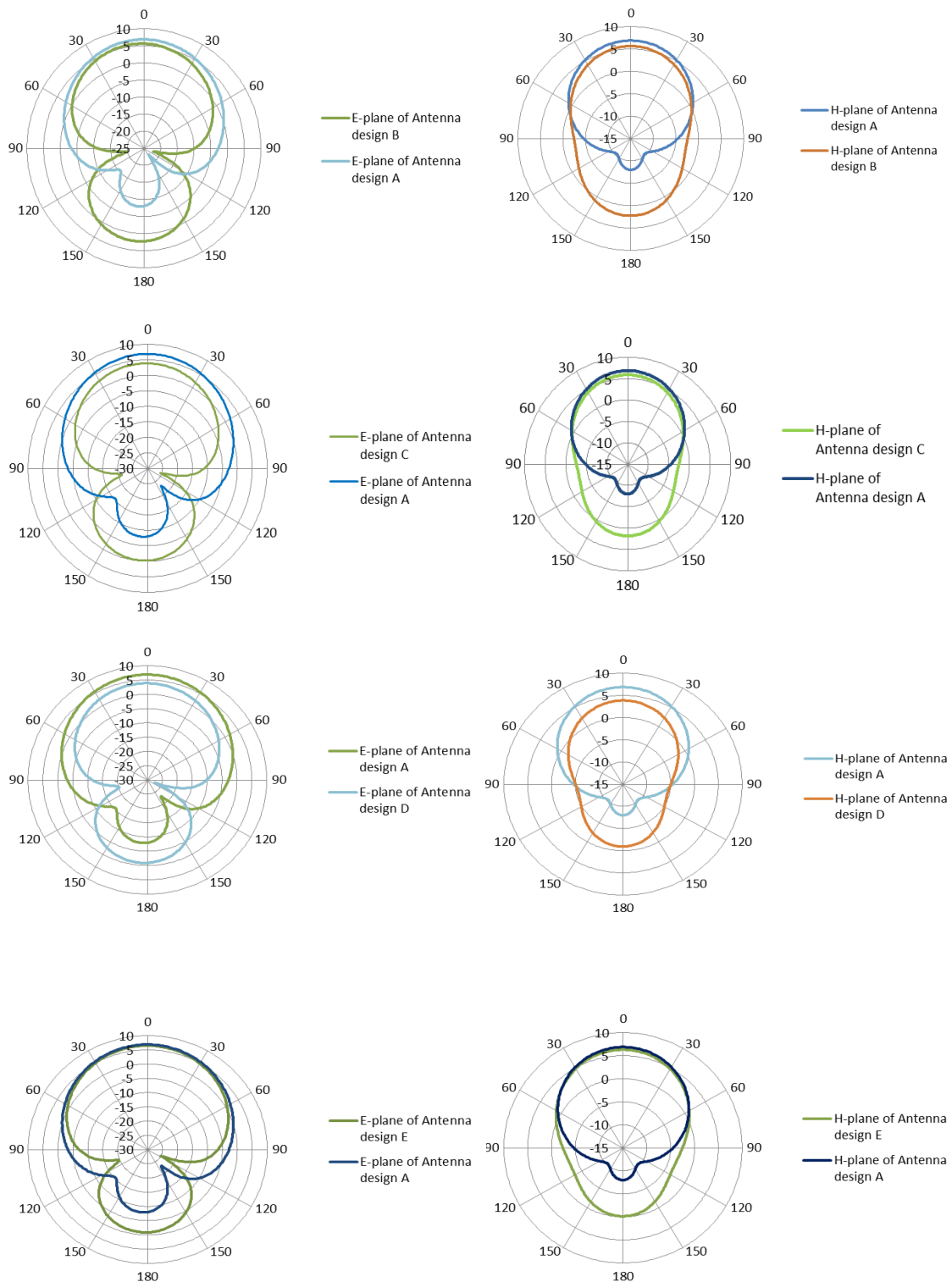
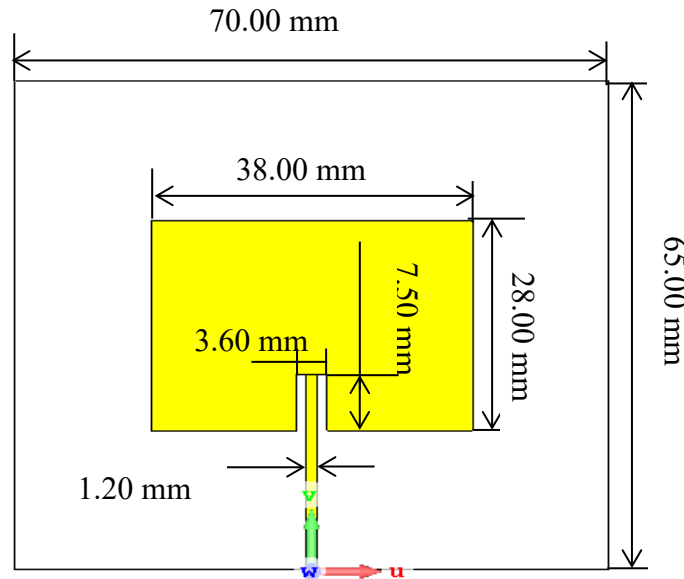


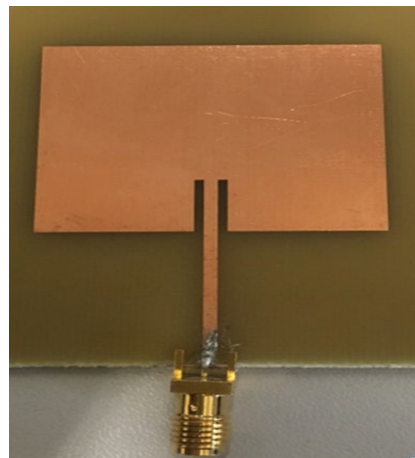
Figure 5.14 Simulated radiation patterns at 2.45 GHz for microstrip antennas with radiating patch and meshed ground compared to Antenna A which has a solid ground plane for meshes details see Table 5.4

### 5.6.5. Microstrip Patch (Inset feed) at 2.45 GHz

The structure and dimension of the proposed microstrip patch antenna is shown in Fig. 5.15. The ground plane covers the entire side of the substrate and is made of copper sheet of 0.035 mm thickness. The radiating element is designed with the same thickness copper. The substrate is FR4 ( $\epsilon_r = 4.3$  and loss tangent  $\delta = 0.018$ ) has a size of  $W_g \times L_g = 70 \text{ mm} \times 65 \text{ mm}$  of substrate height  $h_s = 1.6 \text{ mm}$  is used for all the antennas. The size of the patch  $W_p \times L_p = 38 \text{ mm} \times 28 \text{ mm}$ . The feedline has a characteristic impedance of  $50 \Omega$  for maximum power transfer.



(a)



(b)

Figure 5.15 (a) Simulation model of referenced patch B and (b) Photograph of fabricated microstrip patch (referenced design-inset feed)

The simulated and measured reflection coefficient are shown in Fig. 5.16. The reflection coefficient is at centre frequency of the Wi-Fi band (2.4 – 2.485 GHz). Measured  $S_{11}$  is  $-21.48\text{ dB}$  at  $2.43\text{GHz}$ ,  $-10\text{dB}$  Bandwidth 49 MHz and simulation  $S_{11}$  is  $-25.81\text{ dB}$  at  $2.46\text{ GHz}$   $-10\text{ dB}$  bandwidth 87 MHz.

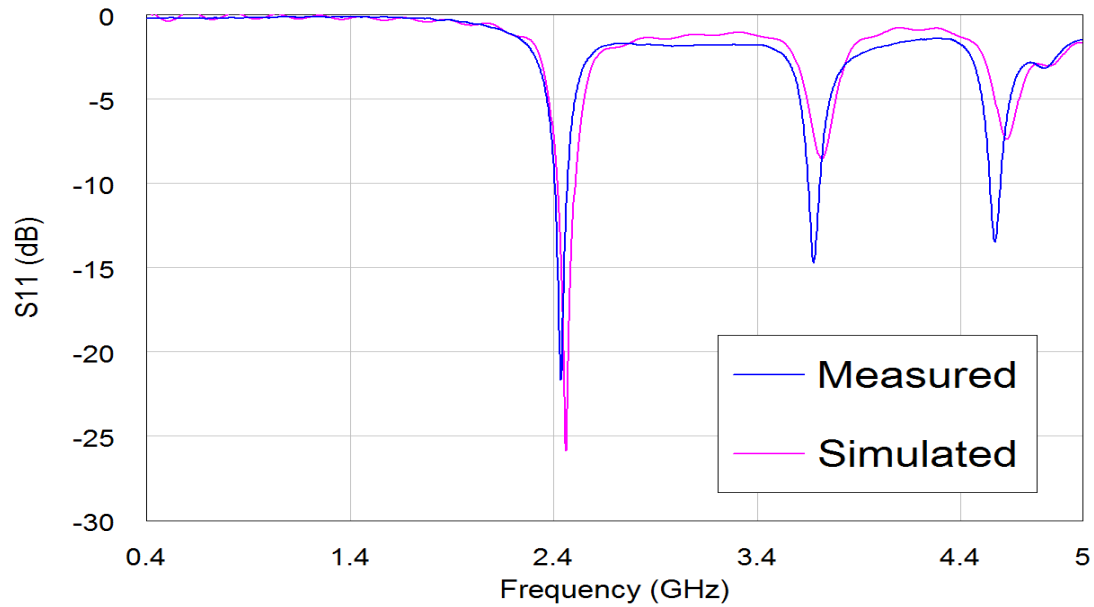


Figure 5.16 Comparison between simulation and measurement of the proposed microstrip patch (inset feed) of Fig.5.15 by means of the  $S_{11}$  plot

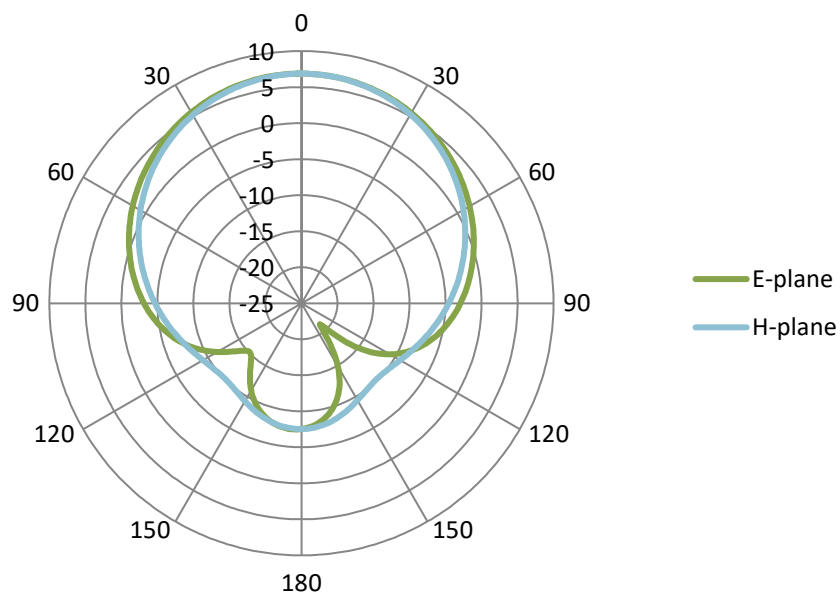


Figure 5.17 Simulated radiation pattern of gain (of Fig 5.15)

A set of four rectangular patch antennas (see Fig.5.15 for the dimension of the patch) with meshed ground plane with line width 0.2 mm were printed on FR4 substrates backed with meshed copper grounds is shown in Table 5.5. The design of meshed patch antenna using three horizontal line were studied by [5.17,5.20]. Similar concepts were used to design the meshed ground plane of the microstrip antennas in this study where three horizontal lines one at the top, one at the bottom and the other at the feed point at the middle were used. This horizontal line at the feed allows current to flow to the vertical lines. Antenna samples (antenna 5 and antenna 6) had a ground plane of 65 mm by 70 mm. The meshed ground of antenna 5 consist of number of vertical lines  $N_v = 25$  and number of horizontal lines  $N_h = 3$ . This antenna has a transparency of 91.5% and metal coverage of 8.5%. Antenna 6 has  $N_v = 36$  and  $N_h = 3$ , the transparency of 88% and metal coverage of 12%. Antenna 5 has a finer meshed ground plane giving a higher resonant frequency and better impedance bandwidth than antenna 6 because the meshed is coarse and closely compact together. The resonant frequency of antennas 5 and 6 are higher than conventional antenna 4 because the electrical lengths of antenna 5 and 6 are shorter as in Fig.5.18 and Fig.5.19.

Antenna 7 and 8 are etched on a FR4 substrate of ground plane (70 mm by 70 mm) but of the same dimension of the patch as antenna 4. Antenna 7 has  $N_v = 15$  and  $N_h = 8$  transparency of 93.5% and metal coverage of 6.5% and Antenna 8 is built with a solid patch (see Table 5.5) over a meshed ground plane and a dielectric constant of substrate between the patch and ground plane is 4.3 and thickness of 1.6 mm. The meshed ground plane consist of  $N_v = N_h = 15$  transparency of the antenna is 91.5% and metal coverage of 8.5%. The transparency of these antenna increased the antenna directivity and the resonant frequency reduces as reported [5.3]. Antenna 7 has higher centre frequency and better impedance bandwidth than antenna 8 because of the reduced number of parallel lines to the length of antenna ground plane.

Table 5.5 Simulated and measured result of representative examples for meshed ground plane


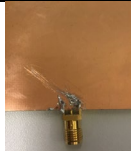

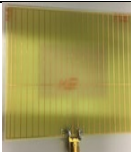

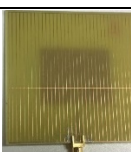

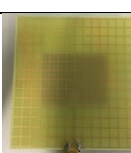

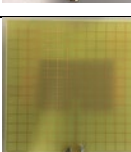
| Antenna design | Patch   | ground  | Simulated $f_0$ (GHz) | Measured $f_0$ (GHz) | Simulated $S_{11}$ (dB) | Measured $S_{11}$ (dB) | Simulated Directivity (dBi) | Simulated Radiation Efficiency (%) |
|----------------|---|---|-----------------------|----------------------|-------------------------|------------------------|-----------------------------|------------------------------------|
| Antenna 4      |    |    | 2.46                  | 2.45                 | -25.8.0                 | -21.4dB                | 6.93                        | 91                                 |
| Antenna 5      |    |    | 2.54                  | 2.53                 | -22.2                   | -37.8                  | 6.48                        | 79                                 |
| Antenna 6      |    |    | 2.52                  | 2.50                 | -14.3                   | -30.1                  | 6.52                        | 84                                 |
| Antenna 7      |   |   | 2.45                  | 2.51                 | -29.6                   | -22.8                  | 5.87                        | 92                                 |
| Antenna 8      |  |  | 2.3                   | 2.25                 | -36.3                   | -14.9                  | 5.67                        | 92                                 |

Figure 5.18 shows the  $S_{11}$  values for three antennas described in the previous paragraph. Antenna 4 has a good impedance match  $-25.7\text{ dB}$  at  $2.46\text{ GHz}$   $-10\text{ dB}$  bandwidth of  $87\text{ MHz}$  and measured values  $-21.5\text{ dB}$  at  $2.43\text{ GHz}$   $-10\text{ dB}$  bandwidth of  $61\text{ MHz}$ . The measured  $S_{11}$  value of Antenna 5 is  $-37.9\text{ dB}$  at  $2.53\text{ GHz}$  and impedance bandwidth  $153\text{ MHz}$  while the simulated result is  $-17.5\text{ dB}$  at  $2.51\text{ GHz}$   $-10\text{ dB}$  bandwidth of  $80\text{ MHz}$ . The measured result shows that antenna 6 resonates  $-21.8\text{ dB}$  at  $2.53\text{ GHz}$  with an impedance bandwidth of  $110\text{ MHz}$  while the simulated results are  $-24.2\text{ dB}$  at  $2.50\text{ GHz}$   $-10\text{ dB}$  bandwidth of  $80\text{ MHz}$ . Meshing the ground plane gives an enhanced bandwidth compared to a solid ground (2.5 %) to meshed ground (7.5%). The difference between simulation results and the measured results may be attributed to inductance offered by the

coaxial probe. Another reason, may be as a result of no nexact values of the dielectric constant of FR4 substrate being available for the process of fabrications.

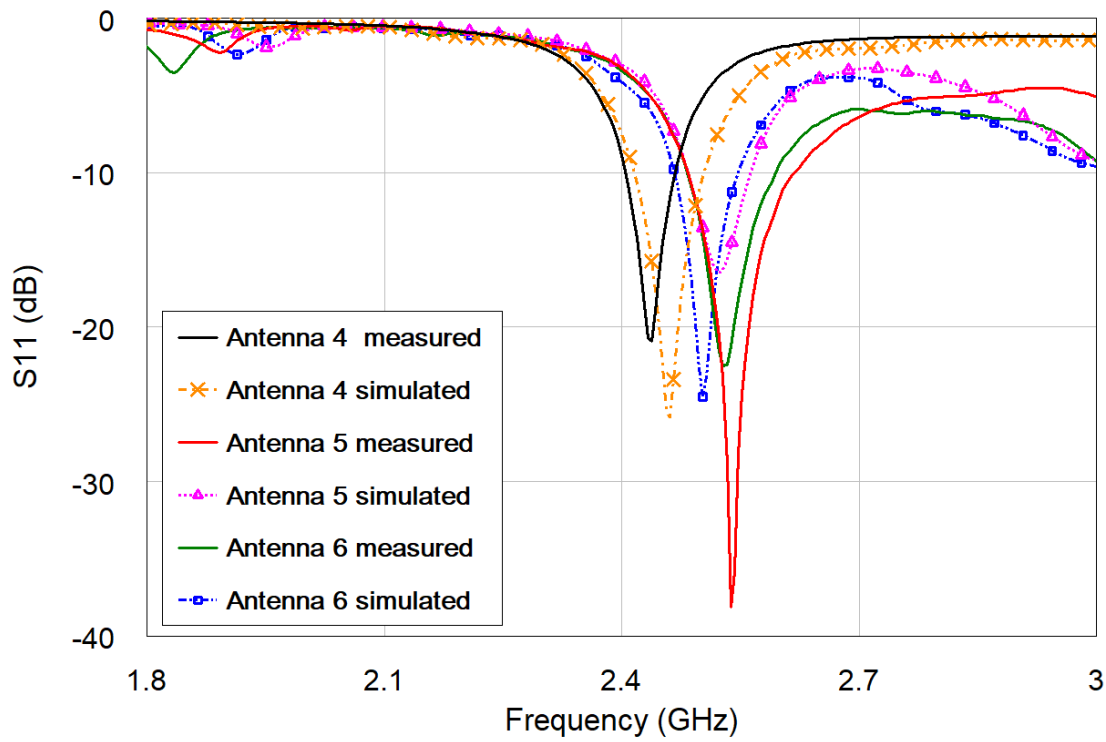


Figure 5.18  $S_{11}$  result for meshed ground plane and conventional patch antenna (antenna 4)

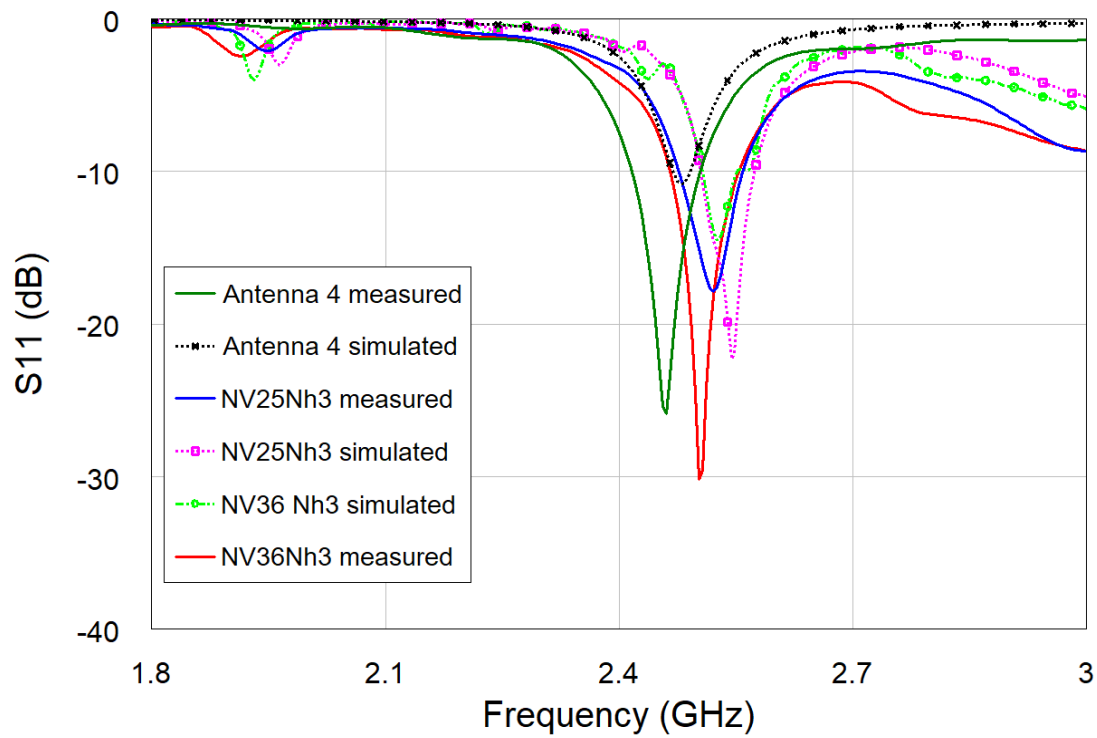


Figure 5.19  $S_{11}$  Simulation results of horizontal lines ( $N_H = 3$ ) and varying vertical lines ( $N_V$ ) of meshed ground plane



Figure 5.20 show the radiation patterns in the E- and H-plane simulated at 2.45 Hz .Antenna 4 has maximum directivity at a peak value of 6.93 dBi whereas antenna 6 has directivity of 6.52 dBi. Both antennas have very similar patterns. Antenna 4 is an inset fed solid patch with a solid ground plane. The other antenna samples 5,6,7 and 8 are solid patch with meshed ground ground on FR4 substrate.

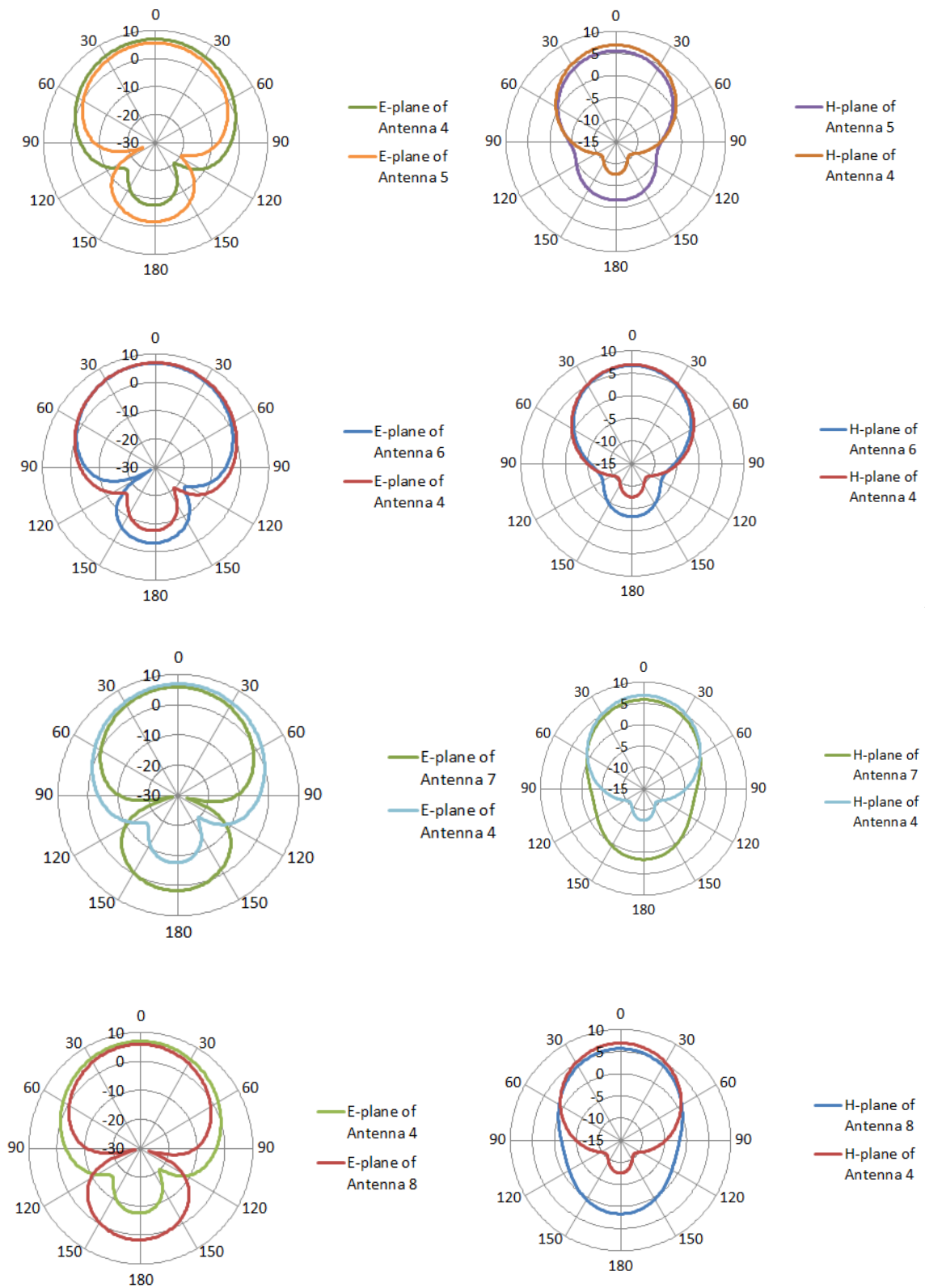
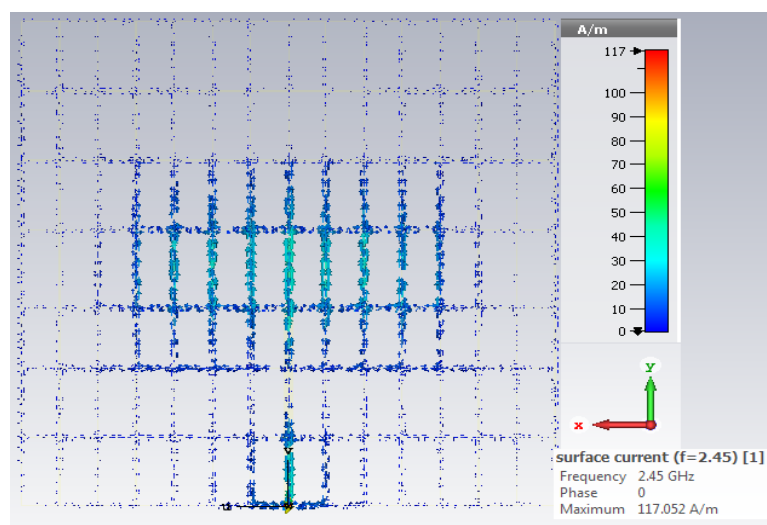


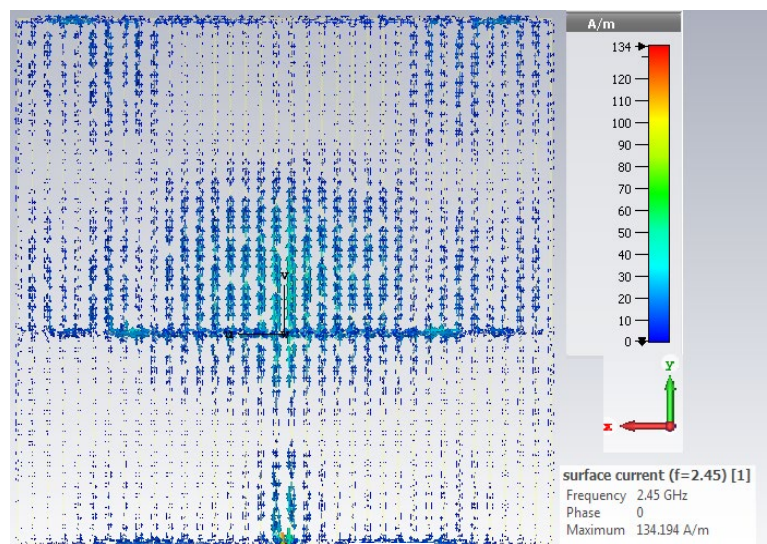
Figure 5.20 Simulated radiation patterns for the Gain of antenna design 4, 5, 6, 7 and 8

### 5.6.6. Simulated surface current for meshed ground plane

The surface current is strong at the feed point and along the feed length. Currents flow along the vertical lines and the horizontal lines shows a decrease in current path as shown in Fig.5.21 (a) and increase the the fundamental resonant frequency. When the number of horizontal lines are reduced to three (3) top, feedpoint and bottom current path decreases (see Fig.5.21(b)) and more current flows along the vertical path causing an increase in the resonant frequency.



(a)



(b)

Figure 5.21 Simulated surface current on the meshed ground plane at 2.45 Hz

## 5.7. Microstrip patch at 5 GHz for evaluation of meshed ground plane

The dimensions of the microstrip patch antennas were approximated from equations (5.6-5.14) from existing literatures [5.13-5.17] as shown in Fig.5.10(a) and (b). The next patch antenna was designed to operate at 5 GHz and the dimensions are listed in Table 5.6. The proposed antennas are constructed with two different substrates: FR4 substrate and fabric substrate. The patch and the inset line are made on the same layer. Antenna dimensions are the same for all meshed ground plane evaluated in this section.

### 5.7.1. Production of textile meshed ground plane

The (Brother Pro PR1000e Entrepreneur) was used to realise the fabrication of the stitched ground plane for the Microstrip patch antennas. The thread used for this study was a Multi-thread conductive yarn Amberstrand Silver 66. One single thread of Amberstrand is made of 66 identical filaments. The diameter of the Amberstrand filament is approximately 17 $\mu$ m [5.9]. The stitching was performed along the horizontal step and vertical step directions for antennas PA2, PA3, PA4 and PA5. The lock stitch method was used where two threads: conductive thread and non-conductive thread were used for stitched formation. A stitch density of 4.5 lines/mm was used for the ground plane. Current prefers to follow path of least resistance rather jump from one yarn to another [5.18]. The number of stitches for the ground plane for antenna PA3 and PA4 was 449. The number of stitches for antenna sample PA2 is 313 and PA5 is 1161. Stitching the ground plane on to fabric material (felt or denim) first, the stitched ground plane is cut and attached to the FR4 substrate using repositionable adhesive.



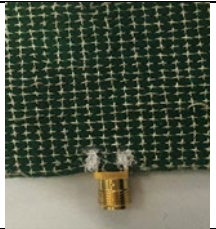


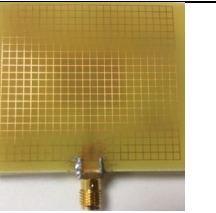
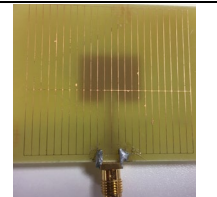
Antennas are named as follows, Antenna PA1 is a solid patch on a solid ground plane, antenna PA2 is a solid patch etched on FR4 and conductive thread stitched on felt material as a ground plane, antenna PA3 is a solid patch and meshed ground (using conductive thread on felt material), antenna PA4 is a solid patch on FR4 substrate and conductive thread stitched on denim fabric as a ground plane, antenna PA5 solid patch on FR4 substrate with a (triangular meshed) on a felt ground plane, MGP1 meshed patch on mesh ground plane (2mm  $\times$  2mm) and antenna MGP3 solid patch on FR4 meshed ground similar (to PA2),

antenna MGP2 meshed patch on solid ground, antenna and antenna MGP4 solid patch on meshed ground ( $2\text{mm} \times 2\text{mm}$ ).

Table 5.6 Microstrip antenna dimensions and parameters

|   |       |
|---|-------|
| Operating frequency, $f$ in GHz               | 5     |
| Dielectric constant                           | 4.3   |
| Length of the patch, $L_p$ in mm              | 14    |
| Width of the patch, $W_p$ in mm               | 18.42 |
| Position of inset feed point, $y_p$ in mm     | 3.5   |
| Distance between feed & patch $W_{fp}$        | 1.2   |
| Width of the microstrip feed line $W_f$ in mm | 1.2   |
| Height of substrate FR4 in mm                 | 1.6   |
| Loss tangent of FR4                           | 0.018 |
| Ground plane length $L_g$                     | 44    |
| Ground plane width $W_g$                      | 48    |
| Thickness $t$ in mm<br>Copper sheet           | 0.035 |
| Linewidth, $L_w$ , in mm                      | 0.2   |

Table 5.7 Simulated and measured parameters of representative examples of meshed and stitched ground planes for microstrip antennas

| Antenna design                    | PA1   | PA2   | PA3  | PA4   | PA5   | MGP1  | MGP3  |
|-----------------------------------|---|---|--|---|---|---|---|
| Ground plane                      |  |  |  |  |  |  |  |
| Measured $f_0$ (Hz)               | 4.97  | 5.48  | 5.32   | 5.31  | 5.02  | 4.7   | 5.07  |
| Measured $S_{11}$ (dB)            | -25.6   | -17.42  | -25.99   | -30.8   | -15.3   | -24.3   | -37.8   |
| Simulated $S_{11}$ (dB)           | -21.4   | -19.21  | -32.59   | -25.34  | -22.39  | -26.9   | -17.8   |
| Measured -10 dB Bandwidth (MHz)   | 150   | 502   | 660  | 780   | 814   | 220   | 180   |
| Simulated -10dB Bandwidth (MHz)   | 200   | 200   | 190  | 424   | 200   | 240   | 80  |
| Simulated Directivity (dBi)       | 7.03  | 5.09  | 6.76   | 6.22  | 6.7   | 6.91  | 7.22  |
| Simulated Radiated efficiency (%) | 91  | 86  | 77   | 84  | 87  | 72  | 88  |

### 5.7.2. Solid patch with solid ground (PA1) and meshed patch with meshed ground

Antenna sample PA1 is a solid patch with solid ground plane and antenna sample MGP1 a meshed patch with meshed ground plane. Both have the same dimensions. They are fabricated on an FR4 substrate of 1.6 mm thickness. The reflection coefficient,  $S_{11}$ , of each antenna sample is shown in Fig. 5.22. PA1 simulation  $S_{11}$  result is  $-21.4\text{ dB}$  at  $4.97\text{ GHz}$ ,  $-10\text{ dB}$  bandwidth of  $200\text{ MHz}$  and measured  $S_{11}$  is  $-25.6\text{ dB}$  at  $4.92\text{ GHz}$ ,  $-10\text{ dB}$  bandwidth  $200\text{ MHz}$  while MGP1 has a measured  $S_{11}$  of  $-24.2\text{ dB}$  at  $4.70\text{ GHz}$ ,  $-10\text{ dB}$  bandwidth of  $220\text{ MHz}$  and simulation  $S_{11}$  result at  $-26.9\text{ dB}$  at  $4.82\text{ GHz}$ ,  $240\text{ MHz}$ . The drop in frequency of meshed patch with meshed ground (MGP1) is lower by  $4.47\%$  as compared to PA1. It has a higher impedance bandwidth. The difference between the measured and simulation as a result errors of substrate permittivity.

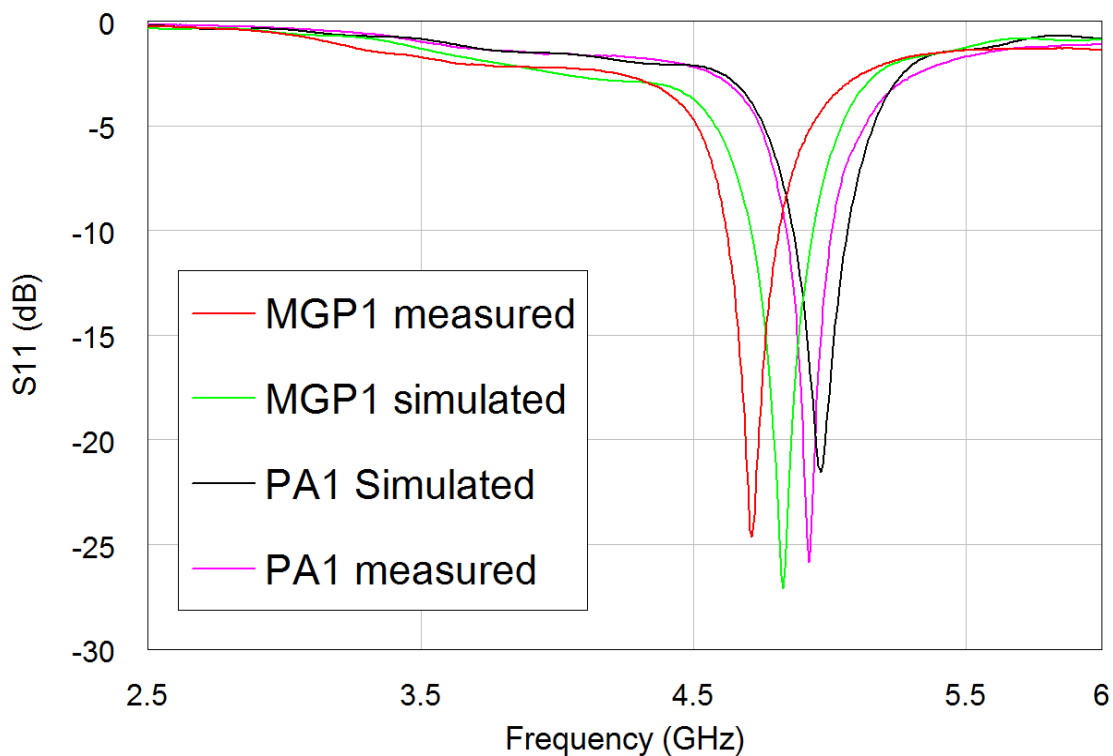


Figure 5.22  $S_{11}$  Measured result compared with simulation of solid patch (PA1) with solid ground and meshed patch (MGP1) with meshed ground

The radiation pattern at 4.82 GHz as shown in Figure 5.23 where the E-plane and H-plane shows the leakages on the meshed ground plane, particularly for the H-plane. The pattern of the meshed patch antenna does not change significantly compared to the solid patch result. The solid patch has a directivity of 7.03 dBi and the directivity of the meshed patch is 6.91 dBi. There is directivity show only a small change when the antenna is meshed. The maximum directivity of the patch antenna (PA1) to the directivity at the rear is given as  $FBR_{dB} = 18.32dB$ .

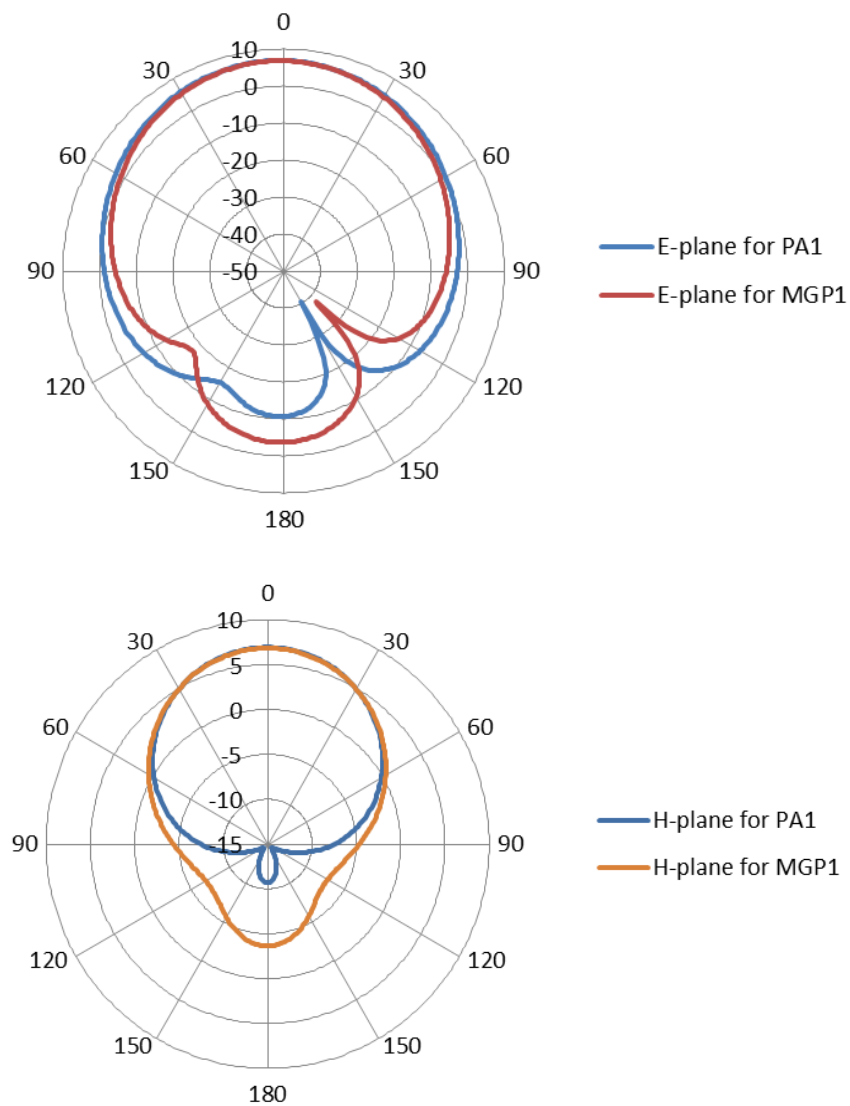


Figure 5.23 Stimulated radiation pattern of antenna samples MGP1 and PA1



### 5.7.3. Comparison of patches with meshed and solid ground planes

The measured input reflection ( $S_{11}$ -parameter) of the antenna samples MGP4 and PA1 is shown in Fig.5.24. The antenna sample MGP4 is solid patch on a meshed ground plane while PA1 is solid patch on a solid ground plane. The measured  $S_{11}$  for of MGP4 is  $-20.2\text{ dB}$  at  $4.72\text{ GHz}$   $-10\text{ dB}$  bandwidth of  $260\text{ MHz}$  (measured) while simulation results gives  $-15.4\text{ dB}$  at  $4.93\text{ Hz}$   $-10\text{ dB}$  bandwidth of  $140\text{ MHz}$ . PA1 simulation result is  $-21.4\text{ dB}$  at  $4.97\text{ GHz}$  will  $-10\text{ dB}$  bandwidth of  $200\text{ MHz}$  and measured  $S_{11}$  of  $-25.6\text{ dB}$  at  $4.92\text{ GHz}$  at  $-10\text{ dB}$  bandwidth  $200\text{ MHz}$ . Antenna sample MGP4 has a directivity of  $6.98\text{ dBi}$  while the solid patch PA1 has a directivity of  $7.03\text{ dBi}$ .

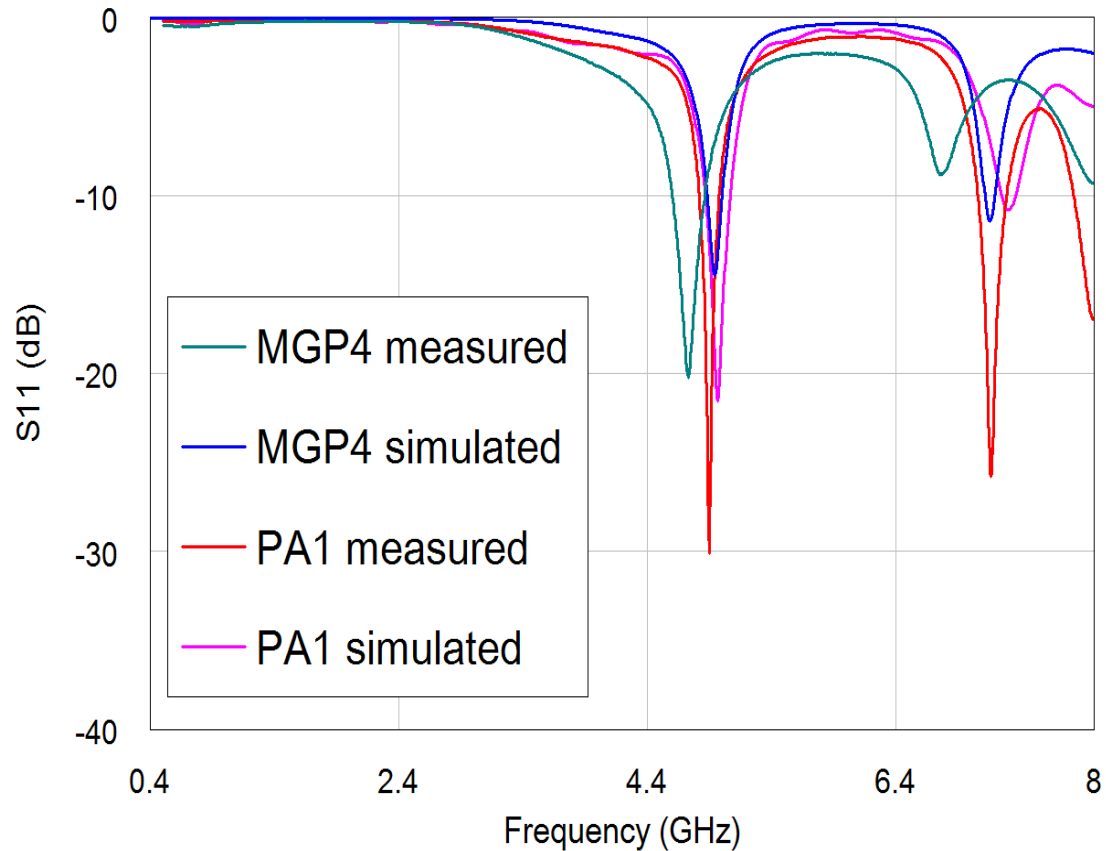


Figure 5.24 Simulated and measured  $S_{11}$  results of the antenna MGP4 and PA1 (solid patch on meshed and solid ground planes)

### 5.7.4. Stitched ground plane on fabric substrate.

Antenna sample MGP3 is a solid patch (for dimensions see Table 5.5) with a meshed ground plane on FR4 substrate. Sample PA2 is solid patch antenna on an FR4 substrate backed with

stitched meshed ground plane of the same dimension as MGP3. Measured  $S_{11}$  results are shown in Fig.5.25. It is shown that two patch antenna were well matched at their resonant frequencies: MGP3 is  $-15.9\text{ dB}$  at  $5.07\text{ GHz}$  and  $-14.4\text{ dB}$  at  $5.48\text{ GHz}$ , with  $600\text{ MHz}$   $-10\text{ dB}$  bandwidth. The stitched ground plane resonance is slightly higher than the copper because the line width of the Amberstrand is thicker. The measured  $S_{11}$  of PA2 is  $-17.2\text{ dB}$  at  $5.48\text{ GHz}$  with  $780\text{ MHz}$   $-10\text{ dB}$  bandwidth. The stitched ground plane has a higher bandwidth than the antenna sample PA1 because the increased thickness of the substrate. PA2 stitched measured is different to the stitched simulated:

- More resonances at low frequency in the PA2 simulation are missing because the stitching at corners may not be fully connected. It is speculated that there should be loop resonances and these are missing.
- More loss at high frequency in the measured and broader band in PA2 stitched connected, because there are losses in the yarn that have not been taken into account in the model

MGP3 has thin traces on the ground plane and hence more inductances which may have given a different result.

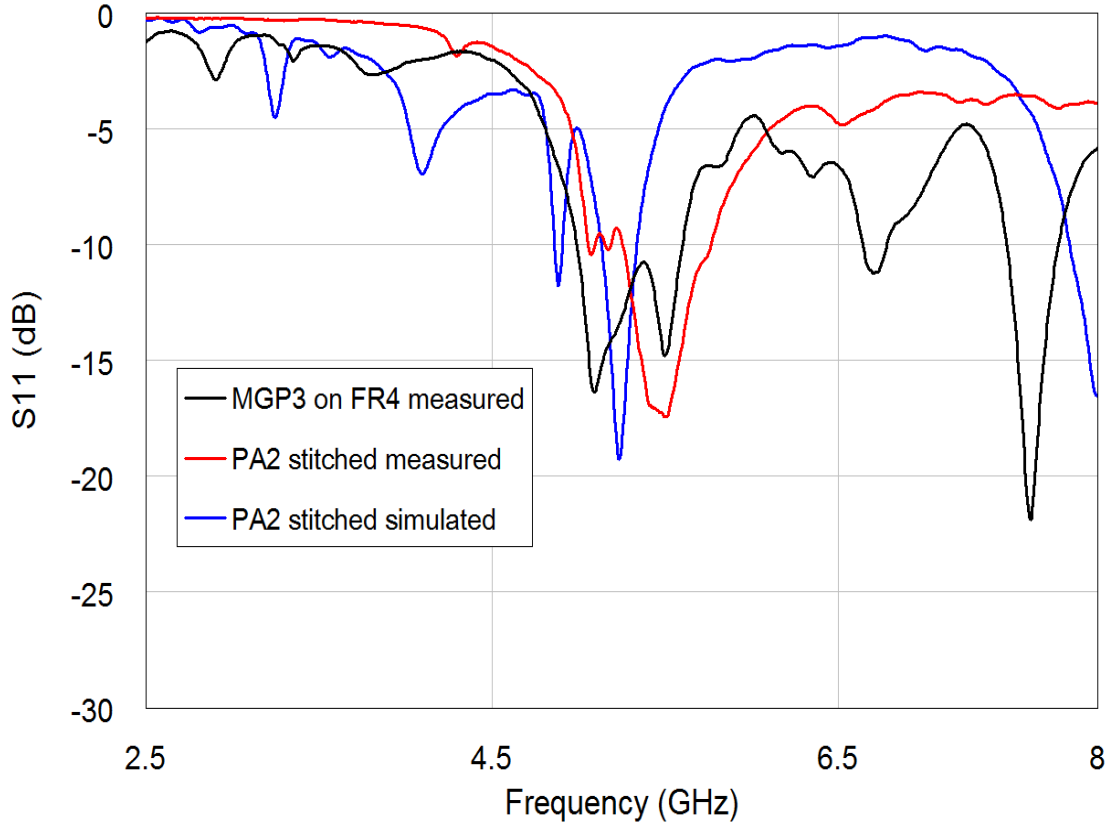


Figure 5.25 Meshed ground (MGP3) and stitched ground plane (PA2) measured results compared with simulation of PA2

The stitched antenna was placed on a rigid substrates, FR4 and compared with the etched antenna, PA1, see Table 5.7. All the stitched pattern was fastened to the FR4 substrate and the stitching were done using 2 mm spacing based on the design from MATLAB. Amberstrand Silver 66 thread was used. This antenna consists of three layers: the top patch, the dielectric substrate (FR4) and a thin fabric material, on which is placed the stitching of the ground plane. The same dimension of the ground plane (44 mm × 48 mm) were used for all the stitching designs. Antenna PA3 is on a felt fabric ground plane with total substrate thickness approximates 2.6 mm. Antenna sample PA4 is placed on denim fabric.

The simulated and measured  $S_{11}$  of three samples of stitched antenna is depicted in Fig. 5.26. Measured  $S_{11}$  of PA3 is -25.8 dB at 5.31 GHz with 800 MHz -10 dB bandwidth, Simulated  $S_{11}$  of PA3: -32.7 dB at 4.56 GHz with 500 MHz -10 dB bandwidth. The differences between the simulation and measurement due to inaccuracy of thickness of the rigid substrate and fabrication errors. Measured  $S_{11}$  result of PA3: -30.7 dB at 5.31GHz with 680 MHz -10 dB bandwidth while the simulated  $S_{11}$  result -25.2 dB at 5.46 GHz 420 MHz -10 dB bandwidth, the

simulation and measurement agreed for the antenna sample PA4. However PA3 has higher impedance bandwidth than PA4 as a result of the substrate thickness. The antenna sample PA4 has a centre frequency of  $-30.7\text{ dB}$  at  $5.31\text{ GHz}$  compared with PA3  $-25.8\text{ dB}$  at  $5.46\text{ GHz}$ . Antenna sample PA5, stitched on a denim substrate in triangular geometry, has a  $-10\text{ dB}$  bandwidth of  $861\text{ MHz}$  at  $-15.2\text{ dB}$ . The difference between the measurement and simulated results may be attributed to two reasons, air gap between the FR4 and fabric layer which was not considered during simulation. The adhesive spray used for fixing the fabric to FR4 was not taken into consideration during simulation.

MPG3 and MPG4 have different meshed ground planes, which explains the difference between measurements (Fig. 5.25 and Fig. 5.24).

The reflection coefficient of antenna PA3 was measured when placed onbody as shown in Fig.5.27. The measurements were carried out considering a  $3\text{ mm}$  gap between the body and the antenna. The  $S_{11}$  off-body measurement has  $S_{11}$  at  $5.18\text{ GHz}$  at  $-23.78\text{ dB}$  with  $-10\text{ dB}$  bandwidth of  $0.651\text{ GHz}$  while the on-body measurement  $4.781\text{ GHz}$  of  $-15.26\text{ dB}$  and  $5.316\text{ GHz}$  at  $-23.55\text{ dB}$ , with  $-10\text{ dB}$  bandwidth of  $0.86\text{ GHz}$ . The  $-10\text{ dB}$  bandwidths in free space and worn does not change significantly. The on body measurement shows the bandwidth has broadened and no change in resonant frequency except in two modes.

The simulated radiation patterns for a conventional microstrip patch antenna (PA1) and a microstrip patch with meshed ground at their resonant frequencies are shown in Fig.5.28. Meshing the ground plane does not change the shape of the pattern for the patch antenna but only causes some back radiation will leakage through the ground plane. The patterns are normalised to the peak gain at each frequency.

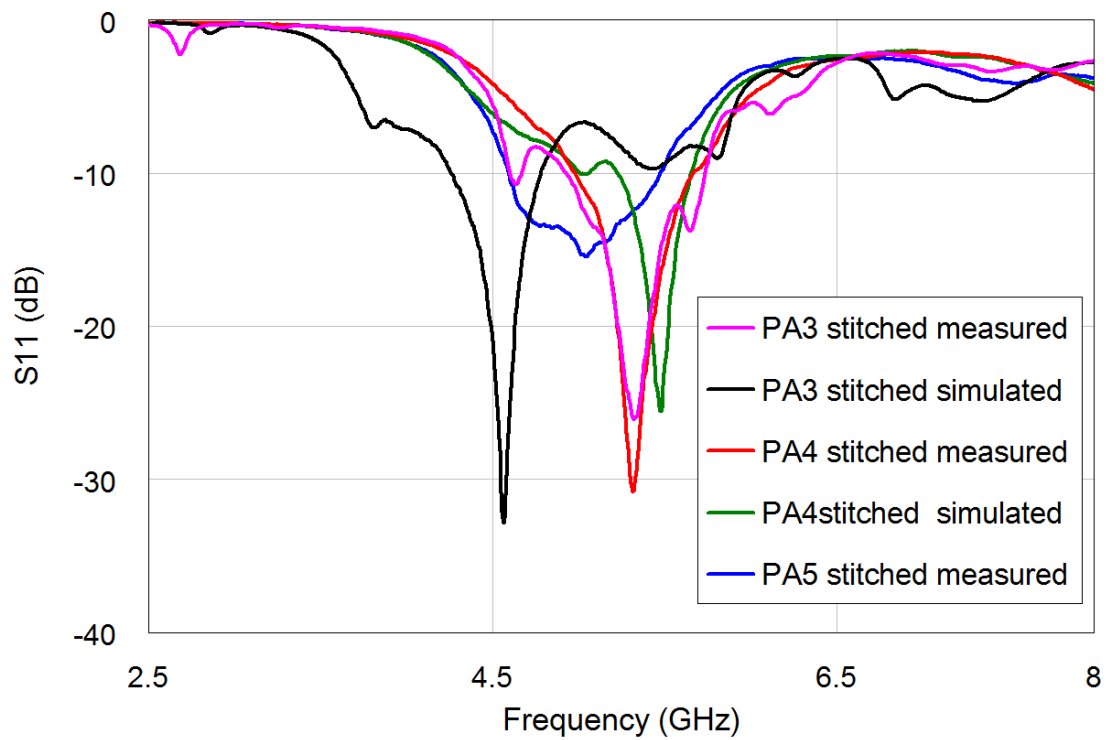


Figure 5.26 Measured  $S_{11}$  results of antennas with different stitched ground plane on different textile substrate

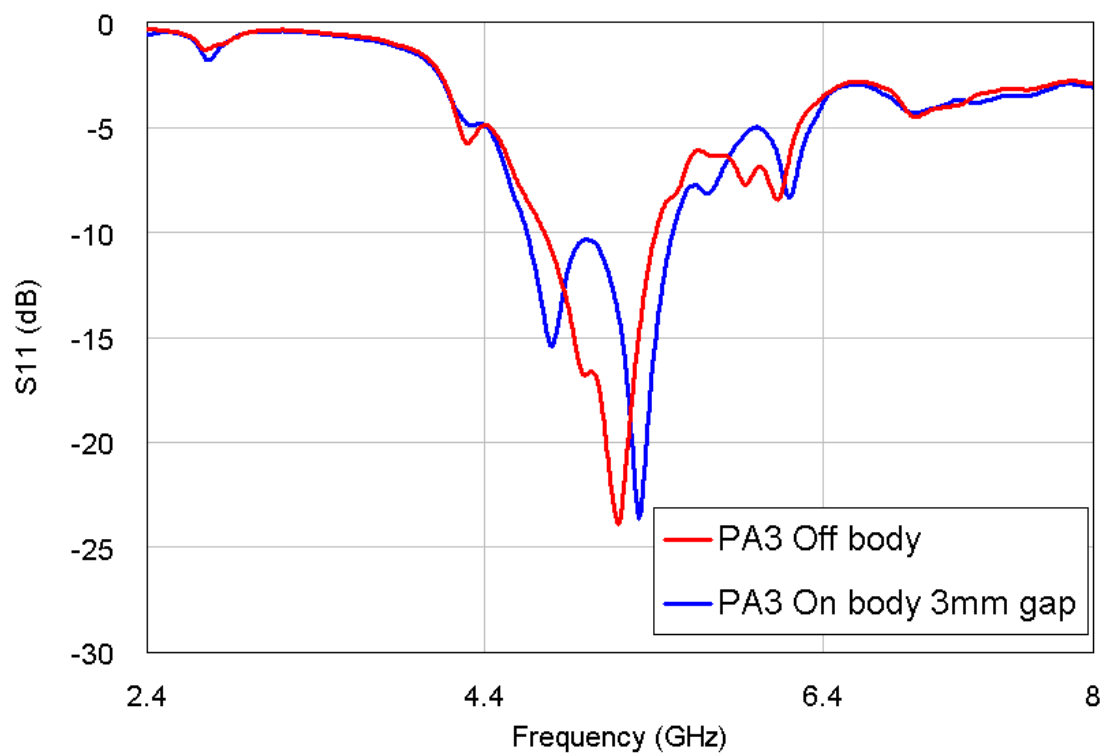


Figure 5.27 Measured  $S_{11}$  of antenna sample PA3 off and on body

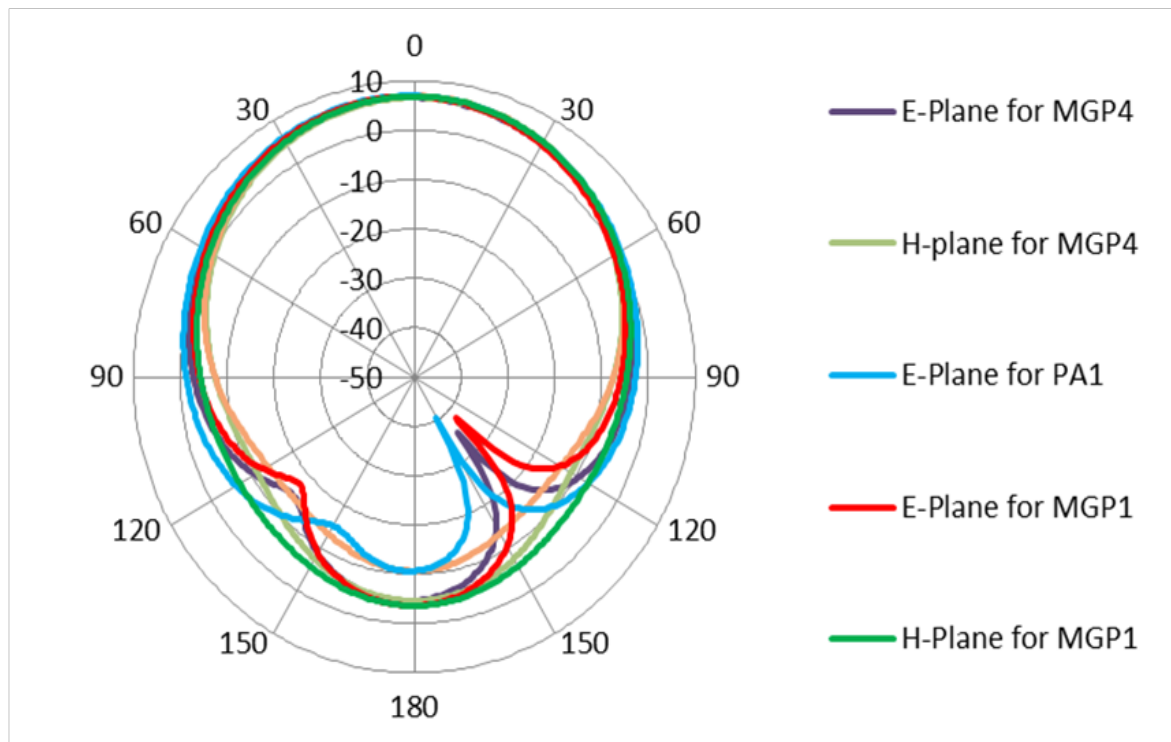


Figure 5.28 Stimulated radiation patterns of antenna samples that are presented in Table 5.7

### 5.7.5. Simulated surface current for meshed ground plane

The surface current is strong at the feed point and along the feed length. Currents flow along the vertical lines and the horizontal lines shows a increase in current path as shown in Fig.5.29 and lowering the the fundamental resonant frequency.

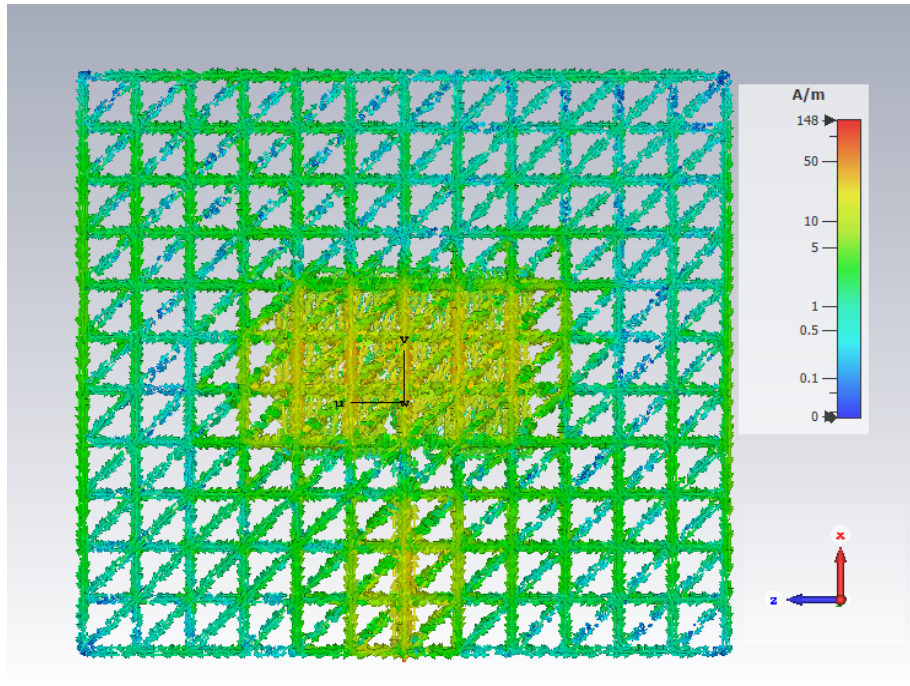


Figure 5.29 Simulated surface current on meshed ground plane for microstrip patch antenna at 5GHz

### 5.7.6. Summary

The bypass method employed in this study shows the possibilities of increased stitch spacing for ground plane of antennas and also at the same time reducing the cost of production of the stitched antennas. Full control of the stitch pattern is achieved. A higher conductive path was achieved on the mesh designs.

Current follows along the stitched path of ground plane. This stitched ground were applied to microstrip patch antennas. The patch antennas was designed at 5GHz with consistent dimensions and with differing format ground plane of the same size. A solid patch with solid ground plane was used for comparison with the stitched ground planes. Closer stitched configuration were achieved which gives resonant frequency at 5GHz. A fabric patch design with stitched ground shows comparable performance to coventional copper patch antenna of same design.

## Conclusion

The bypass method using MATLAB software is used to control the stitching techniques and stitching density. Three sets of geometric patterns were created include rectangular, square and triangular mesh. These patterns were stitched onto denim and felt fabric materials to provide a microstrip patch ground plane. The rectangular and square patterns uses less yarn compared to the triangular patterns. However, the Bypass method can be used to create any geometric pattern desired for any particular antenna ground plane. The solid ground plane of the microstrip antenna were replaced with a stitched ground plane for applications at 2.45 GHz and 5 GHz. This method has proven successful based on results from the ground plane designs carried out in this study.

The meshed ground plane of the size  $8 \times 8$  using an offset distance of  $\frac{1}{2}$  grid was designed using the proposed stitching pattern. The first stitch patterns created were not connecting properly at all node points when measured but to improved connections between the vertical and horizontal sections, an offset grid were generated. Measurement results on the proposed stitched ground planes were compared with the theory of infinite resistive network that shows good agreement.

Two types of feed were considered in the modelling of the microstrip patch antenna. The inset feed gives a better match and higher resonant frequencies than the direct feed microstrip line because the input impedance is clearly defined. The inset fed microstrip antenna has an efficiency of 91 % while the microstrip line fed has an efficiency of 88 % at the centre operating frequency of 2.45 GHz. From the results at  $-10dB$  bandwidth for microstrip patch at 5 GHz, a bandwidth of 150 MHz was realised but the value of 861 MHz bandwidth was achieved using the triangular stitched ground plane pattern. The rectangular stitched pattern used for the same microstrip patch antenna give a  $-10 dB$  bandwidth of 780 MHz. These results of the meshed stitched antennas shows a bandwidth broadening when the antenna is stitched on fabrics. Meshed version of the antenna will be advantageous if applied because less materials is required, implying less weight and cost, they can equally be integrated into clothing for wearable applications.



## References

- 5.1. W. Zeng, L. Shu, Q. Li, S. Chen, F. Wang, and X. M. Tao, “Fibre-based wearable electronics: A review of materials, fabrication, devices, and applications,” *Adv. Mater.*, 26(31), pp. 5310–5336, 2014.
- 5.2. Y. Ouyang and W. J. Chappell, “High frequency properties of electro-textiles for wearable antenna applications,” *IEEE Trans. Antennas Propag.*, 2008.
- 5.3. Clasen and R. Langley, “Meshed patch antennas,” *IEEE Trans. Antennas Propag.*, 52(6), pp. 1412–1416, 2004.
- 5.4. G. Venezian, “On the resistance between two points on a grid,” *Am. J. Phys.*, 62(11), pp. 1000, 1994.
- 5.5. Z. Z. Tan, “Recursion-transform method to a non-regular  $m \times n$  cobweb with an arbitrary longitude,” *Sci. Rep.*, 5, pp. 1–8, 2015. doi: 10.1002/cta.1988
- 5.6. F. Y. Wu, “Theory of resistor networks: The two-point resistance,” *Exactly Solved Model. A Journey Stat. Mech. Sel. Pap.* pp. 489–509, 2009. [Accessed 20-February-2018]. <http://stacks.iop.org/ja/37/6653>, doi:10.1088/0305-4470/37/26/004.
- 5.7. L. Zhang, Z. Wang, D. Psychoudakis, and J. L. Volakis, “E-fiber electronics for body-worn devices,” *Proc. 6th Eur. Conf. Antennas Propagation, EuCAP 2012*, pp. 760–761, 2012
- 5.8. T. Acti, S. Zhang, A. Chauraya, W. Whittow, R. Seager, and T. Dias, “High Performance Flexible Fabric Electronics for Megahertz Frequency Communications,” *Propagation Conference (LAPC), Loughborough* pp.1-4, 2011.
- 5.9. S. Zhang, W. Whittow, R. Seager, A. Chauraya, and J. C. Vardaxoglou, “Non-uniform mesh for embroidered microstrip antennas,” *IET Microwaves, Antennas Propag.*, 11(8), pp. 1086–1091, 2017
- 5.10. V. Safarova, L. Hes, and J. Militky, “An approach to electrical resistance measurement eliminating contact resistance problem,” *Int. Conf. Appl. Electron.*, pp. 259–262, 2015
- 5.11. F. M. Smits, “Measurement of Sheet Resistivities with the Four - Point Probe,” *Bell Syst. Tech. J.*, 37(3), pp. 711-718, 1958
- 5.12. C. Hertleer, H. Rogier, L. Vallozzi, and L. Van Langenhove, “A textile antenna for off-body communication integrated into protective clothing for firefighters,” *IEEE Trans. Antennas Propag.*, 57(4), pp. 919–925, 2009
- 5.13. C. A. Balanis, “Antenna theory analysis and design,” John Wiley and Son's Inc., 2016.

- 5.14. T. Milligan, “Modern Antenna Design,” 2nd Ed. 2005
- 5.15. D. M. Pozar, “Microstrip antennas,” Proc. IEEE, 80(1), pp. 79–91, 1992.
- 5.16. M. A. Matin and A. I. Sayeed, “A design rule for inset-fed rectangular microstrip patch antenna,” WSEAS Trans. Commun., 9(1), pp. 63–72, 2010.
- 5.17. L. I. Basilio, M. A. Khayat, J. T. Williams, and S. A. Long, “The dependence of the input impedance on feed position of probe and microstrip line-fed patch antennas,” IEEE Trans. Antennas Propag., 49(1), pp. 45–47, 2001.
- 5.18. R. Seager, S. Zhang, A. Chauraya, W. Whittow, Y. Vardaxoglou, T. Acti, and T. Dias, “Effect of the fabrication parameters on the performance of embroidered antennas,” IET Microwaves, Antennas Propag., 7(14), pp. 1174–1181, Nov 2013.
- 5.19. T. Yasin, R. Baktur, T. Turpin, and J. Arellano, “Analysis and Design of Highly Transparent Meshed Patch Antenna Backed By a Solid Ground Plane,” Prog. Electromagn. Res. M., 56, pp. 133–144, 2017.
- 5.20. S. Shahin, M. Shokooh-Saremi, “A Rigorous study on Meshed Patch Antenna,” 23<sup>rd</sup> Iranian conference on Electrical Engineering (ICEE), 2015.

## **Chapter 6**

### **Conclusions and Future Work**

#### **6.1. Summary of Results**

In chapter 2 a brief review of wire antennas was presented, showing how the first wire antenna was proposed. Antennas are designed either by a set of equations or using a simulator to create a design and then to analyse the properties. The process of designing an antenna by intuition or trial and error takes quality time since antennas are highly multimodal. Evolutionary optimisation such as by use of genetic algorithms has been used to improve the quality of existing designs, to create new designs and to simplify the design process. Genetic algorithms have been successfully used for the optimisation of linear wire antennas, crooked-wire antennas and microstrip spiral antennas, at different frequency bands.

An understanding of textile antenna design and manufacturing techniques is essential in this study. The properties of the fabrics used as dielectric substrates and their characterisation are highlighted. Embroidery is fast and flexible in creating new patterns and make integrating radio frequency systems into clothing/garments for wearable applications.

The simulation-based optimisation is used for design of linear wire antennas in chapter 3. The genetic algorithm is used for optimisation and the computation of wire antenna characteristics is performed using an electromagnetic solver (NEC2). Results from the GA run were used to produced samples of linear wire antennas. The NEC2 results were compared to CST (a FIT solver) simulations before fabrication. The performance of the linear wire antennas was evaluated for a population of 30 and evolved for 500 generations or 15000 fitness calculations. The GA is flexible and gives better and improved designs of antennas.

Chapter 4 presents the fabrication and measurements of wire, planar and stitched antennas. The antenna samples were named Pocket A, pocket B, pocket C, pocket D and collar A, collar B, collar C, collar D. This procedure of using the GA coupled with NEC2 to optimise parameters of antenna yields good designs, showing remarkable performance in terms of bandwidth and return loss ( $S_{11}$ ). All the four optimised antennas had good efficiency that make them suitable for communication applications.

Chapter 5 focuses on the production of stitched ground planes for textile applications. A meshed resistive grid was evaluated using Kirchhoff's current law and nodal analysis. The

equivalent resistance between nodes are a function of their distance apart. A finite resistive grid was simulated and compared with measured sets of data. For the purpose of implementation of the designs, a microstrip patch antenna was designed and stitched on a meshed ground with denim and felt fabric. A practical mesh ground plane was modelled and designed using MATLAB. The designs were exported to embroidery machine software for production. Representative samples, used as patch ground planes, were validated.

## **6.2. Main Contributions**

The main contributions of this thesis are:

- A generic method of modelling wire antenna is proposed using Numerical Electromagnetic Codes (NEC2) built on the application of genetic algorithm (GA).
- A set of novel pocket and collar antennas were optimised using the generic method to produce covert antennas for civilian applications. These covert antennas can be retrofitted to existing garment designs and there is a high level of flexibility.
- A stitched ground plane for microstrip patch antennas and stitched monopoles were developed and fabricated using the MATLAB interface to computer embroidery.
- The interface method reduces the stitching density and electrical resistance between mesh nodes making the antennas to be flexible and wearable.

## **6.3. Industrial Applications**

This thesis has shown the possibility of designing a novel bent wire antenna (for wearable applications) using an inspired optimisation process. This method was achieved by the use of MATLAB and NEC2 for automating the design cycle. Results were compared with CST Microwave studio before fabrication on printed circuit board (PCB). The stitched wire antennas were integrated in apparel using embroidery.

The work reported in this thesis has produced an approach that answers the motivation behind the work. Cables are expensive to install over some areas in Nigeria. Wearable wire antenna can be used for communication. These stitched antennas could be produced on a large scale

since the embroidery process is easy, reliable and low cost. The wire antenna could be used on children's school bags with other sensors to monitor and track movement in case of kidnapping and to detect of killing of herdsmen in Nigeria.

#### **6.4. Future Research**

This thesis is primarily focussed on covert antennas to be hidden in garments/clothing for wearable applications and produce a technique that could bypass the PE design embroidery machine.

- The linear wire antennas were used as reference for this optimisation procedure to perform the designs although some other types of antennas such as Stitched and printed dipoles could be considered [6.1]- [6.2].
- The stitched antennas will be connected to GSM and Wi-Fi communication modules and performances should be tested.
- In this research, probe fed techniques were used for the rectangular patch antenna designs, circular and triangular patch antennas would be exploited to generate a circular polarisation to manage propagation path problems. Other alternative feeding techniques should be investigated in future to ease the manufacturing processes.
- Finally, an exploration local fabric material in Nigeria and the possibilities of integrating these into textile antennas to reduce the cost of manufacturing should be undertaken. All fabrics need to be characterised.

## References

- 6.1. J. Tak, Y. Hong and J Choi., “Textile antenna with EBG structure for body surface wave enhancement,” *Electronics Letters*, 51, pp.1131-1132, 2015.
- 6.2. P. S. Hall et al., “Antennas and propagation for on-body communication systems,” *IEEE Antennas Propag. Mag.*, 49(3), pp. 41–58, 2007.

## APPENDIX A

### Numerical Methods

#### 1. Finite Difference Time Domain (FDTD)

The FDTD method is a direct implementation of Maxwell's time dependent curl equations to solve the temporal variation of electromagnetic waves within a finite space that contains an object of arbitrary geometry and compositions. A good understanding of the principles on which the software is based is important in order to set relevant parameters of the simulators [1]. The (FDTD) method introduced by Yee in 1966 [2] is one of the grid-based differential time domain numerical methods. The entire computation domain is meshed into individually cuboid cells which each are solved into time domain. He started considering a Cartesian mesh and setting the three components  $E_x, E_y, E_z$  to be located in middle of the edges and the other three components  $H_x, H_y$ , and  $H_z$ . to be located at the centre of the faces. The dual grids were introduced which are called the electric and magnetic grids. The finite-difference time-domain (FDTD) method [3] solves the coupled Maxwell's curl equations directly in the time domain by using finite time steps over small cells in space. The solution domain is discretized. FDTD excels at analysing of inhomogeneous and nonlinear media but its demand for system memory are high because of discretization of the entire solution domain. The FDTD method reduces the differential equations that can be solved by sets of difference equations. A cell has only one material. It may not be homogenous, but it is still one boundary.

#### 2. Finite Integration Technique (FIT)

The Finite Integration Technique was developed and published by Weiland in 1977 [4]. FIT is a theoretical framework for solving the integral rather than differential form of Maxwell's equations in the time domain. The FIT is a discretised form of Maxwell's equations. The method can be applied to static, harmonic and time dependent fields, mainly because it is a computer-compatible reformation of Maxwell's equation in integral form. For many practical problems, both frequency and time domain analysis are essential and only the combination yields successful results [5] - [6]. The equations (A.1) - (A.7) are the continuous form of Maxwell's equations and can be solved by using mathematical properties of the integral. These equations are the integral form.

$$\text{Faraday's Law: } \oint_C \vec{E} \cdot d\vec{l} = -\frac{\partial}{\partial t} \int_S \vec{B} \cdot d\vec{S} \quad (\text{A.1})$$

$$\text{Gauss's Law for magnetic field: } \oint_S \vec{B} \cdot d\vec{S} = 0 \quad (\text{A.2})$$

$$\text{Ampere's Law: } \oint_S \vec{H} \cdot d\vec{l} = \int_S \vec{J} \cdot d\vec{S} + \frac{\partial}{\partial t} \int_S \vec{D} \cdot d\vec{S} \quad (\text{A.3})$$

$$\text{Gauss's Law for electric field: } \int_S \vec{D} \cdot d\vec{S} = \int_V \rho dV \quad (\text{A.4})$$

$$\vec{D} = \epsilon \vec{E} \quad (\text{A.5})$$

$$\vec{B} = \mu \vec{H} \quad (\text{A.6})$$

$$\vec{J}_L = k \vec{E} \quad (\text{A.7})$$

Where  $\vec{E}$  = Electric field vector (V/m);  $\vec{H}$  = Magnetic field vector (A/m);  $\vec{B}$  = Magnetic flux density vector (Tesla);  $\vec{D}$  = Electric Displacement (C/m<sup>2</sup>);  $\vec{J}_L$  = displacement current density (A/m<sup>2</sup>);  $\rho$  = volume charge density (C/m<sup>3</sup>).

Computer Simulation Technology Microwave Studio (CST) is a 3D simulation package for electromagnetic analysis. CST uses a number of different solvers or simulators (Transient solver, Frequency domain, Eigen-mode solver, Integral equation solver) to solve different problems based on their applications. CST uses the Finite Integration Techniques for computing the  $\vec{E}$  and  $\vec{H}$  field at each point [6]. This package is used in the thesis to validate the NEC2 results.

### 3. Numerical solution by the Method of Moments

The Method of Moment transforms an integral or differential equation into a set of simultaneous linear equations that they then be computed numerically. Application of the Method of Moment yields an impedance matrix that may be solved for the current and other properties. The method was first applied to electromagnetic problems in the 1960s by Harrington [7]. The Method of Moments expands the currents on an antenna (or scattering object) in a linear sum of simple basis functions. The Method of Moments is computationally efficient and is easily combined with other frequency domain methods to solve large problems. The Method of Moment is very useful in solving radiation and scattering problems. It is mostly suitable for wire antennas [7]. The assumptions for the formulation are as follows:



The integral equation (A.8) is solved by Method of Moments [9-10]. The solution is an integral or differential equation that has the general for

$$F(g) = h \quad (A.8)$$

where  $F$  is an integral or differential operator,  $g$  is the desired response function (charge or current) and  $h$  is a known source or excitation function. The objective is to find  $g$  once  $F$  and  $h$  is known. The unknown response function can be expanded as a linear combination of  $N$  terms as:

$$g(z') \approx a_1 g_1(z') + a_2 g_2(z') + \dots + a_N g_N(z') = \sum_{n=1}^N a_n g_n(z') \quad (A.9)$$

where  $a_n$  is an unknown operator and each  $g_n(z')$  is a known function usually a basis function. Substituting equation (A.9) into (A.8) and applying the linearity of the  $F$  operator gives (A.10) into

$$\sum_{n=1}^N a_n F(g_n) = h \quad (A.10)$$

The basic function  $g_n$  depends on each value of  $F(g_n)$  in (A.10). The expansion of (3.10) leads to one set of equation. This is accomplished by evaluating (A.10) using the boundary conditions at different points. This method is referred to as point matching (or collocation).

The equation (A.10) takes the form of

$$\sum_{n=1}^N a_n F(g_n) = h_m, \quad m = 1, 2 \dots N \quad (A.11)$$

The equation (A.11) is expressed in matrix form as:

$$[Z_{mn}][I_n] = [V_m] \quad (A.12)$$

where

$$Z_{mn} = F(g_n) \quad (A.13)$$

$$I_n = a_n \quad (A.14)$$

$$V_m = h_m \quad (A.15)$$

The unknown coefficients  $a_n$  can be solved using inverse matrix techniques on equation (A.12) as:

$$[I_n] = [Z_{mn}]^{-1}[V_m] \quad (\text{A.16})$$

The underlying concept of the Method of Moments is the numerical solution of integral equations for currents induced on a structure by the sources and incident electromagnetic fields. The integral is reduced to a series of linear algebraic equations and solved using a matrix method. Linear wire antennas can be solved efficiently by the use of MoM.

#### 4. Integral Equations and Numerical solutions in Numerical Electromagnetic Code

The Numerical Electromagnetic Code is also known as NEC is a user-oriented program for analysing the interaction of electromagnetic waves with conducting wires and surfaces. NEC2 is public domain software for antenna modelling. It uses an integral form of numerical solution. NEC2 uses Method of Moment's codes for analysis. NEC2 is used for the modelling of wire structures in free space or with conducting ground. The NEC2 solver computes current distributions, impedances, power input, radiation pattern, efficiency and gain of a wire antenna.

NEC2 program uses electric-field integral equation (EFIE) for thin wires structures as well as the magnetic-field integral equation (MFIE) for large smooth surfaces. For a structure that combines wires and surfaces NEC2 uses both EFIE and MFIE coupled together [9-10]. The integral representation of the electric field of a volume current distribution  $\vec{J}$  used in NEC2 of the form of EFIE as,

$$\vec{E}(\vec{r}) = \frac{-j\eta}{4\pi k} \int_V \vec{J}(\vec{r}') \cdot (\vec{r} - \vec{r}') dV' \quad (\text{A.17})$$

Where

$$G(\vec{r} - \vec{r}') = (k^2 I + \nabla \nabla) g(\vec{r} - \vec{r}') \quad (\text{A.18})$$

$$g(\vec{r} - \vec{r}') = \exp(-jk|\vec{r} - \vec{r}'|) / |\vec{r} - \vec{r}'| \quad (\text{A.19})$$

$$k = \omega \sqrt{\mu_0 \epsilon_0} \quad (\text{A.20})$$

$$\eta = \sqrt{\frac{\mu_0}{\epsilon_0}} \quad (\text{A.21})$$

Where  $\vec{E}(\vec{r})$  is the radiated electric field,  $I$  is the current on the wire antenna,  $\vec{r}$  is the vector to a point on the wire,  $\vec{r}'$  is the vector to the observation point,  $\mu_0$  is the permeability constant,  $\epsilon_0$  is the free-space dielectric constant,  $k$  is the free-space wave number or propagation constant. When considering the current distribution along the surface of perfectly conducting body Equation (A.17) becomes

$$\vec{E}(\vec{r}) = \frac{-j\eta}{4\pi k} \int_V \vec{J}(\vec{r}') \cdot (\vec{r} - \vec{r}') dA' \quad (\text{A.22})$$

In NEC2, the thin-wire approximation is used, and numbers of approximations were introduced to simplify Equation (A.22).

- $E_{tan} = 0$  along the surface as the conductor is perfect (PEC).
- The circumferential current is negligible and only the axial component needs to be considered.
- The total current is observed and treated as a filament on the wire; boundary condition is enforced on the wire surface

A filamentary current ( $I$ ) in (A.14) replace the axial current around a wire of surface current  $J_s(\vec{r})$

Where

$$I(s)\hat{s} = 2\pi a \vec{J}_s(\vec{r}) \quad (\text{A.23})$$

The magnetic field integral equation is obtaining from the integral representation for a surface current distribution  $\vec{J}_s$  of magnetic field,

$$\vec{H}^S(\vec{r}) = 1/4\pi \int_S \vec{J}_s(\vec{r}') \times \nabla' g(\vec{r} - \vec{r}') dA' \quad (\text{A.24})$$

The differentiation is with respect to the integral variable  $\vec{r}'$ . The current  $\vec{J}_s$  is inducing by the external incident field  $\vec{H}^I$ , which implies that the total magnetic field inside the perfectly conducting surface must be zero.

Wire antennas in NEC2 are divided into short straight segments; this increases current distribution on each segment. NEC2 uses the basis functions for providing both current and charge continuity at junctions. The current on a wire segment in NEC2 is given by equation (A.14) and currents are defined over the sub region of the overall structure [10]. The basis function or the current expansion function have the form of equation (A.15) made of three parts, the constant term, odd function and even functions.

$$I_j(s) = A_j + B_j \sin k_s(s - s_j) + C_j [\cos k_s(s - s_j)] \quad (\text{A.25})$$

$$|s - s_j| < \Delta_j/2 \quad (\text{A.26})$$

Where  $s_j$  is the value of  $s$  at the midpoints of  $j^{th}$  segment with  $\Delta_j$  being the length of the segment  $j$  and  $k_s = \omega\sqrt{\mu_0\epsilon_0}$ . Of the three unknown constants, two terms were eliminated by imposing continuity conditions on the current and charge at the ends of segment. The remaining term is related to current amplitude and solved using matrix form of method of moment.

## APPENDIX B

### GA RESULT AND MONOPOLE ANTENNAS

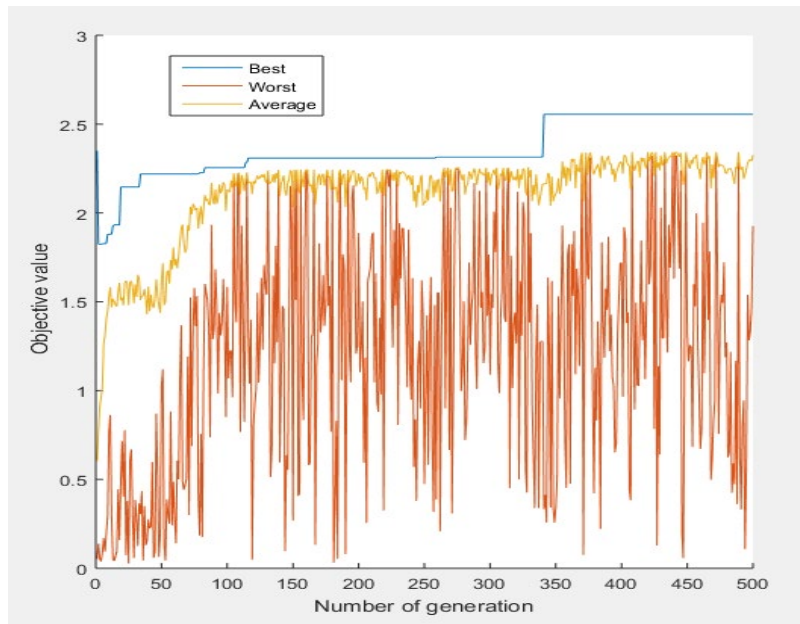


Figure B.1 GA runs for 500 generations

Table B. 1 NEC2 input data structure

| Card | Description                      |
|------|----------------------------------|
| CM   | Command line                     |
| CE   | Comments line                    |
| GW   | Wire specification               |
|      | Tag Number                       |
|      | Number of segments               |
|      | XW1- X coordinate of wire end 1  |
|      | YW1- Y coordinate of wire end 1  |
|      | ZW1 - Z coordinate of wire end 1 |
|      | XW2 - X coordinate of wire end 2 |
|      | YW2 - Y coordinate of wire end 2 |
|      | ZW2 – Z coordinate of wire end 2 |
|      | Rad- radius of the wire          |
| GE   | Geometry End                     |
| EK   | Extended thin-wire approximation |
| Ex   | Excitation source                |
| GN   | Ground parameter                 |
| FR   | Frequency specification          |
| FR   | Frequency Sweep                  |
| LD   | Structure impedance loading      |
| RP   | Radiation pattern                |
| EN   | End of data                      |

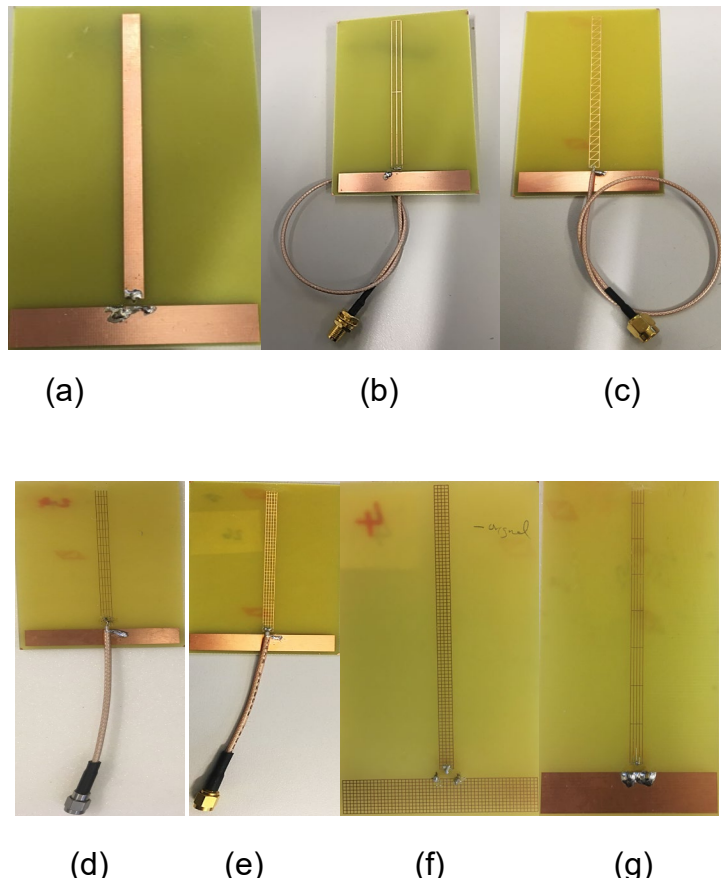


Figure B.2 Meshed monopole antenna samples (a) etched solid monopole (b) antenna sample 25 (c) antenna sample 27 (d) antenna sample 24 (e) antenna sample 26 (f) antenna sample 20 and (g) antenna sample (21)

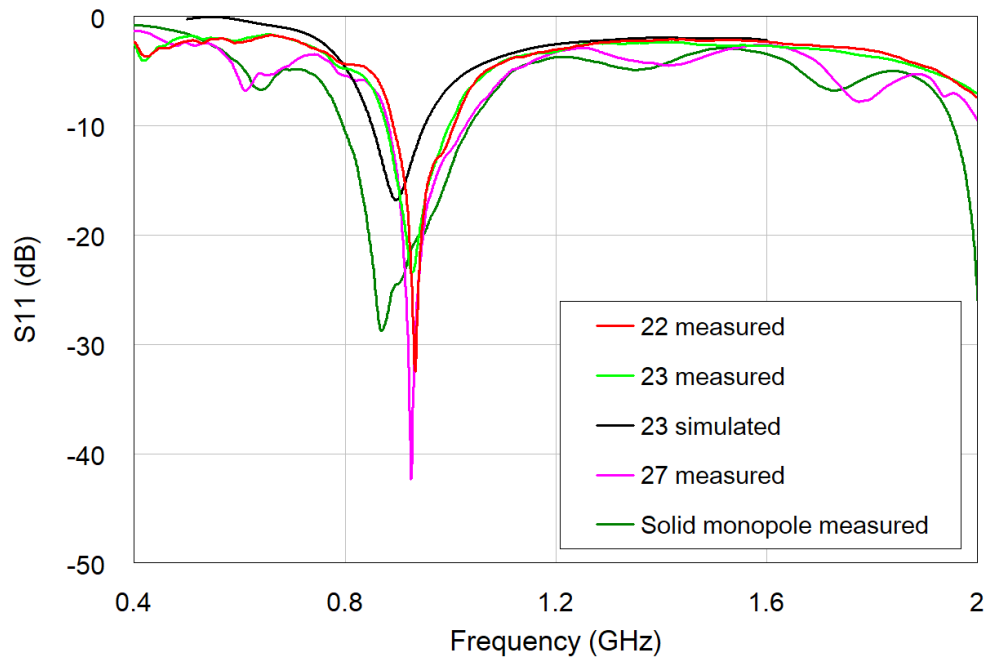


Figure B.3  $S_{11}$  plot for etched meshed antenna samples 22 and 23

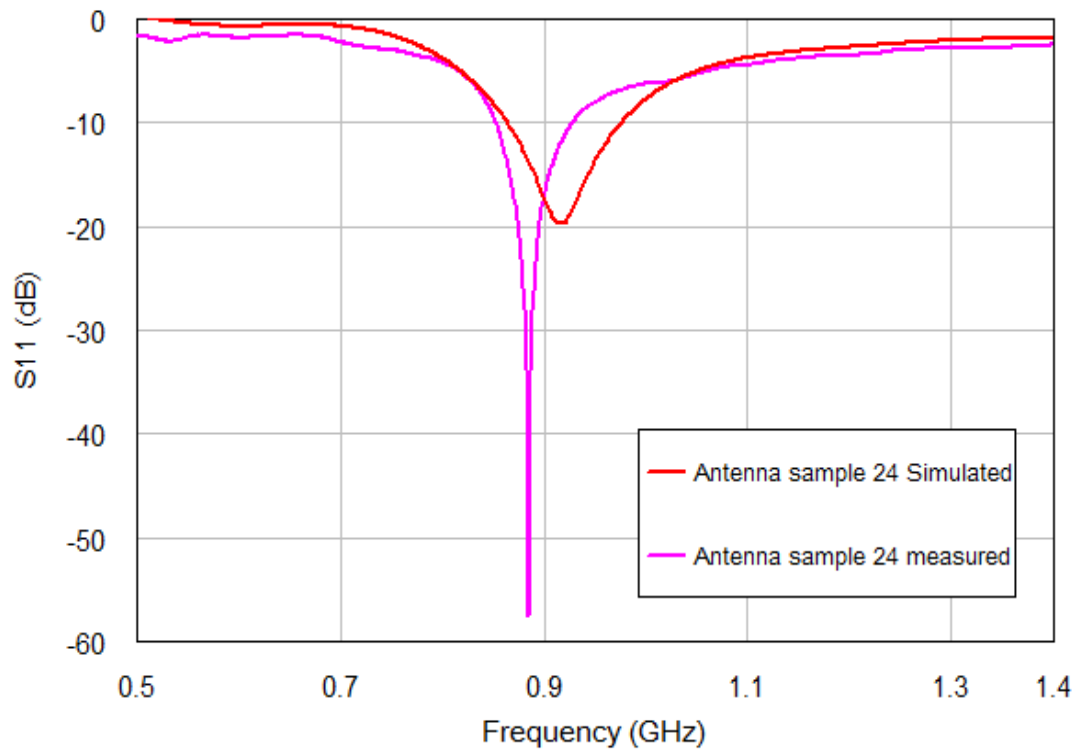

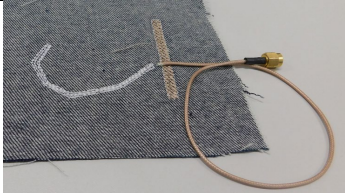


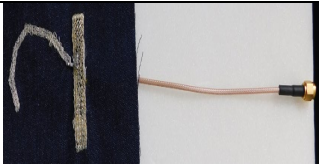
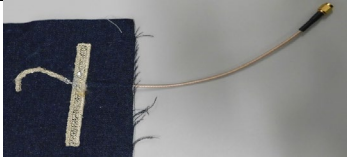


Figure B.4  $S_{11}$  plot of measured antenna sample 24 with simulation

Table B1. Resonant frequencies and bandwidth of stitched antenna samples

| Stitched antenna samples  | Measured $f_0$ (MHz) | Measured $S_{11}$ (dB) | -10dB Bandwidth (MHz) | Radiated efficiency (%) |
|---|----------------------|------------------------|-----------------------|-------------------------|
| <br>EA01   | 879                  | -18.88                 | 126                   | 91                      |
| <br>EA03   | 939                  | -15.87                 | 56                    | 61                      |
| <br>EA04  | 897                  | -42.53                 | 60                    | 54                      |
| <br>EA06 | 972                  | -16.87                 | 115                   | 80                      |
| <br>EA07 | 919                  | -12.50                 | 53                    | 62                      |
| <br>EA08 | 983                  | -51.51                 | 288                   | 74                      |



# MATLAB SCRIPTS FOR AUTOMATING WIRE ANTENNAS

```

Function [THETA1, THETA2, THETA3,THETA4, THETA5, l1,l2,l3, l4,l5,A] =
meander_new( )
close all
clear variables
noantennas = 30;
[THETA1, THETA2, THETA3,THETA4, THETA5, l1,l2,l3, l4,l5] = initialise(noantennas);
[A,newFileLog]= execute(THETA1, THETA2, THETA3,THETA4, THETA5, l1,l2,l3,
l4,l5,noantennas);
l1 = newFileLog(:,1);
THETA1 = newFileLog(:,2);
l2 = newFileLog(:,3);
THETA2 = newFileLog(:,4);
l3 = newFileLog(:,5);
THETA3 = newFileLog(:,6);
l4 = newFileLog(:,7);
THETA4 = newFileLog(:,8);
l5 = newFileLog(:,9);
THETA5 = newFileLog(:,10);
l6 = newFileLog(:,11);
l7 = newFileLog(:,12);
% boundingbox(noantennas, A);
save('l7data.mat', 'l7')
save('l6data.mat', 'l6')
save('alldata.mat')
%%%%%%%%%%%%%%
%%%%%%%%%%
%%%%%%%%%%
% This function initialise the variables
function[THETA1, THETA2, THETA3,THETA4, THETA5, l1,l2,l3, l4,l5] =
initialise(noantennas)
THETA1 = 30+(30)*rand(noantennas,1);
THETA2 = 30+(30)*rand(noantennas,1);
THETA3 = 30+(30)*rand(noantennas,1);
THETA4 = 30+(30)*rand(noantennas,1);
THETA5 = 30+(30)*rand(noantennas,1);
% the antenna length;
% length in millimeter
l1 = 8.3 + (13.9)*rand(noantennas,1); % length of first length
l2 = 8.3 + (13.9)*rand(noantennas,1); % length of second length
l3 = 8.3 + (13.9)*rand(noantennas,1); % length of third length
l4 = 8.3 + (13.9)*rand(noantennas,1); % length of fourth length

```



```

        %plot(linex,line3)
        [iX,iY] = lineintersect(linex,line3);
        if iX~= 10000 || iY~=10000
            THETA3(j) = 30+30*rand(1,1);
            %%%%%%%%%
            loopcount=loopcount+1;
            if loopcount>=10
                [THETA1, THETA2, THETA3,THETA4, THETA5, 11,12,13, 14,15] =
initialise(noantennas);
                reset=1;
            end
        end
    end
    end
    end
    iX = 0;
    iY = 0;
    k=1;
end
if i == 5
    while k<=3
        while (iX~=10000 || iY~=10000)
            A(1,i,j) = l4(j)*cosd(THETA4(j) + THETA3(j)+THETA2(j) + THETA1(j)) +
A(1,4,j);
            A(2,i,j) = l4(j)*sind(THETA4(j) + THETA3(j)+THETA2(j) +THETA1(j)) +
A(2,4,j);
            linex = [A(1,k,j) A(2,k,j) A(1,k+1,j) A(2,k+1,j)];
            line4 = [A(1,4,j) A(2,4,j) A(1,5,j) A(2,5,j)];
            %plot(linex,line4)
            [iX,iY] = lineintersect(linex,line4);
            if iX~= 10000 || iY~=10000
                THETA4(j) = 30+30*rand(1,1);
                k=0;
                iX=10000;
                iY=10000;
                %%%%%%%%%
                loopcount=loopcount+1;
                if loopcount>=10
                    [THETA1, THETA2, THETA3,THETA4, THETA5, 11,12,13, 14,15] =
initialise(noantennas);
                    reset=1;
                end
            end
        end
        k=k+1;
        iX=0;
        iY=0;
    end
    k=1;
    iX = 0;
    iY = 0;

```

```

end
if i == 6
    while k <= 4
        while (iX ~ 10000 || iY ~ 10000)
            A(1,i,j) = l5(j)*cosd(THETA5(j)+ THETA4(j)+ THETA3(j)+THETA2(j)
+THETA1(j)) + A(1,5,j);
            A(2,i,j) = l5(j)*sind(THETA5(j)+THETA4(j) + THETA3(j)+THETA2(j) +
THETA1(j)) + A(2,5,j);
            linex = [A(1,k,j) A(2,k,j) A(1,k+1,j) A(2,k+1,j)];
            line5 = [A(1,5,j) A(2,5,j) A(1,6,j) A(2,6,j)];
            [iX,iY] = lineintersect(linex,line5);
            if iX ~ 10000 || iY ~ 10000
                THETA5(j) = 30+30*rand(1,1);
                k=0;
                iX=10000;
                iY=10000;
                %%%
                loopcount=loopcount+1;
                if loopcount >= 10
                    [THETA1, THETA2, THETA3,THETA4, THETA5, l1,l2,l3, l4,l5] =
initialise(noantennas);
                    reset=1;
                end
            end
            end
            k=k+1;
            iX=0;
            iY=0;
        end
        k=1;
        iX = 0;
        iY = 0;
    end
    disp(strcat('plot',num2str(j)));
    disp(l4(j));
    % axis above zero
    lowest_y = min(A(2,:,j));
    if lowest_y < 0
        A(2,:,j) = A(2,:,j) + abs(lowest_y);
    end
end
if reset == 1
    j=j-1;
    reset=0;
else
    newFileLog(j,:) =
[l1(j),THETA1(j),l2(j),THETA2(j),l3(j),THETA3(j),l4(j),THETA4(j),l5(j),THETA5(j)];
    writeInputFile(A,1,j);
    figure
    % grid on

```

```

        hold on
        title(strcat('j=',int2str(j)))
        plot(A(1,:,j),A(2,:,j),'g');
        % the 10.0000 represents the padding, change as desired.
        plotBoundary(A,j,2,10,10);
% %      plotStaticBoundary();
        drawnow;
        axis square ;
        hold off
    end
    j=j+1;
end
% Set the file paths
cd 'c:\4nec2\'
pwd
cd exe
%if you want to run the monopole simply remove the percentage sign from
%below
for i=1:noantennas%+1
    % i=1:noantennas+1
    % Generate some geometry to run
    filenamestring=sprintf('../out/input%d.nec', i);
    filenamestring2=sprintf('../out/geom%d.out', i);
    fid = fopen('nec2d.tmp', 'wt ');          % Generates the text file
    fprintf( fid, '../out/input%d.nec\n', i);  % that tells nec where to look
    fprintf( fid, '../out/geom%d.out\n', i);  % for the input and output files
    fclose(f)
    % Run nec from the command line
    !Nec2dXS1k5.exe 0<nec2d.tm
    fid = fopen(filenamestring2, 'r');
    tline = fgets(fid);
    while ischar(tline)
        if(findstr(tline, 'FREQUENCY='))
            tline=lower(tline);
            disp(tline)
        end
        tline = fgets(fid);
    end
    fclose(fid);
end
% cd 'F:\project files\'
x = OutputFile(THETA1, THETA2, THETA3, THETA4, THETA5, 11,12,13,14,15, A)

```

## 2. Checking lineintersect

```

function [x,y]=lineintersect(l1,l2)
%This function finds where two lines (2D) intersect
%Each line must be defined in a vector by two points
%[P1X P1Y P2X P2Y], you must provide two has arguments

```

```

%Example:
%l1=[93 388 120 354];
%l2=[102 355 124 377];
%[x,y]=lineintersect(l1,l2);
%You can draw the lines to confirm if the solution is correct
%figure
%clf
%hold on
% line([l1(1) l1(3)],[l1(2) l1(4)])
% line([l2(1) l2(3)],[l2(2) l2(4)])
% plot(x,y,'ro') %this will mark the intersection point
%There is also included in another m file the Testlineintersect
%That m file can be used to input the two lines interactively
%Made by Paulo Silva
%22-02-2011
%default values for x and y, in case of error these are the outputs
x=10000;
y=10000;
%test if the user provided the correct number of arguments
if nargin~=2
disp('You need to provide two arguments')
return
end
%get the information about each arguments
l1info=whos('l1');
l2info=whos('l2');
%test if the arguments are numbers
if (~(strcmp(l1info.class,'double') & strcmp(l2info.class,'double'))))
disp('You need to provide two vectors')
return
end
%test if the arguments have the correct size
if (~all((size(l1)==[1 4]) & (size(l2)==[1 4])))
disp('You need to provide vectors with one line and four columns')
return
end
try
m1=(l1(4)-l1(2))/(l1(3)-l1(1));
m2=(l2(4)-l2(2))/(l2(3)-l2(1));
b1=l1(2)-m1*l1(1);
b2=l2(2)-m2*l2(1);
b=[b1 b2]';
a=[1 -m1; 1 -m2];
Pint=a\b;
%when the lines are paralel there's x or y will be Inf
if (any(Pint==Inf))
disp('No solution found, probably the lines are paralel')
return
end
%put the solution inside x and y

```

```

x=Pint(2);y=Pint(1);
%find maximum and minimum values for the final test
l1minX=min([l1(1) l1(3)]);
l2minX=min([l2(1) l2(3)]);
l1minY=min([l1(2) l1(4)]);
l2minY=min([l2(2) l2(4)]);
l1maxX=max([l1(1) l1(3)]);
l2maxX=max([l2(1) l2(3)]);
l1maxY=max([l1(2) l1(4)]);
l2maxY=max([l2(2) l2(4)]);
%Test if the intersection is a point from the two lines because
%all the performed calculations where for infinite lines
if ((x<l1minX) | (x>l1maxX) | (y<l1minY) | (y>l1maxY) |...
    (x<l2minX) | (x>l2maxX) | (y<l2minY) | (y>l2maxY) )
    x=10000;
    y=10000;
    disp('There's no intersection between the two lines')
    return
end
catch err
%if some strange error occurred show it to the user
rethrow(err)
disp('There's no intersection between the lines (x=nan,y=nan)')
end

```

### 3. This program read the output file and extract the frequency and the magnitude of the normalised impedance

```

% This program read the output file and extract the frequency and the
% magnitude of the normised impedance.
% The magnitude of the normalised impedance is used for computation of
% S11 results Z/50 Ohms.The result are display as plots and array.
% Individul S11 and average S11 results are computed.
function x = OutputFile(THETA1, THETA2, THETA3,THETA4, THETA5, l1,l2,l3, l4,l5, A)
x='true';
generation = 1;
genmax = 10;
while generation <= genmax
    cd 'c:\4nec2\'
    pwd
    cd 'out'
    close all
    % create backup files for genetic algorithm
    foldername = strcat('generation',num2str(generation-1));
    status = mkdir(foldername);
    status1 = copyfile('geom*.out',strcat(foldername,'/'));
    status2 = copyfile('input*.nec',strcat(foldername,'/'));
    status3 = copyfile('s11.txt',strcat(foldername,'/'));
    status4 = copyfile('figure_*.fig',strcat(foldername,'/'));

```

```

FID_S11 = fopen('c:\4nec2\out\s11.txt', 'w', 'n');
targets11=[-1 -1 -1 -2.5 -5 -15 -5 -2.5 -1 -1 -1]
% [-3.4087 -4.3763 -5.6161 -7.0433 -8.2649 -8.5826 -7.8106 -6.5639 -5.3626 -4.3731 -
3.9611];%[1 1 1 .75 .5 0.0001 .5 .75 1 1 1];%%
noantennas=length(THETA1);
fprintf(FID_S11,'Number\t ---l1-- \t -theta1 \t ---l2-- \t -theta2 \t ---l3--\t -theta3 \t ---l4-- \t
-theta4 \t ---l5-- \t -theta5 \t objvalue \t fitvalue \n');
clear PointError
clear s11
clear ObjectiveValue
clear AverageError
clear ReadS11Result
for b=1:noantennas
    fName = sprintf('geom%d.out', b);
    fid=fopen(strcat(fName));
    linecount=0;
    requiredpoint=0;
    reqcount = 1;
    line=0;
    found=0;
    reqstring=cell(50,1);
    while line~= -1
        linecount = linecount+1; %start counting to keep track of the line numbers
        line = fgets(fid); %get the data written and assign it to line
        if findstr(line,'FREQ.')>0 %look for specified string in the line
            requiredpoint = linecount; %record point at which the string was found
        end
        if linecount==requiredpoint+4
            found = 1;
        end
        if found == 1
            reqstring{reqcount}=line;
            reqcount=reqcount+1;
        end
        if linecount > requiredpoint+4 && found==1 && findstr(line,char(10))<=2
            found=0;
        end
    end
    fclose(fid);
    % SPLIT THE PARAMETERS INTO ARRAYS
    try
        for i = 4:50
            disp(reqstring{i})
            c(i-3,:)=strsplit(reqstring{i});
        end
    catch ME
    end
    % calculate the return loss each of the antennas.
    % create an array for the return loss each antennas
    FREQ = str2double(c(:,2));

```



```

% FREQ = str2double(c);
% FREQ = Frequency [MHz]
RESISTANCE =str2double( c(:,3));
REACTANCE = str2double( c(:,5));
clear S11
clear ReflCoeff
ReadS11Result(b)=0;
% MAGNITUDE = NORMALIZED IMPEDANCE
for i = 1:length(RESISTANCE
%   S11 = Return loss.
    ReflCoeff(i) = (RESISTANCE(i) + 1j* REACTANCE(i)- 50)./(RESISTANCE(i) + 1j*
REACTANCE(i) + 50);% calculate the reflection coefficient.
    % ReflCoeff(i) = (str2double(MAGNITUDE(i)) - 1)./(str2double(MAGNITUDE(i)) +
1);% calculate the reflection coefficient.
    % plot the Return loss vs Frequency.
    if ReflCoeff(i) == 0
        S11(i) = 0;
        s11(b,i) = 0;
    else
        S11(i) = (20*log(abs(ReflCoeff(i))));
        s11(b,i) = (20*log(abs(ReflCoeff(i))));
    end
    ReadS11Result(b) = ReadS11Result(b) + S11(i);
end
spe=0;
for p = 1:11 % the number of frequency points
PointError(b,p) = (targets11(p) - s11(b,p))^2/(targets11(p))^2;% targets11(p) - s11(b,p)%
spe = spe + PointError(b,p);
end

AverageError(b) = (spe)/11;
ObjectiveValue(b) = 1/AverageError(b);%1/AverageError(b);
ReadS11Result(b) = ReadS11Result(b)/11;
if ObjectiveValue(b) > 10 % setting the objective value to 1.5 limit
    generation = genmax; % maximum number of geration to run
end
figure
grid on
hold on
title(sprintf('Antenna %d', b));
xlabel('Frequency (MHz)')
ylabel('S11 (dB)')
plot(FREQ,S11);
plot(FREQ,targets11)
hold off
fnamebeginning = 's11_';
fnameextension = '.fig';
fname = strcat(fnamebeginning, int2str(b), fnameextension);
saveas(gcf, fname)
end

```



```

fprintf(FID_nec, strcat('CM Linear wire antenna design', '\n'));
fprintf(FID_nec, strcat('CE File Generated by MatLab', '\n'));
fprintf(FID_nec, 'GW %3i %3i %8.4f %8.4f %8.4f %8.4f %8.4f %8.4f\n', 1, seg, 0, A(1, 1, n), A(2, 1, n), 0, A(1, 2, n), A(2, 2, n), 0.8); %segment length
fprintf(FID_nec, 'GW %3i %3i %8.4f %8.4f %8.4f %8.4f %8.4f %8.4f\n', 2, seg, 0, A(1, 2, n), A(2, 2, n), 0, A(1, 3, n), A(2, 3, n), 0.8); %segment length
fprintf(FID_nec, 'GW %3i %3i %8.4f %8.4f %8.4f %8.4f %8.4f %8.4f\n', 3, seg, 0, A(1, 3, n), A(2, 3, n), 0, A(1, 4, n), A(2, 4, n), 0.8); % segment length
fprintf(FID_nec, 'GW %3i %3i %8.4f %8.4f %8.4f %8.4f %8.4f %8.4f\n', 4, seg, 0, A(1, 4, n), A(2, 4, n), 0, A(1, 5, n), A(2, 5, n), 0.8); %segment length
fprintf(FID_nec, 'GW %3i %3i %8.4f %8.4f %8.4f %8.4f %8.4f %8.4f\n', 5, seg, 0, A(1, 5, n), A(2, 5, n), 0, A(1, 6, n), A(2, 6, n), 0.8); %segment length
% % % % % ground plane4
% % % % % GW 6 1 0.0000 1.0000 1.0000 0.0000 -0.0975 1.0000 0.1000
% % % % % GW 7 1 0.0000 0.0900 1.0000 0.0000 44.7601 1.0000 0.1000
% % % % % GE 0
% fprintf(FID_nec, 'GW %3i %3i %8.4f %8.4f %8.4f %8.4f %8.4f %8.4f\n', 6, 1, 0, 0, 0, 0, 1, 1, 0.75);
% fprintf(FID_nec, 'GW %3i %3i %8.4f %8.4f %8.4f %8.4f %8.4f %8.4f\n', 7, 1, 0, -1, 1, 0, 44, 1, 0.75);
fprintf(FID_nec, 'GW %3i %3i %8.4f %8.4f %8.4f %8.4f %8.4f %8.4f\n', 6, seg, 0, A(1, iLeft, n), 0, 0, 0, 0, 0.8);
fprintf(FID_nec, 'GW %3i %3i %8.4f %8.4f %8.4f %8.4f %8.4f %8.4f\n', 7, seg, 0, 0, 0, 0, A(1, iRight, n), 0, 0.8);
fprintf(FID_nec, 'GW %3i %3i %8.4f %8.4f %8.4f %8.4f %8.4f %8.4f\n', 7, 1, 0, A(1, iRight, n), 0, 0, 0.024, 0, 0.75);
% fprintf(FID_nec, 'GS %3i %3i %8.4f\n', 0, 0, 0.001);

fprintf(FID_nec, strcat('GE 0 \n'));
% fprintf(FID_nec, strcat('GE', '\n'));
fprintf(FID_nec, strcat('EK \n'));
fprintf(FID_nec, 'EX %3i %3i %3i %3i %3i %3i %3i\n', 0, 1, 1, 1, 1, 0, 0); %Excitation Command
wire 1 segment
fprintf(FID_nec, strcat('GN -1 \n'));
% 'GN 2 0 0 0 13 0.005 ' Use this line if ground used
fprintf(FID_nec, 'FR %3i %3i %3i %3i %8.4f %8.4f\n', 0, 1, 0, 0, 900, 0);
fprintf(FID_nec, 'FR %3i %3i %3i %3i %8.4f %8.4f\n', 0, 11, 0, 0, 850, 10);
% % fprintf(FID_nec, 'FR %3i %3i %3i %3i %8.4f %8.4f\n', 0, 17, 0, 0, 400, 100);
fprintf(FID_nec, 'LD %3i %3i %3i %3i %8.4f\n', 5, 1, 0, 0, 58000000);
% %
fprintf(FID_nec, 'RP %3i %3i %3i %3i %8.4f %8.4f %8.4f %8.4f\n', 0, 1, 1, 1000, 90, 0, 0, 0); %calculate gain at boresite
% fprintf(FID_nec, 'RP %3i %3i %3i %3i %8.4f %8.4f %8.4f %8.4f\n', 0, 10, 1, 1000, 0, 0, 10, 90);
fprintf(FID_nec, 'RP %3i %3i %3i %3i %8.4f %8.4f %8.4f %8.4f\n', 0, 361, 1, 1000, -90, 90, 1, 1);
fprintf(FID_nec, 'RP %3i %3i %3i %3i %8.4f %8.4f %8.4f %8.4f\n', 0, 1, 361, 1000, 90, 0, 1, 1);
% %
fprintf(FID_nec, 'RP %3i %3i %3i %3i %8.4f %8.4f %8.4f %8.4f\n', 1, 7, 73, 1000, 180, 0, -30, 5, 1000);
fprintf(FID_nec, strcat('EN', '\n'));
% RP 0 37 73 1003 -180 0 5 5

```

```
fclose(FID_nec);
```

## 5. Execution of the Genetic algorithms

```
function[A,newFileLog] = newexecute(THETA1, THETA2, THETA3,THETA4, THETA5,
l1,l2,l3, l4,l5, noantennas)
A = zeros(2,6,noantennas);
x0 = 1;
y0 = 1;
iX = 0; %intersect point x axis
iY = 0; %intersext point y value
j=1;
loopcount=0;
reset=0;
while j <= noantennas
    A(1,1,j)= x0;
    A(2,1,j)= y0;
    for i = 2:6;
        if i == 2 %first line doesn't need to be checked for intersection
            A(1,i,j) = l1(j)*sind(THETA1(j)) + A(1,1,j);
            A(2,i,j) = l1(j)*cosd(THETA1(j)) + A(2,1,j);
        end
        if i == 3
            A(1,i,j) = l2(j)*cosd(THETA2(j)+THETA1(j)) + A(1,2,j);
            A(2,i,j) = l2(j)*sind(THETA2(j)+THETA1(j)) + A(2,2,j);
            iX = 0;
            iY = 0;
        end
        if i == 4
            A(1,i,j) = l3(j)*cosd(THETA3(j)+THETA2(j)+THETA1(j)) + A(1,3,j);
            A(2,i,j) = l3(j)*sind(THETA3(j)+THETA2(j)+THETA1(j)) + A(2,3,j);
        end
        if i == 5
            A(1,i,j) = l4(j)*cosd(THETA4(j) + THETA3(j)+THETA2(j) + THETA1(j)) + A(1,4,j);
            A(2,i,j) = l4(j)*sind(THETA4(j) + THETA3(j)+THETA2(j) +THETA1(j)) + A(2,4,j);
        end
        if i == 6
            A(1,i,j) = l5(j)*cosd(THETA5(j)+ THETA4(j)+ THETA3(j)+THETA2(j)
+THETA1(j)) + A(1,5,j);
            A(2,i,j) = l5(j)*sind(THETA5(j)+THETA4(j) + THETA3(j)+THETA2(j) +
THETA1(j)) + A(2,5,j);
        end
        %disp(strcat('plot',num2str(j)));
        %disp(l4(j));
    %    axis above zero
    lowest_y = min(A(2,,:j));
    if lowest_y < 0
        A(2,,:j)= A(2,,:j)+ abs(lowest_y);
    end
end
end
```

```

if reset==1
    j=j-1;
    reset=0;
else
    newFileLog(j,:) =
[11(j),THETA1(j),12(j),THETA2(j),13(j),THETA3(j),14(j),THETA4(j),15(j),THETA5(j)];
    writeInputFile(A,1,j);
    figure
%    grid on
    hold on
    title(strcat('j=',int2str(j)))
    plot(A(1,:,j),A(2,:,j),'g');
%    the 10.0000 represents the padding, change as desired.
plotBoundary(A,j,2,10,10);
plotStaticBoundary();
    drawnow;
    axis square ;
    hold off
    filenamebeginning = 'figure_';
    filenameextension = '.fig';
    fName = strcat(filenamebeginning, int2str(j), filenameextension);
    saveas(gcf, fName)
end
j=j+1;
end
save('newdim','THETA1', 'THETA2', 'THETA3','THETA4', 'THETA5', '11','12','13','14','15');
load('newdim');
% Set the file paths
cd 'c:\4nec2\'
pwd
cd exe
%if you want to run the monopole simply remove the percentage sign from
%below
for i=1:noantennas%+1
% i=1:noantennas+1
% Generate some geometry to run
filenamestring=sprintf('../out/input%d.nec', i);
filenamestring2=sprintf('../out/geom%d.out', i);
fid = fopen('nec2d.tmp', 'wt' );          % Generates the text file
fprintf( fid, '../out/input%d.nec\n', i);  % that tells nec where to look
fprintf( fid, '../out/geom%d.out\n', i);   % for the input and output files
fclose(fid);
% Run nec from the command line
!Nec2dXS1k5.exe 0<nec2d.tmp
fid = fopen(filenamestring2, 'r');
tline = fgets(fid);
while ischar(tline)
    if(findstr(tline, 'FREQUENCY='))
        tline=lower(tline);
        disp(tline)
    end
end

```

```

    end
    tline = fgets(fid);
end
fclose(fid);
end

```

## 6. Optimise Genetic algorithm

```

function Fitvalue=optimizedga(THETA1, THETA2, THETA3,THETA4, THETA5, l1,l2,l3,
l4,l5,antenna,objvalue,pointerror)
Oavg = sum(objvalue)/length(objvalue);
Omin = min(objvalue);
Omax = max(objvalue);
Sp = 2;
if (Omin> ((Sp*Oavg)-Omax)/(Sp-1));
    delta = Omax-Oavg;
    A = ((Sp-1)*Oavg)/delta;
    B = (Oavg*(Omax-(Sp*Oavg))/delta);
else
    delta = Oavg-Omin;
    A = Oavg/delta;
    B = -(Omin*Oavg)/delta;
end
Fitvalue = (A*objvalue)+B; % calculate fitness+
[NEWFITNESS, I] = sort(objvalue,'descend'); % sort fitness values in descending order.
remove 'descend' to change order
Selpop = NEWFITNESS/sum(Fitvalue);

%select strongest individuals
for i = 1:15
    newantenna(i,:) = [l1(I(i)) THETA1(I(i)) l2(I(i)) THETA2(I(i)) l3(I(i)) ...
    THETA3(I(i)) l4(I(i)) THETA4(I(i)) l5(I(i)) THETA5(I(i))]; %assign the parameters for
the strongest individuals to the new antenna population
end
crossover(newantenna);
end
function crossover(antenna)
a1 = 0.5; %first alpha value
a2 = 0.8; %second alpha value
for i=1:5 %keep the strongest objective values and crossover the weakest
    mum(i,:) = antenna(i+5,:);
    dad(i,:) = antenna(i+10,:);
    popremainder(i,:) = antenna(i,:);
    offspring1(i,:) = mum(i,:); %give offspring 1 mums genes before performing crossover
    offspring2(i,:) = dad(i,:); %give offspring 2 dads genes before performing crossover
%    xpoint = floor(rand(1,10)); %get the crossover point by rounding down a random
number between one and ten
%    for j=1:xpoint % crossover everything from the start to the xpoint
        Xover = getXPos();
        for j=1:length(Xover) % crossover everything from the start to the xpoint

```

```

        if Xover(j) == 1
            offspring2(i,j) = a1*mum(i,j);%+a1*(dad(i,j)-mum(i,j));
            %offspring2(i,j) = dad(i,j)+a2*(dad(i,j)-mum(i,j));
            offspring1(i,j) = a2*dad(i,j);%+(1-a2)*(dad(i,j)-mum(i,j));
        end
    end
end
%gett all memmbers back into the population
for i=1:5
    newpop(i,:) = popremainder(i,:);%assign the first offspring to be the first five members of
the population
    newpop(i+5,:) = offspring2(i,:);%assign the second offspring to be the members 5-10 of
the population
    newpop(i+10,:) = offspring1(i,:);%assign the uncrossed members to be the members 10-15
of the population
    newpop(i+15,:) = mum(i,:);%assign mum to members 15-20 in the population
    newpop(i+20,:) = dad(i,:);%assign dad to members 20-25 in the populations
end
save('newpop1','newpop')
load('newpop1')
mutate(newpop)
end
function mutate(newpop)
    % define bounds
    %perform mutation
    LLB = 8.31; %line lower bound of the segment length
    LUB = 22.31; %line upper bound of the segment length
    ALB =; %angle lower bound of the segment angle
    AUB =; %angle lower bound of the segment angle
    for i = % no of antennas
        for j = 1:10 % antenna parameters 10
            percentage = rand;% percentage paramter to check if the current element should be
mutated
            if percentage < 0.01
                r = rand; %get the random number to be used in the equations
                switch (j)
                    case {1,3,5,7,9}% if it is an antenna length being mutated then use the length
                        newpop(i,j) = LLB + r*(LUB - LLB);
                    case {2,4,6,8,10}% if it is an antenna angle being mutated then use the length
                        newpop(i,j) = ALB + r*(AUB - ALB);
                end
            end
        end
    end
end
%write them to file
%newpop(:,2) = theta1
%newpop(:,4) = theta2
%newpop(:,6) = theta3

```

```

%newpop(:,8) = theta4
%newpop(:,10) = theta5
%newpop(:,1) = l1
%newpop(:,3) = l2;
%newpop(:,5) = l3
%newpop(:,7) = l4
%newpop(:,9) = l5
%25 = number of individuals

writefiles(newpop(:,2),newpop(:,4),newpop(:,6),newpop(:,8),newpop(:,10),newpop(:,1),newp
op(:,3),newpop(:,5),newpop(:,7),newpop(:,9),25);
end

function writefiles(O1,O2,O3,O4,O5,L1,L2,L3,L4,L5,no)
%no is the number of individuals in the population
%O represents theta
%L represents l
    newexecute(O1,O2,O3,O4,O5,L1,L2,L3,L4,L5,no);
end
function x = getXPos()
%function to decide which chromosomes should be mutated
%this will go through the ten individual chromosomes
    for i=1:10
        r = rand;
        if r>=0.5
            x(i) = 1;
        else
            x(i) = 0;
        end
    end
end
end
end

```



## APPENDIX D

### CREATING SQUARE STITCHING PATTERN AND FINITE ARRAY

#### 1. Creating square stitching pattern

```
clear
fName = 'Square02.csv';    %# A file name
fid = fopen(fName,'w');
x=0;
y=0;

lengthx= 100; %in mm
lengthy= 100; %in mm
% addonx=2; %mm distance between stiches
% addony=2; %mm
jumpx=10; %size of squares in mm
jumpy=10; %size of squares in mm
stitchB = 1; %horizontal stich before and after vertica lstich in mm
locx=[0.0];
locy=[0.0];

for a=0:jumpx:lengthx % full length of line to max X
    x=x+jumpx;
    locx=[locx x];
    locy=[locy y];
    plot (locx, locy)
end

for a=0:jumpy:lengthy % full length of line to max Y
    y=y+jumpy;
    locx=[locx x];
    locy=[locy y];
    plot (locx, locy)
end
count = 1;
for b=lengthx:-jumpx:jumpx % makes vertival lines from right to left
    x=x-jumpx; %one square left
    locx=[locx x];
    locy=[locy y];
    plot (locx, locy)
    if b==jumpx;
        for a=0:jumpy:lengthy % last line on +Y before reaching x=0
            y=y+jumpy;
            locx=[locx x];
            locy=[locy y];
            plot (locx, locy)
            count=1;
        end
    end
end
```

```

    end
else
    if count==1
        for a=0:jumpy:lengthy+jumpx % full length of line to min Y, one over
            y=y-jumpy;
            locx=[locx x];
            locy=[locy y];
            plot (locx, locy)
            count =2;
        end
    else
        for a=0:jumpy:lengthy+jumpx % full length of line to min Y, one over
            y=y+jumpy;
            locx=[locx x];
            locy=[locy y];
            plot (locx, locy)
            count=1;
        end
    end
end
end
end
% x=x-jumpx; %one square left
% locx=[locx x];
% locy=[locy y];
% plot (locx, locy)
end
count=1;
for c=lengthy:-jumpy:-jumpy %makes horizontal lines top to bottom
%
    if c==lengthy;
        for a=0:jumpx:lengthx % full length of line to min x, one over
            x=x+jumpx - stitchB ;
            locx=[locx x];
            locy=[locy y];
            x=x + 2*stitchB ;
            locx=[locx x];
            locy=[locy y];
            plot (locx, locy)
            x=x-stitchB;
            count =2;
        end
    else
        if count==1
            for a=0:jumpx:lengthx+jumpx % full length of line to max x, one over
                x=x+jumpx - stitchB;
                locx=[locx x];
                locy=[locy y];
                x=x + 2*stitchB;
                locx=[locx x];
                locy=[locy y];
                plot (locx, locy)
            end
        end
    end
end

```

```

        x=x-stitchB;
        count =2;
    end
else
    for a=0:jumpx:lengthx+jumpx % full length of line to min x, one over
        x=x-jumpx + stitchB;;
        locx=[locx x];
        locy=[locy y];
        x=x - 2*stitchB;;
        locx=[locx x];
        locy=[locy y];
        plot (locx, locy)
        x=x+stitchB;
        count=1;
    end
end
end
if mod(lengthx/10,2) == 0
    %if even
    if count ==1
        x=x-stitchB;
        y=y-jumpy; %one square left
        locx=[locx x];
        locy=[locy y];
        x=x+stitchB;
    else
        x=x+stitchB;
        y=y-jumpy; %one square left
        locx=[locx x];
        locy=[locy y];
        x=x-stitchB;
    end
    plot (locx, locy)
else
    x=x-stitchB;
    y=y+jumpy; %one square left
    locx=[locx x];
    locy=[locy y];
    x=x+stitchB;
    plot (locx, locy)
    %number is odd
end
end
tablexy = [locx;locy];
fprintf(">","STITCH_COUNT:", "%f\n", length(locx) );
fprintf(">","EXTENTS_LEFT:", "%f\n", round(min(locx)));
fprintf(">","EXTENTS_TOP:", "%f\n", max(locy));
fprintf(">","EXTENTS_RIGHT:", "%f\n", max(locx));
fprintf(">","EXTENTS_BOTTOM:", "%f\n", min(locy));
fprintf(">","EXTENTS_WIDTH:", "%f\n", max(locx)-min(locx) );

```

```

fprintf('">',"EXTENTS_HEIGHT:","%f"\n\n', max(locy)-min(locy));
fprintf('***',"STITCH","%f","%f" \n', tablexy);
fprintf(fid,"**","COLOR","0","0" \n');
fprintf(fid,"**","TRIM","0","0" \n');
fprintf(fid,"**","STITCH","%f","%f" \n', tablexy);
% fprintf(fid,"**","STITCH","%f","%f" \n', tablexy);
fclose(fid);

```

## 2. Create square pattern

```

function result = createSquarePattern(filename, locx, locy)
    fName = filename;      %# A file name
    fid = fopen(fName,'w');
    tablexy = [locx;locy];
%   fprintf(fid,">","STITCH_COUNT:","%f"\n', length(locx) );
%   fprintf(fid,">","EXTENTS_LEFT:","%f"\n', round(min(locx)));
%   fprintf(fid,">","EXTENTS_TOP:","%f"\n', max(locy));
%   fprintf(fid,">","EXTENTS_RIGHT:","%f"\n', max(locx));
%   fprintf(fid,">","EXTENTS_BOTTOM:","%f"\n', min(locy));
%   fprintf(fid,">","EXTENTS_WIDTH:","%f"\n', max(locx)-min(locx) );
%   fprintf(fid,">","EXTENTS_HEIGHT:","%f"\n\n', max(locy)-min(locy));
fprintf(fid,"#","[THREAD_NUMBER]","[RED]","[GREEN]","[BLUE]","[DESCRIPTION]
","[CATALOG_NUMBER]" \n');
    fprintf(fid,"$","1","0","0","0","Black","" \n');
    fprintf(fid,"$","2","112","188","31","Lime Green","" \n');
    fprintf(fid,"$","3","237","23","31","Red","" \n');

    fprintf(fid,"**","COLOR","0","0" \n');
    fprintf(fid,"**","TRIM","0","0" \n');
    fprintf(fid,"**","STITCH","%f","%f" \n', tablexy);
    fclose(fid);
end

```

## 3. Creating a unit cell pattern

```

function result= drawStichingPatternSimple(length, width)
    fName = 'SampleUnitCellPattern.csv';      %# A file name
    fid = fopen(fName,'w');
    result = [];
    for i = 0:width:length - width
        point1 = [0; i]
        point2 = [width; i]
        point3 = [width; i + width]
        point4 = [0; i]
        result = cat(2,result, point1,point2,point3,point4)
    end
    result = cat(2, result, [0; length], [width; length])
    locx = result(1,:);
    locy = result(2,:);
    tablexy = [locx;locy];

```

```

%   fprintf(fid,">","STITCH_COUNT:", "%f" \n', length(locx) );
%   fprintf(fid,">","EXTENTS_LEFT:", "%f" \n', round(min(locx)));
%   fprintf(fid,">","EXTENTS_TOP:", "%f" \n', max(locy));
%   fprintf(fid,">","EXTENTS_RIGHT:", "%f" \n', max(locx));
%   fprintf(fid,">","EXTENTS_BOTTOM:", "%f" \n', min(locy));
%   fprintf(fid,">","EXTENTS_WIDTH:", "%f" \n', max(locx)-min(locx) );
%   fprintf(fid,">","EXTENTS_HEIGHT:", "%f" \n \n \n', max(locy)-min(locy));
fprintf(fid,"#", "[THREAD_NUMBER]", "[RED]", "[GREEN]", "[BLUE]", "[DESCRIPTION]
", "[CATALOG_NUMBER]" \n');
    fprintf(fid,"$", "1", "0", "0", "0", "Black", "" \n');
    fprintf(fid,"$", "2", "112", "188", "31", "Lime Green", "" \n');
    fprintf(fid,"$", "3", "237", "23", "31", "Red", "" \n \n');
    fprintf(fid,"*", "COLOR", "0", "0" \n');
    fprintf(fid,"*", "TRIM", "0", "0" \n');
    fprintf(fid,"*", "STITCH", "%f", "%f" \n', tablexy);
    fclose(fid);
end

```

## APPENDIX E

### Numerical simulation of the infinite array

```
% This code calculates the resistance from the centre of a finite
% grid of resistors to every point in the grid
% we use nodal analysis to do the calculation
clear all
digits(3)
%close all
%%%%%%%%%%%%%%%%%%%%%%%%%%%%%%%%%%%%%%%%%%%%%%%%%%%%%%%%%%%%%%%%%%%%%%%% Mesh build
M= 4; % this is the order of the grid
    % N=1 implies that m= -1, 0, 1 and n= -1, 0 1
    % i.e. a 9-node problem
    % we assume that the nodal voltage at each point is V(i, j)
    % See http://matlabbyexamples.blogspot.co.uk/2011/11/circuit-solver-using-matlab-programming.html
    % Create a finite grid of resistors
    % It is possible to insert defects into the grid at this stage
FractionDefected=0.01; % This is the fraction of the available branches or nodes that have a defect

    % If a resistor does not connect to a node it is
    % deleted from the netlist completely.
    % The resistor visualisation does not account for that.
    % Note that increasing above 0.1 means there is a
    % higher
    % probability that a node will not connect to any of
    % its branches. Thus the resistance to a point can
    % not be computed.
NodeNo= 1; % Keeps a tally of the nodenumbers used so ones can be added onto the list
frequency=2.45e9; % Hz
joincap=1e-12; % Capacitance in Farads of one single join
NetList=[];
centrenode= (2*M+1)^2/2 + 0.5; % for convenience
meshwidth=2*M+1; %
for m=1:meshwidth-1
    for n=1:2*M
        NetList= [NetList ; [n+(m-1)*meshwidth (n+1)+(m-1)*meshwidth 1]]; % last digit is the impedance
        NetList= [NetList ; [n+(m-1)*meshwidth n+m*meshwidth 1]];
    end
end
m=2*M+1;
for n=1:meshwidth-1
    NetList= [NetList ; [n+(m-1)*((2*M)+1) (n+1)+(m-1)*((2*M)+1) 1]];
end
n=2*M+1;
for m=1:meshwidth-1
```

```

NetList= [NetList ; [n+(m-1)*((2*M)+1) n+(m)*((2*M)+1) 1]];
end
NodeNo=meshwidth^2+1; % Set the nodes to the next value to be created
%%%%%%%%%%%%%%%%%%%%%%%%%%%%%%%%%%%%%%%%%%%%%%%%%%%%%%%%%%%%%%%%%%%%%%%%% End mesh build
%%%%%%%%%%%%%%%%%%%%%%%%%%%%%%%%%%%%%%%%%%%%%%%%%%%%%%%%%%%%%%%%%%%%%%%%% Introduce defects - delete a random selection of
%%%%%%%%%%%%%%%%%%%%%%%%%%%%%%%%%%%%%%%%%%%%%%%%%%%%%%%%%%%%%%%%%%%%%%%%% branches
n=round(FractionDefected*size(NetList,1));
idx=randsample(1:size(NetList,1),n) ;
%NetListRows = NetList(idx,:) ; % pick rows randomly % Uncomment if breaks
%NetList(idx,:)=[]; % remove those rows UNCOMMENT
%idx = randsample(1:size(NetList,1),n) ; %random sample of branches
%DeletedResistors= NetList(idx,:); % UNCOMMENT
%%%%%%%%%%%%%%%%%%%%%%%%%%%%%%%%%%%%%%%%%%%%%%%%%%%%%%%%%%%%%%%%%%%%%%%%% END OF DEFECT
%%%%%%%%%%%%%%%%%%%%%%%%%%%%%%%%%%%%%%%%%%%%%%%%%%%%%%%%%%%%%%%%%%%%%%%%% More defects
% Find entries in the netlist that refer to a specific node
% Example
idx = randsample(1:meshwidth^2, n);
for k=1: numel(idx);
    defectnode = idx(k);
    %index1 = NetList(:,1) == defectnode;
    %index2 = NetList(:,2) == defectnode;
    %branches=[NetList(index1, :) ; NetList(index2, :)] % The right and up down and left
nodes
    branches= [find(NetList(:, 1)==defectnode); find(NetList(:, 2)==defectnode)];
    if numel(branches) > 3; % There needs to be 4 branches before this defect will occur
        % This is why the ones on the edge are always
        % connected and it goes to the same value.
        %%%%%%%%%%%%%%%%%%%%%%%%%%%%%%%%%%%%%%%%%%%%%%%%%%%%%%%%%%%%%%%%%%%%%%%%%% Example defect
        % Move up and down branches to a new node and splice a capacitor between
        % the two nodes
        NetList(branches(1),:)= [NetList(branches(1), 1:2) 1]; % Left and right branches the
SAME
        NetList(branches(4),:)= [NetList(branches(4), 1:2) 1]; % Shouldn't make any changes
        % Shift the up down resistors to the new node
        NetList(branches(2),:)= [NodeNo NetList(branches(2), 2) 1];
        NetList(branches(3),:)= [NetList(branches(3), 1) NodeNo 1];
        % Splice in the capacitor between the old and new node
        NetList=[NetList ; [defectnode NodeNo -j/(2*pi*frequency*joincap)]]; % This adds in a
new node and connects it to the branch to the right

        NodeNo=NodeNo+1; % Don't forget to move to the next node number for the next
defect
    end
end
% Inject a test voltage
% Strategy is to change the position of the test voltage and then
% measure the current flowing back out of the zero volts terminal
% by adding the branch currents leading into it.
% Then the resistance can be found.
% This has been validated against a circuit model for a few cases.

```

```

% e.g. M=1 the adjacent node to the left of the centre has a resistance of
% 0.583 ohms. As M-> Infinity the resistance -> 0.5 as predicted by
% theory.
% Iterate over all the nodes in the mesh.
for node=1:meshwidth^2
    if node==centrenode
        Z(node)=0;
    else
        Vnod=[centrenode 0; node 1];
        l=size(NetList,1);
        N=max([NetList(:,1) ;
        NetList(:,2)]);
        A=zeros(N,N);
        B=zeros(N,1);
        % Load A matrix
        for i=1:l
            n1=NetList(i,1);
            n2=NetList(i,2);
            if n1==n2
            else
                A(n1,n2)=A(n1,n2)-1/NetList(i,3);
                A(n2,n1)=A(n2,n1)-1/NetList(i,3);
                A(n1,n1)=A(n1,n1)+1/NetList(i,3);
                A(n2,n2)=A(n2,n2)+1/NetList(i,3);
            end
        end
        % Load B matrix
        for i=1:size(Vnod,1)
            A(Vnod(i,1),:)=zeros(1,N);
            A(Vnod(i,1),Vnod(i,1))=1;
            B(Vnod(i,1),1)=Vnod(i,2);
        end
        Vo=A\B;
        %%%% THE BELOW WORK IS DONE- COMMENTS LEFT IN FOR INFO
        % calculate the resistance by measuring the currents into the ground node
        % Sum of V/R
        % DEVELOPMENT - this needs to automatically work out the currents
        % coming into the node. At the moment it is vastly oversimplified
        % because it tries to work out based on position where the current is
        % coming from
        % AND it does not take the impedance of the branch into account.
        % It needs to interrogate the node list for branches entering the node
        % THEN use their impedances to calculate the currents.
        % THIS ONLY WORKS FOR ALL EQUAL RESISTANCES COMING INTO THE
NODE
        branches=[find(NetList(:, 1)==node); find(NetList(:, 2)==node)];
        current=0;
        for q=1:numel(branches)
            if NetList(branches(q), 1)~=node;
                current=current + (Vo(node)-Vo(NetList(branches(q), 1)))/NetList(branches(q), 3);
            end
        end
    end
end

```



```

    end
    if NetList(branches(q), 2)~=node;
        current=current + (Vo(node)-Vo(NetList(branches(q), 2)))/NetList(branches(q), 3);
    end
end
end
Z(node)= 1/current;
%Z(node)= 1/(Vo(centrenode+1)+Vo(centrenode-
1)+Vo(centrenode+meshwidth)+Vo(centrenode-meshwidth));
end
end
Z=reshape(Z, [meshwidth meshwidth]); % convert to a matrix
Z=flipud(Z(meshwidth/2+0.5:meshwidth, meshwidth/2+0.5:meshwidth));

figure
imagesc([0 M], [-M 0], imag(Z)) % Currently this shows the real part of the voltage
% caxis([0 3])
colorbar
%set(gca,'YTick',[-8:0], 'YTickLabels', [{8}, {7}, {6}, {5}, {4}, {3}, {2}, {1}, {0}]); % A
bodge!!!
axis square
colorbar
colormap(flipud(hot))
title('Imaginary part of the normalised impedance to each grid point for a finite array')

% % Draw a visualisation of the resistors on the plot
% % Horizontal resistors
for m=0:M-1
    for n=0:M
        rectangle('Position',[0.2+m] (-0.15-n) 0.6 0.3], 'FaceColor',[1 1
1], 'EdgeColor','b', 'LineWidth', 1)
    end
end
for m=0:M
    for n=0:M
        line([0.2+m -0.2+m], [0-n 0-n], 'LineWidth', 1, 'Color','b')
    end
end
% Vertical resistors
for m=0:M
    for n=0:M-1
        rectangle('Position',[-0.15+m] (-0.8-n) 0.3 0.6], 'FaceColor',[1 1
1], 'EdgeColor','b', 'LineWidth', 1)
    end
end
for m=0:M
    for n=0:M
        line([0+m 0+m], [0.2-n -0.2-n], 'LineWidth', 1, 'Color','b')
    end
end
end
% blobs

```

```

for m=0:M
    for n=0:M
        rectangle('Position',[-0.05+m -0.05-n 0.1 0.1],'Curvature',[1 1], 'FaceColor',[0 0 0])
    end
end
axis off
%%%%%%%%%%%%%%%%%%%%%%%%%%%%%%%%%%%%%%%%%%%%%%%%%%%%%%%%%%%%%%%%%%%%%%%%%%%%%%
%%%%%%%%%%%%%%%%%%%%%%%%%%%%%%%%%%%%%%%%%%%%%%%%%%%%%%%%%%%%%%%%%%%%%%%%%%%%%%real part
figure
imagesc([0 M], [-M 0], real(Z)) % Currently this shows the real part of the voltage
% caxis([0 3])
colorbar
%set(gca,'YTick',[-8:0], 'YTickLabels', [{8}, {7}, {6}, {5}, {4}, {3}, {2}, {1}, {0}]); % A
bodge!!!
axis square
colorbar
colormap(flipud(hot))
title('Real part of the normalised impedance to each grid point for a finite array')
for m=0:M-1
    for n=0:M
        rectangle('Position',[(0.2+m) (-0.15-n) 0.6 0.3], 'FaceColor',[1 1
1],'EdgeColor','b','LineWidth', 1)
    end
end
for m=0:M
    for n=0:M
        line([0.2+m -0.2+m], [0-n 0-n], 'LineWidth', 1, 'Color','b')
    end
end
% Vertical resistors
for m=0:M
    for n=0:M-1
        rectangle('Position',[(-0.15+m) (-0.8-n) 0.3 0.6], 'FaceColor',[1 1
1],'EdgeColor','b','LineWidth', 1)
    end
end
for m=0:M
    for n=0:M
        line([0+m 0+m], [0.2-n -0.2-n], 'LineWidth', 1, 'Color','b')
    end
end
% blobs
for m=0:M
    for n=0:M
        rectangle('Position',[-0.05+m -0.05-n 0.1 0.1],'Curvature',[1 1], 'FaceColor',[0 0 0])
    end
end
axis off
latex(sym(vpa(Z)))
resistance = real(Z)

```

imaginary = imag(Z)  
worstresistance= max(max(Z))

## References

1. R. Carter, "The Method of Moments in Electromagnetics, by W.C. Gibson," *Contemp. Phys.*, 51, (2), pp. 183–184, 2010.
2. P.B. Johns, "A symmetrical condensed Node for the TLM method" *IEEE Transactions on theory and techniques*, Vol. MTT-35 (4) 1987 pp.370-376.
3. M. Bartsch., "Solution of Maxwell's equations," *Comput. Phys. Commun.*, 73(1–3), pp. 22–39, 1992.
4. T. Milligan, *Modern Antenna Design*, 2nd Ed. 2005.
5. M. Clemens and T. Weiland, "Discrete Electromagnetism with the Finite Integration Technique," *Prog. Electromagn. Res.*, 32, pp. 65–87, 2001
6. S. Akhtarzad and P. B. Johns, "Solution of Maxwell's equations in three space dimensions and time by the t.l.m. method of numerical analysis," *Proc. Inst. Electr. Eng.*, vol. 122, no. 12, p. 1344, 1975.
7. R. F. Harrington, "Matrix Methods for Field Problems," *Proc. IEEE*, 55(2), 1967.
8. T. Weiland, M. Timm, and I. Munteanu, "A practical guide to 3-D simulation," *IEEE Microw. Mag.*, 9(6), pp. 62–75, 2008
9. J. Burke, "Numerical Electromagnetic Code (NEC2)" User Manual January, 1992.
10. Burke, G.J and Poggio, A.J, "Numerical Electromagnetic Code (NEC2) – Method of Moments," Part II, Lawrence Livermore National Laboratory, 1981.